OUKA
The University of Osaka
Institutional Knowledge Archive

Title	MATHEMATICAL AND PHYSIOLOGICAL STUDY ON THE CONTRACTILE MECHANISM OF MUSCLE AND THE NEUROMUSCULAR CONTROL SYSTEM
Author(s)	赤澤, 堅造
Citation	大阪大学, 1974, 博士論文
Version Type	VoR
URL	https://hdl.handle.net/11094/1094
rights	
Note	

The University of Osaka Institutional Knowledge Archive : OUKA

https://ir.library.osaka-u.ac.jp/

The University of Osaka

MATHEMATICAL AND PHYSIOLOGICAL STUDY ON THE CONTRACTILE MECHANISM OF MUSCLE AND THE NEUROMUSCULAR CONTROL SYSTEM

KENZO AKAZAWA

MATHEMATICAL AND PHYSIOLOGICAL STUDY ON THE CONTRACTILE MECHANISM OF MUSCLE AND THE NEUROMUSCULAR CONTROL SYSTEM

by

KENZO AKAZAWA

Submitted in partial fulfillment of the requirements

for the degree of Doctor of Engineering

Faculty of Engineering

Osaka University

March, 1974

PREFACE

One of the most important tasks of the life sciences is to clarify the fine functions found in the biological system, by fully applying all the scientific techniques developed up to the present, and to turn the subsequent knowledge to the advancement of scientific technology and to the promotion of public welfare. Tremendous progress has been made in the areas of electronics, control engineering and computer science. Engineers are now in the position of turing this technique to the advancement of life science or the aid of less fortunate fellow man. However, the problems here are certainly more complex and difficult than expected.

So far engineers interested in Biomechanism or Bio-Medical Engineering have been involved in producing new artificial augmentations and replacements for man's subsystem, such as prostheses and heart-lung machines, and further in developing new artificial limbs, manupilators, walking machines and robots. In these fields, however, there are many unsolved problems significant enough to require detailed investigations. The point we particularly emphasize is that the complex engineering devices such as driving actuators, automatic control instruments and information processing systems, do not yet exhibit the same desirable performance, function and stability as our own muscles and motor control systems. And, in relation to the development of artificial limb, it is particularly necessary to solve the two following problems:

i) the development of compact, sufficiently powerful and flexible actuators, similar to living muscles;

ii) the development of a rational system of controlling the various actuating mechanisms in highly functional limbs, the system to be similar to the neuromuscular control system.

As far as these two problems are concerned, however, present technology is able to reproduce (create) only the simplest of the functions provided in the muscular contractile mechanism and in the motor control system.

In this view, it is of great significance to reveal excellent functions of the living motor system and to find in the system some valuable clues which may lead the way to important developments of new actuators and to a high quality automatic control system.

In general, the mechanisms of muscle contraction and motor control have been extensively studied by the sciences of biology, medicine, physiology and biophysics, but it has been felt that these studies have failed to go beyond a fragmentary explanation of specific phenomena and most investigation proceeds without a unifying theory of muscle contraction and similarly without that of motor control system. A comprehensive approach relating all the studies of the muscle contraction or of the motor system is needed, and development of a unifying theory of them has obviously important and interesting ramifications in applied science as well as basic science.

The present study is indeed along this line, the purpose of which is to clarify the mechanisms of muscle contraction and motor control from the point of view of engineering, paying special attentions to their dynamic functions. However, to our chagrins, the results obtained in the present study are probably far from the principal objects attempted and seem to fail to achieve entire elucidation of the mechanisms of muscle contraction and motor control, although they undoutedly constitute an important and valuable contribution to the study of the question. Of course, the vast field of biological motor activity obviously exceeds the limits of one man's investigation. One short decade of investigation in a new area of research can hardly be expected to have solved more than a fraction of the problems facing us in interpreting the chemo-mechanical coupling of the muscular contractile mechanism and the role of nervous systems in motor control. The results presented in this thesis seem to indicate new openings for further investigations.

ABSTRACT

The present thesis consists of two parts. The purpose of this study is to elucidate the mechanism of muscle contraction and to uncover the control functions of the neuromuscular system in the fully dynamic sense. At the same time, the subject is to find some valuable clues that may lead respectively to the development of artificial muscles and to the synthesis of control systems for artificial limbs or paralyzed limbs.

Part I deals with the mechanism of muscular contraction. First, mechanical properties of skeletal muscle are clarified by various physiological experiments on the frog semitendinosus muscles; the viscous elastic properties of the resting muscle, the force-load-velocity and load-extension relations of the contracting muscle and the time courses of the active state are determined quantitatively.

Second, a mechanical model of the muscle consisting of a contractile component (composed of force generator and viscou-like component) and viscous elastic components, is developed on the basis of these physiological findings. Dynamic characteristics of muscle contraction are accounted for by simulations of the model.

Then, the contractile component is modeled, based on the sliding-filament theory, the chemical reaction mechanism of actin-myosin-ATP system and the excitation-contraction coupling. All the system parameters involved are determined quantitatively from the physiological data obtained from the frog semitendinosus muscle.

Finally, the unified model capable of accounting for all the contractile process from neural impulses to mechanical work is developed by synthesizing the models mentioned above. This model is not only able to explain various steady state properties such as the force-load-velocity, force-energy liberation and force-heat production relations but also to inpetpret the transient

responses such as isometric and isotonic contractions and time courses of inner Ca ion concentraction. The responses of the model show close agreement with those obtained from frog skeletal muscles.

Part II deals with the motor control system, which includes sensory and motor neurons at the spinal cord level and their associated muscles, joint, skeletons and muscle proprioceptors (spindle receptors and Golgi tendon organs) A mathematical model of each physiological element is developed, based on recent physiological and anatomical findings of cat's soleus muscles. Dynamic properties of the muscle spindle is particularly investigated in detail, paying special attentions to variation of position and velocity sensitivities due to the gamma efferent activities.

A model of stretch reflex concerning single muscles is synthesized by connecting the models of muscle, spindle receptor and alpha motoneuron into an equivalent feedback system. Responses of the model of the stretch reflex are in a good agreement with the physiological result. The mechanism of length control as well as the role of spindle receptor and gamma motor system in its reflex is made clear.

A neuromuscular control system model concerning a pair of agonist and antagonist muscles is developed. Computer simulations reveal the mechanisms of postural control, velocity control and tension control, and besides the mechanism of how these control actions are made to cooperate with each other. At the same time, the synergetic actions originating from the functional elements such as gamma motor system, alpha-gamma linkage, spindle group Ia, tendon group Ib and spindle group II afferent fibers are accounted for by analyzing each control action.

Besides, a mathematical model of a human forearm motor system is developed based on anatomical and phsyiological data. Movements of the forearm generated by functional electrical stimulation via surface electrodes as well as normal innervation are explained by the model.

ACKNOWLEDGEMENT

The author wishes to express his gratitude for the guidance and support received from Professor Katsuhiko Fujii, who was closely associated with the research from first to last. It was the author's immeasurable benefits to receive his invigorating advice and stimulation.

He also wishes to express his thanks to Professor Masataro Nishimura and Yutaka Suzuki for their valuable guidance and intriguing comments. Appreciation is extended to Professor Yoshio Inuishi, Professor Kazuo Kawabe and Professor Chiyoe Yamanaka for the guidance and encouragement.

The author's special thanks go to Professor Hidenobu Mashima (School of Medicine, Juntendo University) for his encouraging suggestions, support and invaluable help during the study of muscle contraction as well as in making the physiological experiments. Without his help, the author's work is likely to fail of its purpose. Professor Yuji Tonomura (Faculty of Science, Osaka University) enlightened him on the molecular mechanism of muscle contraction and contributed to valuable suggestions about the mathematical modeling of the contractile machinery.

Sincere thanks are due to Dr. Takeshi Kasai for his encouraging suggestions and helpful discussions in investigating mechanical properties of the muscle. The author is also much indebted to the staff members of Fujii Lab., in particular, to Mr. Eizo Kuroda, Dr. Tatsuya Morita and Mr. Hideo Taguchi for their valuable discussions and criticisms.

He is also indebted to Dr. Moto Matsumura and Dr. Kazuhiro Yamada (School of Medicine, Juntendo University) for their valuable comments about the energetics of muscle contraction, and to Mr. Hiroki Kushima for his help with the physiological experiments on the frog skeletal muscle.

Not forgotten are his research associates, Messrs. Kunihiko Murata, Hiroaki Mikami, Saburo Kajiyama, Makoto Yamamoto and Tadashi Hara, with whom he worked together and had opportunities to discuss many problems and to spend enjoyable time together. Their invaluable help is gratefully acknowledged.

TABLE OF CONTENTS

PART II

STUDY ON THE NEUROMUSCULAR CONTROL SYSTEM

PART I

STUDY ON THE CONTRACTILE MECHANISM OF THE SKELETAL MUSCLE

CHAPTER I

INTRODUCTION

The remarkable difference from ordinary engineering actuators such as electrical, pneumatic and hydraulic actuators is that living muscles are biological machines which convert chemical energy into force development and mechanical work. The contractile machinery is basically composed of contractile proteins, actin and myosin, and the fuel is universally ATP (adenosine triphosphate) with high energy. Furthermore, in comparison with the engineering actuators, the following characteristics of muscle functions can be emphasized.

(i) The muscle is a compact and soft machine capable of generating forcible power; the ratio of output power /weight is surprisingly great (2-10 Kg/cm^2 cross section).

(ii) Viscous and elastic properties vary with contractile activity of muscle contraction. Their coefficients change significantly with the transition from rest to contraction.

(iii) An autogenetic control mechanism is provided in the contractile machinery; energy liberation is effectively regulated according to change in applied load.

These magnificient functional characteristics can neither be provided in the present engineering machines nor be materialized by any possibility even by means of applying the modern progressive techniques. Recently, various kinds of artificial muscles have been developed in parallel with the development of externally-powered prostheses for physically impaired individuals. There are, for instance, McKibben muscle, artificial rubber muscle designed by Kato and Ishida (1969)[55] and artificial mechano-chemical muscle developed by Katchalsky (1954)[54] and Tatara (1973).[81] All these artificial

muscles, however, are far from living muscles in respect to the power/weight ratio. Indeed, to develop such compact, flexible and sufficiently powerful artificial muscles that can generate forces of a magnitude similar to the intact muscles has been strongly urged. In this context, it is of important significance to elucidate the mechanism of contractile machinery in the living muscle from the point of view of engineering.

Indeed, there seems to be significant advances in the last decade in knowledge of the details of muscle structure and of the molecular mechanism of muscle contraction. In spite of them, no comprehensive theory has been proposed yet which satisfactorily explains the molecular events involved in the mechano-chemical process of muscle contraction. A complete explanation of the contractile process can only come when structural, biochemical and physiological findings are melded into a single theory. The present study is essentially under this view. Seeing that the contractile machinery comprises a complex of interacting processes and components, simulation study seems to be quite available for the present purpose. Further, the mathematical modeling can be recognized as being a useful way to quantify the interacting behaviors within the contractile machinery and to determine the dynamic characteristics of the contractile mechanism. In such a case the point that should be emphasized is that a mathematical model of the muscle, treating it as a chemo-mechanical system, should be in such a form as involves the following contents:

1) There be a clear correspondence between the model and the ultrastructure and function of muscle fiber elucidated during the last decade.
2) The characteristics of each component of the model be figured out quantitatively.
3) The various mechanical behaviors during shortening and lengthening exhibited by the contracting and resting muscles be able to be explained quantitatively by the model.

4) Microscopic characteristics (sliding movements of myofilaments, chemical process of the actin-myosin-ATP system) as well as macroscopic ones (tension development, shortening, work, energy liberation, heat production and Ca ion release) be inclusively accounted for by means of the model in the dynamic sense.

Various kinds of models have been presented in order to interpret the functional characteristics of the muscle, as shown in the extensive literature concerned with muscle models (Pringle, 1960[69] ; Sandow, 1970[77]). For example, the classical viscoelastic model of muscle was introduced by Gasser and Hill (1924)[33] and Levin and Wyman (1927)[57] ; a two-component model which consisted of the series elastic component and the contractile component was developed by Hill (1938)[36] , Wilkie (1950)[87] and Ritchie and Wilkie (1958)[71] ; the physicochemical model by Polissar (1952)[68] , the transmutation chain model by Buchthal and Kaiser (1951)[17], and recently the modified viscoelastic model by Bahler (1968)[10]. All these models, however, are not satisfactory in the sense that there is no clear correspondence between the model and the microstructure of muscle fiber elucidated during the last decade, and that the characteristics of each component of the model are not figured out quantitatively. Since 1957, A. F. Huxley and his co-workers (Huxley, 1957[45] ; Gordon et al., 1966[34]) have established the sliding-filament theory in parallel with the electron-microscopic findings on myofilaments made by H. E. Huxley (1957)[47]. Quantitative approaches, involving mathematical descriptions and the formulation of appropriate models of the sliding-filament mechanism, have been presented by many workers : Deshcherevskii (1968)[26], Volkenstein (1969)[86], T. L. Hill (1970)[43], Chaplain and Frommelt (1971)[29] and Huxley and Simmons (1971)[46]. All these models, however, have been rather meagre because none of them goes beyond explanation of specific phenomena in muscular contraction, although they have furnished us with useful information in understanding muscular contraction or in constructung a mathematical model.

The present study is undertaken in order to develop a new model of muscle including the modern concepts of the sliding-filament mechanism, molecular mechanism of the actin-myosin-ATP system and excitation-contraction coupling, paying special attentions to the correspondence between the model and the microstructure of the muscle. This kind of modeling of the muscle may open a useful way not only for the better understanding of the contractile mechanism but also for further application of the contraction principle to the development of small-sized, efficiently powerful artificial muscle and to the analysis of neuromuscular control system.

The current pressing problems are those concerned with the formulation of a mathematical model of muscle contraction, which lies at the junction between experimental evidence and theoretical construct. Although many investigations have been already made on the dynamic properties of the skeletal muscles, it is not easy and even impossible to compare the results of them quantitatively with each other because of the difference of materials and experimental conditions. They can not provide all data needed for the simulations. Therefore, in this study, necessary data for the simulations are obtained by focusing all the physiological experiments on the frog semitendinosus muscle. To sum up, we have carefully made a mathematical model of muscle contraction with an iterative process between physiological experimentation and simulation.

The organization of the present thesis (part I) is as follows.

In chapter II, well-established findings about structure and functions of skeletal muscles are reviewed, detailing the ultrastructure of muscle fiber, the theory of sliding-filament mechanism and the molecular mechanism of contraction. Further, mechanical properties of skeletal muscles are outlined in comparison with the mechanical model. The experimental set-up and preparations of the frog semitendinosus muscle which were used in the physiological experiments are described.

In chapter III, mechanical properties of the resting and contracting states are determined quantitatively from the frog semitendinosus muscle, by designing pertinent physiological experiments by which each mechanical element is identified as independently as possible. That is, viscous and elastic properties of the resting muscles, load-extension relations of the series elastic component of the contracting muscles, force-load-velocity relations of the contractile component and viscous-like force are together determined.

In chapter IV, active contractile forces generated in the contractile component- intensities of active state- are estimated by an analytical method, and are compared with those estimated experimentally by quick-release and quick-stretch techniques.

In chapter V, a mechanical model of the muscel is developed, based on the experimental findings determined in chapters III and IV, and muscle dynamics are explained , comparing the responses of the model with what are actually observed on the muscle.

In chapter VI, a mathematical model of the contractile component is developed, based on the molecular mechanism of contraction (actin-myosin-ATP system), sliding-filament mechanism, excitation-contraction coupling and ultrastructure of muscle fibers. Finally, an unified model of muscle contraction is developed by putting this model into the contractile component of the mechanical model. All the parameters of the model are determined by employing the values obtained in chapter III. Dynamic characteristics of the contractile mechanism are distinctly revealed in a quantitative sense by simulating various contractile phenomena such as isometric and isotonic contractions.

Chapter VII does summarize major findings obtained in the present study.

CHAPTER II

REVIEW OF THE MECHANISM OF MUSCLE CONTRACTION AND METHODS

2.1 MUSCLE STRUCTURE AND CONTRACTILE MECHANISM

a) Muscle structure

The structure of a muscle fiber and organs that compose it offers important clues to understanding of how the muscle does function. Examination of the fine structure of striated muscle fibers, made possible by a electron microscope and X-ray, has shed new light on the question of how the muscle cell translates chemical energy of contraction into mechanical work. We may begin by representing the well-established anatomical findings of the striated muscle cell.

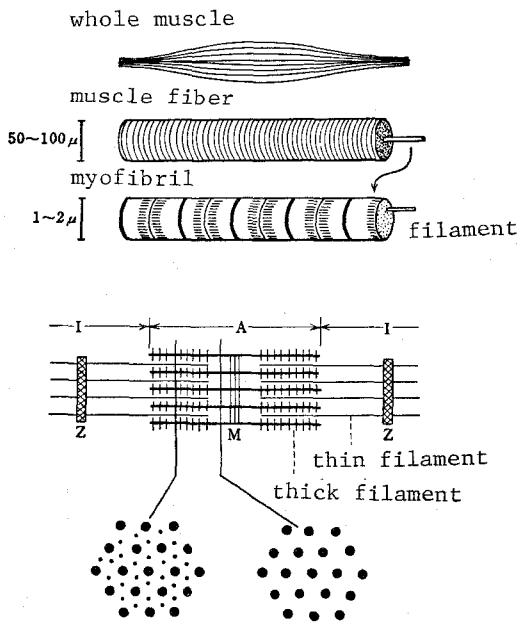

Fig. 2.1 Structure of muscle fiber.

A skeletal muscle (striated muscle) is made up of many individual muscle fibers (Fig. 2.1). Each fiber is a cylindrical, long cell enclosed in a sheath called the sarcolemma. It is made up of a large number of myofibrils. The myo-

fibril is a rod of contractile protein which runs one end of the fiber to the other. The fibril is subdivided by thin partitions called Z-discs (Z-lines) into sarcomere. The sarcomere is a functional unit in the contractile machinery; the contraction of a muscle fiber is produced by the collective and coordinated shortening of many sarcomeres composing it. The myofibril itself is composed of longitudinal fine filaments. The protein filaments are of two types, thin and thick. The thick myosin-containing and thin actin-containing filaments give the regular band pattern of cross-striations (A-band, I-band). The thick filaments are spaced out in a hexagonal lattice 400-450 Å apart, with the thin filaments in between them at the trigonal positions of the lattice. The space between the filaments is occupied by sarcoplasma (a dilute aqueous solution of salts and of other proteins).

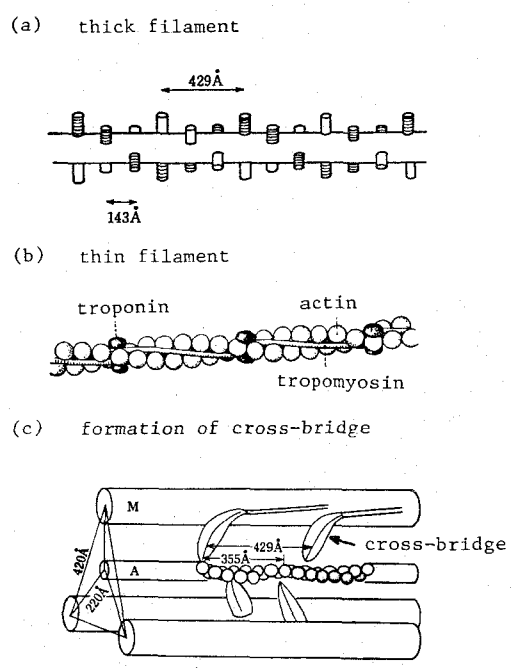

Fig. 2.2 The fine structure of actin and myosin filaments. (a) The six staggered rows of heads on the myosin filament (H. E. Huxley, 1967). (b) Double-stranded super-helix of the actin filement, decorated by troponin and tropomyosin (Ebashi and Endo, 1968). (c) Schematic drawing of the formation of cross-bridges (Mashima, 1972). M, myosin filament; A, actin filament.

b) The fine structure of thin and thick filaments

According to the recent X-ray diffraction observations and electron microscopic recordings of fixed, stained muscles, following conclusions may be outlined (H. E. Huxley, 1969[50]; Bendall, 1969[13]; Davies, 1963[25]).

1) The ultrastructure of the thin and thick filaments is schematically illustrated in Fig. 2.2.

2) The myosin-containing filaments can link with the actin-containing filaments with the formation of cross-bridges *) between them.

3) Thick filaments are in the central region of the sarcomeres, and have a six-fold screw axis of symmetry with a helical arrangement of the cross-bridges which contain the H-meromyosin ATPase. The individual cross-bridges in the myosin filaments are oriented in opposite directions on either side of the center of the filaments.

4) A thin filament is F-actin (two-strings of globular protein arranged in double-stranded chains) decorated by troponin and tropomyosin. The thin filaments are attached to the Z-discs between each sarcomere, and structurally polarized in opposite senses on either side of the Z-discs.

c) Process of muscle contraction

It is commonly believed that the contraction of living muscle is composed of the excitation-contraction coupling followed by the chemo-mechanical coupling (Fig. 2.3). Neural impulses are propagated in the motor nerve fibers from its neuron (in the ventral horn of the spinal cord) to a motor end-plate on a muscle fiber, and all-or-none action potentials are in turn

---

*) A cross-bridge is formed when the myosin head attaches to an actin filament; the cross-bridge results from the attachment of a projecting part of the myosin filament (myosin head, heavy meromyosin subfragment) to specific sites on the actin filaments.

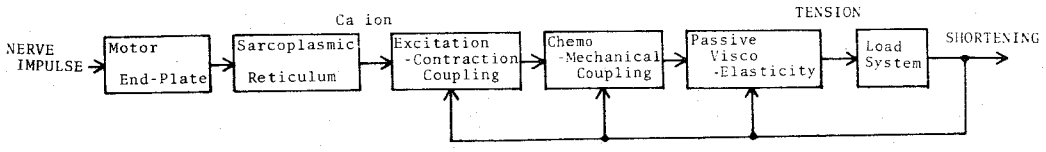

Fig. 2.3 Schematic diagram of the process of muscle contraction

generated in the surface membrane of the muscle fiber. The action potential is conveyed inwards via transverse tubular system of the sarcoplasmic reticulum (SR), where it finally activates the release of Ca ions (excitation-contraction coupling, E-C coupling). Thus, it initiates ATP (adenosine triphosphate) splitting at the active sites on the actin and myosin filaments and the subsequent conversion of the cheminal energy, which turns into work or development of tension (chemo-mechanical coupling, C-M coupling). That is, when Ca ions are bound with reactive sites on the actin filaments, the cross-bridges are formed between myosin and actin filaments, which immediately develop interfilamentary sliding forces. Work is done by the sliding force (contractile force). This active contractile force probably corresponds to the so-called "active state"- defined as a potentiality for force production (Hill, 1949b)[38]. The interfilamentary force can not be observed directly because of the filtering effects of viscous and elastic properties of the muscle, but indirectly measured in the form of tension or shortening of the muscle.

A fundamental response of a skeletal muscle to a single adequate stimulus is a twitch, i.e. a brief period of contraction followed by relaxation. If a second shock is given to the muscle before the response to the first has completely died away, summation occurs. When the stimuli are repeated at high enough frequency, the twitch summations are fused to become a smooth tetanus.

Two types of mechanical recording are commonly done. In one isometric recording, muscle length is fixed and tension development is recorded. In

the other isotonic recording, the muscle is allowed to shorten against a fixed load and a change in muscle length is recorded.

d) Excitation-contraction coupling and Ca ion.

A number of investigations have been made on the action of Ca ion as a regulating agent of the contractile system (Ebashi and Endo, 1968[28]; Sandow, 1970[77]). It is now well-established that Ca ion is the final activator of the contractile system. According to Ebashi and Endo, the troponin-tropomyosin complex is bound uniformly along the whole length of the actin filaments. At rest, the tripartite complex (actin, troponin, tropomyosin) prevents interaction of the actin and myosin filaments, i.e., prevents cross-bridge formation. In the presence of sufficient free Ca ions, troponin (acting specially as the Ca-receptive protein of the whole complex) binds the Ca ions and lifts the inhibition (by some reaction necessarily involving tropomyosin as a sort of intermediary) and thus permits the contractile actomyosin complex to develop. The process of the excitation-contraction coupling is listed as follows (Fig. 2.4).

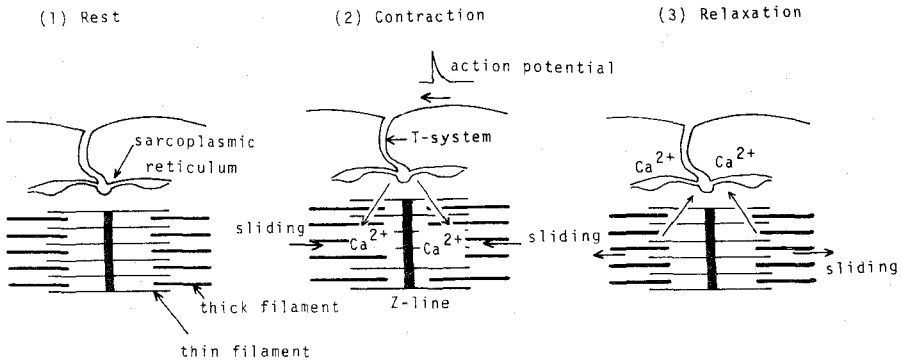

Fig. 2.4 Schematic illustration of the excitation-contraction coupling.

Rising phase of the active state:

1) Action potential and its inward spread through the transeverse tubular system.
2) Release of Ca ion from the sarcoplasmic reticulum.
3) Diffusion of Ca ion to the contractile proteins.
4) Binding of Ca ion to the contractile proteins.
5) Reaction of Ca-bound proteins which affects mechanical responses.

Falling phase of the active state:

6) Uptake of Ca ion by the sarcoplasmic reticulum.
7) Diffusion of Ca ion from the sarcoplasma to the sarcoplasmic reticulum.
8) The contractile proteins release the bound-Ca ions.

Ebashi and Endo (1968)[28] has obtained the steady state relation between the isometric tension and the free Ca ion concentration, by using the skinned fibers (Fig. 2.5). The figure shows that the larger tension is developed as the concentration of Ca ion is increased. At rest, Ca ion concentration is about 10^{-6} Mol (pCa=6.0).

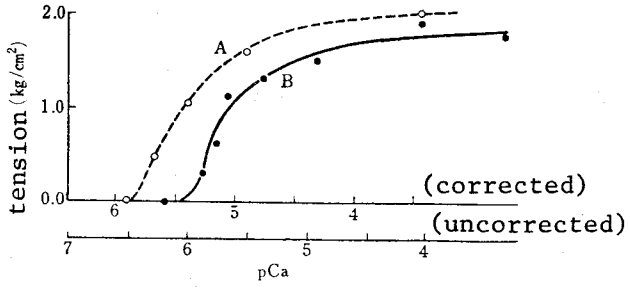

Fig. 2.5 Steady isometric tension developed by skinned fibres as a function of free Ca ion concentration. Curve A, 1 mM Mg; curve B, 12 mM Mg; $pCa=-\log_{10}[Ca^{++}]$, (from Ebashi and Endo, 1968[28]).

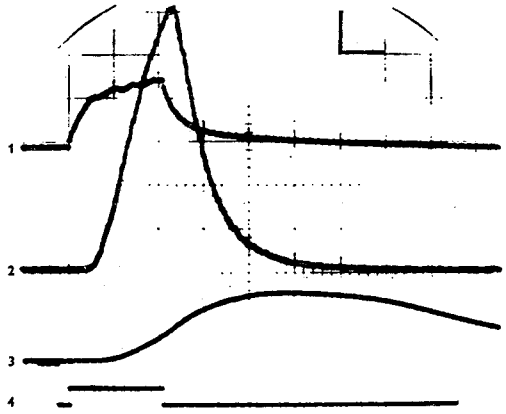

Fig. 2.6 Result of applying a single depolarizing pulse to the fibre membrane. Trace 1, membrane response, 20 $mM.cm^{-1}$; trace 2, calcium-mediated light emission, 1.9 x 10^{-9} $lm.cm^{-1}$; trace 3, isometric tension, 5 $g.cm^{-1}$; trace 4, 1 V calibration pulse and stimulus mark. Horizontal calibration: 100 $msec.cm^{-1}$. Intensity 3.5 V; nominal duration: 200 msec. Temp. 11-12 °C. Resting light emission: 0.64 nlm. Mean resting potential: -56 mV. Calibration bar: 1 cm. (from Ashley and Ridgway, 1970)[8].

Recently, transient responses of the release of Ca ions have been experimentally observed in comparison with the development of tension (Ashley and Ridgway, 1970[8]; Jobsis and O'Connor, 1966[13]). The figure 2.6 is a typical record obtained by Ashley and Ridgway (1970)[8] that shows membrane potential (trace 1), calcium-mediated light emission (trace 2, its height corresponds to the Ca ion concentration) and isometric tension (trace 3). It should be noted that the peak of the Ca ion concentration is at the time when the gradient of isometric tension curve is approximately maximum.

e) The sliding-filament theory

This theory was evolved independently and more or less simultaneously by A. F. Huxley (1957)[45] and H. E. Huxley (1957)[47], and it is now accepted almost universally as a result of the evidence that has been accumulated since that time (Gordon, Huxley and Julian, 1966[34]; Huxley and Simmons, 1971[46]; H. E. Huxley, 1967[49], 1969[50]). Gordon et al. (1966)[34] have accurately measured the re-

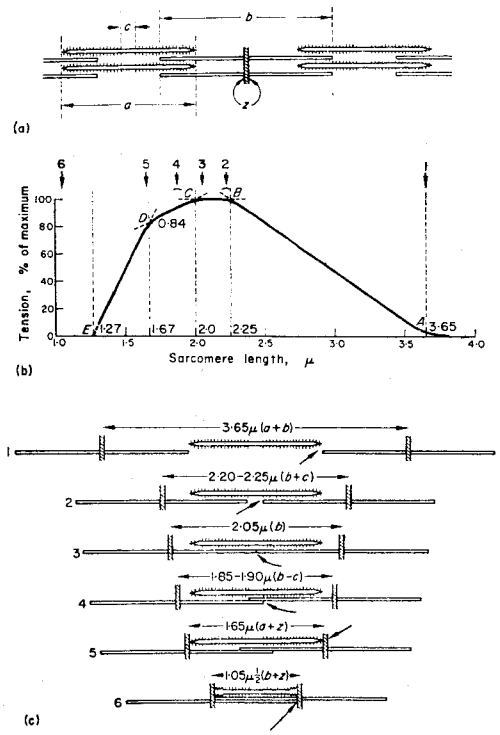

Fig. 2.7 (a) Standard filament lengths. a=1.60 μ; b=2.05 μ; c=0.15 μ; z=0.05 μ. (b) Tension-length curve from part of a single muscle fibre (schematic summary of results). The arrows along the top show the various critical stages of overlap that are potrayed in (c). (c) Critical stages in the increase of overlap between thick and thin filaments as a sarcomere shortens. (from Gordon, Huxley and Julian, 1966)[34].

lation between sarcomere length and active tension in living muscle fibres, and confirmed that the maximum active tension is directly proportional to the length of overlap regions of thick and thin filaments (see Fig. 2.7). According to this theory, shortening and lengthening of the muscle are the relative displacement of thick and thin filaments interdigitating into each other. The theory may be outlined as follows.

1) A force of contraction is developed by the interaction between the thick and thin filaments in the overlap region, and active shortening is caused by movements of the myosin cross-bridges, coupled with hydrolysis of ATP.

2) Lengths of the filaments themselves remain essentially constant. The

myosin and actin filaments slide past one another through the formation of cross-bridges; the actin filaments are drawn further into the array of myosin filaments as the muscle shortens, or are withdrawn again as the muscle is stretched.

3) Tension development, shortening and work follow from the cyclic making and breaking of cross-links between myosin cross-bridges and receptor sites on the actin. That is, an elementary cycle of the contractile machine has two phase; binding and dissociation between actin and myosin; or a force-generating phase and a free phase.

f) Energy sources for contraction

A distinct feature of muscle proteins is their ability to transform energy from chemical to mechanical form. It is well known that the chemical reaction to provide the energy for contraction is the hydrolysis of ATP to ADP (adenosine diphosphate) and Pi (inorganic phosphate).

$$ATP \longrightarrow ADP + Pi \qquad (2.1)$$

The free energy of ATP splitting is approximately 10-11 Kcal/Mol. The resynthesis reaction of ATP is the so-called Lohman reaction, catalysed by creatine kinase:

$$Cr\ P + ADP \rightleftharpoons Cr + ATP \qquad (2.2)$$

The resynthesis of ATP occurs with the greatest rapidity and most of the ATP split is restored at the expence of CrP (creatine phosphate), so that no actual fall in ATP concentration is caused during muscle contractions (both smooth tetanic contractions and twitches). Recent chemical analyses have shown that a total amount of ATP (or creatine phosphate) splitting is approximately proportional to the work done (Tonomura and Oosawa, 1972).[83]

g) Model of the molecular mechanism of muscle contraction

Several models have been proposed, based on the sliding-filament theory, the chemical reaction and the molecular mechanism of muscle contraction (A. F. Huxley, 1957[45]; Davies, 1963[25]; Tonomura et al. 1969[84]; Tonomura, 1972[82]). The models, although they differ in detail, seem to be basically identical. The model in Fig. 2.8 is proposed by Tonomura et al. (1969)[84], which schematically illustrates the molecular mechanism of muscle contraction. This figure shows only a

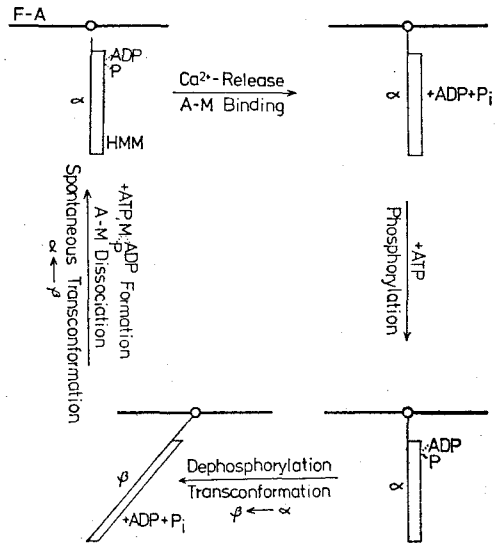

Fig. 2.8 Molecular mechanism of muscle contraction.
F-A (or A) and M indicate F-actin and myosin, respectively. HMM represents the head part of myosin (H-meromyosin). α and β indicate two different types of conformation of the myosin molecule. (from Tonomura et al. 1969[84]).

part of the myofibril, where the essential biochemical reactions occur, i.e., F-actin and the cross-bridge of the myosin filament. The system operates as follows: (i) In the resting state, myosin is in the form of a myosin-phosphate complex. (ii) When Ca ion is set free in the contractile system from the sarcoplasmic reticulum by excitation, Ca ions bind to troponin, which is bound to the F-actin-tropomyosin system. This Ca ion-binding induces a conformational

change in tropomyosin, and the latter produces the change in conformation of F-actin. In consequence, the linkage between myosin and F-actin is formed. (iii) Phosphorylmyosin is rapidly dephosphorylated by the action of F-actin. This energy-releasing process accompanies the transconformation of myosin. Actin filaments are interdigitated into muosin filaments. (iv) ATP produces the myosin-phosphate-ADP complex. Then, the linkage between myosin and F-actin is broken, and myosin is transformed spontaneously to the state (i). The whole system returns to the original state.

2.2 MECHANICAL PROPERTY OF MUSCLE AND ITS MODELS

A muscle in the resting state gives a rubber-like tension-length relation with a small stiffness. The relationship is nonlinear; the muscle is progressively getting stiffer as length is increased. This behavior has been found to reside in the connective tissue surrounding the muscle and in the surface membrane. As far as an unstimulated muscle is concerned, the classical viscoelastic model as shown in Fig. 2.9 (a) would fit satisfactorily, because no interaction between thick and thin filaments takes place. Upon stimulation, muscle is rapidly activated and changes from a passive tissue to a dynamic tissue capable of exerting force or doing work.

Since the study of Gasser and Hill (1924)[33], it has been often pointed out that the viscous and elastic constants of the contracting muscle are much greater than those of the resting muscle. When the muscle is transfered from resting state to activated one, these constants would suddenly be replaced with entirely different values, and would not be considered to increase continuously, because the interaction between myofilaments which are dissociated in the resting state is developed suddenly. Since the work of Hill (1938,[36] 1949a,[37] 1949b)[38] and Wilkie (1950)[87], mechanical behaviors of active muscles have been described by a contractile component (CC) in series with a noncontractile

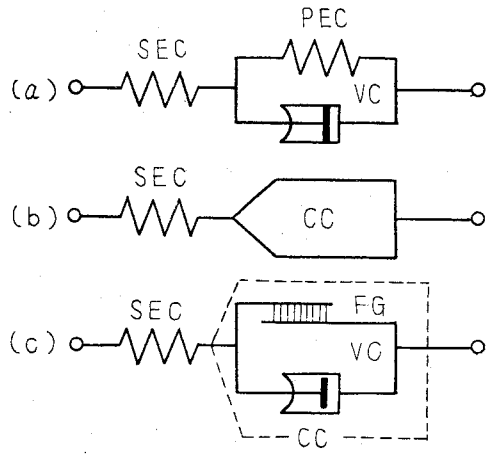

Fig. 2.9 Mechanical model of muscle.
(a) Classical viscoelastic model (Levin and Wyman, 1927)[57],
(b) two-component model (Hill, 1949b[38]; Wilkie, 1950)[87],
(c) new mechanical model (Bahler, 1968[10]; Akazawa et al., 1969)[3].
SEC, series elastic component; PEC, parallel elastic component; VC, viscous component; CC, contractile component; FG, force generator.

series elastic component (SEC). The responses to isotonic quick release would demonstrate the dynamic behavior of an active muscle; a tetanic contracting muscle is quickly released from an isometric condition and allowed to shorten against some fixed load (cf. Fig. 3.6 or Fig. 3.7). The instantaneous shortening occurs immediately after a quick release, which is followed by slower shortening of the contractile machinery. Rapid shortening on the early phase strongly suggests the existence of a series elastic component. The load-extension relation of the series elastic component has been generally determined by this quick release experiment, and identified as being compatible to a nonlinear spring; the elasticity increases as the extension is increased. The structural correspondence of the series elastic component has never been derived yet, while some part of it certainly resides in tendons and Z-lines.

On the other hand, the contractile component has been identified as an element obeying the familiar force-velocity relation. Hill (1938)[36] has derived the famous hyperbolic equation:

$$(P + a)(v + b) = b\,(P_o + a) \qquad (2.3)$$

where a and b are constants, P_o the isometric maximum tension, P the load, and v the velocity of shortening. Recently, Bahler (1968)[10] or Akazawa et al.[3] (1969) have developed a new mechanical model by modifying the two-component model (Fig. 2.9 (c)); that is, the contractile component consists of two elements, a nonlinear force generator (FG) and a nonlinear viscous-like element (VC).

2.3 METHODS

Experiments were performed on the small bundle of the fast muscle fibers prepared from the ventral caput of the semitendinosus muscle of the frog, rana nigromaculata. The muscle was dissected under a binocular microscope until the diameter of the bundle was as small as 500-800 μ. The lengths of different fibers were almost equal in such a preparation. In some experiments the whole muscle or the single fiber preparation was also used.

The experimental arrangement is illustrated in Fig. 2.10. The whole apparatus was set on a special table designed to absorb external mechanical disturbance. The bundle preparation, M, was mounted horizontally in a polystyrol bath (3 × 7 × 1.5 cm) which contained 10 ml of Ringer's solution. On the opposite walls of the bath were placed a pair of platinum foil electrodes (7 × 1.5 cm), E. Thus, the whole length of the preparation could be stimulated simultaneously by the transverse electric field created between these massive electrodes. Usually, 1.0- msec square pulses at 50-100 Hz or AC at 200-500 Hz were applied from a high-current stimulator (about 30 W), G.

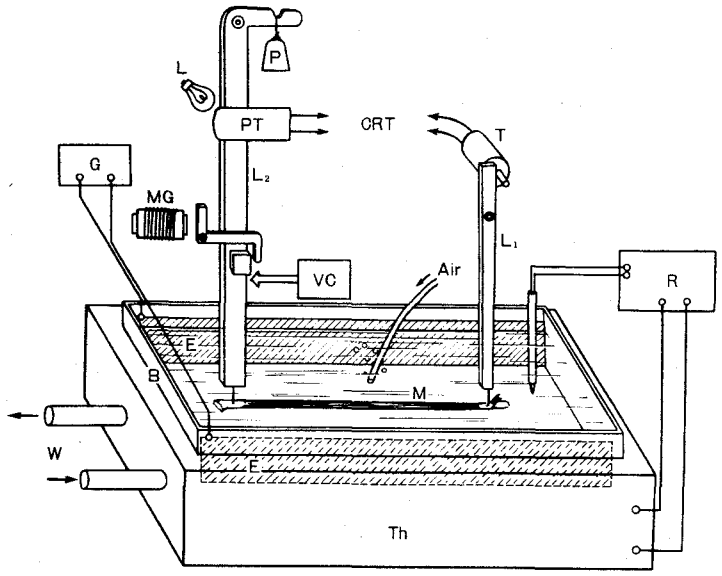

Fig. 2.10 Diagram of the recording system.
B, Ringer's solution bath; E, platinum foil electrodes; G, alternative current or square pulse stimulator; L_1, isometric lever; L_2, isotonic lever; L, light source; M, muscle; MG, electromagnetic relay; P, load; PT, phototube; R, thermoregulator; S, stop; T, RCA 5734 tube; Th, thermoelectric heat exchanger; VC, velocity controller; W, water circulation.

The temperature of the Ringer's solution (110 mM NaCl, 12 mM $NaHCO_3$, 2 mM KCl, 1.8 mM $CaCl_2$, pH 7.2) was maintained at 10 °C by a thermoelectric heat exchanger, Th.

The pelvic tendon of the muscle was penetrated by a stainless steel needle at the tip of the isometric lever, L_1,by which the muscle tension was conveyed to the anodal pin of an RCA 5734 tube, T. The pelvic tendon was usually so thin that it was tied by nylon thread to prevent it from being torn off. The tibial tendon was also tied and penetrated by a stainless steel needle at the tip of the rectangular isotonic lever, L_2, which was made of light

wood, 7 cm in length and 400 mg in weight, and the load P was hung 0.7 cm from the pivot. The movement of the lever was detected photoelectrically; namely, the lever cut the light streaming toward the phototube, PT. Thus, the tension and displacement of the muscle were displayed simultaneously on a cathode-ray oscilloscope, CRO. The compliance of the apparatus was about 5.0 μ/g, measured under a binocular microscope (× 60). This is satisfactorily small for the maximum isometric tension, which was usually less than 10 gwt.

The electromagnetic relay MG was set to the isotonic lever for quick release of the muscle. When it was necessary to adjust the velocity of muscle lengthening or shortening, a velocity controller VC which has been described by Mashima and Matsumura (1960)[63], was connected to the isotonic lever.

The muscle length was varied with an accuracy of 0.1 mm by moving the isometric lever, which was mounted on a sliding scale with a vernier.

Simulation studies were made on analog and digital computers. For the convenience of simulation, a measured tension was always normalized by the maximum tetanus tension, P_o, and a length by the standard length, L_o, at which a muscle generated the maximum tension. The muscle length without containing the tendon length was always measured in the mounted state under a binocular microscope.

CHAPTER III

PHYSIOLOGICAL DETERMINATION OF MECHANICAL PROPERTIES OF THE FROG SKELETAL MUSCLE

3.1 INTRODUCTION

It is well known that resting muscles behave as a flexible rubber-like body and active muscles behave as a two-component system consisting of a contractile component in series with a passive elastic one (Fig. 2.9 (b)); namely, dynamics of muscle contraction depend on the load-extension relation of the series elastic component, the force-velocity relation of the contractile component and the time course of the active state (Hill, 1949b[38]; Ritchie and Wilkie, 1958[71]; Jewell and Wilkie, 1958[52]). In this chapter, mechanical properties of the active and resting muscles are determined quantitatively from adequate physiological experiments on the frog semitendinosus muscles; namely, viscous and elastic properties of the resting muscles, the load-extension relation of the series elastic component and the force-load-velocity relation of the contractile component are determined, while the active state is identified in the following chapter. Much effort is devoted to design pertinent physiological experiments from which these mechanical parameters might be estimated as easily and independently as possible.

First, mechanical properties of the resting muscle are determined from steady-state and transient responses to change in load or in length. The tension-extension relation of isolated tendons is also observed. In addition the steady-state relation between isometric tetanus tension and muscle length is measured.

Second, the load-extension relation of the series elastic component is determined. There are at least three methods of estimating the curve. The first method is to calculate the load-extension curve from two experimental

curves, i.e. the force-velocity curve and the isometric myogram (Hill, 1938,[36] 1949b[38]; Wilkie, 1950[87]). The second is to map out the curve using fast constant-velocity releases (Hill, 1950,[39] 1970[42]). The third is an isotonic quick release technique commonly used (Wilkie, 1956[88]; Jewell and Wilkie, 1958[52]; Bahler, 1967[9]; Cavagna, 1970[19]; Akazawa et al., 1969[3]). The same quick release technique is employed here since the method is the most applicable with the present preparation. Frog semitendinosus muscle at 10 °C does shorten so rapidly that the quick release method is made by taking extreme care over details of technique and is modified to counterbalance the effects of the combined mass (moment of inertia) of the load and lever system. In order to examine the existence of the series elastic component and the correspondence of it with the muscle structure, the effects of various muscle lengths, various times after a single stimulus and different temperatures are investigated.

Further, transient responses to the isotonic quick release are simulated by using the mathematical model in order to estimate analytically the characteristics of the series elastic component. That is, responses of the model are compared with the existing physiological data, and at the same time a slight viscosity within the series elastic component is also estimated by the simulation.

Then, the force-load-velocity relation of the contractile component is determined. The force-velocity relation of the skeletal muscle was described by Hill (1938)[36] on the isotonic shortening of the frog sartorius muscle in terms of a simple hyperbolic equation:

$$(P + a)(v + b) = b (P_o + a) \qquad (3.1)$$

or

$$P_o - P = (P_o + a) v / (v + b) = F_v \qquad (3.2)$$

where P is the load, v is the shortening velocity, P_o is the maximum isometric tension, a is the heat constant and b is the rate constant of energy libera-

tion. The value of ($P_o - P$) or F_v in Eq. (3.2) represents the velocity-dependent tension loss during isotonic shortening or the viscous-like force. Namely, when a muscle shortens at the velocity v, the force P_o is decreased to P as though there were a viscous-like force in the contractile component (Bahler et al., 1967)[9]. Since then, it has been widely confirmed that this equation holds not only in various skeletal muscles (Wilkie, 1950, human muscle[87]; Abbott and Wilkie, 1953, tortoise muscle[2]; Close and Hoh, 1967, kitten muscle)[23] but also in the cardiac (Sonnenblick, 1962[78]; Edman and Nilsson, 1968)[29] and smooth muscles (Csapo, 1955[24]; Mashima and Handa, 1969)[61], although the values of the dynamic constants (a and b) are quite different in these muscles. However, this equation is applicable only to the fully activated muscle, in which the force of the contractile component is steady and equals P_o. Only in a muscle exerting a steady contractile force does the load represent the force during isotonic shortening.

On the other hand, Mashima and Washio (1968)[65] and Mashima and Tsuchiya (1968)[64] showed that it is possible to depolarize the muscle membrane to a certain extent and to maintain the contractile force at a certain level below P_o by applying alternating current (AC) at 200-500 Hz in an excess potassium solution containing 10-20 mM KCl.

The purpose of the present chapter is also to examine the property of the viscous-like force during shortening and lengthening, determining the load-velocity relations at various steady or changing contractile forces.

3.2 MECHANICAL PROPERTIES OF THE RESTING MUSCLE AND THE TENSION-LENGTH CURVE OF THE CONTRACTING MUSCLE

In order to test the elastic properties of the bundle preparation, the load-extension curves of a whole muscle, two bundle preparations, and an iso-

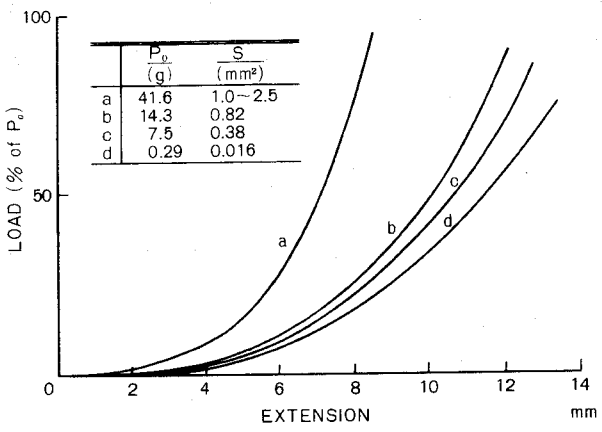

Fig. 3.1 Load-extension curves of the resting muscle; a, whole muscle; b, c, two-bundle preparations; d, single fiber; P_o, maximum tension; S, cross section; L_o, 14 mm in all preparation; 10 °C.

lated single fiber were compared, as shown in Fig. 3.1. The muscle was stretched from the standard length, L_o, at which the maximum isometric tension, P_o, was developed. Curve a was obtained from the whole muscle, curve b and c from two-bundle preparations, and curve d from the single fiber. The standard length, L_o, was 14 mm in all preparations. The values of P_o and the area of cross section S are shown in the insert in Fig. 3.1. As is apparent, curve b and c are far closer to curve d than curve a. The compliance of the bundle preparation is quite similar to that of the single fiber, probably because a small bundle contains less connective tissue. As the size of bundle preparations used in this study was nearly the same as c in the table, the following results would be comparable with those obtained on single fibers.

When the muscle is stimulated, the contractile component develops an active tension, which varies with the length of muscle. The steady tension generated in isometric tetanus of the bundle preparations was measured at different lengths. The result is shown in Fig. 3.2, curve T. The resting tension was also measured for this preparation, curve R. This curve must give

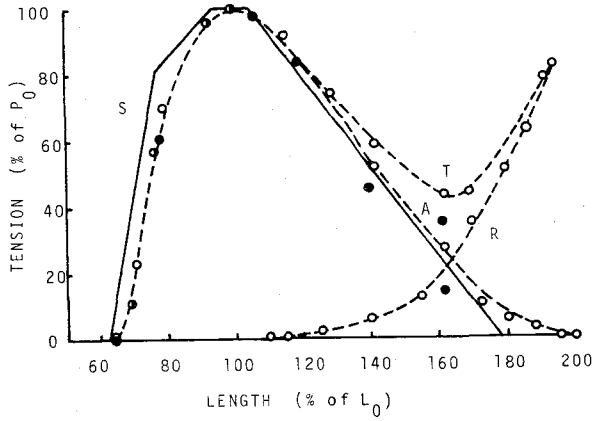

Fig. 3.2 Active tension-length relation. Maximum tension (curve T, total tension; A, active tension, A = T - R) and resting tension (curve R) developed at each muscle length in the frog semitendinosus muscle. ○, P_o=3.1 gwt, L_o=13 mm; ●, P_o=4.4 gwt, L_o=13 mm; ◑, P_o= 3.8 gwt, L_o=14 mm. Solid line, S, redrawn from Gordon et al. (1966).[34]

the elasticity of the parallel elastic component (SEC_1 + PEC_1 in Fig. 3.5). Since the parallel elastic component is structurally parallel with the contractile component (CC), their tension must be added together, so that the intrinsic active tension developed by stimulation is given by curve A (A= T-R). The active tension-length curve of the bundle preparation does also show nearly the same as obtained from a single muscle fiber preparation (see Fig. 2.7; Gordon, Huxley and Julian, 1966)[34]. Note that all these curves were obtained by setting the length of the muscle before it was stimulated tetanically.

In order to determine elastic and viscous characteristics of the resting muscle, following physiological experiments were designed. A typical record of the responses to step change in load is shown in Fig. 3.3. Note that records A and B were obtained from the whole muscle, records C and D from the bundle preparation. Responses to ramp stretching were also recorded (Fig. 3.4);

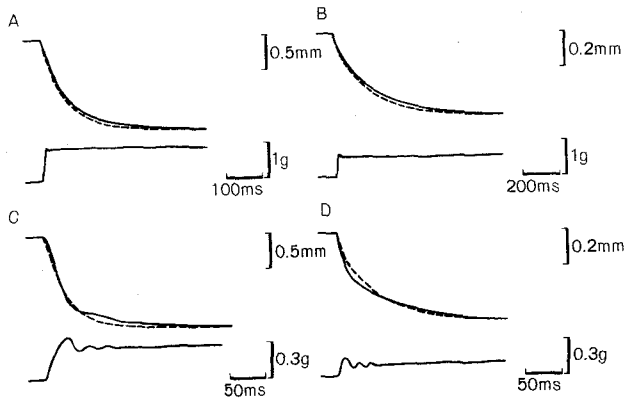

Fig. 3.3 Responses of the resting muscle to step change in load. Upper trace, length(elongation, downward); lower trace, tension on muscle. A, B, whole muscle; C, D, bundle preparation. Solid line, physiological result; broken line, calculated curve obtained with the values in Table III-1.

in these experiments, the muscle was stretched by a small amount at a certain velocity, using a velocity controller, then maintained at the fixed length. All these experimental results indicate that the viscoelastic model illustrated in Fig.3.5 is the simplest and adequate one to interpret the dynamic properties of resting muscles *).

The viscous and elastic constants of the components (viscous constant B_1 of VC_1, elastic constant E_1 of SEC_1 and elastic one E_p of PEC_1) were estimated by applying the curve fitting procedure to the physioloiical data in Fig . 3.3

*) All the experiments show the existence of an elastic element supporting the load. For the early slight quick phase of the elongation curve in Fig. 3.3, two elastic elements SEC_1 and PEC_1 shown in Fig. 3.5 must be introduced where a viscoelastic Voigt model is employed. For the slow phase of the elongation curve in Fig. 3.3 and the phase-lead (differential) characteristics in Fig. 3.4, the viscous element VC_1 in Fig. 3.5 must be introduced. Consequently, at least three components are necessary; series elastic component (SEC_1), parallel elastic component (PEC_1) and viscous component (VC_1). As for the series elastic component, it is convenient to separate it into two subcomponents SEC_t and SEC_p. The former corresponds to definitely non-contractile structures, such as tendons and Z-lines.

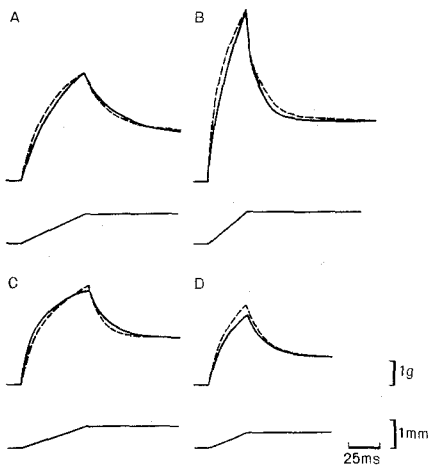

Fig. 3.4 Response of the resting muscle to ramp stretching. Upper trace, tension on muscle; lower trace, length (elongation is upward). A, P_o=4.65 gwt, L_o=10 mm; B, C, D, P_o=8.5 gwt, L_o=11 mm. Solid line, physiological result obtained from the bundle preparation; broken line, calculated curve obtained with the values in Table III-2.

and Fig. 3.4. The estimated values of them are shown in Table III-1 and Table III-2, and the responses obtained with these values are shown in Fig. 3.3 and Fig. 3.4, broken lines. In this estimation, it was not necessary to take account of the nonlinearity in the resting tension-length curve in Fig. 3.1, because the amount of elongation in the stretching experiment was as small as less than 10 % of L_o.

Both the whole muscle and the bundle preparation seem to have a similar dynamic property as seen in Fig. 3.3, but the elastic and viscous damping constants of the whole muscle are naturally greater than those of the bundles as shown in Table III-1. Namely, the former is less compliant as expected from the tension-length curve in Fig. 3.1 and more viscous than the latter, because of more connective tissue between muscle fibers.

TABLE III-1

ELASTIC AND VISCOUS CONSTANTS IN THE RESTING MUSCLE
OBTAINED FROM SUDDEN LOADING EXPERIMENT

PREPARATION	Experiment shown in	L_o (mm)	P_o (gwt)	Load (g)	E_1 (gwt/mm)	E_p (gwt/mm)	B_1 (gwt·sec/mm)
Whole muscle	Fig. 3.3A	13	44	0.9	5.14	0.56	0.112
	B			0.25	6.21	0.69	0.082
	Mean				5.81	0.63	0.097
Bundle preparation	Fig. 3.3C	11	8.4	0.3	1.61	0.23	0.0115
	D			0.1	1.92	0.27	0.0274
	Mean				1.76	0.25	0.0195

TABLE III-2

NORMALIZED ELASTIC AND VISCOUS CONSTANTS IN THE BUNDLE PREPARATION
OBTAINED FROM STRETCH EXPERIMENT

Experiment shown in	L_o (mm)	P_o (gwt)	Velocity of stretch (mm/sec)	Amount of stretch (mm)	E_1 (P_o/L_o)	E_p (P_o/L_o)	B_1 (P_o·sec/L_o)
Fig. 3.4A	10	4.65	37.0	1.85	1.03	0.258	0.0161
Fig. 3.4B			64.0	2.08	1.31	0.186	0.0124
C	11	8.5	24.0	1.32	1.48	0.211	0.0140
D			18.6	0.95	1.35	0.194	0.0129
Mean					1.29	0.212	0.0139

In Table III-2, the values of mechanical parameters are normalized by P_o and L_o in order to make easy a quantitative comparison between differential preparations, e.g., 1.03 P_o/L_o in E_1 is the normalized value of 0.48 gwt/mm by P_o=4.65 gwt and L_o=11.0 mm. These results of estimation indicate that the elastic and viscous constants calculated in the bundle preparations satisfactorily coincided with each other, regardless of the difference in the thickness or length of the bundle. It is concluded that the dynamic behaviors of the resting muscle can be represented by the viscoelastic model, consists of three linear components as shown in Fig. 3.5, within a limit of variation in length less than 10 % of L_o.

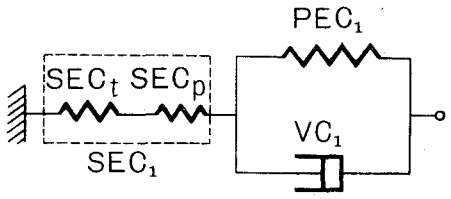

Fig. 3.5 Viscoelastic model of resting muscle.
SEC, series elastic component; PEC, parallel elastic component;
VC, viscous component.

After the experiment two tendons were isolated from both ends of the muscle (L_o=13 mm) and connected together thin metal wire (13 mm). Then the load-extension curve of the tendon was measured in Ringer's solution, neglecting the compliance of the wire. The curve was nearly straight, and the same tension as P_o was obtained when the tendon was stretched by about 1 % of L_o Namely, the elastic constant of the tendon E_t is about $100.0\ P_o/L_o$. This value is so large in comparison with E_1 that the compliance of tendon can be neglected from that of the whole SEC_1.

3.3 THE LOAD-EXTENSION RELATION OF THE SERIES ELASTIC COMPONENT

The load-extension curve of the series elastic component has been commonly determined by the isotonic quick release technique (Hill, 1950[39]; Jewell and Wilkie, 1958[52]; Bahler, 1967[9]). The principle of the quick release is schematically illustrated in Fig. 3.6. The resting muscle (Fig. 3.6 a) is tetanically stimulated and exerts an isometric tension P_o' (Fig. 3.6 b). This muscle was released quickly (Fig. 3.6 c) and allowed to shorten with a certain fixed load P (Fig. 3.6 d). The instantaneous shortening of SEC_2, S, occurs immediately after the release due to a sudden decrease of the force from P_o'

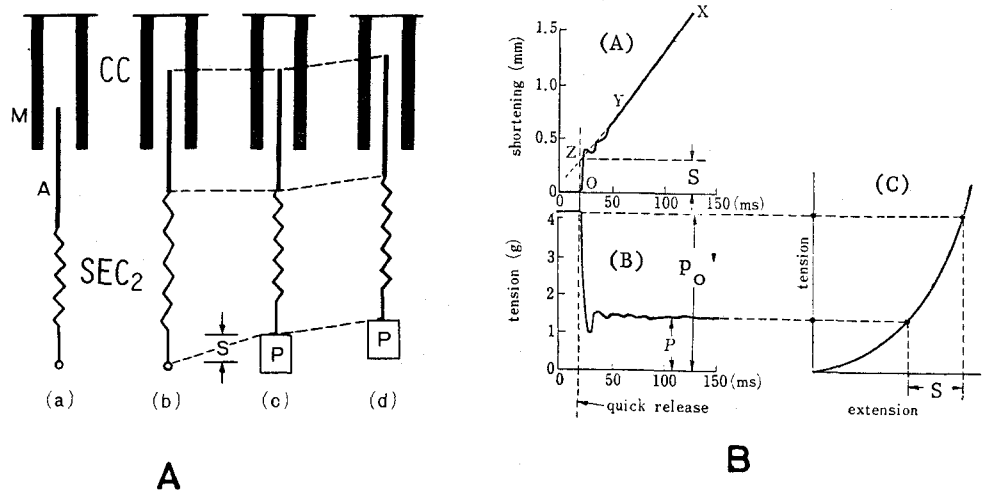

Fig. 3.6 Diagram of estimating the load-extension curve of the series elastic component.

A, schematic illustration of the isotonic quick release experiment. CC, contractile component; M, thick filament; A, thin filament; SEC_2, series elastic component. (a) resting state; (b) isometric contraction; (c) immediately after the quick release with load P; (d) following isotonic contraction; S, intrinsic shortening of the series elastic component.

B, a typical record of the isotonic quick release experiment. Time course of shortening (A) and tension (B) changes after the quick release. Tension (B) on the muscle was suddenly reduced from the isometric tension (P_o'=4.1 gwt) to a fixed isotonic load (p=1.5 g) after 80 msec from the onset of stimulation. Frog semitendinosus muscle, P_o=4.1 gwt, L_o=13 mm, 10 °C. Tension-extension curve (C) of the series elastic component may be obtained from (A) and (B).

to P, because SEC_2 is assumed to shorten much more rapidly than the contractile component for the rapid change in tension. Namely, the load-extension curve of SEC_2 is given as the relation between P and S. In this technique, however, inaccuracy for the estimation of S may be unavoidable due to undesirable factors, such as an active shortening of the contractile component and a slight

viscosity in parallel with the series elastic component. Moreover, in the simple quick release the tension after the release usually shows an undershoot falling to zero tension corresponding to the overshoot in the length curve and keeps zero for a considerable time, especially under light or no load (Fig. 3.7 A, B). While the intersection of the shortening curve and the axis formed by the time of release determines S, this undershoot should cause overestimation of S, because the velocity of active shortening of CC is very rapid under no load. On the other hand, under heavy load the tension falls much slower and the undershoot of tension curve is not so deep. So, there must be no overestimation of S, but rather occur the possibility of slight underestimation due to the slow active shortening, as pointed out by Bahler (1967)[9]. Eventually, it is necessary to control the velocity after release to an appropriate value depending on the load. For this purpose Jewell and Wilkie (1958)[52] added an external viscosity, that is a small dashpot containing castor oil, to the isotonic lever. In the present work, the velocity of instantaneous shortening immediately after the release under light load was adjusted by the velocity controller until the undershoot of tension curve was minimized (Fig. 3.7 C). The velocity of release at which the tension undershoot disappears completely is slow, because the shortening curve becomes round and gives no means to separate the quick shortening from the active contraction.

The load-extension curves obtained by the quick release and the controlled are compared in Fig. 3.8 a and b. The extension at zero load was determined from the shortening at the instant when the tension curve fell to zero under adequately controlled release. Besides these methods, the direct X-Y record was also adopted, in which the tension and length changes immediately after the release fed into X- and Y-axis of CRO (Fig. 3.7 D). The X-Y record of the quick release under no load is shown in Fig. 3.8 c where the velocity of shortening was not controlled at all. In such a case, the compliance of the

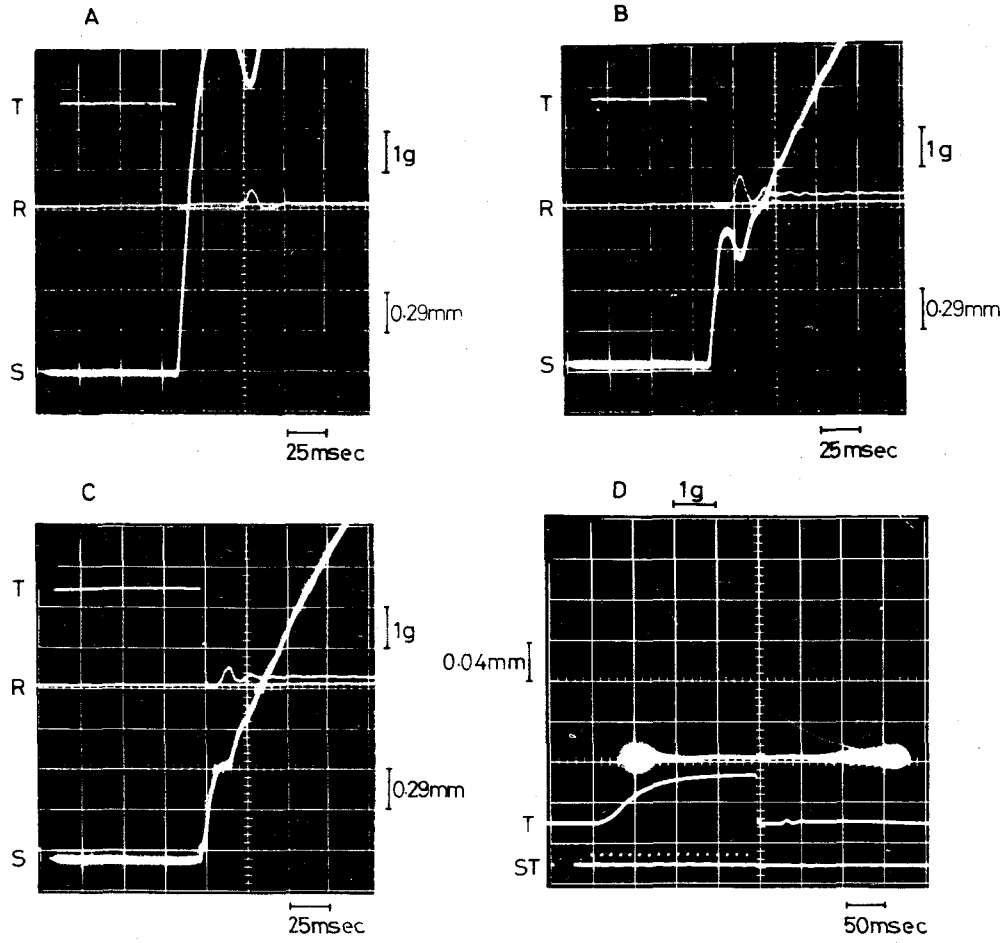

Fig. 3.7 Typical records of isotonic quick release.
A, quick release under no load; B, quick release under light load (P= 0.3 g); C, controlled release under light load (P=0.3 g); D, X-Y record. A, B, C: the same preparation (frog semitendinosus bundle preparation), P_o=2.5 gwt, L_o=12 mm, 10 °C; T, tension curve, 1.0 g/div; S, shortening curve, 0.29 mm/div; R, resting tension level. D: Another bundle preparation, P_o=6.2 gwt, L_o=14 mm, 10 °C; T, tension curve, 5.0 g/div; ST, stimuli; inserted X-Y record, X-axis is tension, 1g/div, Y-axis is shortening, 0.04 mm/div.

series elastic component is underestimated owing to a slight viscosity in parallel with SEC_2, which was estimated as being 0.008 P_o.sec/L_o in the present bundle preparation (See section 3.4) and of the order of 300 dyne.sec/cm in the rat gracilis muscle by Bahler (1967)[9] and in the frog sartorius muscle by Woledge (1961).[89] After all, the most reliable curve is Fig. 3.8 b, and X-Y record obtained by the controlled release was also agreed well with this curve. Any way, the load-extension curve of SEC_2 is not linear, and the maximum extension at P_o is about 3-3.5 % of L_o. The curve b in Fig. 3.8 is expressed with series expanded terms:

$$\left.\begin{aligned} P &= E_2 \, x_2 \\ E_2 &= (2.96 + 51.8 \, \hat{x}_2 + 1.9 \times 10^4 \, \hat{x}_2^{\,2}) \, P_o/L_o \end{aligned}\right\} \qquad (3.3)$$

where E_2 = elastic coefficient, function of extension,

x_2 = extension of SEC_2,

$\hat{x}_2$ = normalized value of x_2 , $\hat{x}_2 = x_2/L_o$.

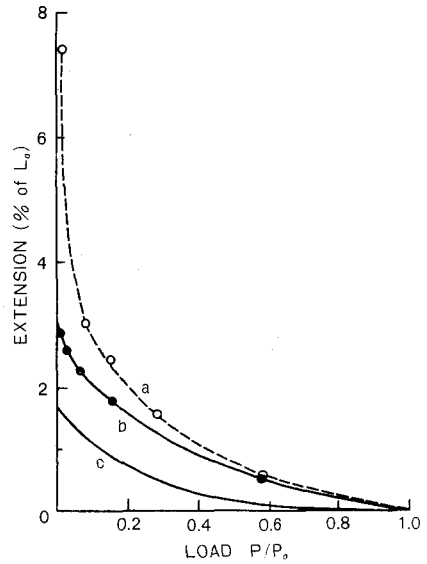

Fig. 3.8 Load-extension curves of the series elastic component obtained by the simple quick release (a), the controlled release (b), and X-Y record of the simple quick release (c). Frog semitendinosus bundle preparation, P_o=2.75 gwt, L_o=12 mm, 10 °C.

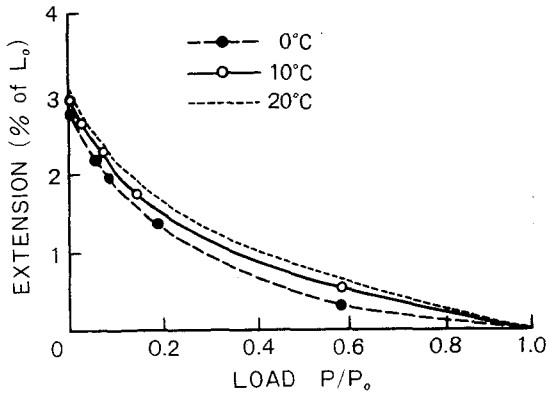

Fig. 3.9 Load-extension curves of the series elastic component at various temperatures. Frog semitendinosus bundle preparation; L_o=12 mm.

a) The effect of temperature

In order to examine how much the active shortening of the contractile component is contained in the load-extension curve determined by the controlled release method the effect of temperature was observed. Normalized load-extension curves at different temperatures are shown in Fig. 3.9. A slight change in the series compliance with temperature as well as in the curvature of load-extension curve was observed. If the compliance contains much active contraction, the differences between these curves are presumed to be more definite, so that a slight change of the compliance would be attributed to the temperature dependence of the passive element.

b) The effect of contractile tension

Applying the controlled release method at various tension levels during tetanic contraction, the effect of contractile tension on the load-extension curve of the series elastic component was examined. One of the results is shown in Fig. 3.10. The curves obtained by the release at more 0.5 P_o are roughly superposable with each other by shifting along the vertical axis. Namely, the compliance of the series elastic component does not alter at near the peak tension, but it is clearly increased at the early beginning of con-

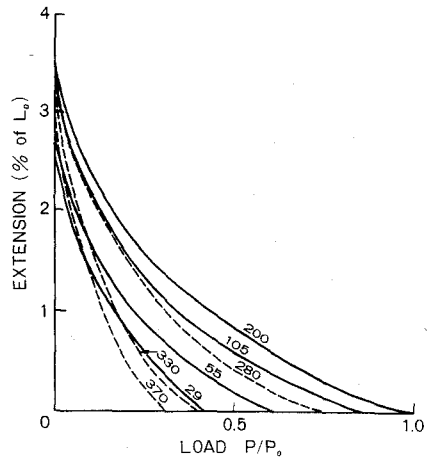

Fig. 3.10 Load-extension curves of the series elastic component at various times during tetanic contraction. Tetanic stimulation (1.0 msec pulse, 100 Hz) was affected for 100 msec. Figure above each curve indicates the time (msec) after the beginning of the stimulation. Frog semitendinosus bundle preparation; L_o=13 mm, 10 °C.

traction and after half relaxation. This result implies that the compliance of the series elastic component is practically independent of the contractile tension, except the very beginning of the contraction and the late relaxation period.

c) The effect of muscle length

As in the contracting muscle the thick and thin filaments are actively connected by cross-bridges at the overlap region, the series elastic component would be divided into two subcomponents, SEC_t and SEC_a. The former is the same as in the resting muscle, and the latter would correspond mainly to the inactive parts of the thin and thick filaments. If so, the length of SEC_a or SEC_2 will be increased with an increase in the muscle length as illustrated schematically in Fig. 3.11. Therefore, the effect of muscle length on the series elasticity was examined. One of the results is shown in Fig. 3.11, in which the load-extension curve was determined at L_o-2 mm (86 % L_o),

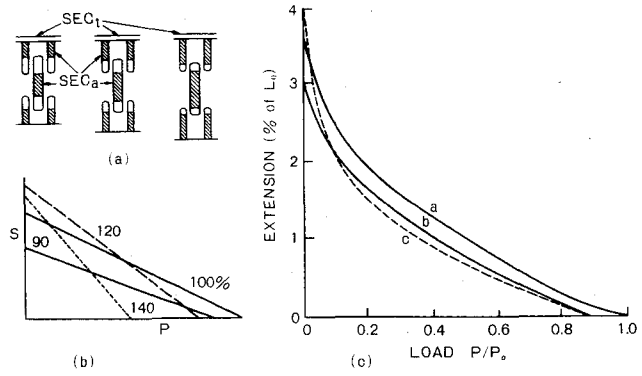

Fig. 3.11 Effect of muscle length on the series elasticity. (a) Schematical illustration of an increase in the length of SEC_a with increasing muscle length from left to right, (b) calculated load-extension curves at various muscle lengths, figures show the muscle lengths in % of L_o, (c) load-extension curves obtained at various muscle lengths ; a, 14 mm (=L_o); b, 12 mm; c, 16 mm; frog semitendinosus bundle preparation; 10 °C.

L_o=14 mm, L_o + 2 mm (114 % L_o). Suppose that the compliance of SEC_t is 0.01 L_o/P_o (see section 3.2) and that of SEC_a is also linear, the total load-extension curves at various muscle lengths are to be as illustrated in Fig. 3.11(b). Of course, the measured load-extension curves shown in Fig. 3.11(c) do not sufficiently agree with the theoretical ones because of the nonlinear property, but apparently the series elastic component is more compliant at the longer length of the muscle. Then it is concluded at least quantitatively that a part of the series elastic component contains the inactive regions of the thick and thin filaments where both filaments do not ovelap each other. For the better fit of the theoretical curves, the nonlinear compliance of SEC_a must be taken into the theory.

3.4 DETERMINATION OF THE LOAD-EXTENSION CURVE OF THE SERIES ELASTIC COMPONENT BY MEANS OF COMPUTER SIMULATIONS

The purpose of this section is to simulate the transient responses to the isotonic quick release and to determine analytically the load-extension curve of the series elastic component and finally to verify the experimental curve determined at section 3.3. In order to do this, a mathematical model in Fig. 3.12 is employed here; the series elastic component is modeled as a purely mechanical spring (SEC_2) in parallel with a weak viscosity (VC_s)*). The contractile component is modeled, based on the molecular mechanism of muscle contraction, its modeling being expressed in detail in chapter VI.

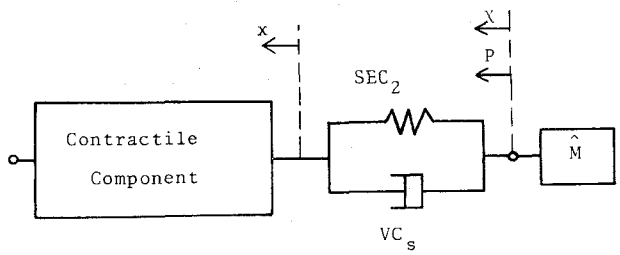

Fig. 3.12 Mechanical model of muscle for quick release experiments. CC, contractile component; SEC_2, series elastic component; VC_s, viscous component; P, tension; x, X, shortening; $\hat{M}$, equivalent mass.

a) Equation of the muscle-load system

Kinetic equation for the muscle and loading system in Fig. 3.12 is

$$\left.\begin{aligned} \hat{M}\,\ddot{X} &= P - \hat{M}\,g_a \\ m\,\ddot{x} &= F_a - P \\ P &= E_2\,(x - X) + B_s\,(\dot{x} - \dot{X}) \\ \ell &= \ell_o - X \end{aligned}\right\} \qquad (3.4)$$

*) This viscous damping element may be neglected on the ordinary contraction, because the velocity of normal shortening is considerably slower than that of instanteneous shortening immediately after the isotonic quick release.

where $\hat{M}$ = equivalent mass, consisting of an applied load and the isotonic lever,

P = tension on muscle,

X = shortening of muscle,

x = shortening of CC,

F_a = force exerted in CC,

m = mass of muscle; we make an approximation of $m\ddot{x}=0$, because of its minor effects on muscle dynamics,

E_2 = elastic coefficient of SEC_2,

B_s = viscous damping constant of VC_s,

ℓ = length of muscle,

ℓ_o = initial length of muscle,

g_a = accerelation of gravity, (980 cm/sec^2).

An equivalent mass of our experimental arrangement is (see Appendix A)

$$\hat{M} = 0.28 + 0.01\ P_e \qquad (3.5)$$

where P_e = mass of the applied load.

The relation between load on SEC_2 (P_{sec}) and extension of SEC_2 (x_2) is expressed as

$$P_{sec} = E_2\ x_2 \qquad (3.6).$$

$$x_2 = x - X$$

b) Mathematical model of the contractile component

When repetitive tetanic stimuli are applied to the muscle, inner Ca ion concentration can be assumed to maintain a steady state (state of equilibrium). This section treats the contractile process under this condition, while chapter VI deals with transient changes in Ca ion concentration. Therefore, descriptions of the model are given in a simplified form of, but equivalent to, those of the complete model described in chapter VI.

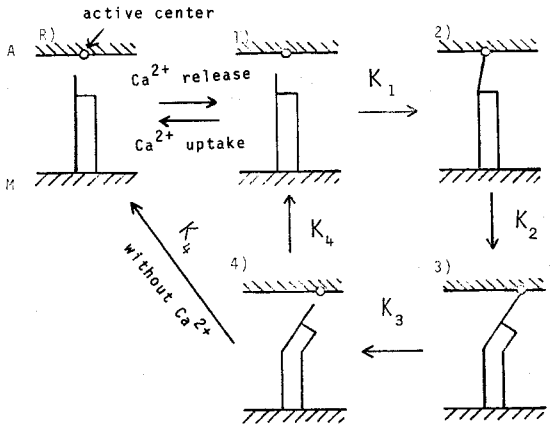

Fig. 3.13 Schematic drawing illustrating the molecular mechanism of contractile process under the steady state of Ca ion concentration. A, actin filament; M, myosin cross-bridge.

It is assumed here that a single working cross-bridge (unit contractile machine) is generating constant active force f with dissipating the force loss f_v in proportion to the velocity v ; thus, the unit machine exerts the net force $f-f_v$. Consequently, the total active force generated in the contractile component F_a is expressed as

$$F_a = n_2 \left(f - f_v \right) \tag{3.7}$$

$$f_v = \begin{cases} \beta v & (v \geqq 0) \\ \beta' v & (v \leqq 0) \end{cases} \tag{3.8}$$

$$v = \dot{x}$$

where β = constant of proportionality during shortening,

β' = constant of proportionality during lengthening,

n_2 = number of working cross-bridges at the state 2) in Fig. 3.13.

Interactions between myosin cross-bridges and Ca ion-receptive proteins (active center) in the thin filaments may be separated into five following states (Fig. 3.13): R) resting state; 1) activation of the active center

resulted from binding of Ca ion; 2) formation of a cross-bridge between both filaments (the cross-bridge is developing a sliding force f);
3) in the instant of breaking down the cross-bridge; 4) the cross-bridge is completely broken down. Note that the cycle 1)→2)→3)→4) is considered to continue as long as the tetanic stimulation lasts. Taking the numbers of the active center at the states 1), 2), 3) and 4) to be n_1, n_2, n_3 and n_4, respectively, we obtain following kinetic equations for the contractile reaction under the steady Ca ion concentration:

$$\begin{aligned} \dot{n}_1 &= K_4 n_4 - K_1 n_1 \\ \dot{n}_2 &= K_1 n_1 - K_2 n_2 \\ \dot{n}_3 &= K_2 n_2 - K_3 n_3 \\ \dot{n}_4 &= K_3 n_3 - K_4 n_4 \end{aligned} \tag{3.9}$$

where K_i, (i= 1, 2, 3, 4) = rate constant of transition from the state i) to the state i+1),

The total number of working active centers N is expressed as:

$$N = n_1 + n_2 + n_3 + n_4 \tag{3.10}$$

The value of N is dependent on an intrinsic length of the overlap region of two kinds of filaments, which depends on the length of muscle, ℓ. Namely,

$$N / N_o = F_\ell(\ell) / F_{\ell o} \tag{3.11}$$

where $F_\ell(\ell)$ = intrinsic length of the overlap region, function of ℓ,

N_o = the value of N where the maximum tension P_o is developed,

$F_{\ell o}$ = maximum of $F_\ell(\ell)$, $F_{\ell o} = F_\ell(L_o)$.

Considering the sliding movement of filaments produced by the cyclic movements of cross-bridges, we introduce following nonlinear properties into the rate constant K_2; K_2 is increased linearly with an increase in the velocity of sliding movement v :

$$K_2 = \begin{cases} \alpha_o + \alpha_1 v & (v \geqq 0) \\ \alpha_o - \alpha_1' v & (v \leqq 0) \end{cases} \tag{3.12}$$

where α_o, α_1, α_1' = constants.

c) Simulated results

Responses of a tetanus muscle to an isotonic quick release are simulated by using equations (3.4)-(3.12), and the elastic coefficient of SEC_2 is estimated. In the simulation, the values in Table III-3 are used for the parameters of the contractile component. These values are determined by investigating the physiological data, such as the force-load-velocity relation and muscle energetics (details are given in section 6.4). The function $F_\ell(\ell)$ is given by Eq. (6.54). Figure 3.14 is a typical record of the isotonic quick release obtained from the frog semitendinosus muscle. The solid line is a traced line of the physiological record; after-load is 0.13 g in (a), 0.34 g in (b) and 0.48 g in (c).

Initial conditions at the time of the quick release (at $t=t_q$) are

$$\ell = L_o,\ X = 0,\quad P = P_o,\ x = P_o / E_2 \qquad (t = t_q) \tag{3.13}$$

and the initial values of n_i (i=1, 2, 3, 4) are

$$n_1 = n_3 = n_4 = 0.017\ N_o\ ,\ n_2 = 0.8\ N_o \qquad (t=t_q) \tag{3.14}.$$

In order to estimate the value of E_2, simulations are done on three cases;

$$\text{case 1,}\quad E_2 = 6.4 \times 10^4\ \hat{x}_2^2\ P_o/L_o \tag{3.15}$$

$$\text{case 2,}\quad E_2 = 2.5 \times 10^4\ \hat{x}_2^2\ P_o/L_o \tag{3.16}$$

$$\text{case 3,}\quad E_2 = 1.1 \times 10^4\ \hat{x}_2^2\ P_o/L_o \tag{3.17}.$$

The load-extension curves of these three cases are shown in Fig. 3.15; the extension of SEC_2 at $P = P_o$ are 2.5 % of L_o, 3.4 % of L_o and 4.5 % of L_o

TABLE III-3

PARAMETERS OF THE CONTRACTILE COMPONENT

α_o = 21.0 /sec, α_1 = 120.0 /L_o , α_1' = 130.0 /L_o , f = 0.125 P_o/N_o,
β = 0.35 P_o.sec/L_o , β' = 3.43 P_o.sec/L_o , $K_1=K_3=K_4$= 258 /sec

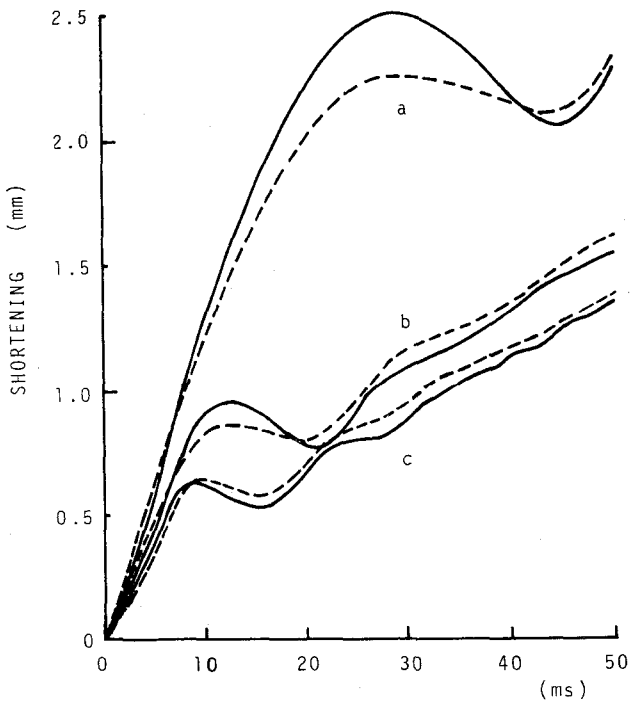

Fig. 3.14 Simulation of responses to the isotonic quick release of tetanically stimulated muscle. Solid line, experimental record obtained from frog semitendinosus bundle preparation, P_o=2.7 gwt, L_o= 13 mm, 10 °C; after-load, (a) 0.13 g, (b) 0.34 g, (c) 0.48 g. Broken line, simulated response obtained from the model by using Eq. (3.16) as E_2 .

in the cases 1, 2 and 3, respectively. On the other hand, eight values of viscous constant B_s were employed in the simulations; B_s = 0.001, 0.002, 0.005, 0.007, 0.008, 0.01, 0.02, and 0.05 P_o.sec/L_o. Simulation experiments were done in all the possible combinations of E_2 and B_s, i.e. 24 combinations.

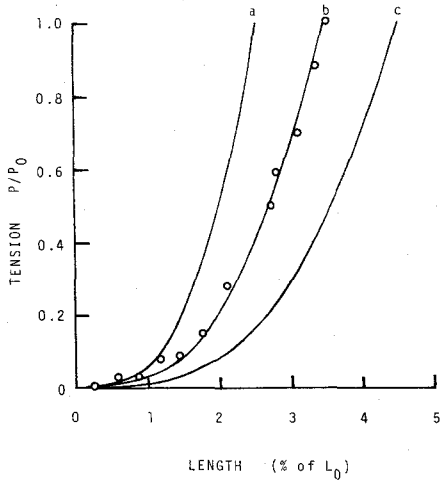

Fig. 3.15 The load-extension curves of the series elastic component, SEC_2. Open circle, experimental curve obtained from the controlled release. Curve a, the relation of case 1; curve b, case 2; curve c, case 3.

Consequently, we obtained such suitable values as could satisfactorily account for the physiological data of the isotonic quick release in Fig. 3.14; namely, E_2 was the relation of case 2 (Eq. (3.16)) and B_s was about 0.007-0.01 $P_o.sec/L_o$. The broken line in Fig. 3.14 is the response of the model obtained from these values (B_s=0.008 $P_o.sec/L_o$), which shows close agreement with the physiological result. As for the cases 1 and 3, we also attempted to fit the responses of the model to the physiological ones by changing the values of B_s over a wide range, but failed. Those responses of the model tended to differ considerably from the experimental results. We may thus conclude that the elastic constant of SEC_2 approximately obeys the relation of Eq. (3.16) and viscous damping constant in parallel with SEC_2 is about 0.008 $P_o.sec/L_o$. It should be noted that, as seen in Fig. 3.15, the load-extension curve of Eq. (3.16) is in a good agreement with that obtained from the frog muscle. Finally, the load-extension curve obtained experimentally at section 3.3 can be recognized as being satisfactorily accurate.

It was also indicated that the viscous damping constant considerably affected the instantaneous quick shortening after a quick release, although it had insignificant effects on normal shortening of contraction because of its slight viscosity and normal slow shortening. The value of its constant has been already identified by Woledge (1961)[89] as being B_s=0.007-0.009 P_o.sec/cm in frog sartorius at 10 °C, and also by Bahler (1967)[9] as being B_s=0.01 P_o.sec/cm in rat gracilis at 17.5 °C. The value obtained here is B_s=0.008 P_o.sec/L_o=0.01 P_o.sec/cm, which is quite the same as Bahler's. These facts also seem to support the simulation result.

3.5 FORCE-LOAD-VELOCITY RELATION OF THE CONTRACTILE COMPONENT AND VISCOUS-LIKE FORCE

a) Load-velocity relations of the shortening muscle determined at various steady contractile forces

The load-velocity relation of the skeletal muscle has usually been determined only in the fully activated muscle. In our research, however, it was first determined in the partially activated muscle as well as in the fully activated one, using the isotonic quick release method.

First, the muscle was isometrically tetanized at the initial length of L_o by square pulses at 50-100 Hz until the tension reached P_o, and then quick release was performed using an electromagnetic relay. Following this, the fully activated muscle shortened against the load P, as seen in Fig. 3.16 A. The shortening velocity v was measured at the linear part of the shortening curve which began immediately after the quick shortening of the series elastic component. Measuring the velocities for various loads at the same initial length L_o, the load-velocity relation was obtained as shown in Fig. 3.17, curve 1. This curve was hyperbolic , and the dynamic constants were a/P_o=

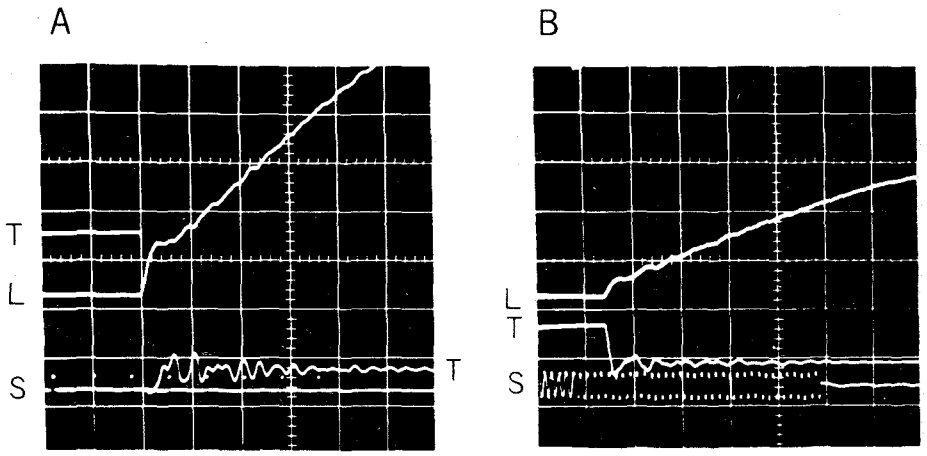

Fig. 3.16. Measurement of the shortening velocity by the isotonic quick release method. The muscle was released after 200 msec from the start of stimulation. A, square pulses stimulation at 50 Hz in Ringer's solution, load=1.0 g; B, AC stimulation at 300 Hz, in 20 mM potassium solution, load=0.7 g; L, shortening curve, 1 mm/div; T, tension curve 2g/div; S, stimulus; time, 25 msec/div; P_o= 7.6 gwt; L_o= 12 mm ; 10 °C.

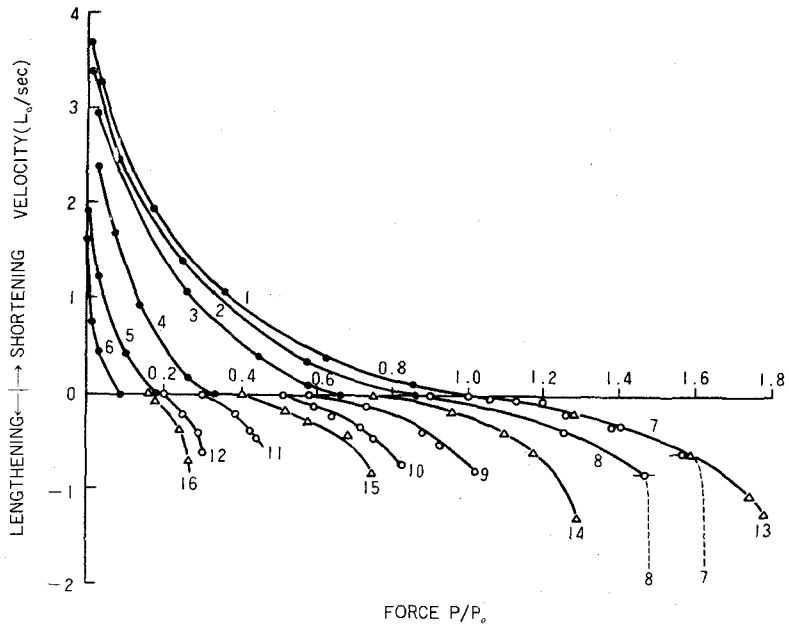

Fig. 3.17. Force-velocity (load-velocity) curves obtained at various contractile forces. Filled circle, determined by isotonic shortening; open circle, determined by isotonic lengthening; triangle, determined by isovelocity stretching; 10°C.

0.23 and b/L_o=0.9/sec. In the average of 10 cases, a/P_o was 0.25 (0.23-0.28) and b/L_o was 0.9/sec(0.85-0.90/sec). Of course, under these experimental conditions, load P means the force of the contractile component during isotonic shortening, and the intrinsic contractile force is P_o.

Second, the potassium concentration of Ringer's solution was raised to 20 mM and the muscle was stimulated by AC at 500 Hz. In such an excess potassium solution, the action potential was abolished and the muscle membrane was partially but uniformly depolarized by AC stimulation (Mashima and Washio, 1968)[65]. Since the depth of depolarization depends on the potassium concentration and the field strength, various steady tensions were obtained by applying various field strenghts. Thus, the contractile force was kept at a certain level without changing the muscle length. In the partially activated muscle thus obtained, the contractile force, F,was less than P_o;for example, F is 0.35 P_o in Fig. 3.16B. Repeating the velocity measurements for various loads, a set of load-velocity curves was obtained, as shown in Fig. 3.17, curves 2-6.

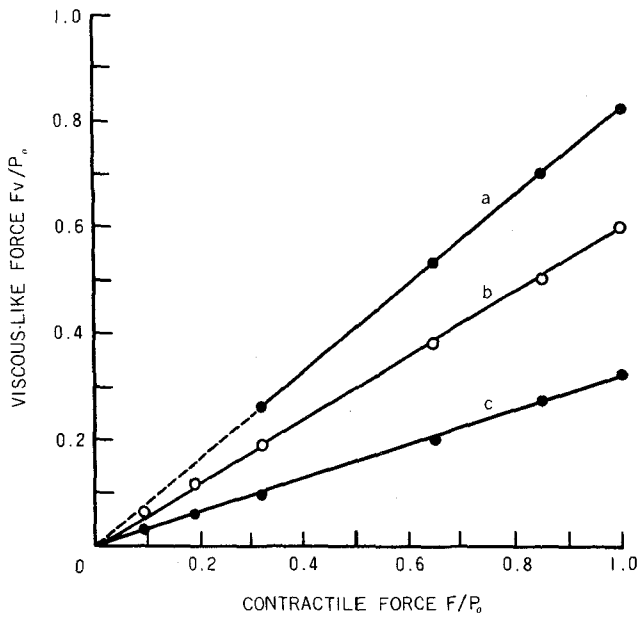

Fig. 3.18 Relation between the viscous-like force and the contractile force at various shortening velocities. a, at 2.0 L_o/sec; b, at 1.0 L_o/sec; c, at 0.4 L_o/sec.

The intersection of each curve and the abscissa (at v = 0) represents the isometric tetanus tension before release, that is, the contractile force of that curve. For example, in Fig. 3.17, curve 3, F is 0.65 P_o.

According to Bahler et al. (1967)[11], the fact that the faster a muscle shortens the less force it exerts is interpreted as meaning that part of the force is dissipated internally as a function of the velocity, as though there were an internal load or viscous-like force. This viscous-like force, F_v, is the difference between the contractile force and the load, i.e. $F_v = F - P$. In order to examine the property of the viscous-like force, the quantity (F - P) at a certain velocity was plotted against F, as shown in Fig. 3.18. It is remarkable that the relation is exactly linear at every shortening velocity arbitrarily selected. Thus, we concluded that the viscous-like force is not only a hyperbolic function of velocity, as shown in Eq.(3.2), but also a linear function of contractile force in the partially as well as the fully activated muscle. Consequently, the following equation is proposed, instead of Eq.(3.2):

$$F_v(v,F) = F - P = \frac{F}{P_o}(P_o + a)\frac{v}{v + b} \qquad (3.18)$$

Further, the load-velocity equation of the fully activated muscle [Eq. (3.1)] is generalized to the following force-load-velocity equation,

$$(P + A)(v + B) = B(F + A)$$

or

$$v(A + P) = b(F - P) \qquad (3.19)$$

where $A = (F/P_o)a$ and $B = b$. Using Eq. (3.19) and the dynamic constants ($a/P_o = 0.23$, $b/L_o = 0.9$/sec), the load-velocity curves were calculated for various contractile forces, and it was confirmed that curves 1-6 in Fig.3.17 showed a good coincidence with these calculated curves. Therefore, Eqs.(3.18) and (3.19) are applicable to any contractions of partially activated muscle

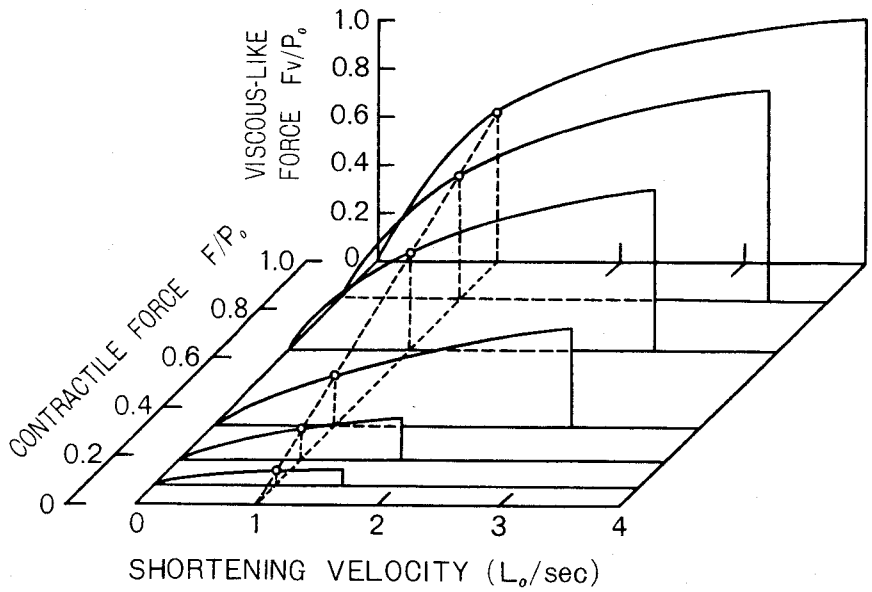

Fig. 3.19 Three-dimensional diagram of the contractile force, viscous-like force and shortening velocity at L_o.

where $F \leqq P_o$, at least during steady state activity. Furthermore, it was derived that the heat constant A increases linearly with an increase of the contractile force, and Hill's constant a is the maximum value at $F = P_o$, whereas the constant b does not change in the partially activated muscle. In order to show the property of the viscous-like force represented by Eq. (3.18), the relation between the contractile force, the viscous-like force, and the shortening velocity at L_o is illustrated as a three-dimensional diagram, as seen in Fig. 3.19. From these results it is suggested that the contractile component of the muscle involves the viscous-like element, which works as a function of the velocity and the contractile force.

The effect of muscle length on the load-velocity relation was also examined by repeating the same experiments at muscle lengths between 0.8 L_o and 1.2 L_o. Thus, similar hyperbolic curves were obtained, as shown in Fig. 3.20, and the dynamic constants were $a/P_o = 0.28$ and $b/L_o = 0.9/\text{sec}$.

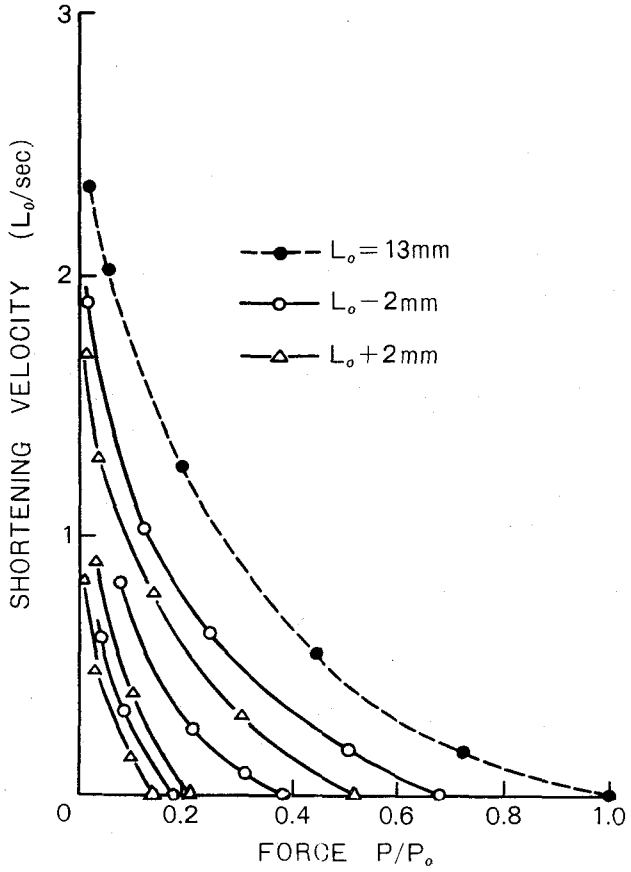

Fig. 3.20. Force-velocity curves obtained at various muscle lengths. Contractile force was changed by AC stimulation in the excess potassium solution. P_o=15 gwt; 10 °C.

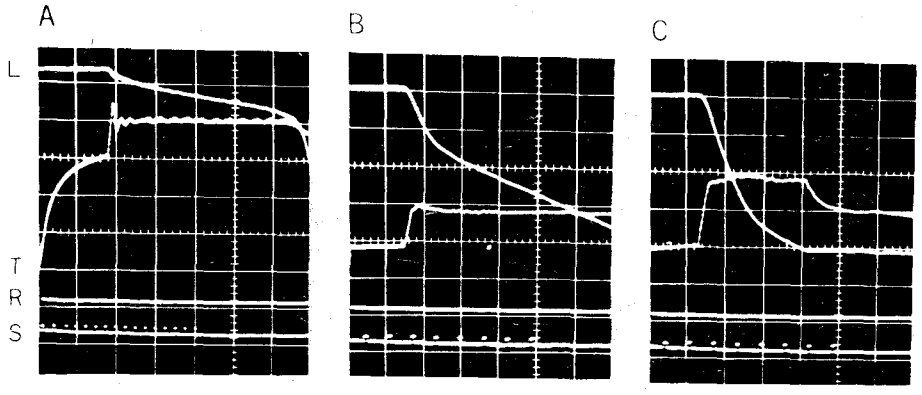

Fig. 3.21. Changes in tension and length during the lengthening by a load larger than P_o. L, lengthening curve, 0.4 mm/div; T, tension curve, 0.7g/div in A, 1.4g/div in B and C; time, 50 msec/div in A, 20 msec/div in B and C; R, resting tension level; S, stimulus, 80HZ; A, quick stretch by 1.3 P_o (3.5g); B, controlled stretch by 1.5 P_o (4g); C, controlled stretch by 2.0 P_o (5.5g); P_o= 2.7 gwt; L_o=12 mm; 10 °C.

It was confirmed that these curves fit Eqs. (3.18) and (3.19) within this range of muscle length.

b) The velocity of isotonic lengthening induced by loads larger than P_o

The viscous-like force in the contractile component also worked when the muscle was lengthened by a stretch or during isometric relaxation, at which time the contractile component is stretched by the series elastic component. In order to examine the viscous-like force of the lengthening muscle, the load-velocity relation of the lengthening muscle was determined.

First, the muscle was isometrically tetanized at L_o by square pulses at 80 HZ, and at the maximum tension P_o it was stretched isotonically by a load larger than P_o, removing the stop for the isotonic lever suddenly. The changes in tension and muscle length during isotonic lengthening were recorded simultaneously, as shown in Fig. 3.21A. As pointed out by Katz (1939)[56], the lengthening curve consists of two phases, that is, an immediate downstroke and slow uniform lengthening, when the load is less than 1.6 P_o. As the tension curve was maintained at the load level, the lengthening velocity was measured in the linear part of the lengthening curve after the immediate downstroke due to the lengthening of the series elastic component. The lengthening velocity, -v, thus obtained was plotted against the load, as shown in Fig. 3.17, curve 7. This curve is not completely identical to curve 1, but it is also hyperbolic. As seen in Fig. 3.21A, an overshoot appeared in the tension curve, corresponding to the immediate downstroke of the lengthening curve. A large overshoot might accelerate the initial "giving" of the contractile component. Therefore, the maximum lengthening velocity was confined by the velocity controller, in order to minimize the overshoot. Thus, the lengthening velocity for loads up to 1.6 P_o was measured (Fig. 3.21B).

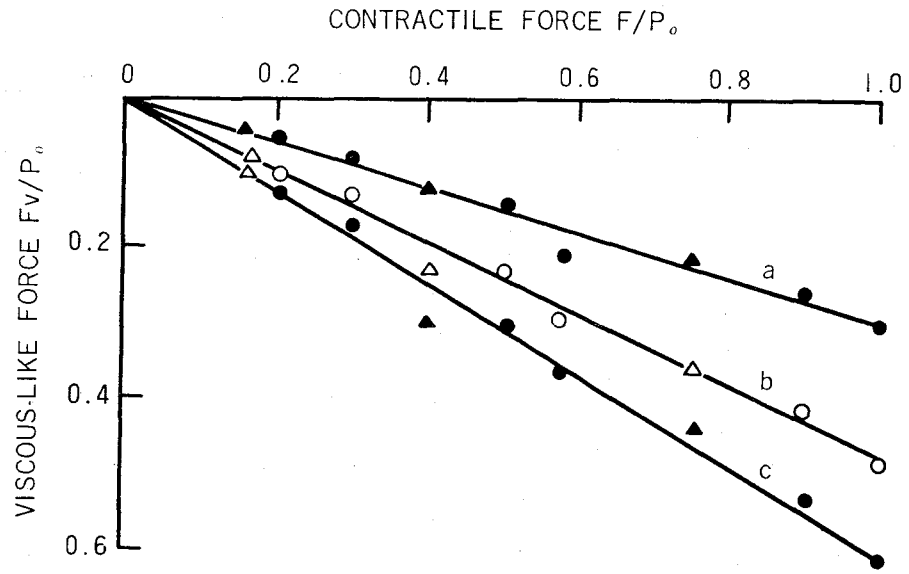

Fig. 3.22 Relation between the viscous-like force and the contractile force at various lengthening velocities. a, at 0.2 L_o/sec; b, at 0.6 L_o/sec. Circles, obtained by isotonic lengthening; triangles, obtained by isovelocity stretching.

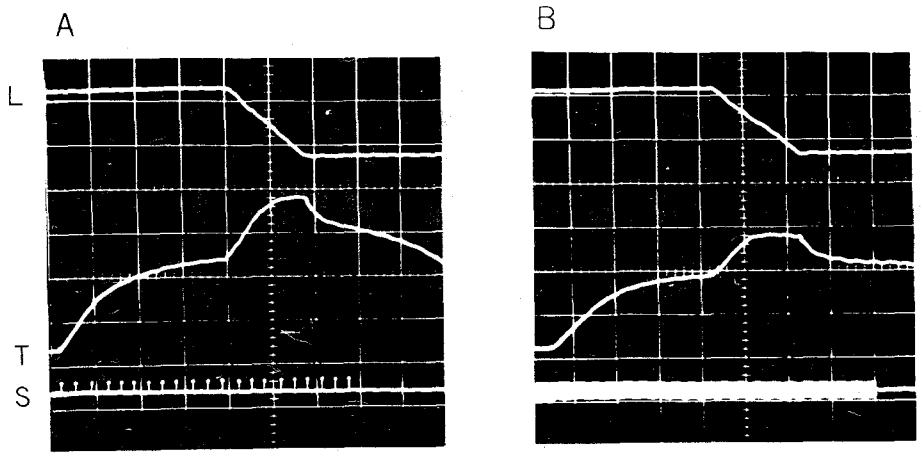

Fig. 3.23 Measurement of tension developed by the isovelocity stretching. A, in Ringer's solution, stimulated by square pulsed at 80 Hz, stretched by 0.4 mm at a velocity of 4.4 mm/sec, P_o = 4.3 g; B, in excess potassium solution, stimulated by AC at 500 Hz, stretched by 0.4 mm at a velocity of 3.7 mm/sec, F = 0.7 P_o; L, length, 0.24 mm/div; T, tension, 2 g/div; time, 50 msec/div; L_o=14 mm, 10 °C.

For loads between 1.6 P_o and 1.8 P_o, however, various lengthening velocities were observed for a certain load by repeating the same experiments, so that it was difficult to determine the real velocity. This situation is expressed by the dotted line in curve 7. For loads larger than 1.8 P_o, a large downstroke was followed by a rapid "giving" or relaxation, as seen in Fig. 3.21C, and no linear lengthening was observed, as though myofilaments had slipped off. When the maximum velocity was not controlled, the tension curve was raised steadily over the load level during the stretch and isotonic condition was no longer realized. Therefore, within the load range of less than 1.6 P_o or the velocity range of less than 1.0 L_o/sec, the following equations were obtained:

$$(2P_o - P + a')(-v + b') = b'(P_o + a') \tag{3.20}$$

or

$$P - P_o = (P_o + a')\frac{v}{v + b'} \tag{3.21}$$

In curve 7, $a'/P_o = 0.4$ and $b'/L_o = 0.85$/sec. Namely, the heat constant a' during lengthening is about 1.6 times larger than a during shortening. The rate constant of energy liberation b' during lengthening, however, is the same as b during shortening.

Second, the muscle was soaked in excess potassium solution containing 10-20 mM KCl and stimulated by AC at 300 Hz at various intensities. Thus, a set of load-velocity curves at various contractile forces was determined on the lengthning muscle, as shown in Fig.3.17, curves 8-12. All these curves were also hyperbolic, unless the lengthening velocity exceeded about 1.0 L_o/sec.

The viscous-like force during lengthening at a certain velocity was plotted against the contractile force, as shown in Fig. 3.22. The relation was also linear, as observed on shortening in Fig. 3.18. Thus, the following equation

is introduced instead of Eq. (3.21):

$$F_v = P - F = \frac{F}{P_o}(P_o + a')\frac{v}{v - b'} \qquad (3.22)$$

And the generalized force-load-velocity relation of the lengthening muscle becomes

$$(P - 2F - A')(v - B') = B'(F + A.) \qquad (3.23)$$

or

$$v\,(P - 2F - A') = B'(F - P)$$

where $A'=a'(F/P_o)$ and $B'=b'$. Finally, it was concluded that the viscous-like force in the contractile component was increased linearly with increasing contractile force not only on shortening but also on lengthening in the velocity range of less than 1.0 L_o/sec.

c) The force-velocity relation determined by isovelocity stretching

Another method of determing the force-velocity relation was also adopted. The muscle was tetanized isometrically at L_o and , after the maximum tension was attained, it was stretched at various constant velocities, using the velocity controller. The tension and muscle length during the stretch were recorded simultaneously, as shown in Fig. 3.23. The tension curve attained a new steady level about 50 msec after the beginning of the stretch. Then the lengthening velocity, -v, and the developed steady force, P, were measured and plotted, as seen in Fig. 3.17, curve 13. The maximum tension measured by this method was about 1.8 P_o at the velocity of 1.0 L_o/sec, that is , a little larger than the value obtained by the isotonic lengthening method.

Second, by AC stimulation in excess potassium solution (Fig. 3.23) , a set of P-v relations was determined at various contractile forces, as

shown in Fig. 3.17, curves 14-16. These curves are essentially similar to curves 7-12 which were obtained by isotonic lengthening. The viscous-like force measured from these curves also coincided with those obtained by isotonic lengthening, as seen in Fig. 3.22. Using Eq. (3.23) and $a'/P_o=0.4$, $b'/L_o=0.85$ /sec as dynamic constants, the force-velocity curves were calculated. These curves coincided satisfactorily with experimental curves 7-16 in Fig. 3.17.

These results are also confined within the velocity range of less than 1.0 L_o/sec. When the velocity of stretch was larger than 1.0 L_o/sec, the tension curve rose rapidly and continuously, so that no plateau in the tension curve was observed.

Comparing Fig. 3.18 with Fig. 3.22, it is found that the viscous-like force during lengthening is about 1.4 times larger than that during shortening, if contractile forces and velocities are identical.

d) Force-velocity relation during the change in contractile force

In order to apply Eqs. (3.18) -(3.23) to a transient state during contraction, it is necessary to examine whether these relations represent an instantaneous contractility or not, because these relations were determined only in steady state activity. On the falling phase of the tension in a relaxing muscle, Jewell and Wilkie (1960)[53] determined the force-velocity relation and stated that Hill's hyperbolic equation fit at any instance during relaxation. In our research, the force-velocity relation during the rising phase of contraction was also determined. As it was impossible for the quick release method to measure an instantaneous velocity during the rapid change in tension, the muscle was soaked in the excess potassium solution and stimulated by AC at 500 Hz, the voltage of which was increased almost linearly with time. By this stimulation the rate of tension rise was slowed down to 1.5 P_o/sec, as seen in Fig. 3.24A. Then the muscle was released at a given time

after the start of stimulation, and the changes in tension and length of the muscle were recorded simultaneously. Immediately after quick shortening due to the series elastic component came linear shortening of the contractile component against a certain load (Fig. 3.24B). This shortening velocity was plotted against the load, as shown in Fig. 3.25. The load-velocity curves in Fig. 3.25 were obtained by using Eq.(3.19), taking $a/P_o = 0.25$ and $b/L_o = 0.9$ /sec as the dynamic constants. Observed points in Fig. 3.25 fit satisfactorily with the calculated curves. Therefore, we concluded that Eq. (3.19) holds not only during steady state activity but also for any instance during the change in contractile force, so that F in Eq. (3.19) can be generalized to a function of time, F(t), at least in the observed rate of tension rise. Actually, the transition from isometric to isotonic contraction is so quick, as seen in Fig. 3.24B, that the above generalization may be valid for the rising phase of normal contraction.

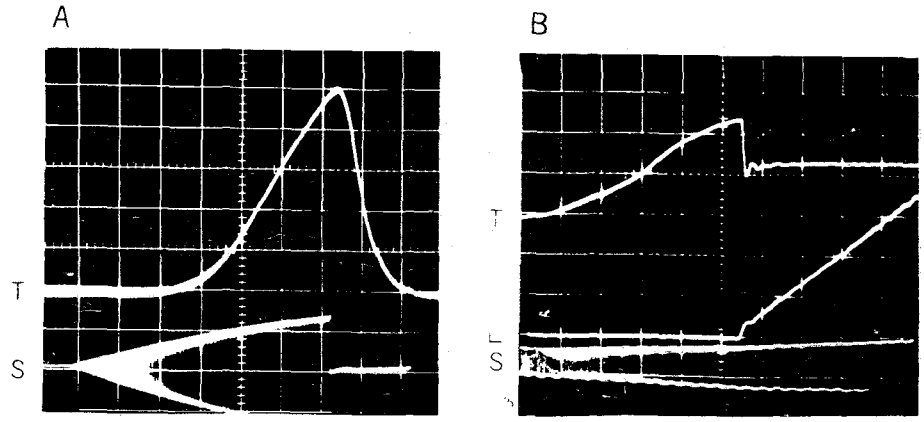

Fig.3.24 Measurement of shortening velocity during the rising phase of contraction generated by increasing AC stimulation at 500 Hz in excess potassium solution. T, tension, 0.1g/div in A, 0.9g/div in B; L, length, 0.3 mm/div; S, stimulus; time, 200 msec/div in A,50 msec/div in B; A, whole course of contraction, L_o = 12mm; B, isotonic quick release at 700 msec from the start of stimulation, L_o = 11mm; 10°C.

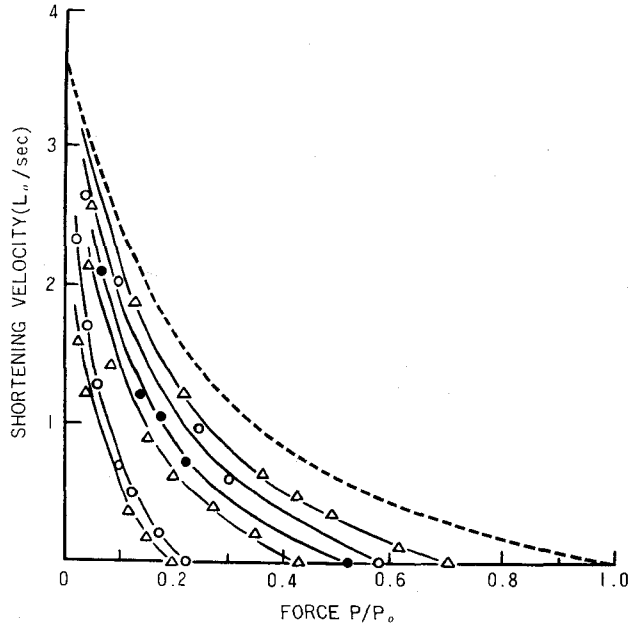

Fig. 3.25 Force-velocity curves calculated from Eq. (3.19), taking $a/P_o = 0.25$ and $b/L_o = 0.9$/sec. Observed points determined by the isotonic quick release method during the rising phase of contraction fit with calculated curves; three preparations; 10°C.

3.6 DISCUSSION

a) The series elastic component

The series elastic component has been commonly identified by isotonic quick release experiments. As to this technique, Podolsky (1960)[67] and Civan and Podolsky (1966)[21] pointed out as follows; the non-steady phase of the motion following lever release could not be attributed solely to mechanical interaction of lever inertia with the series elastic element, and there was an additional component that appeared to be originated in the contractile element of the muscle. Certainly, seeing that the series elastic component does work together with the contractile component, it is very hard or

impossible to identify solely the series elastic component from performing any mechanical experiments. Further, mechanical measurement would not lead to a clear decision for the question because of inaccuracy of measuring instantaneous rapid movements after quick releases. So, simulation study described at section 3.4 is considered to be of important significance in leading to the explicit conclusion for this problem. Especially the simulated result is worthy to be emphasized; namely, the load-extension relation of the series elastic component, being separated from effects of the contractile component, was determined quantitatively and close agreements were obtained between the simulated results and the experimental ones.

The question has been often posed whether the series elastic component is all in the tendon or whether part of it may be located within the the microstructure of the muscle fibers. The present work showed that about one third of the whole series elasticity corresponded to the tendons. For the residual series compliance, it is difficult to say the structural correspondence in the present study, while Z-lines would be contained in it. However, the failure of the series elastic component to change remarkably with temperature or time after a single shock (Fig. 3.9 and Fig. 3.10) in addition to the dependence of series compliance on muscle length (Fig. 3.11) would strongly suggest that the cite must be located in a region not subject to the profound change which occurs in the contractile proteins during activity; namely, the fact may point to its being in an inactive region and may probably include the possibility that it is in the inactive parts of thin and thick filaments, and not dominantly in the working sites of the filaments. This consideration would be supported by electron-microscopic observations demonstrated by Galey (1969)[32]. On the other hand, Huxley and Simmons (1971)[46] have accurately recorded the change in tension after a stepwise length change and pointed out that the instantaneous elasticity is mostly in the filament themselves, i.e., resides in the cross-bridges them-

selves. If so, at least a part of the series compliance actually observed does come from the movement of the cross-bridges, and it seems to be suggestive that the series compliance of the active muscle is larger at the beginning of contraction and at late relaxation. It is pity that the mechanical experiments can not lead to a clear decision for the question; whether a partial participation of the cross-bridges in the series elasticity or ambiguity of mechanical measurement would be the cause. Any way, macroscopically the total extension of the series elastic component of the frog semitendinosus muscle was about 3-3.5 % of L_o under the maximum tension.

b) The viscous-like component

In the present study the load and the contractile force were separated. The contractile force, F, is defined as the steady isometric tension, which may represent the intensity of the active state, and the maximum contractile force in the fully activated state is P_o, while the load P means the force during the isotonic shortening or lengthening. And the difference between F and P is the viscous-like force, F_v, because when the muscle is released from isometric to isotonic contraction, the force is decreased from F to P, as though there were a viscous-like force, which works as a function of velocity v. Hill's equation, Eq. (3.2), describes the viscous-like force as a hyperbolic function of v. However, Eq. (3.2) holds only in the fully activated muscle, where $F=P_o$. The present study on partially activated muscles, where F is less than P_o, showed that the viscous-like force is a linear function of F, and Eqs. (3.18) and (3.19) were introduced. Of course, the viscous force should be a mere function of v. But from the viewpoint of the sliding filament theory (H. E. Huxley, 1957[47]; A. F. Huxley, 1957[45]), the cross-bridges between myofilaments functioning

as force generators are all in parallel, as in shown schematically in Fig. 3.26. Assuming that each cross-bridge has a proper force f and viscosity f_v, the total viscosity F_v or the total force F may become the sum of the viscosity or force of each cross-bridge. Thus, it should not seem strange that the viscous-like force is proportional to the contractile force, because both of them are proportional to the number of active cross-bridges.

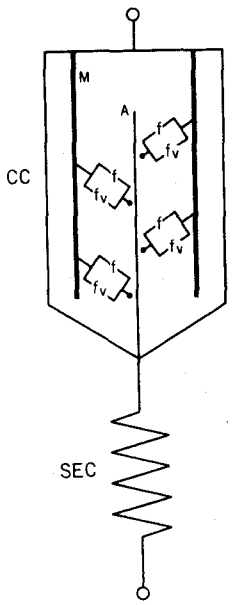

Fig. 3.26 Schematic drawing of the contractile component (CC) and the series elastic component (SEC). M, thick filament; A, thin filament; f, and f_v, contractile force and viscous-like force of a unit force-generator.

From the finding that for a given velocity, the viscous-like force is exactly proportional to the contractile force, it is apparent that the load-velocity curves in Fig. 3.17 converge to a common maximum velocity when P=0. This fact suggests that each cross-bridge has an all-or-none property even in the partially activated muscle, that F and F_v depend on the number of active

cross-bridges, and that a hyperbolic equation similar to Eq. (3.1) must be valid for each force generator.

According to Bahler et al. (1968),[12] the shortening velocity is not only a function of load and length, but is also a function of an additional variable related to the time lapse after the onset of stimulation. Of course, there is a definite relation between the contractile force and muscle length as determined by Gordon et al. (1966),[34] but most tension-length relations are significant only in the fully activated muscle. It is apparent from our results that the contractile force is much more important than the length in explaining the viscous-like force during the sliding of myofilaments.

Abbott and Wilkie (1953)[2] and Matsumoto (1967)[66] showed that the force-velocity relationship was valid for all lengths less than L_o. Our results also showed that between 0.8 L_o and 1.2 L_o the dynamic constants remained fixed. While Gordon et al. (1966)[34] found that the observed velocity was lower than that predicted by the force-velocity curve at sarcomere lengths below 1.7 μ (0.85 L_o) in unloaded contractions of single fibers, Bahler et al. (1968),[12] on the other hand, found that the velocity of shortening achieved at a given length was lower for longer initial lengths, when the muscle was allowed to shorten from different initial lengths. Probably, an increase in the viscous-like force or some other resistance to shortening might account for these lower velocities in the length region below 0.8 L_o or beyond 1.2 L_o.

As for the additional variable related to time, especially in the beginning of contraction, the fact should be taken into consideration that the muscle is only partially activated at that point. Not Eq.(3.1) but Eq. (3.19) might be applicable to such a transient state. Although our experiments were conducted during slowly rising tension, Jewell and Wilkie (1960)[53] obtained similar results in experiments of the falling phase of tension in a relaxing muscle. Jewell and Wilkie (1958)[52] also concluded that the change of velocity followed very quickly on the change in force ——

probably in less than 1 msec. If each cross-bridge has an all-or-none property and the contractile force in the partially activated state expresses the change in the number of active cross-bridges participating in contraction, Eq. (3.19) may represent the instantaneous contractility of the skeletal muscle, at least in the first approximation. And for the estimation of the active state, which is nothing but the contractile force F(t) as a function of time, in the beginning of contraction Eq. (3.19) should be used instead of Eq. (3.1), together with the tension-extension relation of the series elastic component.

From Eq. (3.19), it was proposed that the heat constant A increased proportionally with the contractile force. According to Hill's study on the shortening heat (1964)[41], the heat constant α increased linearly with increasing load. But the relation between a and α is not yet known. Thus, a further problem is whether the shortening heat depends on the load or on the contractile force itself. According to Katz (1939)[56], the velocity of reversible lengthening was much smaller than the value calculated from Eq. (3.1), and the temperature coefficient (Q_{10}) of the lengthening velocity was 1.56, while that of shortening velocity was about 2. In our results also the heat constant during lengthening was 1.6 times larger than that during shortening, confirming to the fact that the viscous-like force on lengthening was 1.4 times larger than that on shortening. The increase in heat or viscous-like force during lengthening may be interpreted as the result on an increase in the friction between myofilaments (Dumoulin and Marechal, 1970)[27], but another interpretation is also possible, i.e., that these increases are due to an activation of cross-bridges by stretching. Abbott and Aubert (1952)[1] reported that if a tetanically stimulated muscle was stretched it was generating more tension and able to do more work. Recently, Ruegg et al (1970)[72] observed a delayed rise in tension caused by abrupt stretching and suggested that an activation of contractile linkages caused by stretching may

account for this tension rise. In any case, further research on the viscosity or friction-loss in an individual cross-bridge must be done in relation to the submolecular mechanism of the sliding of myofilaments.

3.7 CONCLUSION

Mechanical properties of the resting and contracting states were determined from the physiological experiments on small bundles dissected from the frog semitendinosus muscle.

1. The tension-extension curve of the bundle was nearly the same as that of single fibers.

2. Dynamic properties of the resting muscles were interpreted with the three-component model, consisting of the series elastic element (elastic constant=1.3 P_o/L_o), the parallel elastic element (elastic constant=0.21 P_o/L_o) and the viscous element (viscous constant=0.014 $P_o.sec/L_o$), within a limit of length change less than 10 % of L_o. Compliance of the tendon was estimated as about 0.01 L_o/P_o.

3. The load-extension curve of the series elastic component (SEC_2) in the contracting muscle was determined by the controlled release technique, and the maximum extension at P_o was about 3-3.5 % of L_o. The series elastic coefficient E_2 was increased with an increase in extension x_2; $E_2 = (2.96 + 51.8\ \hat{x}_2 + 1.9 \times 10^4\ \hat{x}_2^2)\ P_o/L_o$, $\hat{x}_2 = x_2/L_o$.

4. The series compliance of the contracting muscle was not affected remarkably by the change in temperature or contractile force and was increased slightly at longer muscle length.

5. A kinetic model of the contractile component was developed, based on the molecular mechanism of contraction and the sliding filament theory. A mathematical model of muscle consisting of this kinetic model, the series

elastic component (SEC_2) and slight viscosity in parallel with SEC_2, was simulated on a digital computer. Then, the load-extension curve of SEC_2 was estimated analytically by simulating the transient responses to isotonic quick release. The estimated curve was in a good agreement with the experimental ones.

6. The viscous element in parallel with SEC_2 was identified, and its viscous constant was about 0.008 P_o.sec/L_o.

7. The load-velocity curves of shortening muscle obtained at the standard length L_o fit Hill's hyperbolic equation at any contractile force in the partially activated muscle, and the dynamic constants were a/P_o=0.25 and b/L_o=0.9 /sec at 10 °C. The viscous-like force F_v at a given velocity increased linearly with increasing contractile force F. These results were valid in the length region between 0.8 and 1.2 L_o.

8 The load-velocity curves of lengthening muscle were also hyperbolic at any contractile force and F_v was also proportional to F, unless the velocity exceeded 1.0 L_o/sec. The dynamic constants were a'/P_o=0.4 and b'/L_o= 0.85 /sec, i.e., a'/P_o was 1.6 times larger than a/P_o.

9. Hill's force-velocity equation was generalized to the force (F)-load (P) - velocity (v) equation $(P + A)(v + b) = b\ (F + A)$, $A=a\ F/P_o$; or the force-F_v-velocity equation $F_v = (F/P_o)(P_o + a)\ v/(v + b)$.

10. The value of F_v on lengthening was 1.4 times larger than that on shortening under the same contractile force and velocity.

11. These force-load-velocity equations were valid not only during steady contractile force but also for any instance during the change in contractile force.

12. The significance of F_v, or force-dependent viscosity, is discussed with respect to the sliding theory.

CHAPTER IV

GRAPHICAL ANALYSIS AND EXPERIMENTAL DETERMINATION OF THE ACTIVE STATE

4.1 INTRODUCTION

Since the studies of Hill (1938)[36] and Wilkie (1950)[87], it has been generally considered that the skeletal muscle contains an active contractile component capable of generating tension in series with a noncontractile elastic component. On stimulating the muscle, the contractile component is brought into an " active state", which is defined by Hill (1949b)[38] as the tension developed when the contractile component is neither lengthening nor shortening. To determine the time course of the active state during a twitch, several experimental methods have been proposed. A first method described by Hill (1949b)[38] in frog sartorius muscle depends on quick stretch of the muscle at various times after stimulation. It was aimed primarily at determining the resistance to stretch or how quickly muscle reached its full capability for generating tension. A second method designed by Ritchie (1954)[70] is the quick-release method which concerns the peak of redeveloped twitch tension after a small amount of quick release at various times after stimulation. According to Hill's definition, the peak of tension curve coincides with the active state, because at the peak the change in tension with time is zero. This method, however, gave only the falling phase of the active state after the peak tension. A third method was described by Jewell and Wilkie (1960)[53]. They measured the velocity of isotonic shortening after the quick release. This gave almost the whole course of the active state, but there is some doubt about the idea that the capacity to shorten has the same physiological meaning as the capacity to develop tension.

Recently, Bahler et al. (1967)[11] presented a new analytical method for determining the whole course of the active state in rat gracilis anticus muscle. They defined the active state as a force-generating capability of the contractile component. The fact that the faster a muscle shortens the less force it exerts is interpreted as meaning that part of the force is dissipated internally as a function of the velocity, as though there were an internal load or viscous-like force. This analytical method is based on the three-component model which contains force generator, viscous-like component and series elastic component, as shown in Fig. 4.1. The active state curve was drawn as the sum of the isometric tension curve and the viscous-like force which was calculated from the force-velocity curve as the difference between the maximum force and the force exerted at each instant. This method has successfully been applied to frog cardiac muscle by Mashima and Kushima (1971)[62].

In this paper, almost the same analytical method as Bahler's was employed but difinite difference depends on the force-velocity curve. While Bahler and his co-workers applied the simple force-velocity curve of fully activated muscle to a twitch, we used the force-load-velocity curves, which are a set of load-velocity curves obtained not only on fully but also on partially activated muscle. The force-load-velocity relation has been described in chapter III. It must be emphasized that in the beginning of a twitch or during the relaxation the muscle is only partially activated.

All the physiological experiments were done on the small bundle of the frog semitendinosus muscle fibers (see section 2.3). In this place, in order to make a quick release of the muscle, an electromagnetic relay to produce instantaneous withdrawal of a small hook was connected to the isotonic lever. When it was necessary to control the shortening or lengthening velocity of the muscle, the velocity controller was connected to the isotonic

lever. A quick stretch was made by a quick release of the lever with a sufficiently heavy load. The amount of quick release was set before stimulation by adjusting the position of a stop for the lever and measured on the enlarged photograph with an accuracy of 0.01 mm. The initial length of the preparation excluding tendons is always L_o, at which it can exert the maximum tension P_o.

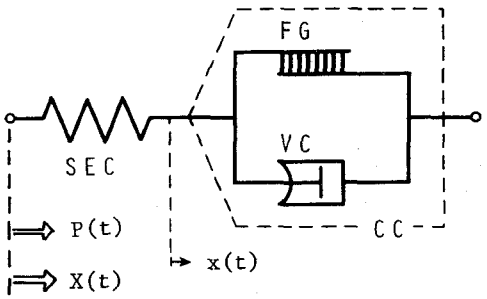

Fig. 4.1 Mechanical model of muscle. CC, contractile component; FG, force generator; VC, viscous-like component; SEC, series elastic component. P(t), measured tension; X(t), shortening of the muscle; x(t), shortening of CC.

4.2 ANALYTICAL METHOD

a) Mechanical model

It has been accepted that the mechanical behavior of the skeletal muscle can be described by a contractile component (CC) in series with a non-contractile series elastic component (SEC). Upon stimulation, the active state develops in the CC, which generates force or shortens at the velocity obeying Hill's force-velocity relation (Hill, 1938)[36]. According to Bahler et al. (1967)[11], the force-velocity curve is characterized by the CC which

develops a force, part of which is transmitted through the muscle so that it exerts tension, and part of which is dissipated internally as a fucntion of the velocity with which the CC shortens. From these considerations a new mechanical model shown in Fig. 4.1 is proposed. In this three-component model, the contractile component consists of a force generator (FG) and a viscous-like component (VC). And the muscle tension as a function of time, P(t), can be expressed by the difference between the force developed in the FG, F(t), and the velocity-dependent tension-loss in the VC, $F_V(t)$. Then we obtain

$$P(t) = F(t) - F_V(t) \tag{4.1}$$

As expressed in section 3.5, $F_V(t)$ is a hyperbolic function of the velocity and at the same time it is a linear function of the force. It is reasonable to assume that F(t) is nothing but the intensity of the active state which is difined by Hill (1949b)[38] as the intrinsic strength of the contractile component, because F(t) is a time course of the force-generating capability of the contractile component. Then the active state can be determined from P(t) and $F_V(t)$, which can be obtained from the force-load-velocity relation of CC and the tension-extension relation of SEC when P(t) is given. However, it is necessary to obtain these relations in the same muscle and under the same conditions.

b) Force-load-velocity relation of the contractile component

In the previous section 3.4, Hill's force-velocity relation,

$$(P + a)(v + b) = b\ (P_o + a)$$

was generalized to the following force-load-velocity equation:

$$(P + A)(v + b) = b\ (F + A) \qquad (v \geq 0) \tag{4.2}$$

$$A = a(F/P_o)$$

where P is the load or the force during isotonic contraction, F is the intensity of the active state or the force during isometric contraction,

v is the shortening velocity of the contractile component, P_o is the maximum isometric force, a is the heat constant and b is the rate constant of energy liberation. The value of a/P_o was 0.25 and b/L_o was 0.9 sec^{-1} in our preparation at 10 °C.

When the muscle was lengthened by a load heavier than the developed force, the relation was also described by a hyperbolic equation:

$$(P - 2F - A')(v - b') = b' (F + A') \qquad (v < 0) \qquad (4.3)$$

$$A' = a'(F/P_o)$$

The value of a'/P_o was 0.4 and b'/L_o was 0.85 sec^{-1} at 10 °C. These results were used in this chapter (see Fig. 4.4 D).

c) Tension-extension relation of the series elastic component

The tension-extension curve of SEC was directly determined by the controlled quick-release method using the velocity controller (see section 3.3). The tension-extension curve obtained is shown in Fig. 4.2. Curve A was obtained from the preparation with short tendons, in which the pelvic and tibial tendons were tied near the end of muscle fibers in order to make the tendons as short as possible. On the other hand, curve B was obtained from the long tendon preparation, both tendons of which were tied near the bones. Usually each tendon was 1-2 mm long in the long tendon preparation. In the short tendon preparation the extension of SEC was about 3.5 % of L_o at the tension of P_o but it was 4.5 % of L_o in the long tendon preparaion. Obviously, the compliance of the preparation depends on the length of tendon.

Although Sandow (1958) employed an exponential equation at the experimental formula of the tension-extension curve, we approximated this with a third power equation to facilitate computer calculation. We obtain

$$P = E_2 x_2 \qquad (4.4)$$

$$E_2 = (2.9 + 51.8 \hat{x}_2 + 1.9 \times 10^4 \hat{x}_2^2) P_o/L_o \quad \text{(for curve A)}$$

$$E_2 = (2.3 + 31.4\,\hat{x}_2 + 0.9 \times 10^4\,\hat{x}_2^2)\,P_o/L_o \qquad \text{(for curve B)}$$

$$x_2 = x - X$$

where x_2 is the extension of SEC, $\hat{x}_2$ is the normalized value of x_2 ($\hat{x}_2 = x_2/L_o$) , X is the shortening of the muscle and E_2 is the elastic coefficient of SEC.

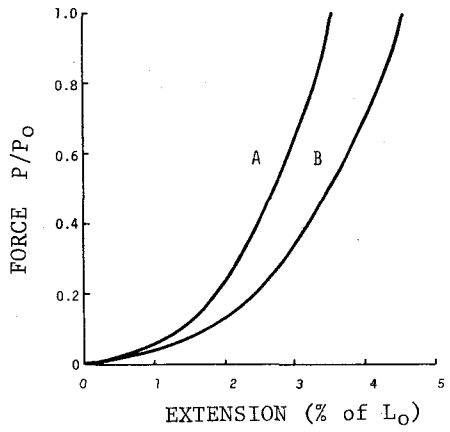

Fig. 4.2 Tension-extension curve of SEC. A, short tendon preparation; B, long tendon preparation.

d) Mathematical formulation

The active state curve, F(t), can be obtained from the force-load-velocity relation of CC expressed by Eqs. (4.2) and (4.3) and the tension-extension relation of SEC expressed by Eq. (4.4), when the tension curve, P(t), and the shortening curve of muscle, X(t), during the contraction are given.

Rearranging Eqs. (4.2) and (4.3), we obtain

$$F = f(v)\,P \tag{4.5}$$

$$f(v) = \frac{b + v}{b - \dfrac{a}{P_o}\,v} \qquad (v \gtrsim 0) \tag{4.6}$$

$$f(v) = \frac{b' - v}{b' - \left(2 + \frac{a'}{P_o}\right) v} \qquad (v \leqq 0) \qquad (4.7)$$

F, P and v are functions of time. And the velocity of CC as a function of time, v(t), can be obtained from the equation:

$$v(t) = \frac{dx_2(t)}{dt} + \frac{dX(t)}{dt} \qquad (4.8)$$

If P(t) is given, $x_2(t)$ can be calculated from Eq. (4.4). Finally, F(t) can be obtained from the tension curve P(t) and the shortening curve of muscle X(t). The blockdiagram of computer calculation of the above-described formula is shown in Fig. 4.3. If P(t) and X(t) are measured simultaneously, this analytical method to determine the active state curve is applicable not only to the isometric but also to the isotonic or any other type of contraction.

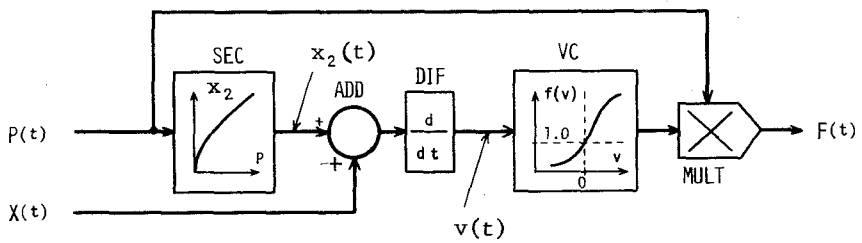

Fig. 4.3 Blockdiagram for computer calculation of the active state curve F(t), from tension curve P(t) and shortening curve X(t). SEC, function element generating the tension-extension (P-x_2) relation of SEC, (input, P; output, x_2); VC, function element generating the v - f(v) relation of VC, (input, v; output, f(v)); ADD, adder; DIF, differentiator; MULT, multiplier.

On the other hand, from Eq. (4.1) the viscous-like force is

$$F_v(t) = F(t) - P(t) \qquad (4.9)$$

Therefore, $F_v(t)$ can be obtained from P(t) and F(t). Furthermore, substi-

tuting Eqs. (4.5)-(4.7), F_v can be also expressed as a function of v and P.

$$\left.\begin{aligned} F_v &= \frac{(P_o + a)\, v}{P_o\, b - a\, v}\, v \qquad (v \geq 0) \\ F_v &= \frac{(P_o + a')\, v}{P_o\, b' - (2P_o + a')\, v}\, v \qquad (v < 0) \end{aligned}\right\} \tag{4.10}$$

4.3 DETERMINATION OF THE ACTIVE STATE DURING ISOMETRIC TWITCH

The time course of the active state, F(t), was determined from the tension curve, P(t), by the analytical method, that is, computer calculation or graphical analysis. The procedure of graphical analysis is illustrated in Fig. 4.4 on the isometric twitch of the short tendon preparation. In Fig. 4.4 A, the tension curve, P(t), at L_o is traced. As shown in Fig. 4.4 B the time course of the lengthening of SEC, $x_2(t)$, is obtained by converting P(t) through the tension-extension curve of SEC, which is the trace of Fig. 4.2 A. The curve $x_2(t)$ thus obtained is shown in Fig. 4.4 C. In the isometric contraction, X(t) is zero and the amount of the lengthening of SEC is equal to that of the shortening of CC. Then, the time course of shortening velocity of CC, v(t), is the differential of $x_2(t)$, i.e. $dx_2(t)/dt$, which is also shown in Fig. 4.4 C. The time course of f(v) in Eq. (4.6) or (4.7) is obtained by converting the curve v(t) through the v-f(v) curve which is seen in Fig. 4.4D. During the relaxation v(t) has minus sign, because the CC is lengthened, so that the v-f(v) curve in the third quardrant of Fig. 4.4 D is used. The curve f(v) thus obtained is shown in Fig. 4.4 E. Finally, the active state curve, F(t), can be drawn by the relation of Eq. (4.5) as the product of P(t) and f(v), as illustrated in Fig. 4.4 A. The viscous-like force curve, $F_v(t)$, is also drawn by using the relation of Eq. (4.9) as the difference

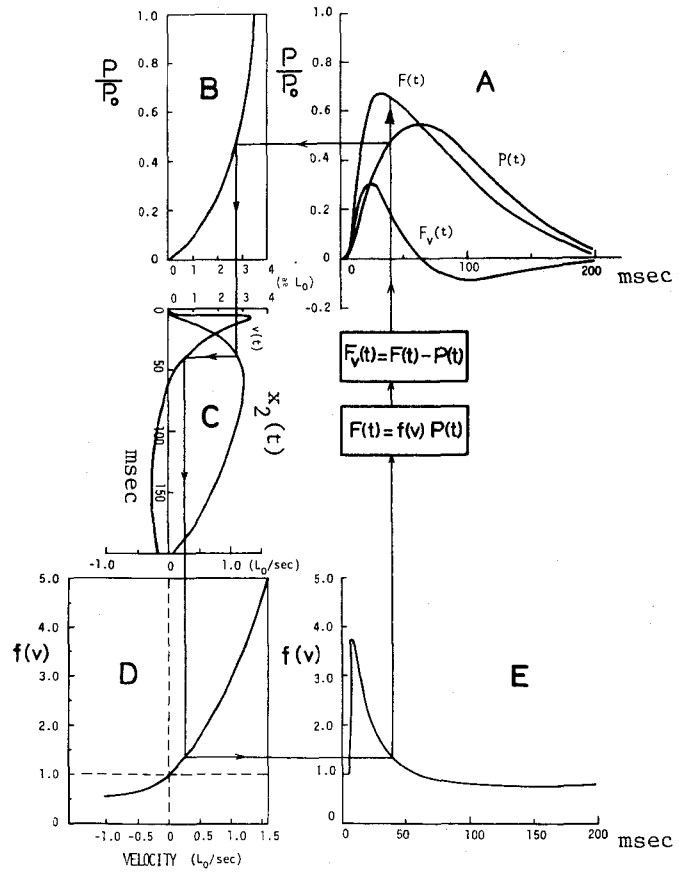

Fig. 4.4 Graphical analysis of the active state curve during isometric twitch of short tendon preparation. A, tension curve, P(t), active state curve, F(t), and viscous-like force curve, $F_v(t)$; B, tension-extension curve of SEC; C, lengthening curve of SEC, $x_2(t)$, and velocity of CC, $v(t)=dx_2(t)/dt$; D, v-f(v) curve of VC; E, f(v) curve. Arrows indicate the order of procedure.

between F(t) and P(t), as also illustrated in Fig. 4.4 A. With the long tendon preparation, the active state curve is also determined as shown in Fig. 4.5 by the same procedure, using the curve B in Fig. 4.2 as the tension-extension curve of SEC. In both preparations F(t) curve does not attain the

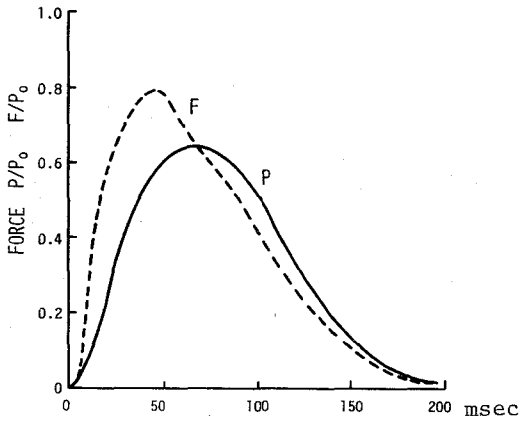

Fig. 4.5 The active state curve during isometric twitch of long tendon preparation. P, tension curve; F, active state curve determined by graphical analysis; P_o=3.7 gwt, L_o=14 mm, 10 °C.

full extent of P_o and no plateau appears during the isometric twitch. The peak value of F(t) is about 0.7 P_o in the short tendon preparation and 0.8 P_o even in the long tendon preparation. The reason for this result may be explained by the fact the long tendon preparation is more compliant and the rate of rise of tension is faster than that of the short one.

The time course of the active state developed by repetitive stimuli was also drawn by the same procedure. One of the results is shown in Fig. 4.6, where the square pulses at 100 Hz, which corresponds to the critical fusion frequency at 10 °C, are applied. The curves in Fig. 4.6 P are the isometric tension curves generated by 1, 2, 3, 4, 6 and 10 pulses. The active state curves of these contractions are shown in the lower part of Fig. 4.6. Generally, 2 or 3 pulses were necessary for the summated active state to reach the full intensity of P_o. When more pulses are applied the plateau is maintained at the level of P_o. In particular, the plateau duration at more than 6 pulses is prolonged every pulse by the amount of pulse interval. The half time of the rising phase of the active state is about 20 msec independently of the number of pulses. The half time of the falling phase increases

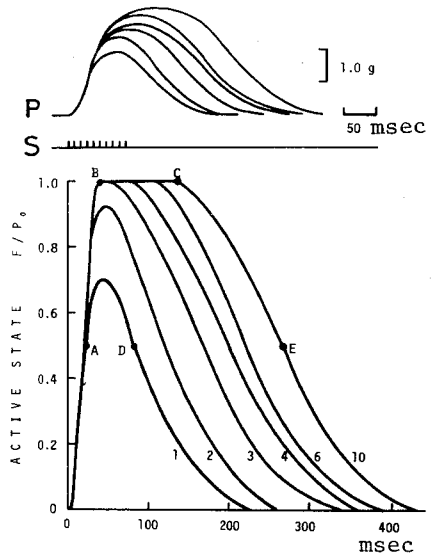

Fig. 4.6 Effect of the number of stimuli on the active state curve of isometric contraction (short tendon preparation). Upper, P, isometric tension curves generated by 1, 2, 3, 4, 6 and 10 pulses at the interval of 10 msec; S, stimuli. Lower, active state curve determined by graphical analysis; curve 1, 2, 3, 4, 6 and 10 are generated by 1, 2, 3, 4, 6 and 10 pulses, respectively. The instants A, B, C, D, E and F correspond to A, B, C, D, E, and F in Fig.4.7, respectively.

with increasing number of pulses, for example in Fig. 4.6, about 60 msec at a single pulse, 75 msec at 2 pulses and 125 msec at 3 pulses, but no more increase is observed at more than 3 pulses.

As shown in Figs. 4.4 and 4.5, the time to peak of the active state is about 40 msec in the isometric twitch of the short tendon preparation, while it is about 50 msec in the long tendon preparation. The time to plateau of the active state in the isometric tetanus is also about 40 msec as seen in Fig. 4.6, point B.

If the active state reaches its full activity during a twitch, the P-v relation at that time should satisfy the load-velocity relation at $F=P_o$. Whether the active state really reached full activity or not was checked in

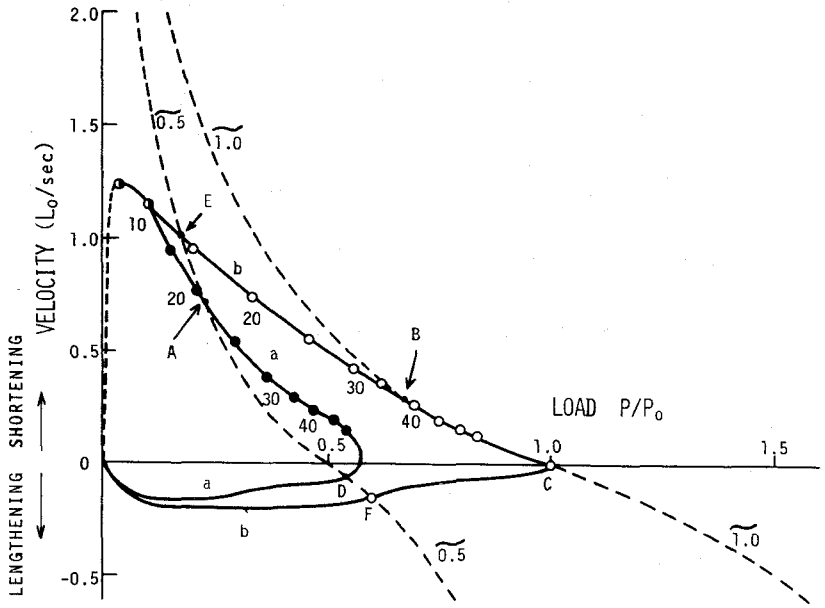

Fig. 4.7 Force-velocity relation during the twitch (filled circle, curve a) and tetanus (open circle, curve b). Dotted line 0.5 and 1.0 are P-v curves at F=0.5 P_o and F=1.0 P_o, respectively. Number under the circle represents the time after the first stimulus. A, B, C, D, E and F show the instants of A, B, C, D, E and F in Fig. 4.6 respectively.

the following way. Curve $\widetilde{1.0}$ in Fig. 4.7 shows the load-velocity curve at F= P_o which was obtained by substituting F=1.0 P_o for Eqs. (4.2) and (4.3). Curve a is the Lissajous' figure showing the relation between the muscle tension, P(t), and the velocity of CC, v(t), during the isometric twitch in Fig. 4.6. Apparently, curve a does not intersect curve $\widetilde{1.0}$. This means that the full active state is never attained at any instant during the twitch. On the other hand, curve b in Fig. 4.7 is the P-v Lissajous' curve during the 10-pulse tetanic contraction in Fig. 4.6. This curve coincides with curve $\widetilde{1.0}$ between points B and C, that is, the active state was maintained at full extent of 1.0 P_o during the period between B and C, which is about 40 to 150 msec after the first stimulus. Points B and C in Fig. 4.7 correspond to

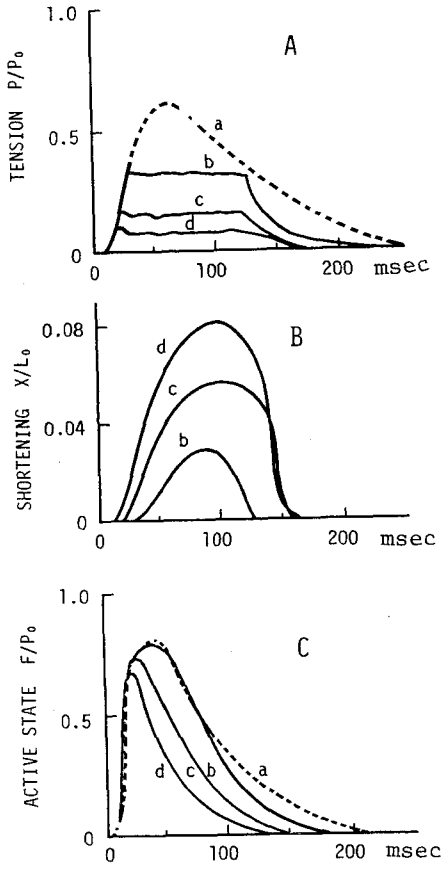

Fig. 4.8 The active state curve during isotonic contraction determined by graphical analysis. A, tension curve; B, shortening curve; C, active state curve; a, isometric twitch; b, c, d, isotonic twitch (after-load: b, 0.2 g; c, 0.45 g; d, 0.9 g); P, tension; X, shortening of muscle; F, active state. P_o=3.0 gwt; L_o=14 mm; 10 °C.

points B and C in Fig. 4.6, respectively.

Furthermore, curve $\widetilde{0.5}$ in Fig. 4.7 is the load-velocity curve at F=0.5 P_o, which was obtained by substituting F=0.5 P_o for Eqs. (4.2) and (4.3). This curve intersects curve a at A and D, and curve b at E and F. Therefore, at the instants corresponding to these ponts, the intensity of the active state is 0.5 P_o. The points A, D, E and F in Fig. 4.7 correspond to A, D, E and F in Fig. 4.6, which are the instants after 21, 75, 21 and 270 msec from the start of stimulation, respectively.

4.4 DETERMINATION OF THE ACTIVE STATE DURING ISOTONIC TWITCH

According to Mashima et al. (1972)[59], the force-load-velocity relation was valid even when the muscle length was changed between 0.8 and 1.2 L_o. Therefore, the analytical method described above is applicable to determining F(t) curve of the isotonic contraction during which the muscle length is changing, provided that the tension curve, P(t), and the shortening curve, X(t), are given. For example, Fig. 4.8 A and B are the tension and shortening curves of the after-load twitches against various after-loads. While the initial length was always kept at the slack length of L_o by the stop for the isotonic lever, the pre-load was zero. Curve a is the isometric twitch, and curves b, c and d are the after-load twitches against the load of 0.9 g, 0.45 g and 0.2 g, respectively.

Firstly, the extension of SEC, $x_2(t)$, was obtained from P(t) through the tension-extension curve of SEC. Secondly, the velocity of CC, v(t), was calculated from Eq. (4.8), using $x_2(t)$ and X(t). Finally, the active state curve F(t) was calculated from Eqs. (4.5)-(4.7). The active state curves thus obtained are shown in Fig. 4.8 C. Apparently, the time course of the active state varies with load, especially in duration. With a decrease in the load, the duration, time to peak and peak intensity clearly decrease. All of them are largest under the isometric condition. Although the rate of rise or fall of the active state is almost unchanged, the rate of rise increases slightly at the transition from isometric to isotonic contraction.

4.5 INSTANTANEOUS RECORDING OF THE ACTIVE STATE WITH ISOMETRIC TENSION CURVE

Instead of the graphical analysis described above, of course, it is possible to record the active state curve of the isometric contraction simultaneously with the tension curve, using an on-line computer which operates the electronic circuit shown in Fig. 4.3. But this procedure is too compli-

cated for the practical use, because the circuit contains two variable function elements and a multiplier. Therefore, we assumed that the elastic coefficient of SEC, $\hat{E}_2$, is a constant which is independent of tension and that the viscous coefficient of VC, $\hat{B}_2$, is a constant which is independent of force or velocity, because the displacement of CC is sufficiently small in an isometric contraction and the viscosity would be a linear function of velocity as the first approximation. Then, we obtain the following equation instead of Eq. (4.4),

$$P(t) = \hat{E}_2 \, x_2(t) \tag{4.11}$$

and also obtain instead of Eq. (4.1)

$$P(t) = \hat{F}(t) - \hat{B}_2 \frac{dx_2(t)}{dt} \tag{4.12}$$

Then we obtain

$$\hat{F}(t) = P(t) + k \frac{dP(t)}{dt} \tag{4.13}$$

$$k = \hat{B}_2 / \hat{E}_2$$

where $\hat{F}(t)$ is the approximate value of F(t). From Eq. (4.13), $\hat{F}(t)$ can be obtained as the sum of the isometric tension curve, P(t), and its differential curve, dP(t)/dt. These calculations can easily be made by a more

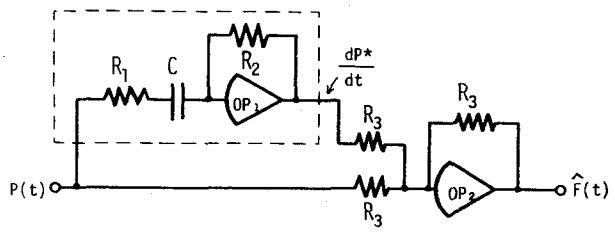

Fig. 4.9 Operational circuit for calculating the approximate active state curve, $\hat{F}(t)$, during isometric contraction(see Eq. (4.14)); OP_1 and OP_2, linear operational amplifiers.

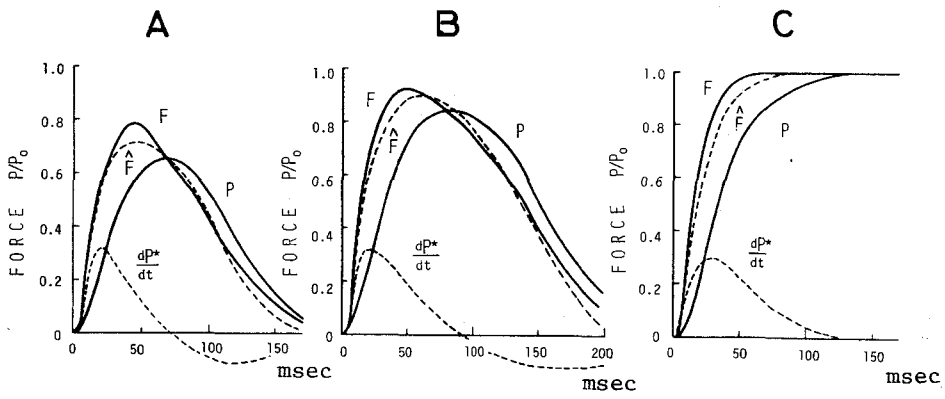

Fig. 4.10 Comparison of the approximate curve ($\hat{F}$) with the active state curve determined by graphical analysis (F). $\hat{F}$ = P + dP*/dt; P, measured isometric tension curve; A, single pulse; B, 2 pulses; C, 16-pulse stimulation; stimulus interval, 12.5 msec.

simplified circuit, containing only linear operational amplifiers as shown in in Fig. 4.9. Thus, an instantaneous recording of the active state becomes far easier. Theoretically, a complete differential operation can be made when R_1 in Fig. 4.9 is zero. If so, the circuit would become unstable because of the overload for the amplifier. Therefore, the approximate differential circuit seen in Fig. 4.9 (broken line) was used for practical application. The transfer function of the circuit is $ks/(1+\tau s)$, where $k=CR_2$, $\tau=CR_1$ and the symbol s represents Laplace transform variable. If the time constant, τ, is set to be sufficiently small compared with that of tension response, the differential operation is accurate enough, at least for practical use. Finally, the approximate calculation is expressed by the following equation instead of Eq. (4.13),

$$\hat{F}(t) = P(t) + \frac{dP(t)^*}{dt} \tag{4.14}$$

$$\frac{dP(t)^*}{dt} = \mathcal{L}^{-1}\left[\frac{k\,s}{1+\tau s}\,P(s)\right]$$

where the symbol $\mathcal{L}^{-1}[G(s)]$ denotes inverse Laplace transform of G(s), and P(s) is the Laplace transform of P(t).

In order to operate this equation, the time constants, k and τ, have to be determined. In frog ventricle, it has been confirmed experimentally by Mashima and Kushima (1971)[62] that the value of k is almost unchanged with the change in muscle length, taking the nonlinearity of SEC and VC into consideration, and the value of k is 0.05-0.056 sec at 20 °C. But in the skeletal muscle, it is impossible to estimate theoretically or experimentally this value of k, because of the complicated nonlinearity of VC. Therefore, the values of k and τ were estimated by trial and error so as to let $\hat{F}(t)$ coincide closely with the active state curve determined by the graphical analysis. Eventually, best fit was obtained when k=17.0 msec and τ=4.2 msec in our preparation at 10 °C. One of the results of computer calculation in the long tendon preparation is shown in Fig. 4.10. Fig. 4.10 A represents the isometric twitch, Figs. B and C the isometric contractions by 2 and 16 pulses with the interval of 12.5 msec, respectively. Curve P is the measured tension curve, curve F is the active state curve determined by graphical analysis and curve $\hat{F}$ is the approximate curve obtained from Eq. (4.14). The $\hat{F}(t)$ curve shows fairly good coincidence with the F(t) curve in these isometric contractions, when the above-mentioned time constants are employed.

On materialization of the circuit shown in Fig. 4.9, the values of k=17.0 msec and τ=4.2 msec were selected, for example, by setting C=1.0 μF, R_1=4.2 KΩ and R_2=17.0 KΩ. But even if the value of R_1 is not accurately 4.2 KΩ but, for example, 5.0 KΩ , there would be very little effect on $\hat{F}(t)$. Moreover, on inspection of Fig. 4.4 or 4.10, it is seen that the peak value of $F_v(t)$ is about half that of P(t) in an isometric twitch. Therefore, it is not necessary to look for the most adequate value of R_2 by the trial and error method described above, rather it is far more practical to adjust the gain of differential curcuit in the following way. Firstly, P(t) and dP/dt

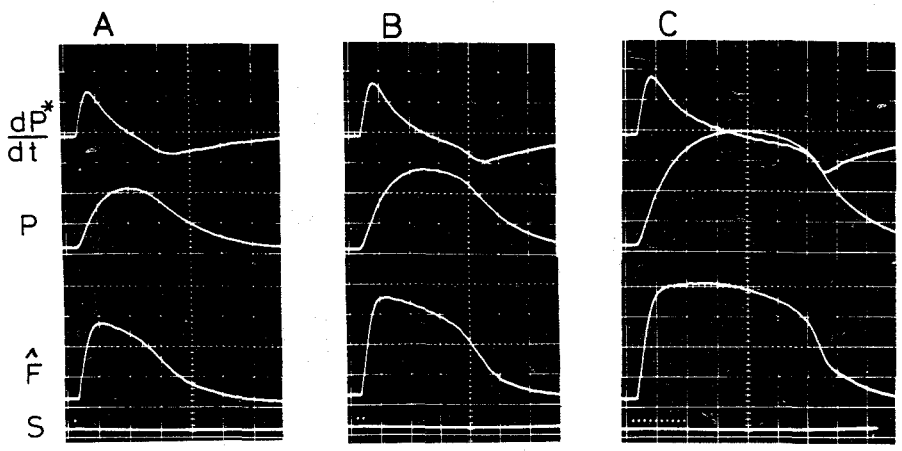

Fig. 4.11 Simultaneous recording of isometric tension P, dP*/dt and $\hat{F}$ curves. A, single pulse; B, 2 pulses; C, 10-pulse stimulation; stimulus interval, 10 msec; ordinate, 2.0 g/div; sweep, 50 msec/div; S, stimulus; long tendon preparation; L_o=14 mm; 10 °C.

curves of isometric twitch are displayed simultaneously on a CRT. Secondly, the gain of the amplifier for dP/dt, that is, the value of R_2, is adjusted until the maximum amplitude of dP/dt becomes about half that of P(t). In this way, P(t), dP/dt and $\hat{F}(t)$ curves were recorded simultaneously as shown in Fig. 4.11. Another piece of evidence which may verify this conventional way is the fact that the plateau phase in the $\hat{F}(t)$ curve of isometric tetanus was completely smoothed at the level of P_o as shown in Fig. 4.11 C, when the maximum dP/dt of the twitch was adjusted so as to be about half the maximum P(t) of the twitch as seen in Fig. 4.11 A. If the gain of dP/dt is raised higher than that, a spike-like hump higher than P_o appears in the initial phase of $\hat{F}(t)$ curve of the tetanus.

4.6 EXPERIMENTAL DETERMINATION OF THE ACTIVE STATE

a) Quick-release method

The active state after the peak of isometric curve was determined experimentally by the quick-release method devised by Ritchie (1954)[70], and it was

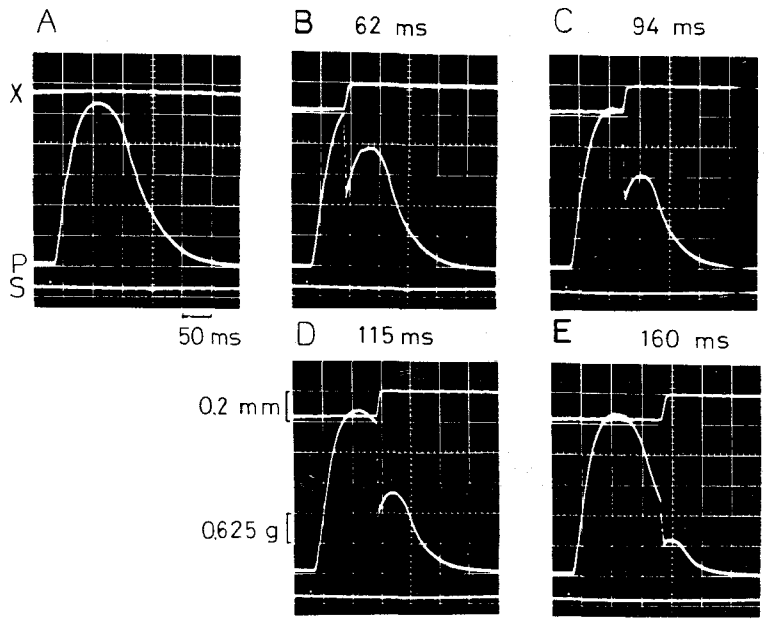

Fig. 4.12 Changes in tension curve by quick release during isometric twitch. A, isometric twitch; B, released at 62 msec; C, 94 msec; D, 115 msec; E, 160 msec after stimulus; amount of release, 0.18 mm (1.5 % of L_o); X, length curve, 0.2 mm/div; P, tension curve, 0.625 g/div; S, stimulus; sweep, 50 msec/div; P_o=5.4 gwt; L_o=12 mm, 10 °C.

compared with the active state curve determined by graphical analysis. According to Jewell and Wilkie (1960)[53], Ritchie's method might underestimate the duration of the active state, but it was possible to reduce this error by decreasing the amount of quick release; for example, in the frog sartorius muscle when the release was 1.6 % L_o (L_o=31 mm, amount of release =0.5 mm, 0 °C), the measured active state curve almost conincided with the correct one. In the present study, the amount of release was set at 1.5-7.5 % L_o. One of the results when the amount of release was 1.5 % L_o (L_o=12 mm) is shown in Fig. 4.12. The muscle was released from L_o+0.18 mm to L_o at various times after stimulation. Tension curve, P, and shortening curve, X, were recorded simultaneously. The curve connecting a series of peaks of the redeveloped tension after the release gave the tail of the active state. In order to

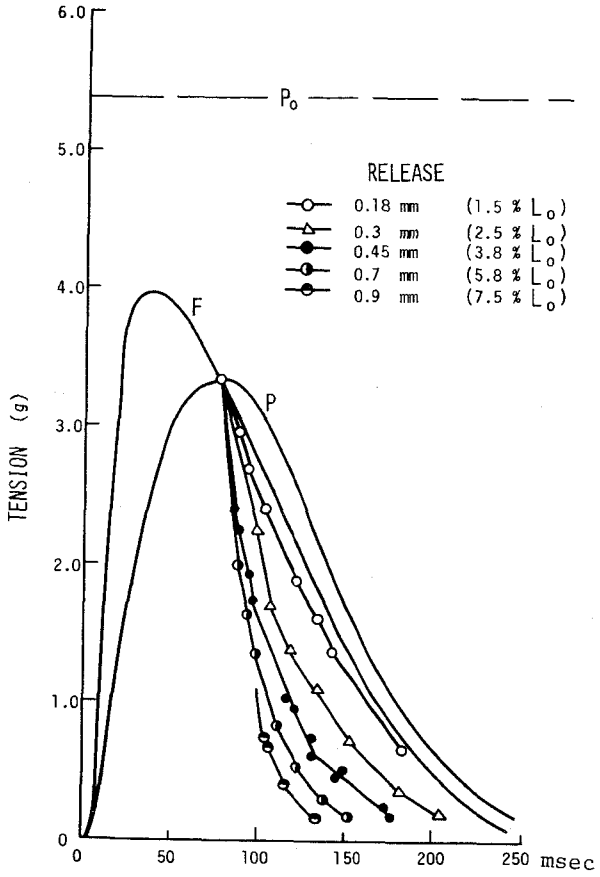

Fig. 4.13 Effect of the amount of quick release on the falling phase of the active state during isometric twitch. Amount of release is shown in the figure. P, Tension curve; F, active state curve determined by graphical analysis; P_o=5.4 gwt; L_o=12 mm; 10 °C.

examine the effect of the amount of release on the time course of the active state, various amounts of quick releases, such as 0.3, 0.45, 0.7 and 0.9 mm, were also applied. The curves obtained are traced in Fig. 4.13. Even when the amount of release is as small as 1.5 % L_o, the experimental curve agrees only approximately but not completely with curve F which is determined by the graphical analysis. As the amount of release increases, the experimental curve decays more quickly, and the duration of the active state decreases,

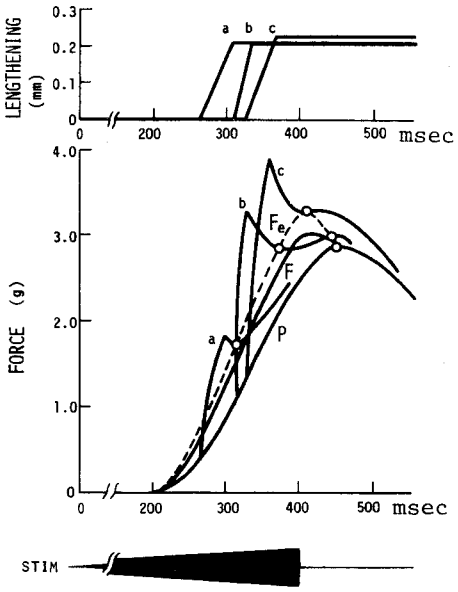

Fig. 4.14 The rising phase of the active state determined by quick stretch method (open circle). Upper trace, length curves. Lower, tension curves; P, tension curve; F, active state curve determined by graphical analysis; F_e, active state curve determined by quick stretch method; STIM, AC at 300 Hz with linearly increasing voltage, in the excess potassium solution; time and amount of stretch: a, at 265 msec after the start of stimulation and 0.21 mm; b, at 310 msec and 0.21 mm; c, at 325 msec and 0.22 mm; P_o=6.3 gwt; L_o=13 mm; 10 °C.

conforming to the observation by Briden and Alpert (1972).[15] These results suggest that a quick release causes some deactivation of the contractile mechanism and its degree increases with increasing amount of quick rlease.

b) Quick-stretch method

It is impossible to determine the rising phase of the active state curve by Ritchie's quick-release method. However, applying quick stretches at various times during the rising phase and plotting the troughs of redeveloped tension, the early part of the active state curve can be obtained, because at the trough, as well as at the peak, the contractile component is neither

lengthening nor shortening. We applied the quick stretch during the rising phase of the isometric twitch. But it was extremely difficult fo observe a measurable trough in tension curve at 10 °C, because the peak time was only 75 msec from the stimulus and the rate of rise of tension was too fast. In order to slow down the tension development, the muscle was soaked in excess potassium Ringer's solution([KCl] = 14 mM) and stimulated by AC at 300 Hz with linearly increasing voltage, as described by Mashima and Tsuchiya (1968)[64]. The tension curve thus obtained is curve P in Fig. 4.14. The muscle (L_o = 13 mm) was stretched at constant speed using a velocity controller by 0.21 mm (1.6 % L_o) from L_o-0.21 mm to L_o. The instant of stretch was 265 msec in a, 310 msec in b and 325 msec in c from the start of stimulation. Immediately after the quick stretch the tension shows a sudden rise and stress relaxation, and then it redevelops, forming a trough. At the bottom of the trough, P(t)= F(t), because v(t)=0 and f(v)=1.0 in Eqs. (4.5) and (4.6). Curve F_e in Fig. 4.14 was obtained by plotting these troughs. Curve F represents the active state curve determined from curve P by graphical analysis. Both curves agree approximately in the rising phase but they differ considerably near the peak. While the difference increases with tension, it is suggested that the contractile component must be activated even by such a small amount of stretch and the degree of activation depends on the contractile force.

When the temperature was lowered to 0 °C, the rate of rise of tension was sufficiently slowed for the application of quick stretch. Therefore, the stretch experiment was repeated at 0 °C using a single pulse stimulation. One of the results is shown in Fig. 4.15. The tension, P, and muscle length, X, are recorded simultaneously. The original record of isometric twitch curve at L_o is shown in A. In B, C and D, the muscle was stretched from L_o-0.25 mm to L_o (L_o=14 mm) by 0.25 mm (about 1.8 % L_o) at 42, 55, and 72 msec after the stimulus, respectively. In Fig. 4.16, curve P is the trace of tension curve P in Fig. 4.15. Curve a is the active state curve obtained by

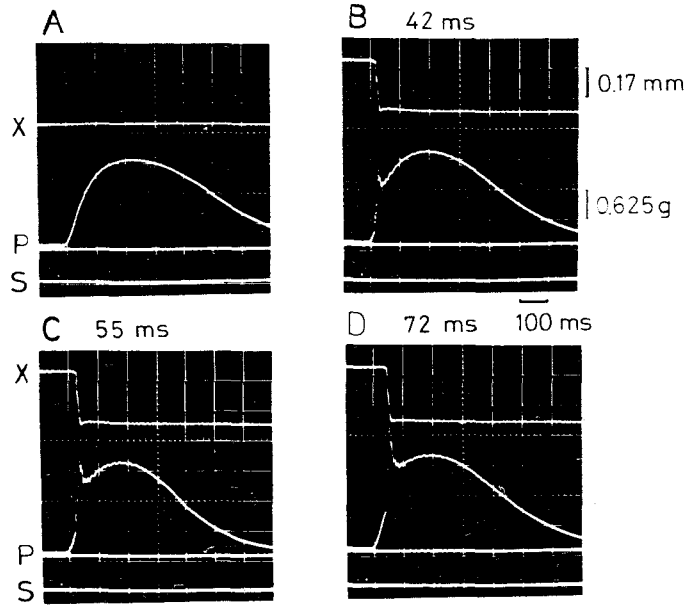

Fig. 4.15 Changes in tension curve by quick stretch during isometric twitch. A, isometric twitch; B, stretched at 42 msec; C, 55 msec; D, 72 msec after stimulus; amount of stretch, 0.25 mm (1.8 % L_o), from L_o-0.25 mm to L_o; X, length curve, 0.17 mm/div; P, tension curve, 0.625 g/div; S, stimulus; sweep, 100 msec/div; P_o=2.25 gwt; L_o=14 mm; 0 °C.

plotting the troughs after the stretch. In order to examine the effect of the amount of stretch on the time course of the active state, the amount of stretch was varied to 0.36, 0.46 and 0.57 mm, always keeping the final length at L_o. Curves b, c and d in Fig. 4.16 are the active state curves obtained by these experiments. Obviously, as the amount of stretch increases, the active state increases and the rate of rise becomes quicker, that is, the degree of activation caused in the contractile mechanism depends on the amount of quick stretch. But it is confirmed that the active state does not reach its full extent of P_o during the isometric twitch even at 0 °C and even in th the muscle activated by the quick stretch of 3.6 % L_o.

Finally, it is concluded that the analytical method is more favorable than the experimental method for derermineing the active state curve,

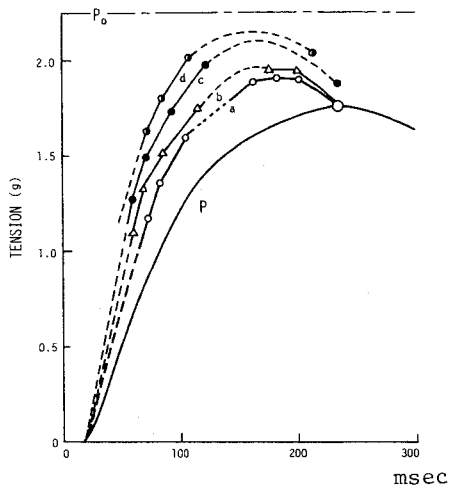

Fig. 4.16 Effect of the amount of quick stretch on the rising phase of the active state during isometric twitch. Amount of stretch: a, 0.25 mm; b, 0.36 mm; c, 0.46 mm; d, 0.57 mm; P, tension curve; P_o= 2.25 gwt; L_o=14 mm; 10 °C.

because no release or stretch is applied during the contraction. Only an approximate curve can be obtained by the quick-release or -stretch method, when the amount of release or stretch is less than 2 % of the muscle length.

4.7 DISCUSSION

The material used in the present study was a small bundle preparation obtained from the semitendinosus muscle of the frog. The elastic property of this preparation was quite similar to that of the single fibers examined in chapter III or Mashima et al. (1972).[59] Therefore, the results obtained would be comparable with those obtained on a single fiber. And most of the experiments were performed at 10 °C, because the sarcoplasmic reticulum is ready to release Ca ion below 10 °C in caffeinized muscle fiber (Sakai, 1965)[73] and even in normal muscle fiber a cooling contracture begins to occur below 5 °C (Sakai, 1967)[74], although the mechanical measurement after quick release is far easier at 0 °C than at 10 °C.

The contractile force, F, and the load, P, were separated and discussed in detail by Mashima et al. (1972).[59] They stated that the difference between F and P was the viscous-like force, F_v, because when the muscle was released from isometric to isotonic contraction, the force was decreased from F to P, as though there were a viscous-like force, which worked as a function of velocity. The three-component model in the present study was derived from this consideration. The active state curves during isometric and isotonic contraction were obtained by computer calculation or graphical analysis based on the model by assuming that the force of the force generator in the contractile component, F(t), is nothing but the active state, as proposed by Bahler et al. (1967).[11] The three-component model is not a mere extension of the classical viscoelastic model established by Gasser and Hill (1924)[33] and Levin and Wyman (1927),[57] but a natural conclusion derived from the modern concept of the sliding filament mechanism. The force generator may correspond to a sliding-force generator at the cross-bridge between myofilaments.

The analytical method described in the present study is similar to that proposed by Bahler et al. (1967),[11] but we employed the force-load-velocity relation which fits at any contractile force (at $F \leqq P_o$), instead of the conventional force-velocity relation which fits only when the contractile force is maintained at the maximum force (at $F = P_o$). Actually, the contractile force is less than P_o during the rising phase or relaxation, probably because some of the cross-bridges are not in active state. The advantages of the analytical method for the determination of the active state are as follows: (i) quantitative calculations are possible for the entire course of the active state of isometric and isotonic contrations, (ii) when the tension-extension curve and the force-load-velocity curves of the preparation are known, only the tension curve is needed to determine the active state curve during isometric

contraction and no quick release or quick stretch is required, (iii) the active state curve can be obtained simultaneously with the tension and shortening curves, using the operational circuit shown in Fig.4.3, (iv) the approximate active state curve during isometric twitch can easily be recorded by means of the simple circuit shown in Fig. 4.9, which contains only a linear operational amplifier.

Since the study of Hill (1949)[38], the abrupt transition from rest to full activity has generally been accepted in the frog sartorius muscle at $0^{o}C$ and many studies (Ritchie, 1954[70]; Jewell and Wilkie, 1960[53]; Edman and Kiessling, 1971[31]) have been done along this line. However, Bahler et al. (1967)[11] pointed out that the active state does not reach the maximum value of P_o but 0.92 P_o at $17.5^{o}C$ in rat gracilis anticus muscle. Our results showed that the peak intensity of the active state during the isometric twitch reached only 0.7-0.8 P_o at $10^{o}C$ or $0^{o}C$, and no plateau phase was observed. Two or three stimuli were necessary for the active state to reach its full intensity and form a plateau. The muscle force does not reach its full extent so abruptly but it takes about 40-50 msec at $10^{o}C$. Therefore, the force-velocity relation at $F < P_o$ should be applied during this period. Edman and Kiessling (1971)[31] analyzed the rising and falling phases of the active state by applying four shocks and plotting the peaks and troughs of the isometric myogram. From these experiments, however, it is difficult to conclude that the active state reaches its full intensity by a single shock, because the peak or trough produced by the second or later shocks may indicate an intensity of the summated active state, which, of course, reaches the maximum intensity.

According to Jewell and Wilkie (1958)[52], the active state takes approximately 60 msec to become fully established at $0^{o}C$. Our result was about 40 msec at $10^{o}C$. Taking the temperature difference into account, these results agree rather well. The peak time of dP/dt curve is considerably shorter

than the peak time of the active state as seen in Fig 4.10A. This would explain the value of 40 msec at 0^{o}C obtained by Close (1962)[22]. The very rapid rise of the active state reported by Edman (1970)[30] may depend not on the initial development of tension but on the development of tension enhanced by previous stimuli.

The rate of rise of the active state increased slightly at the transition from isometric to isotonic contraction. More precise measurement was impossible because of the disturbance caused by mechanical oscillation at the transition, but a quicker rate of rise in the isometric one was clearly shown in the frog ventricle by Mashima and Kushima (1971)[62]. This fact suggests that the active cross-bridge requires a higher rate of force development or energy liberation when it moves against the viscous-like force, although the duration of the active state is shortened.

It was pointed out by Jewell and Wilkie (1960)[53] that the active state can be determined accurately when the amount of quick release is less than 2% L_o. In our results also the active state curve determined by the experimental method is, practically speaking, accurate enough when the amount of release or stretch is less than 2% L_o. But as seen in Fig. 4.16, the intensity of the active state increases with increasing amount of quick stretch almost in proportion to the amount of stretch. According to Abbott and Aubert (1952)[1], if a tetanically stimulated muscle were stretched to a given length it would generate more tension and be able to do more work that during an isometric contraction at that length. Ruegg et al. (1970)[72] observed a transient delayed rise in tension caused by abrupt stretch and suggested that an activation of contractile linkages caused by stretching may account for this tension rise. The measured increase in the active state may be brough about by such activation of cross-bridges, and contractile machinery may have a mechanism to store part of the energy supplied by stretching.

Contrary to this, as seen in Fig. 4.13, the intensity of the active state obtained by quick release decreases almost proportionally with increasing amount of quick release. Recently, Briden and Alpert (1972)[15] found that the active state decreased as the extent of shortening or release was increased and for each 0.1 mm of isotonic shortening there was a 2% decrease in active state force. From these observations it is apparent that quick release produces a large decrement in the muscle force. As pointed out by Rüegg et al. (1970),[72] a deactivation of the contractile mechanism caused by shortening might account for the decrease in contractile tension after a quick release. And the muscle may have a mechanism to sustain part of the declining energy which is rapidly exhausted by a quick release or even by an active shortening. In order to simulate the change in active state caused by the quick change of length, parallel elasticity within the contractile component must be assumed. Although the physiological meaning of this elasticity is unknown, the presence of an elastic element and another elastic element with viscous as well as elastic properties in the myofilaments has recently been suggested by Huxley and Simmons (1971).[46]

The analytical method described in the present study is more favorable than the experimental method for determining the active state, because no release or stretch is applied during the contraction. Of course, the quick release is employed when the tension-extention curve or the force-velocity curve is determined. According to Civan and Podolsky (1966),[21] the contractile force reaches a steady value before the velocity becomes steady when the load is changed, and the characteristics of the nonsteady state depend on the change in load and on temperature. But the force-velocity relation is usually mesured after the nonsteady period, where the CC shortens at a constant speed. And the nonsteady period can be shortened when the oscillation in shortening curve is minimized by the device of controlled release. Moreover, Jewell and Wilkie (1960)[53] and Mashima et al. (1972)[59] verified that the force-velocity relation is applicable any time during contraction.

4.8 CONCLUSION

1. The time course of the active state was calculated by mathematical analysis based on the three-component model, and compared with the experimental curve determined by quick release or stretch in the small bundle preparation dissected from frog semitendinosus muscle at $10^{o}C$.

2. The three-component model contains a contractile component, which consists of a force generator and a viscous-like component, and a series elastic component. The active state as the force of the force generator is determined by substituting the tension and velocity curves of the contractile component for the force-load-velocity relation.

3. By this analytical method, the entire active state curve can be determined not only in the isometric but also in the isotonic contraction.

4. The active state of the isometric twitch does not reach its full extent of P_o but only 0.7-0.8 P_o.

5. In the isotonic contraction the duration of the active state decreases with decreasing load, and the rate of rise of the active state increases at the transition from isometric to isotonic contraction.

6. The active state curve determined by quick release or quick stretch agrees approximately with the curve determined by the analytical method when the amount of release or stretch is less than 2% of the muscle length, although the experimental curve varies with the amount of release or stretch.

CHAPTER V

ANALYSIS OF DYNAMIC CHARACTERISTICS OF MUSCLE CONTRACTION BY A MECHANICAL MODEL

5.1 INTRODUCTION

High quality physiological data concerning the behaviors of skeletal muscles have been accumulated by a wide range of physiological experiments, which have led to the establishment of certain basic concepts of muscle contraction (Hill, 1938[36]; A. F. Huxley, 1957[45]; Jewell and Wilkie, 1958[52]). Since the classical viscoelastic model was introduced by Gasser and Hill (1924)[33], several kinds of mechanical models have been presented in parallel with extensive physiological recordings (Levin and Wyman, 1927[57]; Hill, 1949b[38]; Wilkie, 1950[87]; Buchthal and Kaiser, 1951[17]; Bornholst and Minardi, 1970[14]). Eventually, the two-component model consisting of the contractile component and the series elastic component has been generally accepted as a basic one (Ritchie and Wilkie, 1958[71]; Pringle, 1960[69]; Houk, 1966[44]; McRuer et al., 1969[58]; Apter and Graessley, 1970[7]). More recently, Bahler (1968)[10] has developed an analytical model based on an analysis of experimental data in rat gracilis anticus muscle. Bahler's approach is similar to that proposed by Carlson (1957)[18] which consists of factoring the pertinent variables of muscle contraction into a series of functions. However, these quantitative approaches involving mathematical descriptions and formulation of the models have been rather meagre, because none of them goes beyond a fragmentary explanation of specific phenomena.

In this chapter, a mathematical model of skeletal muscle is developed based on physiological findings revealed in chapters III and IV. The model consists of a force generator and elastic and viscous components of the resting and contracting states. Mechanical behaviors, including nonlinear properties, exhibited by the muscle under various physiological conditions are

plainly interpreted in the fully dynamic sense by means of simulation studies. Responses of the model obtained from the simulations are compared with those from frog semitendinosus muscles. Physiological meanings of viscous and elastic components are discussed with reference to the ultrastructure of the sarcomere and the sliding-filament theory. The present study is evidently useful to engineers interested in the neuromuscular control system and in the design of an orthotic system that utilizes paralyzed skeletal muscles. In fact, the proposed model is extended to investigation of the neuromuscular control system in Part II.

5.2 VISCOELASTIC MODEL

a) Modeling

In order to understand how the muscle system works in the fully dynamic sense and to obtain the required quantitative data on mechanical internal system variables, different mechanical experiments such as isovelocity lengthening and step change in load were made on the resting and contracting muscles. The model illustrated in Fig. 5.1 is postulated as the simplest and adequate one to explain those experimental results, which is the complete model elaborated by assembling the two partial models in the resting and active muscles. The model consists of the elastic components (SEC_1 and PEC_1) and the viscous one (VC_1) in the resting state, and the force generator (FG), the elastic component (SEC_2) and the viscous-like component (VC_2) in the contracting state. It comprises also the elastic element (SEC_t) corresponding to the tendon. The features of the model are as follows.

i) Mechanical properties of the resting muscle can be exhibited by passive elements such as tendon, membrane, sarcoplasma and connective tissue. Examing the responses of the resting muscle to ramp-wise increase of

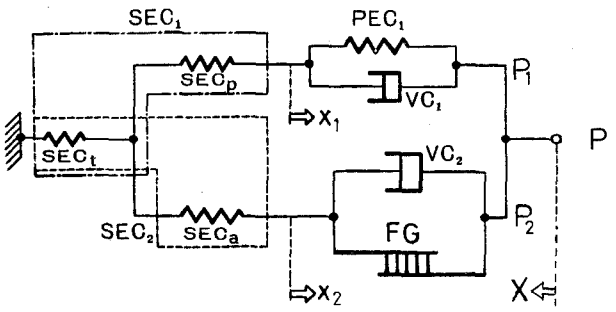

Fig. 5.1 Mechanical model of skeletal muscle. SEC, series elastic component; PEC, parallel elastic component; VC, viscous component; FG, force generator. P, P_1, P_2, tension; x_1, x_2, extension of SEC; X, shortening of muscle.

the muscle length, it is indicated at section 3.2 that the muscle dynamics can be described by the three-component model in Fig. 5.1 (SEC_1, PEC_1 and VC_1).

ii) Because linkages between actin and myosin filaments are produced in the contracting state, additional elements should be introduced. According to Hill (1938[36], 1949b[38]) and Jewell and Wilkie (1958)[52], contracting muscle has been divided into two components; a nonlinear series elastic and a contractile one obeying hyperbolic force-velocity relation. On the other hand, according to Bahler (1968)[10], the contractile component consists of two components, a force generator and a velocity-dependent (viscous-like) component which explains the nonlinear property of the force-velocity curve. Thus, the similar mechanical model in Fig. 5.1 which consists of FG, VC_2 and SEC_2 is chosen for the contracting muscle. The mass of muscle has minor effects on muscle dynamics and may be neglected.

b) Quantitative estimations

Each characteristics of the components was determined by the input-output relations between change in length and in tension of muscle which were obtained from various kinds of mechanical experiments. Since possible length

TABLE V-1

MECHANICAL PARAMETERS OF THE MUSCLE

PEC_1	$E_p = 0.21\ P_o/L_o$	
SEC_t	$E_t = 100.0\ P_o/L_o$	
SEC_1	$E_1 = 1.3\ P_o/L_o$	
SEC_2	$E_2 = (2.96 + 51.8\ \hat{x}_2 + 1.9 \times 10^4\ \hat{x}_2^2)\ P_o/L_o$	
VC_1	$B_1 = 0.014\ P_o/(L_o/\text{sec})$	
VC_2	$B_2 = \dfrac{F\ (P_o + a)}{P_o\ (v + b)}$	$a/P_o=0.25$, $b=0.9\ L_o/\text{sec}$, $(v \geqq 0)$
	$B_2 = \dfrac{F\ (P_o + a')}{P_o(b' - v)}$	$a'/P_o=0.4$, $b'=0.85\ L_o/\text{sec}$, $(v \leqq 0)$

change of the intact muscle is less than about 10 % of L_o, characteristics of each component were measured within this limit of variation in length. Measured viscous and elastic constants are shown in Table V-1. They were estimated as follows.

Dynamic chracteristics exhibited by the resting muscle were approximately linear ones, and described by the transfer function (Akazawa, Fujii and Kasai, 1969)[31]:

$$\frac{P_1(s)}{X(s)} = -\frac{K_o\ (1 + T_2 s)}{(1 + T_1 s)} \tag{5.1}$$

$$K_o = E_1\ E_p\ /(E_1 + E_p)\ ,\quad T_1 = B_1/(E_1 + E_p),\quad T_2 = B_1/\ E_p \tag{5.2}$$

where P_1 = tension on muscle at the resting state,

X = shortening of muscle,

E_1 = elastic constant of SEC_1,

E_p = elastic constant of PEC_1,

B_1 = viscous constant of VC_1,

K_o = constant,

T_1, T_2 = time constants.

Equation (5.1) was programmed on an analog computer. The constants K_o, T_1 and T_2 were chosen so that the model responses might give a good fit to the experimental data of the resting muscles at ramp stretching as shown in Fig. 5.3. Then, the elastic constants E_1 and E_p and the viscous constant B_1 were automatically estimated from Eq. (5.2). The results are given in Table V-1.

The load-extension relation of the series elastic component SEC_2 is obtained from the relation between the applied load and the instantaneous shortening immediately after the quick release of an active muscle (see section 3.3). The obtained load-extension curve of SEC_2 did not obey Hook's law. The curve in Fig. 3.8 b is expressed by the equation;

$$f_s(x_2) = E_2\, x_2$$

$$E_2 = (2.96 + 51.8\, \hat{x}_2 + 1.9 \times 10^4\, \hat{x}_2^{\,2})\, P_o/L_o \qquad (5.3)$$

where x_2 = extension of SEC_2,

$\hat{x}_2$ = normalized extension of SEC_2, $\hat{x}_2 = x_2/L_o$,

$f_s(x_2)$ = force across SEC_2, function of x_2,

E_2 = elastic coefficient of SEC_2,

P_o = maximum tension developed at the length L_o,

L_o = standard length of muscle.

The load-extension curve of isolated tendons was nearly straight. The same tension as P_o was obtained when the tendon was stretched about 1 % of L_o; namely the elastic constant of the tendon E_t in this preparation is about 100.0 P_o/L_o.

The viscous-like force of the contracting muscle might be developed in the force-generating-machine which accounts for the sliding of the filaments. Thus the viscous-like component VC_2 is nothing but the velocity-dependent element in the contractile component. From this, the relation between viscous-like force and velocity can be determined from the load-velocity relation of the contracting muscle. The load-velocity relation of shortening muscles at various contractile forces has been already determined in section

3.5 and Hill's (1938)[36] hyperbolic equation is generalized:

$$(P + A)(v + b) = b\,(F + A) \qquad (v \geqq 0) \qquad (5.4)$$

$$A = a\,(F/P_o)$$

$$v = \dot{x}_2 + \dot{X}$$

where P = tension on muscle,

v = velocity of the contractile component,

a, b = dynamic constants of Hill's (1938)[36] equation,

F = contractile force generated in FG.

The dynamic constants were $a/P_o=0.25$ and $b=0.9\ L_o$/sec. Note that P_o is the maximum value of the contractile force F and that P is not the exerting force but the load (tension) of muscle. Namely, the viscous-like force is expressed by F-P (Mashima, Akazawa, Kushima and Fujii, 1972)[59]. From Eq. (5.4), viscous coefficient B_2 is expressed as a function of v and F:

$$F_v = F - P \qquad (5.5)$$

$$= B_2\, v$$

$$B_2 = F\,(P_o + a)/P_o\,(v + b) \qquad (5.6)$$

where

F_v = viscous-like force in VC_2,

B_2 = viscous-like coefficient of VC_2.

The load-velocity relation of the lengthening muscle has been also determined as a hyperbolic equation:

$$(P + 2\,F - A')(v - b') = b'\,(F + A') \qquad (v \leqq 0) \qquad (5.7)$$

$$A' = a'\,(F/P_o)$$

where a', b' = dynamic constants.

The constants were $a'/P_o=0.4$ and $b'= 0.85\ L_o$/sec. Then, viscous-like constant of the lengthening muscle becomes

$$B_2 = F\,(P_o + a')/\,P_o\,(b' - v) \qquad (5.8)$$

The remarkable point on the relation is that the viscous constant is a hyperbolic function of the velocity and that it increases linearly with an increase in the contractile force. The dynamic constant a' during lengthening is about 1.6 times larger than a during shortening.

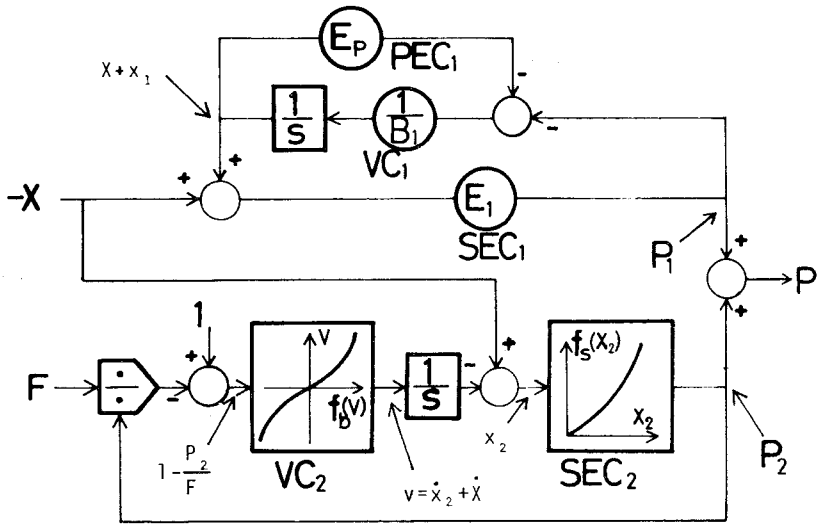

Fig. 5.2 Blockdiagram of the mechanical model programmed on an analog computer.

c) Equation of motions

For the convenience of simulation, Eqs. (5.5), (5.6) and (5.8) are rewritten as

$$\left.\begin{aligned} F_v &= F\ f_b(v) \\ f_b(v) &= (P_o + a)\, v / P_o\,(v + b) \qquad (v \geq 0) \\ &= (P_o + a')\, v / P_o\,(b' - v) \qquad (v \leq 0) \end{aligned}\right\} \qquad (5.9)$$

Then, due to $E_t \gg E_1$, the dynamic equations of the model in Fig. 5.1 are simplified as

$$\begin{aligned} P &= P_1 + P_2 \\ P_1 &= E_1 x_1 \\ P_1 &= E_p\,(-X - x_1) + B_1\,(-\dot{X} - \dot{x}_1) \end{aligned} \qquad (5.10)$$

$$P_2 = f_s(x_2)$$

$$P_2 = F - F\, f_b(\dot{X} + \dot{x}_2)$$

The blockdiagram programmed on an analog computer is shown in Fig. 5.2.

5.3 SIMULATED RESULTS

In the previous studies (Akazawa et al., 1969[3], 1970a[4], 1970b[5]), it has been ascertained through simulation procedures that the model interprets not only our experimental results but also the results of vibration experiment by Buchthal and Kaiser (1944)[16] and quick stretch experiment by Hill (1949b)[38]. It was shown qualitatively that the dynamic properties of the muscle during contraction were different from those at rest and vary with contractile activity. In this section, by simulating the responses of the resting and contracting muscles (frog semitendinosus muscle) to isovelocity stretching, it is shown quantitatively that in what way the nonlinear characteristics of the mechanical components affect the contraction and in what fashion the mechanical properties of the muscle vary with the degree of contractile activity. Validity of the proposed model is also examined.

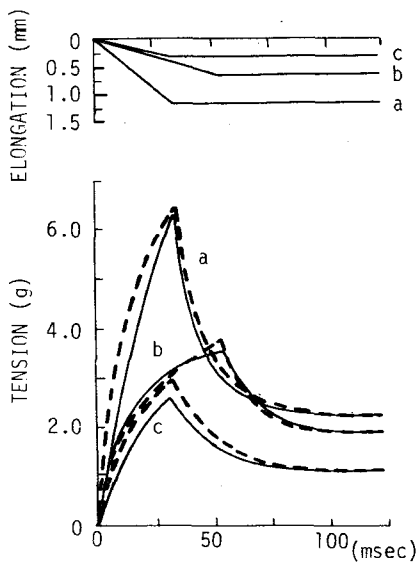

Fig. 5.3 Tension change (lower trace) of the resting muscle increased by ramp-wise stretch (upper trace). Solid line, experimental result; dashed line, simulated result. a, speed of stretching was 64 mm/sec, stretched amount was 2.1 mm; b, 24 mm/sec, 1.3 mm; c, 18 mm/sec, 0.9 mm. Frog semitendinosus muscle, P_o=8.5 gwt, L_o=11 mm, 10 °C.

a) Responses of the unstimulated muscle

Time courses during linear elongation of the resting muscle are shown in Fig. 5.3, solid line. In these experiments the muscle was stretched by a small amount at certain constant velocities, using a velocity controller, then maintained at the stretched length. Upper traces in Fig. 5.3 show length changes and lower traces (solid lines) show the resulted tension changes. The results of computer simulation are shown with broken lines in Fig. 5.3. On the simulations, F=0 and the values of E_1, E_p and B_1 in Table V-1 were used. The simulated curves show close agreement with the physiological data.

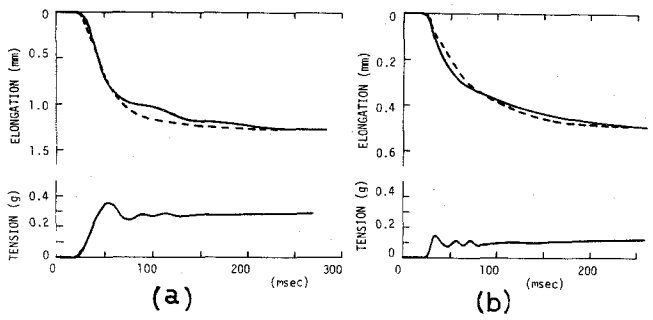

Fig. 5.4 Elongation of muscle length (upper trace) and tension change (lower) in the resting muscle after sudden loading; (a) load =0.3 g, (b) 0.1 g. Solid line, experimental result; broken line, simulated curve. Frog semitendinosus muscle, P_o=8.4 gwt, L_o=11 mm, 10 °C.

Responses of the resting muscle to sudden loading are simulated. Solid curves in Fig. 5.4 show the elongation of muscle length and tension changes which occured when the force on the muscle was step-wisely increased from zero to the fixed load. The loads 0.3 g and 0.1 g were applied on the experiments in Fig. 5.4. Dashed lines show the simulated results on a computer where the lowere traces in Fig. 5.4 were employed as the time course of the load P_1. The simulated curves are in a good agreement with the physiological results.

b) Responses of the contracting muscle

The muscle exerting a certain force was lengthened by a certain small amount (less than 10 % of L_o) giving ramp stretch at various speeds by means of the velocity controller, and the tension and length changes were recorded simultaneously. One of the results is shown in Fig. 5.5 (a). Then, the exerting force of the muscle was changed and the lengthening experiment was repeated. When the muscle was immersed in 14-18 mM KCl-Ringer's solution and stimulated with alternating current (100-500 Hz), the exerting isometric force of the muscle was easily maintained at a desired level by adjusting the intensity of the current (Mashima and Tsuchuya, 1968)[64]. One of the results is shown in Fig. 5.5 (b). Note that the more the contractile force was exerted, the larger the tension was increased by stretching.

Dashed lines in Fig. 5.5 show the simulated results on a computer, where time courses of upper traces in the figure were used as those of muscle elongation -X, steady isometric tension as the contractile force F and the dynamic constants in Table V-1 were used. In order to simulate these muscle responses, time course of the contractile force F which are masked by the filtering effect of viscous and elastic properties must be identified. The contractile force coincides with the isometric steady tension because no change in both tension and muscle length occured in this case; v=0 when dX/dt=0 and dP/dt=0, thus we have F=P from Eq. (5.4). Dynamic properties of the contractile component would be scarcely affected by the small amount of stretch less than 10 % of L_o, so that time courses of the contractile force during and after stretching can be considered to be approximately the same as those of isometric force. Simulated results obtained from this assumption showed close agreement with the experimental ones.

It was, however, noticed that simulated curve was always below the experi-

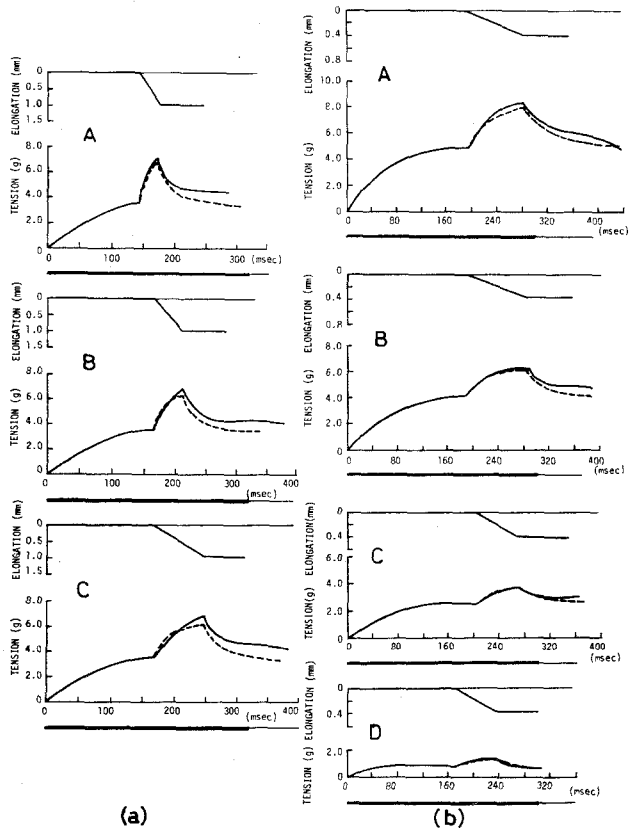

Fig. 5.5 Simulation of tension responses to stretching the muscle exerting the steady isometric force. Top trace, elongation of muscle length; middle trace, solid line, experimental tension change, dashed line, simulated curve; bottom trace, AC stimulation.

(a) Effect of stretch at various speed on the tension of the muscle. Contractile force before the stretch was maintained at 0.75 P_o by stimulating with AC (500 Hz) in 18 mM KCl-Ringer's solution. Speed of stretch; A, 32.9 mm/sec; B, 21.0 mm/sec; C, 12.9 mm/sec. P_o=4.65 g, L_o=10 mm, 10 °C.

(b) Effect of stretch on the muscle exerting various contractile forces. Contractile force was varied by stimulating with AC (500 Hz) in 14 mM KCl-Ringer's solution; A, 1.0 P_o; B, 0.75 P_o; C, 0.4 P_o; D, 0.16 P_o. Speed of stretch was about 4.0 mm/sec. P_o=5.3 g, L_o=14 mm, 10 °C.

mental curve at late stress relaxation phase after the stretch. Further, the ratio of the difference (offset) P_e between experimental and simulated tension to the amount of stretch X_e was roughly proportional to the contractile force. For example, $P_e/X_e = 7.8\ P_o/L_o$ at $F=1.0\ P_o$; $5.5\ P_o/L_o$ at $F=0.75\ P_o$; $3.8\ P_o/L_o$ at $F=0.4\ P_o$. This fact implies that the higher tension after stretch is not an error nor artifact but some activation by the stretch in the contractile component.

While responses of the muscle exerting the steady contractile force ($dF/dt = 0$) were simulated later, dynamics of the muscle during transient phase ($dF/dt \neq 0$) are analyzed here. Solid lines in Fig. 5.6 show the experimental results illustrating tension responses to ramp stretching at different instants after stimulus. The muscle was stretched at the constant speed by the small and nearly the same amount (0.3 mm), and maintained at the stretched length. The contraction was isometric until the stretch was applied. Curve P in Fig. 5.6 is the isometric tension curve measured when stretching was not applied. A supramaximal square pulse was applied on the experiment in Fig. 5.6 (a). In Fig. 5.6 (b), the muscle was stimulated in excess potassium Ringer's solution by alternating current (300 Hz), whose intensity was increased linearly in order to increase the contractile force slowly.

Dashed lines in Fig. 5.6 (a) and (b) show the tension responses simulated in the same manner as Fig. 5.5. On these simulations, however, curves F were determined from the analytical method described in the later chapter IV or by Mashima and Kushima (1971)[62] or Akazawa et al. (1971).[6] The simulated curves were well compatible with the experimental results. The tension responses to stretching were not the same, in spite of the nearly same mechanical input X and were dependent on the instant of stretching. Thus this fact showed apparently the nonlinear property of the contracting muscle; variation of the properties with time after the stimulation. It was also indicated through the simulation that these nonlinear mechanical properties in the contracting muscle

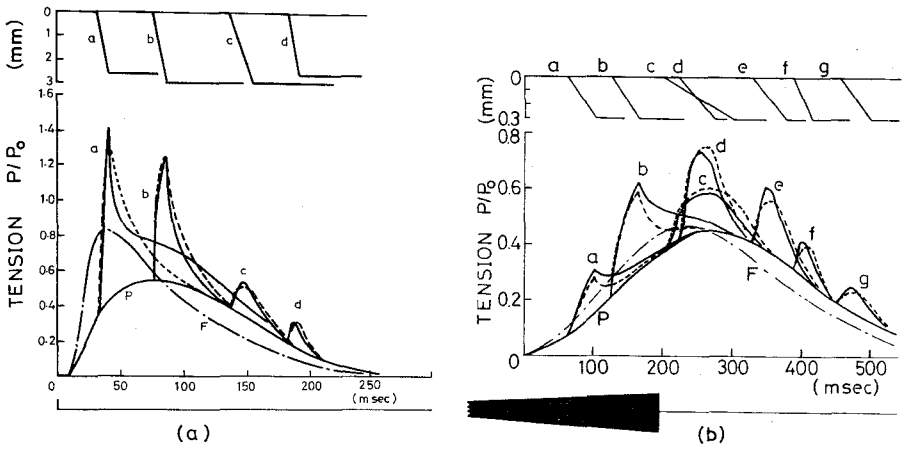

Fig. 5.6 Simulation of tension responses to stretching the contracting muscle at different instants after the onset of stimulation.
Solid line, experimental result; dashed line, simulated curve. P, isometric tension; F, exerting contractile force. Top trace, elongation of muscle length; middle trace, tension; bottom trace, stimulation.

(a) Single square pulse was applied to the muscle. A, speed of stretch =24 mm/sec, length change =0.26 mm; b, 24 mm/sec, 0.3 mm; c, 16 mm/sec, 0.3 mm; d, 29 mm/sec, 0.26 mm. Frog semitendinosus muscle, P_o=7.4 g, L_o=12 mm, 10 °C.

(b) Alternating current (300 Hz) whose intensity was increased gradually was applied. a, speed of stretch =7.5 mm/sec; b, 8.5 mm/sec; c, 2.9 mm/sec; d, 6.0 mm/sec; e, 10.0 mm/sec; f, 10.0 mm/sec; g, 6.7 mm/sec. Frog semitendinosus muscle, P_o=6.3 g, L_o=11 mm, 10 °C.

came from the nonlinearity of VC_2, especially the dependence of the viscous coefficient upon the contractile force, rather than SEC_2.

5.4 DISCUSSION

a) Modeling

According to Bahler (1968)[10], the mammalian skeletal muscle is modeled as a nonlinear force generator, bridged by a viscous-like element obeying hyperbolic force-velocity relations, in series with a nonlinear series elastic element. We also have developed the same viscous elastic model based on the results obtained from the frog skeletal muscle. Since the study of Hill (1938)[36], the force-velocity relation has been explained as a property of the contractile component, so that the classical visoelastic theory of muscle contraction introduced by Gasser and Hill (1924)[33], Levin and Wyman (1927)[57] has been abandoned. When the viscoelastic model of muscle is proposed again, it may give an uncommon impression to most of the physiologists. Though the theory seems to turn back to the early thirties, this new viscoelastic model is based on the recent electron microscope and X-ray diffraction findings of the ultrastructure of muscle fibers (H. E. Huxley, 1957[47], 1969[50]) and on the sliding-filament theory (A. F. Huxley, 1957[45]; Gordon et al. 1966[34]), so that the model is quite different in such meanings from the classical one in which muscle was thought to be the viscoelastic system as a whole. The simulated results obtained from the model closely resembled the experimental data from the frog skeletal muscle; that is, this fact means that this new viscoelastic model can explain the mechanical properties of muscular contraction quantitatively with sufficient accuracy, and the following usefulness can be also proposed.

Since the model is applicable to the muscle-limb system in the neuromuscular control system, it can be analyzed quantitatively how effectively the mechanical properties of muscular contraction and the nonlinear properties of

elastic and viscou-like components work on the system. These analyses may indicate important suggestions not only in developing artificial muscles or artificial limbs but also in synthesizing an external control system of human extremities as pointed out by Vodovnik et al. (1971).[85]

b) Structural correspondence of the model to the microstructure

Taking account of the microstructure of the muscle fiber and the sliding-filament theory, a viscoelastic model with distributed parameters illustrated in Fig. 5.7 can be proposed as one being equivalent to the lump parameter model in Fig. 5.1. The correspondence between each component and structure is assumed as follows. SEC_t is the elastic part of tendon and Z-lines. SEC_p, PEC_1 and VC_1 are the elastic and viscous elements in sarcomeres, such as surface membrane, surrounding connective tissue and sarcoplasma. Since its plasticity in resting muscles is attributed to the absence of cross-bridges between the two set of filaments, the mechanical properties are explained simply by these elements.

FG would correspond to a sliding-force generator at the sites of myofilament overlap in the sliding-filament theory in the contracting state. VC_2 is the viscous-like component developed in the contracting muscle and the viscous-like force is explained as the velocity- and force-dependent tension loss which is probably a certain sliding-loss dissipated during sliding movements or molecular interactions at the active cross-bridges. As pointed out by Mashima, Akazawa, Kushima and Fujii (1972),[59] the linear relation Eq. (5.9) between the viscous-like force and the contractile force can be explained under the assumption that both of them are proportional to the number of active cross-bridges. If we consider simply, SEC_a would correspond to the elastic element due to the active cross-bridges or due to the inactive parts of the thick and thin filaments where both filaments do not overlap each other.

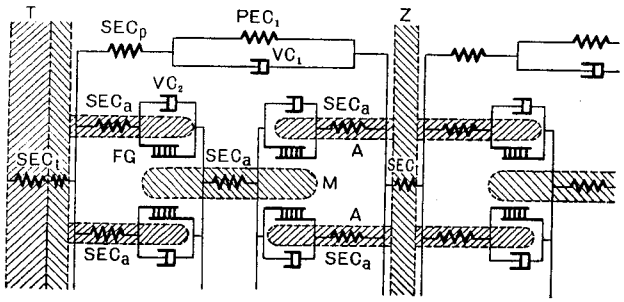

Fig. 5.7 Illustration showing the correspondence of each mechanical component of the model to the microstructure of sarcomere. A, thin filament; M, thick filament; T, tendon; Z, Z-line.

This scheme seems to correspond most closely with the electron-microscopic evidence (H. E. Huxley, 1957)[47] and the sliding-filament theory (A. F. Huxley, 1957[45]; Gordon et al., 1966)[34]. But it is difficult to say explicitly the structural correspondence in the present study. Though many attempts have been made to determine the structural correspondence of the series elastic component to the muscle fiber (Civan and Podolsky, 1966[21]; A. F. Huxley and Simmons, 1971[46]; Galey, 1969)[32], different conclusions are expressed. Any way, identification of the series elastic component is an important and interesting problem left in the future.

c) Simulation

As shown in Fig. 5.2, muscle system was expressed as two inputs (X and F) -one output (P) system and two inputs were treated as independent ones without interactions. Of course, there is a difinite relation between the contractile force and muscle length as determined by Gordon et al. (1966)[34]. We also obtained the relation from the frog semitendinosus muscle in isometric contractions in chapter III (Fig. 3.2). Since the simulations were done on

the muscle contraction at the length near L_o and within the variation less than 10 % of L_o, it was assumed, considering the relation in Fig. 3.2, that the contractile force F was not affected by a small amount of length change even in the transient phase ($dF/dt \neq 0$) as well as in the steady state ($dF/dt = 0$). That is, as shown in the simulation of stretch experiments of Figs. 5.5 and 5.6, time course of the contractile force F(t) estimated in the isometric contraction was used as that during and after the stretching. Although the simulated results showed slight differences such as offset tension, they closely resembled the principal parts of the experimental results obtained from the muscle. This fact implies that the proposed model is valid and that it can be used sufficiently to analyze the intrinsic mechanical property of muscle contraction.

Following discussion may be done on mechanical phenomena which were not explained by the model. Namely the simulated tension curves in the stretch experiment came always below the experimental tension curves as seen in Figs. 5.5 and 5.6, whereas no such difference was seen in the resting muscle as seen in Fig. 5.3. This offset tension was found to be in proportion to the elongation of the muscle length and to the contractile force before stretching. Therefore, those offset tensions would not be resulted from the inactive parallel elastic component (see the resting tension curve in Fig. 3.2), but from the active tension of the contractile component. They, however, could not be interpreted by the relation between the steady contractile force and muscle length in Fig. 3.2, because the muscle was stretched by a small amount from L_o. As pointed out by Abbott and Aubert (1952)[1] and Ruegg et al.(1970),[72] an activation of contractile linkages caused by stretching may account for this tension development after the stretch. As simple a model as possible was intended to construct in the present study because of great importance to simulation. However, if the model is allowed to be more complex, in order to

interpret this tension development, it may be necessary to introduce another intrinsic parallel elasticity of the contractile machine, although the physiological meaning of this elasticity in the sliding-filament theory is not yet known. In any case, further research on the dynamic relation between the contractile force and length change must be done in relation to the sliding-filament mechanism.

5.5 CONCLUSION

1. A mechanical model of a skeletal muscle was developed, based on the physiological results obtained from the bundle preparation of frog semitendinosus muscle at 10 °C. The model consists of a force generator, viscous and elastic components of the resting and contracting states.

2. Responses of the unstimulated muscle to ramp stretch and to step change in load were simulated on an analog computer. Simulated curves showed close coincidence with the experimental results obtained from the muscle.

3. Responses to isovelocity lengthening of the muscles generating steady contractile force and changing contractile force were simulated. A close agreement exists between the simulated results and the experimental ones.

4. Mechanical properties of the contracting muscle vary with time after the stimulation and with the exerting force. Simulation studies indicate that those nonlinear muscle dynamics are mainly due to the nonlinear property of the viscous-like component.

5. Physiological meaning of each component of the model are discussed with reference to the microstructure of sarcomere and the sliding-filament theory.

CHAPTER VI

MATHEMATICAL MODEL OF THE CONTRACTILE MECHANISM OF MUSCLE

6.1 INTRODUCTION

Muscular contraction has been extensively studied from the disciplines of physiology, biochemistry, thermodynamics, anatomy and so on. During the last decade, there have been significant advancements of knowledge about the molecular mechanism of muscle contraction and the ultrastructure of muscle cell. For example, the ultrastructure of sarcomere have been clearly revealed by electron-microscopic observations (H. E. Huxley, 1964[48], 1967[49]) and X-ray diffraction recordings (Hanson and Lowey, 1963)[35]; the molecular mechanism of actin-myosin-ATP system, by Szent-Gyorgyi (1951)[79] and Tonomura (1972)[82]; the excitation-contraction coupling and the role of Ca ion, by Sandow (1952)[75] and Ebashi and Endo (1968)[28]; the sliding-filament theory by A. F. Huxley (1957)[45] and H. E. Huxley (1957)[47]. In spite of these significant advances, no comprehensive theory has been yet proposed which satisfactorily explains the molecular events involed in the mechano-chemical process of muscle contraction. It is thus ardently desired to develop a completely unified model, i.e., to explain how each of the subsystem at the molecular level cooperatively works during contraction, and consequently how the muscle behaves as a whole.

In fact, several kinds of macroscopic models have been proposed (Wilikie, 1950[87]; Pringle, 1960[69]; Bahler, 1968[10]). These models are indeed useful in understanding the mechanical behaviors of muscle as a whole, because of plain and simple representation of the model, although they give no deeper insight into the mechano-chemical process of the contractile machinery. More recently, in order to investigate analytically the mechanism of contraction at the molecular level, many different kinds of microscopic models have been proposed in parallel with the establishment of the sliding-filament

theory (A. F. Huxley, 1957[45]; Deshcherevskii, 1968[26]; Volkenstein, 1969[86]; Chaplain and Frommelt, 1971[29]). However, none of these models goes beyond qualitative explanation of steady state behaviors exhibited by muscles. A model which is capable of explaining the contractile mechanism at the transient phase as well as at the steady state, has been eagerly desired.

The purpose of the present chapter is to interpret not only macroscopic features(force development, shortening, force-velocity relation, energy liberation and heat production) but also microscopic ones (sliding movements of myofilaments, kinetic behaviors of the actin-myosin-ATP system, and releasing or uptaking of Ca ion). Much effort is devoted to develop a new model of the contractile machinery, i.e. to develop a single theory including the modern concepts of the sliding-filament mechanism, the molecular mechanism of the actin-myosin-ATP system and the excitation-contraction coupling. After then, not only the force-velocity, load-energy liberation and load-heat production relations are explained by the model but also transient responses of isometric and isotonic contractions in the frog semitendinosus muscles are simulated on a digital computer. In these processes, all the parameters of the model are determined quantitatively, and dynamic characteristics of the muscle contraction are explicated quantitatively.

6.2 OUTLINE OF THE MECHANISM OF MUSCULAR CONTRACTION

The contractile mechanism, being described in detail in chapter II, is outlined here emphasizing those needed for mathematical modeling of it. The process of contraction is schematically illustrated in Fig. 2.3. A stimulus is conveyed to sarcoplasmic reticulum (SR), which in turn brings about release of Ca ion from SR, followed by binding of Ca ion to contractile proteins in actin filaments. When concentration of inner Ca ion exceeds a thresh-

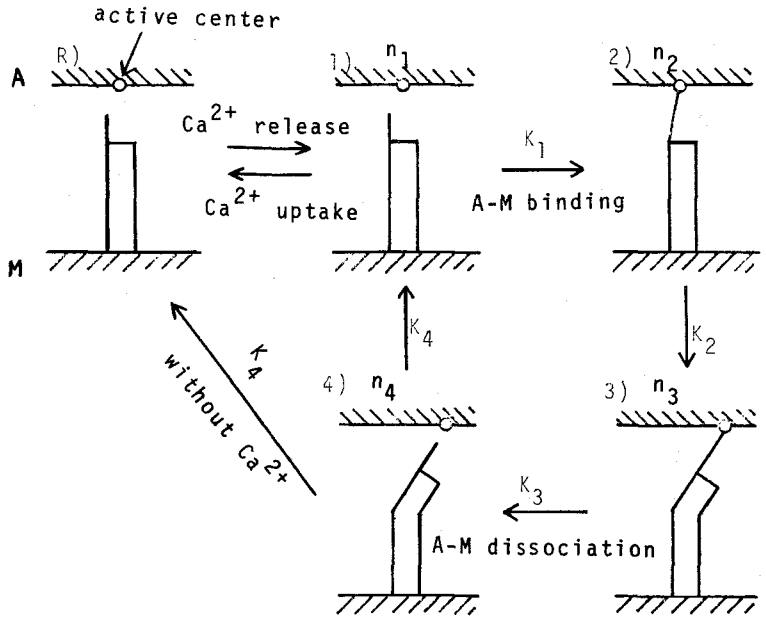

Fig. 6.1 Schematic diagram of the molecular mechanism of muscle contraciion. K_i (i=1,2,3 4), rate constant; n_i (i=1,2,3,4), numbers of the active centers at each state i).

old, the reaction of actin-myosin-ATP system is activated. Consequently, thin filaments slide past into thick filaments, by which a muscle generates force or does shorten.

Binding of Ca ion to troponin (Ca ion-receptive cite) causes some interaction between actin and myosin , which immediately results in the formation of cross-bridges linking between active centers *) of thin filaments and myosin heads. The cross-bridges, moving cyclically as though they were pulling on an oar, make a thin filament slide past into thick filaments. So long as the stimulation continues, cyclical making and breaking of the cross-bridges last, and relaxation begins to occur as Ca ion is uptaken from troponin by sarcoplasmic reticulum.

*) An active center is defined as a site of a thin filament onto which a myosin head is able to attach.

The molecular mechanism of contraction is illustrated schematically in Fig. 6.1; state R) is the resting state; state 1) is activation of an active center, resulted from binding of Ca ion to troponin; state 2) is a state of developing an active contractile force through formation of a cross-bridge; state 3) is at the very instant of breaking the cross-bridge; state 4) is under complete dissociation of the cross-bridge. Note that the state 2) is a force-generating phase and otherwise is a free phase. The transition from the state 4) to 1) occurs when Ca ion is bound to a corresponding troponin, and that from 4) to R) occurs when the troponin has no Ca ion, and besides that from 1) to R) occurs with uptaking the bound Ca ion from the state 1). To sum up, a fundamental process of contraction is the cyclic reaction 1)→ 2)→3)→4)→1), while the relaxaxion accompanies the reaction from 1) to R) or from 4) to R).

6.3 DEVELOPMENT OF THE MODEL

The two-component model in Fig. 6.2 is adopted as a mechanical model and most of organized effort is devoted to develop a model of the contractile component. The contractile component is modeled, based on the excitation-contraction coupling and the molecular mechanism of contraction involving the reaction process of actin-myosin-ATP system and the sliding-filament mechanism.

a) Equation of the two-component model

The equation of an external loading system is

$$\hat{M}\,\ddot{X} = P - \hat{M}\,g_a \tag{6.1}$$

$$\hat{M} = 0.28 + 0.01\,P_e \tag{6.2}$$

where P = tension on muscle,

X = shortening of muscle,

g_a = acceleration of gravity (980 cm/sec^2),

$\hat{M}$ = equivalent mass of the load-isotonic lever system (see Appendix A),

P_e = load applied to the isotonic lever.

The kinetic equation of the muscle is

$$m\ddot{x} = F_a - P \tag{6.3}$$

$$P = E_2 (x - X) \tag{6.4}$$

where m = mass of the muscle,

x = shortening of the contractile component (CC),

F_a = force generated in CC,

E_2 = elastic coefficient of SEC.

Note that we make an approximation $m\ddot{x} = 0$, because of its minor effects on the dynamic characteristics of muscle contraction. The muscle length is

$$\ell = \ell_o - X \tag{6.5}$$

where ℓ_o = initial length of muscle,

ℓ = length of muscle.

It is assumed that a single cross-bridge develops a proper constant force $\underline{f}$ accompanying a force loss $\underline{f_v}$ which depends on the velocity of sliding. Thus, the net force produced by a single cross-bridge is $f-f_v$. Denoting the number of cross-bridges developing forces (working cross-bridges) by $\underline{n_2}$, we may express the total force $\underline{F_a}$ generated in the contractile component as

$$F_a = n_2 (f - f_v) \tag{6.6}$$

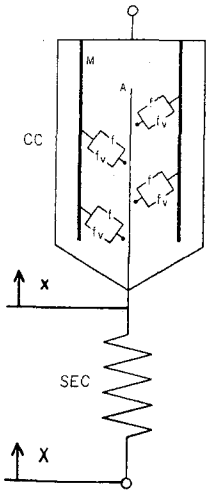

Fig. 6.2 Mechanical two-component model, consisting of the contractile component (CC) and the series elastic component (SEC). M, thick filament; A, thin filament; f and f_v, contractile force and force-loss of a unit cross-bridge (force-generator); x, shortening of CC; X, shortening of muscle.

For simplicity, f_v is assumed to be directly proportional to the velocity of sliding movement $\dot{x}$:

$$f_v = \begin{cases} \beta \dot{x} & (\dot{x} \geq 0) \\ \beta' \dot{x} & (\dot{x} < 0) \end{cases} \qquad (6.7)$$

where β, β' =constants of proportionality.

b) Model of the excitation-contraction coupling

This section is to express the number of the active centers capable of forming cross-bridges between myofilaments , as a function of muscle length and inner Ca ion concentration. For convenience' sake, following symbols are employed for the active center;

A_S^* = active center with Ca ion; the site is activated by the reaction of Ca ion-troponin-tropomyosin complex which results from binding of Ca ion to troponin,

A_s^- = active center without Ca ion; A_s^* is transformed to A_s^- when Ca ion is uptaken from A_s^* . Reversely, A_s^- is transformed to A_s^* when Ca ion binds to A_s^- (Ca ion itself attaches to A_s^-).

N^* = number of A_s^* in the overlap region of thin and thick filaments.

A_s^* is considered to be distributed uniformly along the whole length of thin filaments, so that N^* is directly proportional to the length of the overlap region; namely,

$$N^* = F_\ell(\ell)\ F_c(ca) \tag{6.8}$$

where $F_\ell(\ell)$ = length of the overlap region of myofilaments, function of muscle length, ℓ ,

$F_c(ca)$ = number of A_s^* per unit length of thin filaments; function of ca,

ca = inner calcium ion concentration.

Then, we get

$$\dot{N}^* = \dot{F}_c(ca)\,F_\ell(\ell) + F_c(ca)\,\dot{F}_\ell(\ell) \tag{6.9}$$

$$= \frac{dF_c(ca)}{dca}\,\dot{ca}\,F_\ell(\ell) + F_c(ca)\,\dot{F}_\ell(\ell)$$

In the present chapter, length change of the muscle is within a limit of 10 % of L_o around L_o, where the second term in the right hand side of Eq. (6.9) is considerably smaller than the first term. Hence,

$$\dot{N}^* \cong \frac{dF_c(ca)}{dca}\,\dot{ca}\,F_\ell(\ell) \tag{6.10}$$

We denote by $\dot{C}_r$ the rate at which Ca ion is released from sarcoplasmic reticulum (SR) , and by $\dot{c}_u$ the rate at which Ca ion is uptaken by Sr. Then, the rate of change in inner Ca ion concentration, $\dot{ca}$, is expressed as

$$\dot{ca} = \dot{c}_r - \dot{c}_u \tag{6.11}$$

Substituting Eq. (6.11) into Eq. (6.10),

$$\dot{N}^* = \frac{dF_c(ca)}{dca}\,\dot{c}_r\,F_\ell(\ell) \quad - \frac{dF_c(ca)}{dca}\,\dot{c}_u\,F_\ell(\ell) \tag{6.12}$$

On the other hand, we can write

$$\dot{N}^* = \dot{N}_r - \dot{N}_u \tag{6.13}$$

where $\dot{N}_r$ ($\dot{N}_u$) = rate of increase (decrease) in the number of A_s^* in the ovelap region which results from releasing (uptaking) of Ca ion.

Comparing Eq. (6.12) and Eq. (6.13), finally we get

$$\dot{N}_r = \frac{dF_c(ca)}{dca}\,\dot{c}_r\,F_\ell(\ell)$$

$$\dot{N}_u = \frac{dF_c(ca)}{dca}\,\dot{c}_u\,F_\ell(\ell) \tag{6.14}$$

While above investigations are concerned with the muscle length greater than L_o, they may be applied to the length less than L_o. As shown in Fig. 3.2, an active tension is decreased with decreasing length of the muscle from L_o. This relationship is assumed to originate from a decrease in numbers of the active centers A_s^* actually participating in contraction.

c) Model of the molecular mechanism of muscular contraction

A model of the contractile mechanism is developed with introducing the concept of the sliding filament mechanism into the mechano-chemical process of contraction in Fig. 6.1. We take five assumptions here.

[1] Binding of Ca ion to troponin and releasing of bound-Ca ion from troponin are not affected by reactions of the actin-myosin-ATP system.

Both binding and releasing take place uniformly over a whole length of myofilaments and without time lag (dissociation constant K_c).

[2] All the active centers A_s^* and A_s^- at the states 2) and 3) are transformed to the state 4).

[3] A single cycle of the reaction 1)→2)→3)→4) accompanies with splitting of one molecule of ATP.

[4] The rate constants K_1, K_3 and K_4 are constant where K_1 is the rate constant at the transition from the state 1) to 2), K_3 is that from 3) to 4) and K_4 is that from 4) to 1) or from 4) to R).

[5] The rate constant of the reaction from the state 2) to 3), K_2, is increased directly in proportional to the velocity of sliding $\dot{x}$:

$$K_2 = \begin{cases} \alpha_o + \alpha_1 \dot{x} & (\dot{x} \geq 0) \\ \alpha_o - \alpha_1' \dot{x} & (\dot{x} < 0) \end{cases} \qquad (6.15)$$

where α_o = constant,

α_1 (α_1') = constant of proportionality during shortening (lengthening).

Above assumptions correspond to the molecular mechanism schematically illustrated in Fig. 6.3. The arrows $\rightleftharpoons$ show the dissociation reactions based on the assumption [1] and the arrows $\longrightarrow$ show the kinetic reaction process of the actin-myosin-ATP system.

Then, following symbols are employed:

N^R = number of active centers at the state R),

n_1^*, n_2^*, n_3^*, n_4^* = numbers of A_s^* at the states 1), 2), 3) and 4), respectively,

n_1^-, n_2^-, n_3^-, n_4^- = numbers of A_s^- at the states 1), 2), 3) and 4), respectively.

The assumption [1] is expressed mathematically as follows. The rate of change in numbers of the active centers changing from the state R) to 1) is expressed as $\dot{N}_r N^R/(N^R + N^-)$. Similarly the rate of change in numbers

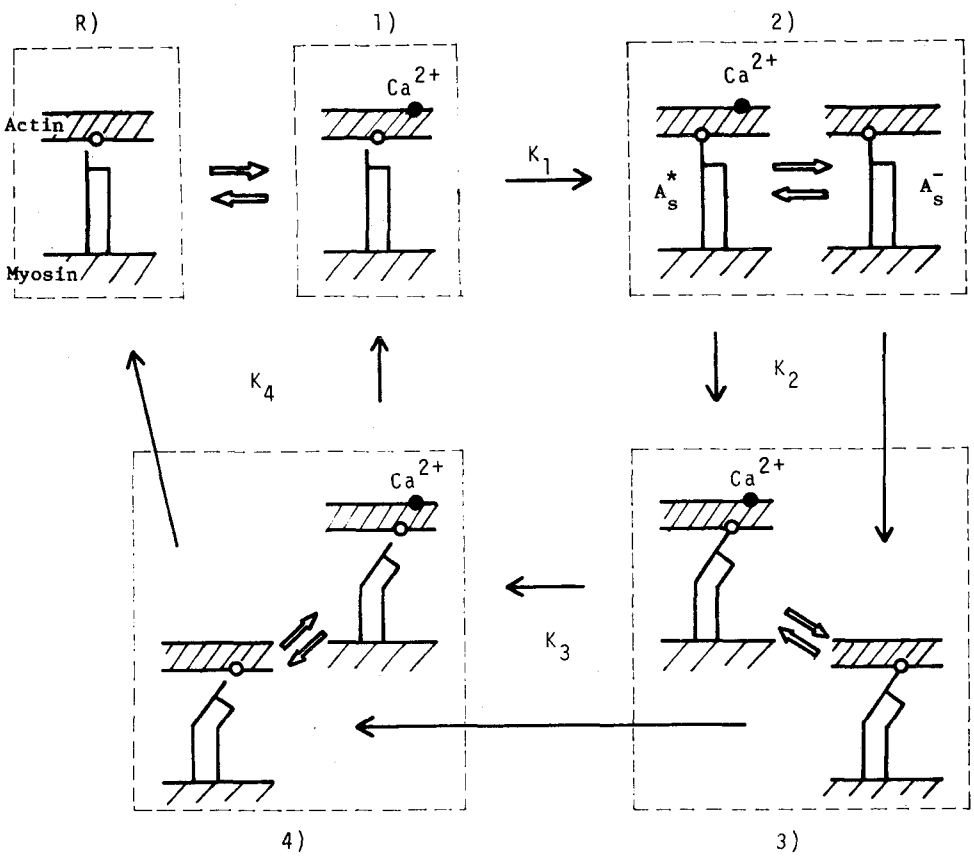

Fig. 6.3 Illustration of the molecular mechanism of contractile process, based on the assumption [1]. The arrow $\longrightarrow$ indicates the chemical reaction of the actin-myosin-ATP contractile system ; individual rate constants of the reaction are K_1, K_2, K_3 and K_4. The arrow $\Longrightarrow$ indicates the dissociation reaction between Ca ion and Ca ion receptive sites of the actin filaments; dissociation constant is K_c. The state R) is the resting state; 1) binding of released Ca ion to troponin; 2) formation of cross-bridge (developing an acitve force and sliding a thin filament) : 3) at the very instant of breaking the cross-bridge; 4) complete dissociation of the cross-bridge.

of the active centers which are changing from A_s^- to A_s^* within the same states are $\dot{N}_r\, n_j^-/(N^R + N^-)$, (j=2,3,4). Here N^- is

$$N^- = n_2^- + n_3^- + n_4^- \tag{6.16}$$

We take $n_1^- = 0$, because A_s^- at the state 1) is quite the same as the state R). Further , the rate of change in numbers of the active centers which are changing from A_s^* to A_s^- within the same states are $\dot{N}_u\, n_j^* / N^*$, (j=1,2,3,4), where N^* is

$$N^* = n_1^* + n_2^* + n_3^* + n_4^* \tag{6.17}$$

The assumption [5] about K_2 is one of the characteristic feature of the proposed model. This assumption is based on following consideration. Cross-bridges are probably broken down (dissociated) when the bridges have finished sliding thin filaments by a certain relative displacement (a stroke). If so, the cross-bridges may be transformed more rapidly from the state 2) to 3) as the velocity of sliding of myofilaments is increased. Hence, the rate of change in the numbers of active centers changing from the state 2) to 3), i.e., the rate constant K_2 must be increased with an increase in velocity of sliding, as expressed by Eq. (6.15).

As for A_s^* , above explanations lead to the following equations:

$$\begin{aligned}
\dot{n}_1^* &= \dot{N}_r \frac{N^R}{N^R + N^-} + K_4\, n_4^* - K_1\, n_1^* - \dot{N}_u \frac{n_1^*}{N^*} \\
\dot{n}_2^* &= \dot{N}_r \frac{n_2^-}{N^R + N^-} + K_1\, n_1^* - K_2\, n_2^* - \dot{N}_u \frac{n_2^*}{N^*} \\
\dot{n}_3^* &= \dot{N}_r \frac{n_3^-}{N^R + N^-} + K_2\, n_2^* - K_3\, n_3^* - \dot{N}_u \frac{n_3^*}{N^*} \\
\dot{n}_4^* &= \dot{N}_r \frac{n_4^-}{N^R + N^-} + K_3\, n_3^* - K_4\, n_4^* - \dot{N}_u \frac{n_4^*}{N^*}
\end{aligned} \tag{6.18}$$

The left hand side of the first equation of Eq. (6.18), $\dot{n}_1^*$, indicates the rate of change in n_1^* . The first and second terms of the right hand side indicate the rates of its decreases. Similar are the differential equations concerning $\dot{n}_2^*$, $\dot{n}_3^*$ and $\dot{n}_4^*$.

In addition, the differential equations concerning A_s^- are

$$\begin{aligned}
\dot{n}_2^- &= \dot{N}_u \frac{n_2^*}{N^*} - K_2 n_2^- - \dot{N}_r \frac{n_2^-}{N^R + N^-} \\
\dot{n}_3^- &= \dot{N}_u \frac{n_3^*}{N^*} + K_2 n_2^- - K_3 n_3^- - \dot{N}_r \frac{n_3^-}{N^R + N^-} \\
\dot{n}_4^- &= \dot{N}_u \frac{n_4^*}{N^*} + K_3 n_3^- - K_4 n_4^- - \dot{N}_r \frac{n_4^-}{N^R + N^-}
\end{aligned} \tag{6.19}$$

Then we define the total numbers of the active centers at the states 1), 2), 3) and 4) as n_1, n_2, n_3, and n_4, respectively. As a result, we can write

$$\begin{aligned}
n_1 &= n_1^* \\
n_2 &= n_2^* + n_2^- \\
n_3 &= n_3^* + n_3^- \\
n_4 &= n_4^* + n_4^-
\end{aligned} \tag{6.20}$$

From Eqs. (6.18)-(6.20), we can also represent the equation for $\dot{n}_i$:

$$\dot{n}_1 = \dot{N}_r \frac{N^R}{N^R + N^-} + K_4 n_4^* - K_1 n_1 - \dot{N}_u \frac{n_1}{N^*}$$

$$\begin{aligned}
\dot{n}_2 &= K_1 n_1 - K_2 n_2 \\
\dot{n}_3 &= K_2 n_2 - K_3 n_3 \\
\dot{n}_4 &= K_4 n_3 - K_4 n_4
\end{aligned} \tag{6.21}$$

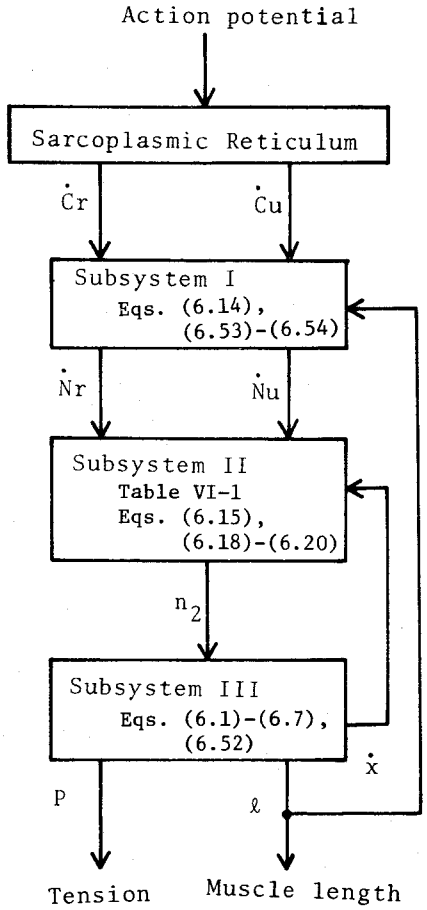

Fig. 6.4 Organization of the total model of muscle contraction. Subsystem I, excitation-contraction coupling; subsystem II, actin-myosin-ATP contractile system; subsystem III, two-component model and external loading system.

d) Development of the total model

Finally, a mathematical model of muscle contraction is constructed by synthesizing the above three subsystem models expressed in sections a), b) and c). The organization of the model is schematically shown in Fig. 6.4 with representing the number of the equation. The subsystem I corresponds to the excitation-contraction coupling, the subsystem II to the molecular mechanism of actin-myosin-ATP system and the subsystem III to the mechanical

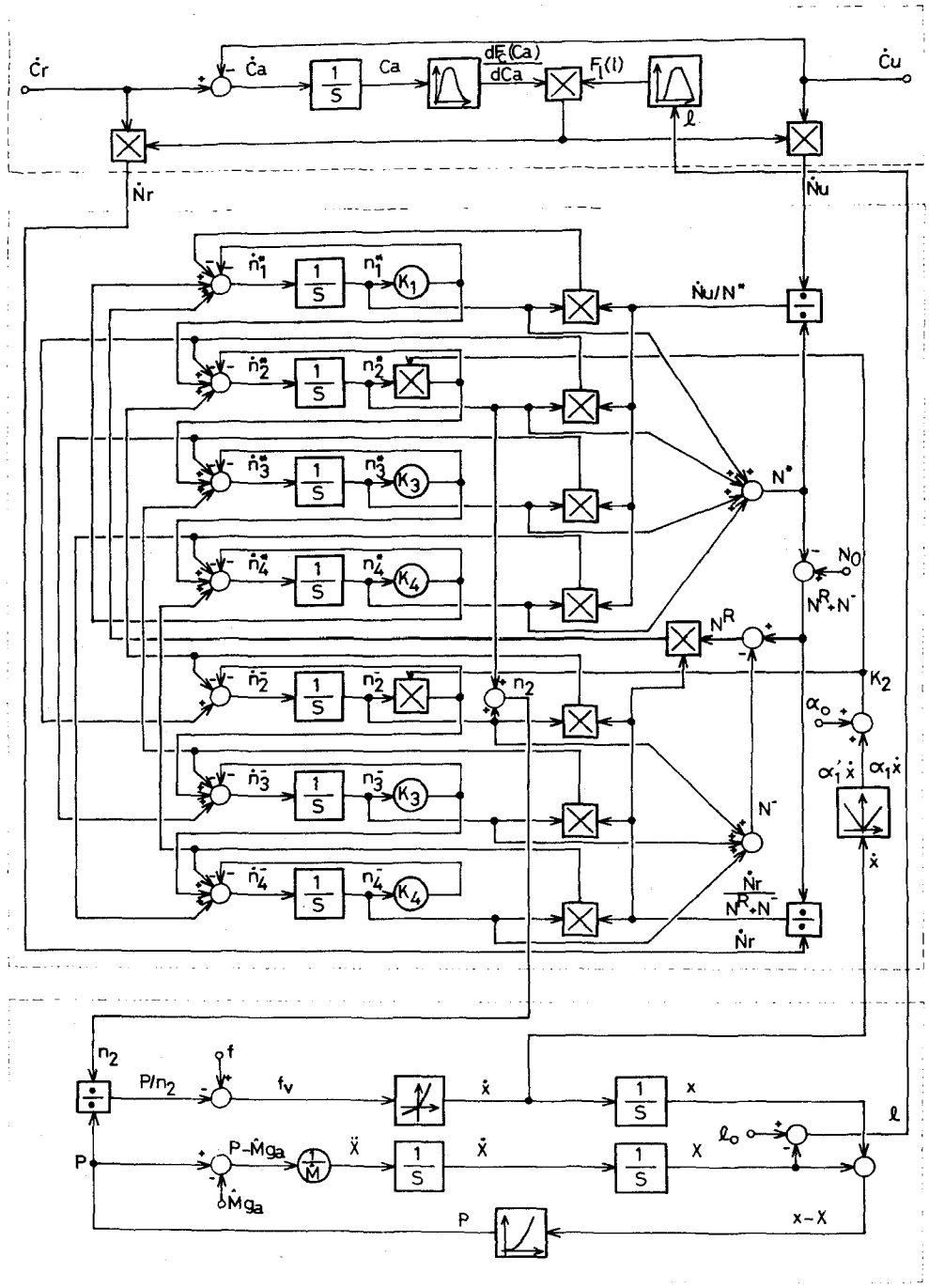

Fig. 6.5 Mathematical model of muscle contraction programmed on a computer.

system involving SEC and external loading. As shown in Fig. 6.4, the contractile system of muscle itself furnishes feedback mechanisms, i.e., ℓ and velocity $\dot{x}$ turn back to the subsystems I and II. In particular, it is of obvious interest that the contractile reaction is regulated by the velocity of shortening and lengthening $\dot{x}$. For deeper understanding, a whole diagram which is equivalent to the diagram of Fig. 6.4 is also shown in Fig. 6.5. Inputs to the whole system are $\dot{c}_r$ and $\dot{c}_u$, i.e., the rate of releasing Ca ion from sarcoplasmic reticulum and that of uptaking Ca ion, respectively, and outputs are tension on the muscle P and shortening of the muscle X.

6.4 SIMULATION OF STATIC CHRACTERISTICS

In this section, the force-load-velocity, load-energy liberation and load-heat production relations are simulated together by means of the proposed model. By comparing them with the physiological results obtained in chapter III, validity of the model is ensured and all the parameters involved are also estimated quantitatively.

a) Preliminary consideration of the steady state characteristics

On the steady state, numbers of the active centers, n_1, n_2, n_3 and n_4 do not change with time, so that the equation (6.21) becomes

$$\begin{aligned} 0 &= K_1 n_1 - K_2 n_2 \\ 0 &= K_2 n_2 - K_3 n_3 \\ 0 &= K_3 n_3 - K_4 n_4 \end{aligned} \tag{6.22}$$

Denoting N by

$$N = n_1 + n_2 + n_3 + n_4 \tag{6.23}$$

and substituting Eq. (6.22) into Eq. (6.23), we get

$$n_i = \frac{N\ K\ K_2}{(K + K_2)\ K_i} \quad , \quad (i=1,2,3,4) \tag{6.24}$$

$$1/K = 1/K_1 + 1/K_3 + 1/K_4 \tag{6.25}$$

Because K_2 is dependent on velocity v (see Eq. (6.15)), n_i (i=1, 2, 3, 4) does vary with v. The relation between n_i and v is shown in Fig. 6.6. As velocity of shortening or lengthening is increased, n_2 is decreased but n_1, n_3 and n_4 are increased. It is an important aspect that the number of cross-bridges developing an active force, n_2, is decreased with an increase in velocity v.

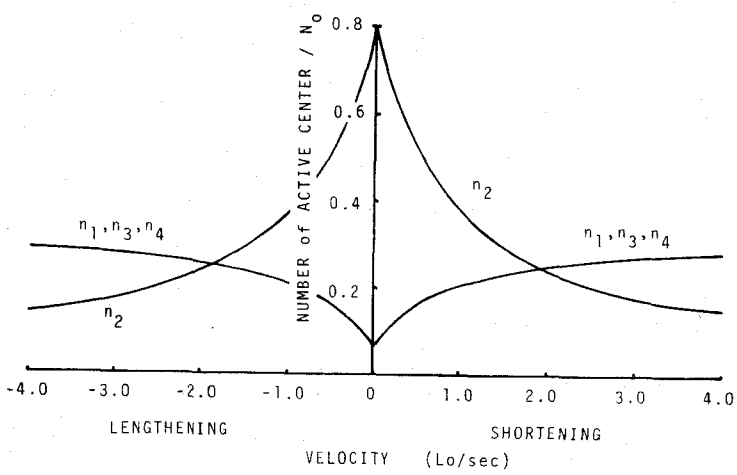

Fig. 6.6 Relation between velocity and number of each active center (n_1, n_2, n_3, n_4). The parameter values in Table VI-1 are employed.

b) The force-load-velocity relation

At the steady state when a muscle continues to shorten with a steady velocity v against a fixed load P, the velocity v is equal to that of the contractile component ($v=\dot{x}=\dot{X}$), and $x=X=0$ then $F_a - P=0$. Putting the

equations (6.6), (6.7), (6.15) and (6.24) into the relation $F_a - P = 0$,

$$F_a = n_2 (f - f_v) \tag{6.6}$$

$$f_v = \beta v \tag{6.7}$$

$$K_2 = \alpha_o + \alpha_1 v \tag{6.15}$$

$$n_2 = \frac{N K}{(K + K_2)} \tag{6.24}$$

then we can obtain the load (P) - velocity (v) relation during shortening:

$$v \left(\frac{N K \beta}{\alpha_1} + P\right) = \frac{K + \alpha_o}{\alpha_1} \left(\frac{N K f}{K + \alpha_o} - P\right) \tag{6.26}$$

Equation (6.26) is quite equivalent to the experimental equation Eq. (3.19) obtained in chapter III:

$$v (A + P) = b (F - P) \tag{6.27}$$

$$A = a (F/P_o)$$

where F = contractile force in CC,

a = heat constant of Hill's hyperbolic equation,

b = dynamic constant of Hill's equation,

P_o = maximum tension developed at L_o.

Consequently, following relations hold among the parameters:

$$A = \frac{N K \beta}{\alpha_1} \quad , \quad a = \frac{N_o K \beta}{\alpha_1} \quad , \quad b = \frac{K + \alpha_o}{\alpha_1}$$

$$F = \frac{N K f}{K + \alpha_o} \quad , \quad P_o = \frac{N_o K f}{K + \alpha_o} \tag{6.28}$$

where N_o = value of N, when the muscle is developing the maximum force, P_o.

Note that the force-velocity relation introduced by Hill (1938)[36]

$$v\ (\ a + P\ ) = b\ (\ P_o - P\ ) \tag{6.29}$$

is a special case of Eq. (6.27) at $F = P_o$.

The same procedure is applied to the lengthening muscle. Substituting the following equations into the relation $F_a = P$,

$$F_a = n_2(f - f_v) \tag{6.6}$$

$$f_v = \beta'\ v \tag{6.7}$$

$$K_2 = \alpha_o - \alpha_1'\ v \tag{6.15}$$

$$n_2 = \frac{N\ K}{(K + K_2)} \tag{6.24}$$

then we can obtain

$$v\ (\frac{N\ K\ \beta'}{\alpha_1'} - P) = \frac{K + \alpha_o}{\alpha_1'}\ (\frac{N\ K\ f}{K + \alpha_o} - P) \tag{6.30}$$

Equation (6.30) is also equivalent to the force-load-velocity relation of lengthening muscles (see Eq. (3.23) in chapter III):

$$v\ (\ 2F + A' - P\ ) = b'\ (\ F - P\ ) \tag{6.31}$$

$$A' = a'\ (\ F/P_o\ )$$

Consequently, we immediately find

$$A' + 2F = \frac{N\ K\ \beta'}{\alpha_1'} \quad , \quad a' + 2P_o = \frac{N_o K\ \beta'}{\alpha_1'}$$

$$b' = \frac{K + \alpha_o}{\alpha_1'} \quad , \quad F = \frac{N\ K\ f}{K + \alpha_o} \quad , \quad P_o = \frac{N_o K\ f}{K + \alpha_o} \tag{6.32}$$

A common maximum velocity v_m at which a muscle is capable of shortening at $P = 0$ is of obvious interest. Introducing $P=0$ into Eq. (6.26),

we get

$$v_m = \frac{f}{\beta} \tag{6.33}$$

This result means that the maximum velocity is dependent only on the property of single cross-bridges, and thus that it would not vary with length of muscle. On the other hand, Gordon et al. (1966)[34] observed that shortening velocities of single fibers obtained at very light loads, which would closely approach the maximum velocity, were approximately identical at various muscle lengths greater than L_o. This evidence would support Eq. (6.33), or the proposed model.

c) Load-energy liberation and load-heat production relations

Energy of a muscle (E), supplied by splitting of ATP, is converted to work (W) and heat (H). There are two distinct kinds of heat, shortening heat, H_s, and maintenance heat, H_m, (Hill, 1949 a).[37]

$$\begin{aligned} E &= W + H = W + H_s + H_m \\ \dot{E} &= \dot{W} + \dot{H}_s + \dot{H}_m \end{aligned} \tag{6.34}$$

Work done per unit time, $\dot{W}$, is given by the product of load P and velocity v:

$$\dot{W} = P\, v \tag{6.35}$$

Substituting the load-velocity relation Eq. (6.29) into Eq. (6.35), we get the relation between P and W:

$$\dot{W} = \frac{b\, P\, (P_o - P)}{P + a} \tag{6.36}$$

Shortening heat is assumed to be closely associated with the force loss f_v, so that the heat produced per unit time $\dot{H}_s$ may be expressed as

$$\dot{H}_s = \frac{d}{dt} \int n_2 f_v \, dx = \frac{d}{dt} \int n_2 f_v \frac{dx}{dt} \, dt$$

$$= n_2 f_v v \qquad (6.37)$$

Substituting Eqs. (6.7), (6.15), (6.24), (6.26),and (6.28) into Eq. (6.37), we obtain the relation between P and $\dot{H}_s$:

$$\dot{H}_s = \frac{a b (P_o - P)^2}{(P_o + a)(P + a)} \qquad (6.38)$$

Hill and Woledge (1962)[40] found values for the rate of maintenance heat production $\dot{H}_m$ about equal to the product of a and b;

$$\dot{H}_m = a b \qquad (6.39)$$

From Eqs. (6.36)-(6.39), finally we obtain

$$\dot{E} = \dot{W} + \dot{H}_s + \dot{H}_m$$

$$= \frac{b P_o}{P_o + a} \left\{ P_o + \frac{a}{P_o} (P_o + a) - P \right\} \qquad (6.40)$$

As seen from Eqs. (6.38) and (6.40), both the rate of shortening heat $\dot{H}_s$ and that of energy liberation $\dot{E}$ can be calculated against load P, by introducing the values of a and b. Experimentally, P-$\dot{E}$ and P-$\dot{H}_s$ relations were measured from the thermodynamical experiments on frog sartorius muscles at 0 °C by Hill (1964)[41]. The physiological result is shown with solid line in Fig. 6.7. Because the dynamic constants, a/P_o=0.25 and b/L_o=0.325 sec^{-1}

were also evaluated on the same preparation by Hill, those values are put into Eqs. (6.38) and (6.40), and $\dot{E}$ and $\dot{H}_s$ are calculated against various values of P. Calculated results are shown with broken line in Fig. 6.7. As a whole, the relation obtained from the model, although slight difference is seen, seems to show the same feature as obtained from the sartorius muscle; namely, $\dot{E}$ and $\dot{H}_s$ are decreased with an increase in load.

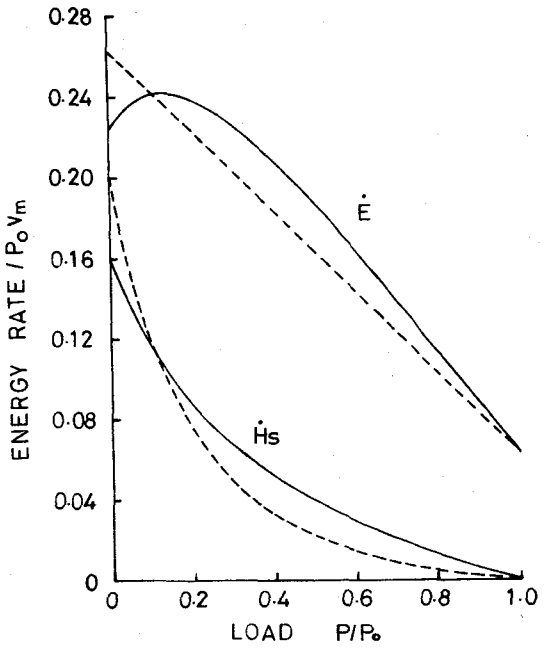

Fig. 6.7 Steady state relation between load P and rate of energy liberation $\dot{E}$, and between load and rate of shortening heat production $\dot{H}_s$ Solid line, physiological result obtained from frog sartorius muscle at 10 °C (Hill, 1964)[41]; broken line, the relations obtained from the model; v_m, maximum shortening velocity.

On the other hand, the energy liberation rate, $\dot{E}$, can be expressed in terms of the energy of ATP hydrolysis. It is assumed in the present work that one molecule ATP is hydrolyzed during single cycles of the contractile reaction 1)→ 2)→ 3)→ 4). It is not fully clarified where nor when ATP splitting takes place, although the stage is presumably at the reaction from the state 2) to 3) or that from the state 3) to 4). So two cases are considered here. As a result, both cases are identical at the steady state.

That is, if ATP splitting occurs at the reaction from 2) to 3), the energy rate, $\dot{E}$, can be written as

$$\dot{E} = e_a K_2 n_2 \tag{6.41}$$

where e_a = free energy exerted by hydrolysis of one molecule of ATP.
If it occurs at the reaction from 3) to 4),

$$\dot{E} = e_a K_3 n_3 \tag{6.42}$$

As seen from Eq. (6.24), $K_2 n_2$ is equal to $K_3 n_3$ at the steady state so that both equations are quite identical.

$$\dot{E} = e_a K_2 n_2 = e_a K_3 n_3 \tag{6.43}$$

Putting Eqs. (6.15), (6.24), (6.26) and (6.28) into Eq. (6.43), we get

$$\dot{E} = \frac{e_a N_o K^2 / \alpha_1 b}{P_o + a} \left\{ \frac{\alpha_o (P_o + a) + K P_o}{K} - P \right\} \tag{6.44}$$

Because Eqs. (6.40) and (6.44) have to be equal, we immediately find

$$\left.\begin{aligned} b\ P_o &= \frac{e_a\ N_o\ K^2}{\alpha_1\ b} \\ P_o + \frac{a}{P_o}(P_o + a) &= \frac{\alpha_o\ (P_o + a) + K\ P_o}{K} \end{aligned}\right\} \qquad (6.45).$$

d) Determination of the parameters

In this section, all the parameters introduced into the model are determined, by using the relations of Eqs. (6.28), (6.32) and (6.45) besides the physiological results.

i) The parameters of the molecular mechanism model

Equations (6.28) and (6.45) can lead to the following relations:

$$\left.\begin{aligned} &K = (1 + a/P_o)\ b\ P_o / e_a\ N_o\ , \quad \alpha_o = a\ K / P_o\ , \\ &\alpha_1 = (K + \alpha_o)/ b\ , \quad \beta = a\ \alpha_1 / K\ N_o\ , \\ &f = (K + \alpha_o)\ P_o / K\ N_o \end{aligned}\right\} \qquad (6.46).$$

It is clear that the parameters K, α_o, α_1, f and β can be easily calculated when the values of P_o, N_o, e_a, L_o, $\underline{a}$ and $\underline{b}$ are together given.

First, the dynamic constants $\underline{a}$ and $\underline{b}$ have been already evaluated (see section 3.5)

$$a/P_o = 0.25, \qquad b/L_o = 0.9\ \text{sec}^{-1} \qquad (6.47)$$

TABLE VI-1

ESTIMATED PARAMETERS OF THE MOLECULAR MECHANISM OF CONTRACTION

SHORTENING		LENGTHENING	
K	86 /sec	K	86 /sec
α_0	21 /sec	α_0	21 /sec
α_1	120 /L_0	α_1'	130 /L_0
f	1.25 P_0/N_0	f	1.25 P_0/N_0
β	0.35 P_0sec/L_0	β'	3.43 P_0sec/L_0

$1/K=1/K_1+1/K_3+1/K_4$

Second, following values described by H. E. Huxley and Hanson (1960)[51] are employed.

$$\left.\begin{aligned} P_o &= 3.0 \text{ Kgwt/cm}^2 \text{ cross section,} \\ L_o &= 1.1\ \mu \text{ / half sarcomere} \\ N_o &= 0.55 \times 10^{13} \text{ /1.1 } \mu \text{ half sarcomere/cm}^2 \text{ cross section} \end{aligned}\right\} \quad (6.48).$$

Third, the energy e_a is calculated. The energy supplied by ATP splitting is about 11 Kcal/Mol (Tonomura, 1972)[82], so that the energy supplied by one molecule of ATP , e_a, is

$$e_a = 11.0 \text{ KCal}/n_o = 7.7 \times 10^{-13} \text{ ergs}$$

where n_o = Avogadoro's number , 6.03×10^{23} /Mol.

Then, 1.0 erg is normalized by P_o, L_o and N_o,

$$1.0 \text{ erg} = 1.7 \times 10^{10}\ P_o.L_o/N_o$$

and consequently we obtain

$$e_a = 1.3 \times 10^{-2}\ P_o.L_o/N_o \quad (6.49).$$

Finally, the values in Table VI-1 are obtained by substituting Eqs. (6.47)-(6.49) into Eq. (6.46).

The same procedure is applied to the lengthening muscle. The relation concerning K, f and α_o is the same as expressed in Eq. (6.46). The constants α_1' and β' are derived from Eq. (6.32);

$$\alpha_1' = \frac{K + \alpha_o}{b'} , \qquad \beta' = \frac{(a' + 2P_o)\ \alpha_1'}{N_o\ K} \tag{6.50}$$

The dynamic constants a' and b' of the lengthening muscle have been already determined as (see section 3.5)

$$a'/P_o = 0.4 , \qquad b'/L_o \approx 0.85\ \text{sec}^{-1} \tag{6.51}.$$

By putting these dynamic constants and the obtained values of α_o, K, P_o and N_o into Eq. (6.50), we can obtain the values of α_1' and β' in Table VI-1. As seen from Table VI-1, remarkable difference between the parameters of lengthening muscles and those of shortening ones is found in the constants of proportionality concerning the force loss, f_v; namely, β' is about ten times greater than β.

ii) The elastic coefficient of the series elastic component

The load-extension relation of the series elastic component (SEC) has been determined at section 3.4. The relation is adopted here. The elastic coefficient E_2 is expressed as

$$\begin{aligned} P &= E_2\ x_2 \\ E_2 &= (2.96 + 5.18\ \hat{x}_2 + 1.9 \times 10^4 \hat{x}_2^{\,2})\ P_o/L_o \end{aligned} \tag{6.52}$$

where x_2 = extension of SEC, $\hat{x}_2 = (x - X)/L_o$.

iii) Estimation of $F_c(ca)$ and $F_\ell(\ell)$

The function of $F_c(ca)$ is determined, based on the physiological data

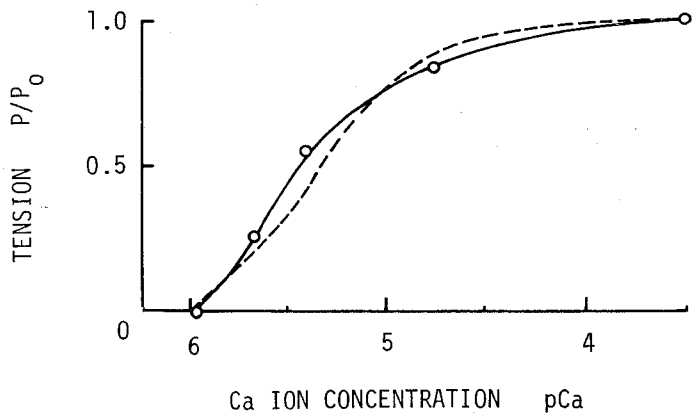

Fig. 6.8 Relation between Ca ion concentration and active tension. Open circle, experimental result obtained from the skinned fibers (see Fig. 2.5 curve A; Ebashi and Endo, 1968); broken line, the relation obtained from Eq. (6.53).

showing the relation between Ca ion concentration (ca) and active tension (P_{act}) at a fixed length ,i.e., $F_{\ell}(\ell)$ is constant. Solid line in Fig. 6.8 shows the relation obtained by Ebashi and Endo (1968). It may be assumed that the value of ca is 10^{-6} Mol at the resting state and 10^{-4} Mol at the tetanic contraction. Because the steady active tension is directly proportional to N*, we can obtain the following relation by applying the curve fitting technique to Fig. 6.8:

$$F_c(ca) = \frac{F_{co}\left(1 - \dfrac{1}{1 + K_c\, ca^2} - \dfrac{F_{cr}}{F_{co}}\right)}{1 - \dfrac{F_{cr}}{F_{co}}} \qquad (6.53)$$

where $K_c = 3.0 \times 10^{10}$ Mol^{-2}, dissociation constant,

F_{cr} = the value of $F_c(ca)$ at $ca=10^{-6}$ Mol,

F_{co} = the value of $F_c(ca)$ at $ca=10^{-4}$ Mol,

$F_{cr}/F_{co} = 0.03$.

The relation of Eq. (6.53) is shown in Fig. 6.8, broken line.

On the other hand, it has been already described that $F_{\ell}(\ell)$ representing the intrinsic length of overlap region of myofilaments corresponds to the tetanic active tension depending on the length of muscle (see section 6.3 b)). The steady active tension developed by tetanic stimuli is directly proportional to $F_{\ell}(\ell)$ because $F_c(ca)$ is considered to be constant F_{co}, so that the active tension-length relation in Fig. 3.2, curve S is applied here. The relation has been also confirmed on the bundle preparation of frog semitendinosus muscle as shown in Fig. 3.2, curve A. Hence, we get

$$\frac{F_{\ell}(\ell)}{F_{\ell o}} = \begin{cases} 0 & ;(1.74 \leqq \ell/L_o) \\ -1.5\ \ell/L_o + 2.01 & ;(1.07 \leqq \ell/L_o < 1.74) \\ 1 & ;(0.95 \leqq \ell/L_o < 1.07) \\ 1.02\ \ell/L_o + 0.038 & ;(0.8 \leqq \ell/L_o < 0.95) \\ 4.42\ \ell/L_o + 2.37 & ;(0.61 \leqq \ell/L_o < 0.8) \\ 0 & ;(\ell/L_o < 0.61) \end{cases} \tag{6.54}$$

$$F_{\ell o} = F_{\ell}(L_o)$$

6.5 SIMULATION OF THE TRANSIENT CHARACTERISTICS

In this section, transient characteristics of muscle contraction involving time courses of tension development, shortening , energy liberation and heat production, are simulated on a digital computer with using the model and the parameters estimated in the former section 6.4. And further, time courses of release and uptake of Ca ion are estimated. Through these simulations, dynamic behaviors of the contractile mechanism and interactions among the internal subsystems are examined.

a) Dynamic behaviors of the model

Most of the parameters have been determined quantitatively in the former section. In order to simulate transient responses of muscle contraction, values of additional parameters such as K_1, K_3 and K_4, and time course of the rate of releasing of Ca ion, $\dot{c}_r(t)$, and that of uptaking, $\dot{c}_u(t)$, are needed. It is pity that those values and the time courses of them have never been observed nor determined experimentally in vivo. Therefore, in order to make preliminaty estimations of the unknown parameters and to comprehend how the model does behave with varying those parameters, simulation experimetns of isometric twitch contractions were made on a digital computer.

First, various values of the parameters K_1, K_3 and K_4 were choosen on the simulations with satisfying the relations $1/K = 1/K_1 + 1/K_3 + 1/K_4$ and $K = 86\ \text{sec}^{-1}$ (see Table VI-1). Second, time courses of the rates of releasing and uptaking of Ca ion, i.e., $\dot{c}_r(t)$ and $\dot{c}_u(t)$ which are produced by a single stimulus are taken as follows*):

$$\dot{c}_r = \begin{cases} 0 & (t \leqq 0) \\ C \dfrac{t}{T_r^2} e^{-\frac{t}{T_r}} & (t > 0) \end{cases}$$

$$\dot{c}_u = \begin{cases} 0 & (t \leqq t_o) \\ C \dfrac{t-t_o}{T_u^2} e^{-\frac{t-t_o}{T_u}} & (t > t_o) \end{cases} \qquad (6.55)$$

where T_r (T_u) = time constant of releasing (uptaking) of Ca ion,

C = constant

t_o = time delay, from the onset of stimulation to the beginning of uptaking of Ca ion.

---

*) $\mathcal{L}[\dot{c}_r(t)] = \dfrac{C}{(1 + T_r s)^2}$, $\mathcal{L}[\dot{c}_u(t)] = \dfrac{C}{(1 + T_u s)^2} e^{-t_o s}$

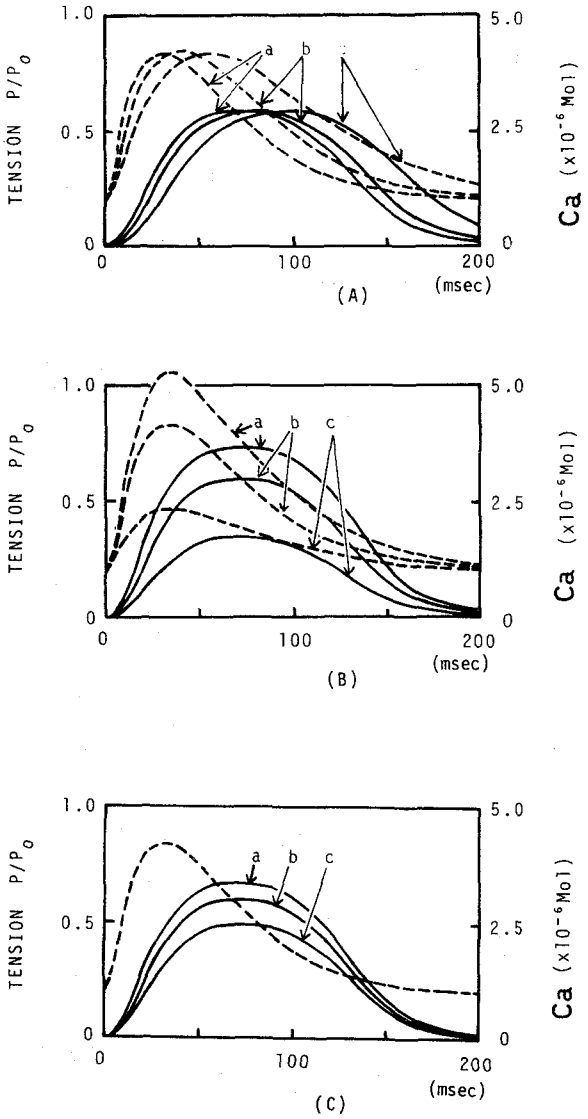

TABLE

Shown in Fig.	(A)			(B)			(C)		
curve	a	b	c	a	b	c	a	b	c
P_{max}/P_o	0.58			0.74	0.58	0.35	0.67	0.58	0.50
t_{pmax} (ms)	70	80	95	70			70		
ca_{max} (x10^{-6}Mol)	4.2			5.8	4.2	2.6	4.2		
t_{camax} (ms)	30	40	55	30			30		
C (x10^{-6}Mol)	4.0	2.8	2.5	6.0	4.0	2.0	4.0		
T_r (ms)	25	25	30	25			25		
T_u (ms)	25.5	27.7	35	25.5			25.5		
t_o (ms)	5			5			5		
K_1 (/sec)	258			258			515	258	129
$K_3.K_4$ (/sec)	258			258			206	258	515

Fig. 6.9 Behaviors of the model for isometric twitch. Solid line, tension curve; broken line, time course of inner Ca ion concentration, ca(t). (A) Effects of changing t_{camax} ; variation of t_{camax} is obtained by changing the values of C, T_r, and T_u, as shown in the inserted table. (B) Effects of changing ca_{max}. (C) Effects of changing K_1.

As represented in Eq. (6.53), inner Ca ion concentration, ca, is taken to be 10^{-6} Mol at the resting state (t = 0). Time course of inner Ca ion concentration, ca(t), is thus expressed as

$$ca(t) = 10^{-6} + \int_0^t (\dot{c}_r - \dot{c}_u)\, dt \qquad (6.56)$$

Third, initial conditions are represented as follows. The muscle is wholly relaxed before onset of stimulation, so that we can write $n_i^* = 0$, $(i = 1.\ 2.\ 3.\ 4)$, $n_i^- = 0$, $(i = 2,\ 3,\ 4)$ and $x = 0$ at $t = 0$. During the isometric contraction, the muscle is fixed at the standard length, L_o, on our experiments, i.e., X=0 and $\ell = L_o$ at t=0.

After these preparatory considerations, then, simulation experiments ts were made on a digital computer with varying the above parameters , T_r, T_u, C, t_o, K_1, K_3 and K_4 over a wide range. Typical results obtained from the simulation experiments are shown in Fig. 6.9. As expected from the figure, the simulation study can lead to following conclusions.

i) Isometric peak tension of twitch contraction, P_{max}, is dependent on both K_1 and maximum value of inner Ca ion concentration, ca_{max}, and it is independent of other parameters.

ii) P_{max} is increased with an increase in K_1 and/or in ca_{max}.

iii) The instant of attaining P_{max}, t_{pmax}, is only dependent on the time of ca_{max}, t_{camax}. The time t_{pmax} becomes earlier as the time t_{camax} is earlier.

iv) As shown in the physiological result (see Fig. 6.10), P_{max} is about at 70 msec(t_{pmax}= 70 msec). In order to satisfy this, t_{camax} has to be about 30 msec.

v) When the value of K_1 is fixed, isometric twitch tension curves are not affected by changing the values of K_3 nor K_4.

b) Simulation of isometric contraction

Solid line in Fig. 6.10 show an isometric twitch tension curve obtained from the bundle preparation of frog semitendinosus muscle fibers at 10 °C. On the basis of above preliminary simulations, following parameter values are taken to account for the twitch contraction in Fig. 6.10; namely, $C = 4.0 \times 10^{-5}$ Mol, $T_r = 25$ msec, $T_u = 25.5$ msec, $t_o = 5$ msec, $K_1 = 190$ sec^{-1}, $K_3 = 310$ sec^{-1} and $K_4 = 310$ sec^{-1}. The response obtained with these values is shown with broken line in Fig. 6.10. The tension curve obtained from the model closely agrees with that obtained from the frog muscle. In this simulation, ca_{max} reaches about 4.2×10^{-6} Mol and the time, t_{camax}, is round 30 msec after the onset of stimulus. It is evident that the time closely coincides with the instant when the rate of tension development, dP/dt, is about maximum. Note that the result is in a good agreement with the experimental evidence demonstrated by Ashley and Ridgway (1970)[8] (see Fig. 2.6). Time courses of $n_i^*(t)$, $n_i^-(t)$, (i=1, 2, 3, 4), $N^*(t)$ and $N^-(t)$ which are obtained from the simulation are also illustrated in Fig. 6.10. It is very interesting that during the relaxation phase (in particular, after about 100 msec from the onset of stimulation), N* is remarkably less than N^-; that is, greater parts of working active centers remain the state of A_s^- (active centers have no Ca ion) in the phase.

c) Simulation of isotonic contraction

Solid lines in Fig. 6.11 show tension and shortening curves in an isotonic twitch contraction which were obtained from the frog semitendinosus muscle at 10 °C. After-load was 1.5 g (0.23 P_o) in curve a , and 2.5 g (0.4 P_o) in curve b. Initial length was L_o in the both experiments.

These isotonic twitches are simulated with applying the model and the same parameter values as used in the simulation of isometric twitch of Fig. 6.10. The responses obtained in such a way are shown in Fig. 6.11, with

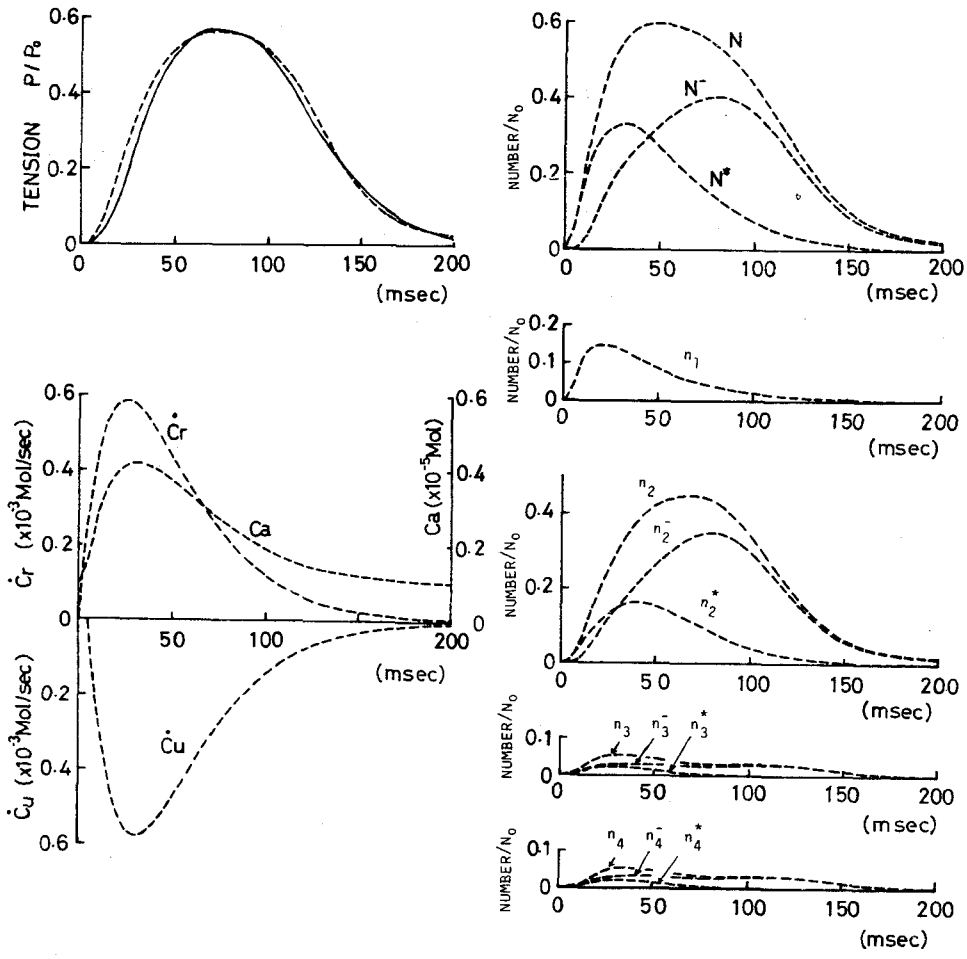

Fig. 6.10 Simulation of isometric twitch contraction.
Solid line, experimental result ontained from the bundle preparation of frog semitendinosus muscle at 10 °C; P_o=6.0 gwt, L_o=13 mm. Broken line, response of the model; T_r=25 msec, T_u=25.5 msec, t_o= 5 msec, C=4.0 × 10^{-5} Mol, K_1=190 sec^{-1} and K_3=K_4=310 sec^{-1}.

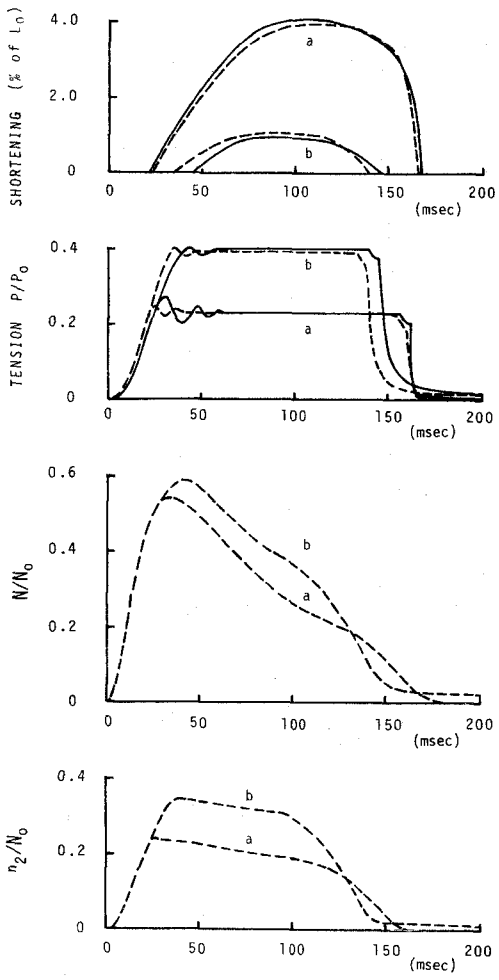

Fig. 6.11 Simulation of isotonic twitch contraction. Solid line, physiological result obtained from the bundle preparation of the frog semitendinosus muscle at 10 °C; P_o=6.0 gwt, L_o=13 mm; curve a, after-load was 1.5 g (0.23 P_o); curve b, 2.4 g (0.4 P_o). Broken line, response of the model; T_r=25 msec, T_u=25.5 msec, t_o=5 msec, K_1=190 sec^{-1}, K_3=K_4=310 sec^{-1}.

broken line. Both shortening and tension curves obtained from the model show close agreements with those from the frog muscle. It is of obvious interest that the number of force-generating cross-bridges, n_2, which are working against heavier load (curve b) is greater than that against lighter load

(curve a). This feature would evidently imply an excellent function of the contractile mechanism of muscle; i.e., the muscle generates greater force against heavier load and smaller force against lighter load.

d) Energy liberation and heat production during twitch

Both energy and heat produced during the period from the beginning of stimulus (t=0) to t_m are calculated where t_m is the time when maximum shortening of isotonic twitch is achieved. It is assumed here, similar to section 6.4, that one molecule of ATP is hydrolyzed during single cycles of the contractile reaction, 1)→2)→3)→4) in Fig. 6.3. However, it is not clear whether the hydrolysis occurs at the stage of reaction from 2) to 3) or from 3) to 4), so that we examine two cases.

Case (1): ATP hydrolysis takes place at the reaction from 2) to 3).

Case (2): ATP hydrolysis takes place at the reaction from 3) to 4).

The rate of energy liberation of case (1), $\dot{E}_1$, and that of case (2), $\dot{E}_2$, are

$$\dot{E}_1 = e_a K_2 n_2 \tag{6.50}$$

$$\dot{E}_2 = e_a K_3 n_3 \tag{6.58}$$

Total energy liberated during the period from t=0 to $t=t_m$ is

$$\begin{aligned} &\text{case (1):} \quad E_1 = \int_0^{t_m} \dot{E}_1 \, dt \\ &\text{case (2):} \quad E_2 = \int_0^{t_m} \dot{E}_2 \, dt \end{aligned} \tag{6.59}$$

On the other hand, work done, W, is expressed as the product of load, P, and maximum shortening attained at $t=t_m$, X_{max};

$$W = P X_{max} \tag{6.60}$$

On the assumption that the shortening heat, H_s, is produced with force-loss, we can write

$$H_s = \int_0^{t_m} \dot{H}_s \, dt \tag{6.61}$$

$$\dot{H}_s = n_2 f_v v \tag{6.37}$$

Activation heat, H_a, and total heat, H, can not be expressed directly but they can be estimated by employing the above calculated values of E, H_s and W. That is, activation heat, H_a, is obtained by

$$\begin{aligned} &\text{Case (1):} \quad H_{a1} = E_1 - H_s - W \\ &\text{Case (2):} \quad H_{a2} = E_2 - H_s - W \end{aligned} \tag{6.62}$$

Further, total heat, H, is given by

$$\begin{aligned} &\text{Case (1):} \quad H_1 = E_1 - W \\ &\text{Case (2):} \quad H_2 = E_2 - W \end{aligned} \tag{6.63}$$

We made computer simulations for isotonic twitches against various after-loads in the same way as described in the above section c), and calculated W, E_1, E_2, H_s, H_{a1}, H_{a2}, H_1 and H_2 with employing Eqs. (6.57)-(6.63). Calculated results are shown in Fig. 6.12 (A). As seen in the figure, E_1 is slightly greater than E_2. In either case, total energy liberated (E_1 or E_2) and the shortening heat H_s were decreased with increasing load. But activation heat, H_a, was gradually increased with an increase in load. Total heat (H_1 or H_2) decreased steeply at lighter load with an increase in load, while it tended to decrease gradualllly at greater load. For comparison, Fig. 6.12 (B) is given which is the experimental result obtained from frog sartorius and toad semi-membrainosus muscle at 0 °C (Hill, 1949a).[37] As seen from Fig. 12 (A) and (B), the relations obtained from the model give the same features as actually observed on the muscles, although quantitative comparison can not be made satisfactorily because of differences of the preparations and the experimental conditions between (A) and (B).

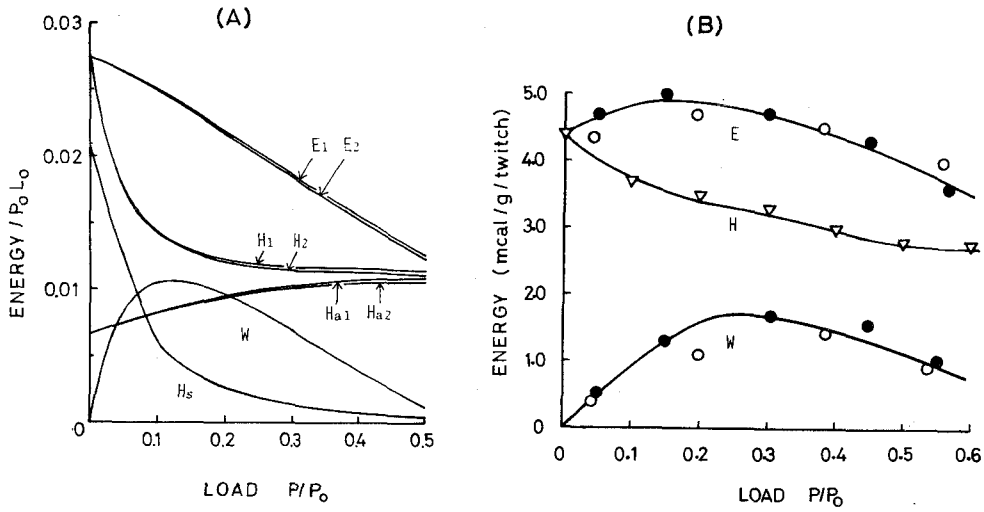

Fig. 6.12 Overall energy balance during twitch, plotted against the load. E, total energy; H_1, total heat for case (1) ; H_2, total heat for case (2); H_s, shortening heat; H_{a1}, activation heat for case (1); H_{a2}, activation heat for case (2); W, work.
(A) Simulated result obtained from the model; (B) experimental result obtained from frog sartorius(open circle, open triangle) and semi-membrainosus muscle (closed circle) by Hill (1949a).[37]
The figure (B) is redrawn from Bendall (1969).[13]

6.6 DISCUSSION

The present study has an important significance in building the single unified theory of muscle contraction by synthesizing recent findings such as minute observations of the ultrastructure of muscle fiber, biochemical speculations about the contractile process at the molecular level, and physiological data on mechanical and thermodynamical properties of muscle contraction. Hitherto, such an approach has tended towards qualitative investigations all along, but the present work does take a quantitative and dynamical view of the muscle contraction. In such an investigation is one of the characteristics features of the present work. Serious difficulties have been encountered in building the model because several matters have not

TABLE VI-2

COMPARISON OF THE ESTIMATED VALUES OF RELATIVE DISPLACEMENT AND SLIDING FORCE

	ℓ_c Å	f dyne	Estimation	W ergs	e_a ergs	η %	P_o $\frac{dyne}{cm^2}$	N_o $\frac{/cm^2}{1.1\ \mu}$
Huxley (1960)	120							
Davies (1963)	100	3×10^{-7}	$\ell_c=W/f$ $f=P_o/N_o$	ne_a	7×10^{-13}	44	2×10^{6}	6.5×10^{12}
Deshcherevskii (1968)	100	3×10^{-7}	$\ell_c=W/f$ $f=P_o/N_o$	3×10^{-13}			3×10^{6}	5.0×10^{12}
Volkenstein (1968)		4.6×10^{-7}	$f=P_o/N_o$				3×10^{6}	6.5×10^{12}
Chaplain (1971)	127							
Tonomura et al. (1972)	100	3×10^{-7}	$\ell_c=W/f$	ne_a	6×10^{-13}	50		
This thesis	92	6.7×10^{-7}	$\ell_c=1/\alpha_1$ $f=1.25P_o/L_o$	$\alpha_1=120/L_o$ $L_o=1.1\mu$			3×10^{6}	5.5×10^{12}

η =efficiency of transformation from chemical to mechanical one

been fully established by biochemical nor by physiological studies. Nevertheless, by introducing reasonable and probable assumptions, all the static and dynamic characteristics of muscle contraction could be satisfactorily accounted for.

In this place, we try to examine three following problems of particular interest and of significance with making reference to the proposed model.

i) How far cross-bridges can make thin filaments slide past in single cycles of the contractile reaction? That is, how long is the relative displacement (the stroke) of cross-bridges?

ii) How does the interaction of Ca ion occur with the contractile system, actin-myosin-ATP system?

iii) In what stage or when does the hydrolysis of ATP take place ? How many molecules of ATP are hydrolyzed in single cycles of the contractile reaction?

a) Relative displacement of cross-bridges

The mean relative displacement of cross-bridges, ℓ_c, can be estimated by applying the same technique as proposed by Deshcherevskii (1968)[26]. Namely,

according to Deshcherevskii, a mean value of conformational transformation of the molecule of myosin, equal to the interval in which the cross-bridge develops an active force, is given as $\ell_c = 1/\alpha_1$. As given in Table VI-1, the value of α_1 has been estimated as $\alpha_1 = 120\ L_o^{-1}$. Consequently, the relative displacement during shortening becomes

$$\ell_c = 1/\alpha_1 = L_o/120 = 92\ \text{Å} \tag{6.64}$$

where L_o = 1.1 μ/half sarcomere.

Similarly, a relative displacement during lengthening, ℓ_c', is calculated by applying $\alpha_1' = 130\ L_o^{-1}$ (see Table VI-1).

$$\ell_c' = 1/\alpha_1' = L_o/130 = 85\ \text{Å} \tag{6.65}$$

As shown in Fig. 2.2, a pitch of the myosin head is about 429 Å and that of F-actin is about 355 Å , and thus the difference is 74 Å . The relative displacement of cross-bridges would be associated with the difference of both pitches, and it is interesting that the estimated values, $\ell_c = 92$ Å and $\ell_c' = 85$ Å , are in the same order.

On the other hand, many workers have suggested, performing different kinds of calculations, that maximum value of the relative displacement of the cross-bridges is about 100 Å, as shown in Table VI-2. Our result was also in the same order. Seeing that the problem as to how the cross-bridges move and slide past thin filaments remains unaccounted for at all, it would be an important future subject to observe ℓ_c or ℓ_c' experimentally.

b) Alternative model I: Interaction of Ca ion with the contractile machinery

In the present work, we assumed that binding or uptaking of Ca ion from Ca-receptive cites is independent of contractile processes of the actin-myosin-ATP system, and introduced the concept of A_s^* and A_s^- with respect to active centers of thin filaments. However, following assumtions [a] and [b] would also be possible and actually suggested by some workers.

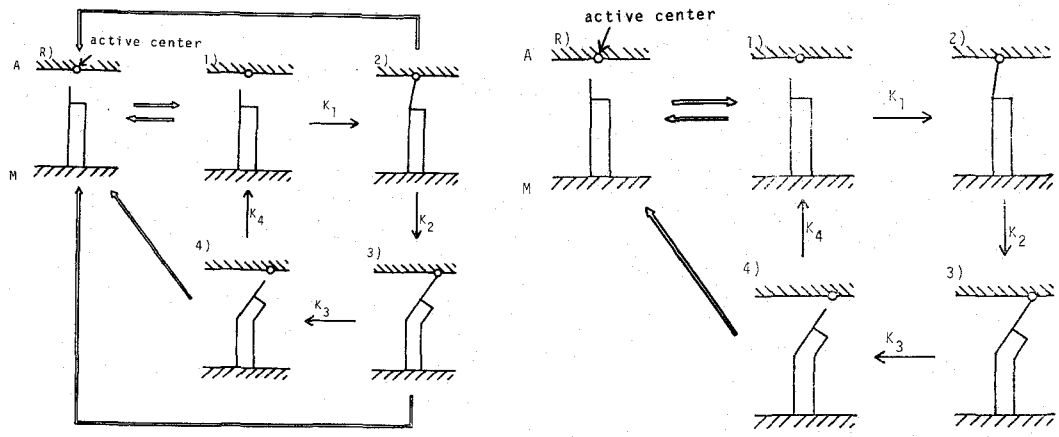

(A) (B)

Fig. 6.13 Schematic illustration of the mechanism of muscle contraction (A), assumption [a]; (B), assumption [b]. The arrow $\longrightarrow$ shows the chemical reaction of actin-myosin-ATP contractile system , the rate constant of which is K_i , (i= 1, 2, 3, 4). The arrow $\Longrightarrow$ shows the dissociation reaction associated with binding and uptaking of Ca ion; a dissociation constant of which is K_c.

Assumption [a]: When Ca ion is uptaken from troponin, cross-bridges dissociate from thin filaments, and the corresponding active centers are immediately returned to the resting state.

Assumption [b]: Binding-Ca ion is uptaken only from the states 1) and 4), and then the active centers are returned to the resting state.

In order to examine the possibility of their assumptions, an isometric twitch contraction is simulated with using them. The simulated results, later shown, lead to the conclusion that both assumtions can not explain the experimental findings demonstrated by Ashley and Ridgway (1970)[8], about the time courses of Ca ion concentrateon. Namely, the conclusive remark is that our assumption [1] (see section 6.3 c)) is most probable as regards the interaction of Ca ion

with the contractile machinery.

i) Mathematical formulation

Assumption [a] :

The molecular mechanism of contraction is schematically shown in Fig. 6.13 (A). The state A_s^- is not necessary to be considered under this assumption at all. The kinetic equation for this case is

$$\begin{aligned}
\dot{n}_1^* &= \dot{N}_r + K_4 n_4^* - K_1 n_1^* - \dot{N}_u n_1^* /N^* \\
\dot{n}_2^* &= K_1 n_1^* - K_2 n_2^* - \dot{N}_u n_2^*/N^* \\
\dot{n}_3^* &= K_2 n_2^* - K_3 n_3^* - \dot{N}_u n_3^*/N^* \\
\dot{n}_4^* &= K_3 n_3^* - K_4 n_4^* - \dot{N}_u n_4^*/N^*
\end{aligned} \qquad (6.66)$$

Assumption [b] :

The molecular mechanism of contraction is shown in Fig. 6.13 (B). The kinetic equation for this case is

$$\begin{aligned}
\dot{n}_1^* &= \dot{N}_r + K_4 n_4^* - K_1 n_1^* - \dot{N}_u n_1^*/(n_1^* + n_4^*) \\
\dot{n}_2^* &= K_1 n_1^* - K_2 n_2^* \\
\dot{n}_3^* &= K_2 n_2^* - K_3 n_3^* \\
\dot{n}_4^* &= K_3 n_3^* - K_4 n_4^* - \dot{N}_u n_4^*/(n_1^* + n_4^*)
\end{aligned} \qquad (6.67)$$

ii) Simulated results

Solid line in Fig. 6.14 is the isometric twitch tension curve obtained from the bundle preparation of frog semitendinosus muscle at 10 °C. Now we simulate this twitch contraction with applying above equations (6.66) and (6.67) and compare them with the physiological result. It should be noted that the steady state characteristics of muscle obtained from both assumptions, [a] and [b], are quite the same as obtained from the assumption

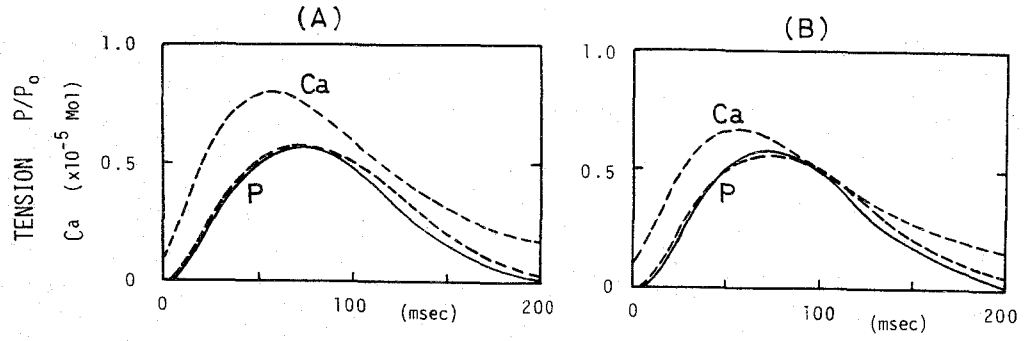

Fig. 6.14 Simulation of isometric twitch. Solid line, isometric twitch tension curve obtained from the bundle preparation of frog semitendinosus muscle, P_o=6.0 gwt, L_o=13 mm, 10 °C. Broken line, responses of the model; P, isometric tension curve; ca, inner Ca ion concentration; (A), response obtained from the assumption [a], $K_1=K_3=K_4=258\ sec^{-1}$, T_r=27.5 msec, T_u=35 msec, t_o=5 msec, $C=4.0 \times 10^{-5}$ Mol; (B), response obtained from the assumption [b], $C=3.2 \times 10^{-5}$ Mol, other parameters are identical to (A).

[1]. Consequently, the parameter values in Table VI-1 can be employed.

Eq. (6.66) is employed for the assumption [a] instead of Eq. (6.18), while other relations used in the simulation are the same as expressed at sections 6.4 and 6.5. The parameters concerning Eq. (6.55) ,i.e., the rates of Ca ion-releasing and of Ca ion-uptaking, are choosen so that the response of the model could closely agree with the experimental tension curve. Namely, we took the parameter values given in Fig. 6.14. Fig. 6.14 (A) shows the response of the model obtained by using the assumption [a] and the parameter values. Close agreement was obtained between the experimental tension curve (solid line) and the simulated one (broken line). However, as seen from the figure, the peak of inner Ca ion concentration was nearly at the time when the peak tension was attained, and it is not at the time of maximum of dP/dt. Namely, the assumption [a] could not by any possibility

explain the experimental result demonstrated by Ashley and Ridgway (1970)[8]. Of course, we varied the values of above parameters (K_i, T_r, T_u, t_o , C) to a wide extent but failed to account for Ashley's results.

As to the assumption [b], similar simulation experiments were made. The simulated result is shown with broken line in Fig. 6.14 (B), where the parameter values of K_i, T_r, T_u, t_o and C are given. As seen from the figure, the assumption [b] can not explain Ashley's findings neither.

c) Alternative model II : ATP splitting

According to A. F. Huxley (1957)[45] and Davies (1963)[25], it was assumed in the present work that one molecule of ATP is hydrolyzed in single cycles of the contractile reaction, 1)→2)→3)→4) in Fig. 6.3. On the other hand, according to the molecular mechanism model proposed by Tonomura (1972)[82] (see Fig. 2.8), it may be also probable to assume that two molecules of ATP are splitted in the single cycles. Although the model proposed in the present study would be enough to be as a basic one, it is also of interest and of significance in offering a clue for further studies to examine the concept of splitting of two molecules of ATP. Here we term the concept of splitting of one molecule of ATP case [1ATP], and that of two molecules case [2ATP]. The parameter values are estimated for the concept of case [2ATP] and then they are compared with those for case [1ATP]. The procedure for case [2ATP] is similar to that described in section 6.4. c) where case [1ATP] is treated.

It is assumed that one molecule of ATP is hydrolyzed at the reaction of changing from the state 2) to 3) and the other one molecule of ATP at the reaction from 3) to 4). Namely, we get the rate of energy liberation as

$$\dot{E} = n_2 K_2 e_a + n_3 K_3 e_a \qquad (6.68)$$

Substituting Eqs. (6.24), (6.26) and (6.28) into Eq. (6.68), we can get

TABLE VI-3

Parameters estimated from the assumption that two molecules of ATP are splitting in single cycles of the contractile reaction.

SHORTENING		LENGTHENING	
K	43 /sec	K	43 /sec
α_0	11 /sec	α_0	11 /sec
α_1	60 /L_0	α_1'	63 /L_0
f	1.25 P_0/N_0	f	1.25 P_0/N_0
β	0.35 P_0sec/L_0	β'	3.43 P_0sec/L_0

$$\dot{E} = \frac{2\, e_a\, N_o K^2/\alpha_1\, b}{P_o + a} \left\{ \frac{\alpha_o (P_o + a) + K\, P_o}{K} - P \right\} \qquad (6.69)$$

Because the rate of energy dissipation represented by Eq. (6.40), $\dot{W} + \dot{H}_s + \dot{H}_m$, has to be equal to Eq. (6.69), the following relations can be obtained:

$$\begin{aligned} b\, P_o &= 2\, e_a\, N_o K^2/\alpha_1\, b \\ P_o + a(P_o + a)/P_o &= \left\{ \alpha_o (P_o + a) + K\, P_o \right\}/K \end{aligned} \qquad (6.70)$$

Consequently, from Eqs. (6.28), (6.32) and (6.70), following relations are obtained:

$$\begin{aligned} &K = (1 + a/P_o)\, b\, P_o/\, 2\, e_a\, N_o\,, \quad f = (K + \alpha_o)\, P_o/\, K\, N_o \\ &\alpha_o = a\, K/\, P_o\,, \quad \alpha_1 = (K + \alpha_o)/\, b\,, \quad \alpha_1' = (K + \alpha_o)/\, b' \\ &\beta = a\, \alpha_1/\, N_o K\,, \quad \beta' = \alpha_1'(a' + 2P_o)/\, N_o K \end{aligned} \qquad (6.71)$$

Putting the values of a, b, P_o, N_o, L_o and e_a in Eqs. (6.47)-(6.51), finally we get the parameters for case [2ATP] given in Table VI-3. Comparing them

with those of case [1ATP] given in Table VI-1, we may conclude as follows.

i) Force generated by single cross-bridges, f, and constants concerning the force-loss, β and β' are identical with each other.

ii) The rate constants of K, α_o, α_1, and α_1' of case [2ATP] are half the values of case [1ATP].

iii) Relative displacements of cross-birdges for case [2ATP] are

$$\ell_c = 1/\alpha_1 = L_o/60 \cong 184 \text{ Å} \qquad (6.72)$$

$$\ell_c' = 1/\alpha_1' = L_o/63 \cong 170 \text{ Å}$$

These values are also half the values obtained from case [1ATP], as seen from comparison of Eq. (6.72) with Eq. (6.64)-(6.65).

Indeed , it is pity that we can not conclude whether case [1ATP] or case [2ATP] is true , from these calculations. But, as expected from these comparisons, to measure the relative displacement of cross-bridges is of great significance and would give an important clue for the problem of stages of ATP splitting. Further studies such as electron microscopic observations in vivo or X-ray diffraction recordings, would be necessary to determine the relative displacements.

d) Force-loss of the muscle contraction

A velocity-dependent force-loss of cross-bridges is assumed to be produced in the state 2) in the present work (see Eq. (6.7)), while it was assumed to be in the state 3) by Deshcherevskii (1968). Considering sliding movements of the cross-bridges in the viscous sarcoplasma some one would presume such a viscous force as being dependent on the velocity of sliding, or would introduce a force-loss (friction-like force) generated by some what relative movements on the attachments between myosin heads and thin filaments. This view corresponds to our assumption. On the other hand, somewhat force loss is presumably developed when cross-bridges dissociate from thin fila-

ments. This view seems to correspond to Deshcherevskii's. The force-loss of contraction would be undoubtedly due to the molecular movements of myofilaments, but it is now difficult and rather impossible to conclude what the nature of the force-loss is nor by what mechanisms the loss is produced. This problem is certainly associated with the energy conversion of muscle contraction. At any rate, further study of the mechanism of energy conversion is strongly required.

6.7 CONCLUSION

A mathematical model of muscle contraction was developed, which could account for various mechanical and thermodynamical properties of contraction, and molecular events of the mechano-chemical coupling and excitation-contraction coupling in the fully dynamic sense.

1. The two-component model consisting of the contractile component (CC) and the series elastic component (SEC) was adopted as a mechanical model. The CC was modeled, based on the microstructure of muscle fiber, the molecular mechanism of actin-myosin-ATP system, the sliding-filament mechanism and the excitation-contraction coupling involving regulation of Ca ion.

2. A leading nonlinear characteristic of the CC model was an increase in the rate constant K_2 produced by increasing velocity of sliding movements (see Eq. (6.15)).

3. The force-load-velocity relation, load-energy liberation relation and load-heat production relation were accounted for by the model.

4. All the parameters involved in the model (rate constants, dissociation constant, force generated by single cross-bridges, etc.) were determined quantitatively by using the physiological data obtained in chapter III.

5. Isometric twitch contraction was simulated on a digital computer by the model, and close agreements were shown between the responses of the

model and the experimental curves of tension and inner Ca ion concentration.

6. Isotonic twitches against various loads were also simulated on a digital computer. Tension and shortening curves obtained from the model showed close coincidence with those from the frog semitendinosus muscle.

7. A mean value of the relative displacement of cross-bridges was estimated to be about 92 Å during shortening and about 85 Å during lengthening.

8. Following problems are discussed ; i) regulation of the reaction of actin-myosin-ATP system by Ca ion; ii) number of molecules of ATP which are hydrolyzed during single contractile reaction.

CHAPTER VII

CONCLUSION

Both dynamic behaviors of the contractile mechanism and mechanical properties of the muscle contraction were explicated by means of simulation studies on a computer and physiological experiments made on the bundle preparations dissected from frog semitendinosus muscle at 10 °C. Every possible effort was devoted to develop the unified model of muscle contraction. An outline of the obtained results is given here, since details of them are represented in the section of conclusion of each chapter.

1. Mechanical properties of the resting and contracting muscles were determined quantitatively by the physiological recordings (chapter III).

i) Viscous and elastic properties of the resting muscles were determined (Table III-2).

ii) The load-extension relation of the series elastic component of the contracting muscles was determined. The series elasticity was expressed as a function of extension by Eq. (3.3).

iii) Transient responses to the isotonic quick releases were simulated on a digital computer using the model, and the experimental load-extension relation , Eq. (3.3), was confirmed (section 3.4).

iv) The force-load-velocity relations of the contracting muscle during shortening and lengthening were determined (Eqs. (3.19) and (3.20)). The viscou-like force was expressed as a function of force and velocity by arranging the force-load-velocity equations(Eqs. (3.18) and (3.22)).

2. The time courses of the active state were estimated by mathematical analyses based on the three-component mechanical model consisting of the force generator, the viscous-like and series elastic components (sections 4.3 and 4.4). The analytical curves were compared with the experimental

ones estimated by quick release or stretch in the bundle preparation (section 4.6). The analytical active state curve agreed approximately with the experimental curve, when the amount of release or stretch was less than 2 % of the standard length.

3. A mechanical model consisting of force generator, viscous and elastic components under the resting and contracting states was developed, based on the results obtained in chapters III and IV (section 5.2). Dynamic characteristics of muscle contraction were explained quantitatively in terms of the model (section 5.3). Correspondence of the model to the microstructure and to the sliding-filament theory was represented (section 5.4).

4. A mathematical model of the contractile component was developed, based on the actin-myosin-ATP reaction system, the sliding-filament theory and the excitation-contraction coupling (section 6.3). A total model of the muscle contraction was developed by introducing the contractile component model into the two-component model consisting of the series elastic and contractile components.

i) All the parameters of the contractile component model were determined quantitatively by employing the physiological data obtained in chapter III (section 6.4).

ii) The model accounted for the force-load-velocity, load-energy liberation and load-heat production relations (section 6.4).

iii) Transient responses of isometric and isotonic twitches were simulated on a digital computer. The simulated results showed close agreements with the physiological data obtained from frog semitendinosus muscle (section 6.5).

iv) Time courses of the rate of releasing of Ca ion and that of uptaking, and those of inner Ca ion concentration were estimated (section 6.5).

v) It was shown that, when heavier load was applied, number of the force-developing cross-bridges was increased and less energy was liberated.

vi) Mean values of the relative displacement of cross-bridges in single cycles of the contractile reaction were estimated to be 92 Å during shortening and 85 Å during lengthening (section 6.6).

REFERENCES

1) Abbott, B. C. and Aubert, X. (1952) The force exerted by active striated muscle during and after change of length. J. Physiol., 177, 77-86.

2) Abbott, B. C. and Wilkie, D. R. (1953) The relation between velocity of shortening and the tension-length curve of skeletal muscle. J. Physiol., 120, 214-223.

3) Akazawa, K., Fujii, K. and Kasai, T. (1969) Analysis of muscular contraction mechanism by viscoelastic model. Tech. Repts. of Osaka Univ., 19, 577-595.

4) Akazawa, K., Fujii, K., Kasai, T. and Mashima, H. (1970a) Simulation of muscular contraction based on sliding mechanism. Jap. J. Medical Electronics and Biol. Engineering, 8, 203-211. (in Japanese).

5) Akazawa, K., Fujii, K., Kasai, T. and Mashima, H (1970b) Dynamic properties of viscous and contractile components. Jap. J. Medical Electronics and Biol. Engineering, 8, 212-219. (in Japanese).

6) Akazawa, K., Fujii, K. and Mashima, H. (1971) Mechanical properties of skeletal muscle. The 2nd domestic symposium of Biomechanism, Minami-Izu, Japan, 175-188. (in Japanese).

7) Apter, J. P. and Graessley, W. W. (1970) A model of muscular contractile elements suitable for quantifying human muscular action. AMRL-TR-70-60, The use of computers for man-machine modeling. 6-26.

8) Ashley, C. C. and Ridgway, E. B. (1970) On the relationship beween membrane potential, calcium transient and tension in single barnacle muscle fibres. J. Physiol., 209, 105-130.

9) Bahler, A. S. (1967) Series elastic component of mammalian skeletal muscle. Am. J. Physiol., 213, 1560-1564.

10) Bahler, A. S. (1968) Modeling of mammalian skeletal muscle. IEEE Trans. on Bio-Medical Engineering, BME-15, 249-257.

11) Bahler, A. S., Fales, J. T. and Zierler, K. L. (1967) The active state of mammalian skeletal muscle. J. Gen. Physiol., 50, 2239-2253.

12) Bahler, A. S., Fales, J. T. and Zierler, K. L. (1968) The dynamic properties of mammalian skeletal muscle. J. Gen. Physiol., 51, 369-384.

13) Bendall, I. R. (1969) "Muscles, molecules, and movement." Heinemann Educational Books LTD.: London.

14) Bornholst, W. J. and Minardi, J. E. (1970) A phenomenological theory of muscular contraction. Biophysical J., 10, 137-171.

15) Briden, K. L. and Alpert, N. R. (1972) The effect of shortening on the time course of active state decay. J. Gen. Physiol., 60, 202-220.

16) Buchthal, F. and Kaiser, E. (1944) Factors determining tension development in skeletal muscle. Acta physiol. scand., 8, 38-74.

17) Buchthal, F. and Kaiser, E. (1951) The rheology of the cross striated muscle fibre. Dan. Biol. Medd., 21, 1-318.

18) Carlson, F. D. (1957) Kinematic studies on mechanical properties of muscle. In "Tissue elasticity." Remington, J. W., Ed., Am. Physiol.Soc., 55-72.

19) Cavagna, C. A. (1970) The series elastic component of frog gastrocnemius. J. Physiol., 206, 257-262.

29) Chaplain, R. A. and Frommelt, B. (1971) A mechanochemical model for muscular contraction. I: The rate of energy liberation at steady state velocities of shortening and lengthening. J. Mechanochem. Cell Motility, 1, 41-56.

21) Civan, M.M. and Podolsky, R. J. (1966) Contraction kinetics of striated muscle fibres following quick changes in load. J. Physiol., 184, 511-534.

22) Close, R. (1962) The pattern of activation in the sartorius muscle of the frog. J. Gen. Physiol., 46, 1-18.

23) Close, R. and Hoh, J. F. Y. (1967) Force:velocity properties of kitten muscle. J. Physiol., 192, 815-822.

24) Csapo, A. (1955) The mechanism of myometrial function and its disorders. In "Modern Trends in Obstetrics and Gynecology." Bowes, K. Ed., Butterworth and Co., London, Ser. 2, Chap. 2, 20-49.

25) Davies, R. A. (1963) A molecular theory of muscle contraction. Nature, 199, 1068-1074.

26) Deshcherevskii, V. I. (1968) Two models of muscular contraction. Biofisika, 13, 1093-1101.

27) Dumoulin, C. and Marechal, G. (1970) Transient changes in the force-velocity relationship during tetanic contractions of frog sartorius muscles, normal or poisoned with 1-fluoro-2, 4-dinitrobenzene. Pflugers Arch., 316, 114-131.

28) Ebashi, S. and Endo, M. (1968) Calcium and muscle contraction. Prog. in Biophysics and Molecular Biol., 18, 123-183.

29) Edman, K. A. P. and Nilson, E. (1968) The mechanical parameters of myocardial contraction studied at a constant length of the contractile element. Acta Physiol. Scand., 72, 205-219.

30) Edman, K. A. P. (1970) The rising phase of the active state in single skeletal muscle fibres of the frog. Acta Physiol. Scand., 79, 167-173.

31) Edman, K. A. P. and Kiessling, A. (1971) The time course of the active state in relation to sarcomere length and movement studied in single skeletal muscle fibres of the frog. Acta Physiol. Scand., 81, 182-196.

32) Galey, F. R. (1969) Elastic properties of fixed and fresh muscle. J. Ultrastruct. Res., 26, 424-441.

33) Gasser, H. S. and Hill, A. V. (1924) The dynamics of muscular contraction. Proc. Roy. Soc. B, 96, 398-437.

34) Gordon, A. M., Huxley, A. F. and Julian, F. J. (1966) The variation in isometric tension with sarcomere length in vertebrate muscle fibres. J. Physiol., 184, 170-192.

35) Hanson, J. and Lowey, J. (1963) The structure of F-actin and of actin filaments isolated from muscle. J. Mol. Biol., 6, 46-60.

36) Hill, A. V. (1938) The heat of shortening and the dynamic constants of muscle. Proc. Roy. Soc. B, 126, 136-195.

37) Hill, A. V. (1949a) The heat of activation and the heat of shortening in a muscle twitch. Proc. Roy. Soc. B, 136, 195-211.

38) Hill, A. V. (1949b) The abrupt transition from rest to activity in muscle. Proc. Roy. Soc. B, 136, 399-420.

39) Hill, A. V. (1950) The series elastic component of muscle. Proc. Roy. Soc. B, 137, 273-280.

40) Hill, A. V. and Woledge, R. C. (1962) An examination of absolute values in myothermic measurements. J. Physiol., 162, 311-333.

41) Hill, A. V. (1964) The effect of load and the heat of shortening of muscle. Proc. Roy. Soc. B, 159, 297-318.

42) Hill, A. V. (1970) "The first and last experiment in muscle mechanics." Cambridge: Cambridge University Press.

43) Hill, T. L. (1970) Sliding filament model of muscular contraction. J. Theor. Biol., 29, 395-410.

44) Houk, J. (1966) The stretch reflex in human muscle systems. In " The application of control theory to physiological systems." Milhorn, H. T. Ed. 283-316, London: W. B. Saunders.

45) Huxley, A. F. (1957) Muscle structure and theories of contraction. Prog. Biophys. Biophysical Chem., 7, 255-318.

46) Huxley, A. F. and Simmons, R. M. (1971) Proposed mechanism of force generation in striated muscle. Nature, 233, 533-538.

47) Huxley, H. E. (1957) The double array of filaments in cross-striated muscle. J. Biophys. Biochem. Cytol., 3, 631-648.

48) Huxley, H. E. (1964) Structural arrangements and the contraction mechanism in striated muscle. Proc. Roy. Soc. B, 160, 442-448.

49) Huxley, H. E. (1967) Recent X-ray diffraction and electron microscope studies of striated muscle. J. Gen. Physiol., 50, 71-83.

50) Huxley, H. E. (1969) The mechanism of muscular contraction. Science, 164, 1356-1366.

51) Huxley, H. E. and Hanson, J. (1960) The molecular basis of contraction in cross-striated muscle. In "Structure and function of muscle, Vol. 1." Bourne, G. H. Ed. London: Academic Press.

52) Jewell, B. R. and Wilkie,D. R. (1958) An analysis of the mechanical components in frog's striated muscle. J. Physiol., 143, 515-540.

53) Jewell, B. R. and Wilkie, D. R. (1960) The mechanical properties of relaxing muscle. J. Physiol., 152, 30-47.

54) Katchalsky, A. (1954) Progress in Biophysics and Biophysical Chemistry. Pergamon Press.

55) Kato, I. and Ishida, T. (1969) Development of artificial rubber muscle. Proc. of 3rd International Symposium on External Control of Human Extremities. Dubrovnik, Aug., 1969.

56) Katz, B. (1939) The relation between force and speed in muscle contraction. J. Physiol., 96, 45-64.

57) Levin, A. and Wyman, J. (1927) The viscous elastic propoerties of muscle. Proc. Roy. Soc. B, 101, 218-243.

58) McRuer, D. T., Magdaleno, R. E. and Moore, G. P. (1969) A neuromuscular actuation system model. IEEE Trans. on Man-Machine System, MMS-9, 61-71.

59) Mashima, H., Akazawa, K., Kushima, H. and Fujii, K. (1972) The force-load-velocity relation and the viscous-like force in the frog skeletal muscle. Jap. J. Physiol., 22, 103-120.

60) Mashima, H., Akazawa, K., Kushima, H. and Fujii, K. (1973) Graphical analysis and experimental determination of the active state in frog skeletal muscle. Jap. J. Physiol., 23, 217-240.

61) Mashima, H. and Handa, M. (1969) The force-velocity relation and the dynamic constants of the guinea-pig taenia coli. J. Physiol. Soc. Japan, 31, 565-566.

62) Mashima, H. and Kushima, H. (1971) Determination of the active state by the graphical, experimental and instantaneous methods in the frog ventricle. Jap. Heart J., 12, 545-561.

63) Mashima, H. and Matsumura, M. (1960) On the relation between force and shortening during muscle twitch. Jap. J. Physiol., 10, 602-609.

64) Mashima, H. and Tsuchiya, H. (1968) Mechanical response generated by alternating current or repetitive square pulses in the frog skeletal muscle. Jap. J. Physiol., 18, 417-431.

65) Mashima, H. and Washio, H. (1968) The changes in membrane potential produced by alternating current or repetitive square pulses in the frog skeletal muscle fibres. Jap. J. Physiol., 18, 4.3-416.

66) Matsumoto, Y. (1967) Validity of the force-velocity relation for muscle contraction in the length region, $\ell \leqq \ell_o$. J. Gen. Physiol., 50, 1125-1137.

67) Podolsky, R. J. (1960) The kinetics of muscular contraction: The approach to the steady state. Nature, 188, 666-668.

68) Polissar, M. J. (1952) Physical chemistry of contractile process in muscle. Amer. J. Physiol.,168, 766-811.

69) Pringle, J. W. S. (1960) Models of muscle. Symposia of the Society of Experimental Biology, No. XIV, Models and Analogues in Biology, Cambridge University Press, 40-68.

70) Ritchie, J. M. (1954) The effects of nitrate on the active state of muscle. J. Physiol., 126, 155-168.

71) Ritchie, J. M. and Wilkie, D. R. (1958) The dynamics of muscular contraction. J. Physiol., 143, 104-113.

72) Ruegg, J. C., Steiger, G. J. and Schadler, M. (1970) Mechanical activation of the contraction system in skeletal muscle. Pflugers Arch., 319, 139-145.

73) Sakai, T. (1965) The effects of temperature and caffein on activation of the contractile mechanism in the striated muscle fibres. Jikei Med. J., 12, 88-102.

74) Sakai, T. (1967) Mechanism of contraction-relaxation cycle. Proc. 17th Ann. Meeting of Jap. Med. Assoc., 203-206.

75) Sandow, A. (1952) Excitation-contraction coupling in muscle response. Yale J. Biol Med., 25, 176-201.

76) Sandow, A. (1958) A theory of active state mechanisms in isometric muscular contraction. Science, 127, 760-762.

77) Sandow, A. (1970) Skeletal muscle. Ann. Rev. Physiol., 32, 87-138.

78) Sonnenblick, E. H. (1962) Force-velocity relations in mammalian heart muscle. Amer. J. Physiol., 202, 931-939.

79) Szent-Gyorgyi, A. (1951) Chemistry of muscular contraction (2nd edition). New York: Academic Press.

80) Taylor, C. P. S. (1969) Isomotric muscle contraction and the active state: An analog computer study. Biophysical J., 9, 759-780.

81) Tatara, Y. (1973) Mechano-chemical system. J. Jap. Soc. Mechanical Engineers, 76, 1000-1007. (in Japanese).

82) Tonomura, Y. (1972) Muscle proteins, muscle contraction and cation transport. Tokyo: University of Tokyo Press.

83) Tonomura, Y. and Oosawa, F. (1972) Molecular mechanism of contraction. Ann. Rev. Biophysics and Bioengineering, 1, 159-190.

84) Tonomura, Y., Nakamura, H., Kinoshita, N., Onishi, H. and Shigekawa, M. (1969) The pre-steady state of the Myosin-Adenosine Triphosphate system. J. Biochem., 66, 599-618.

85) Vodovnik, L. (principal investigator) et al. (1971) The development of orthotic systems using functional electrical stimulation and myoelectric control. Final report , Project No. 19-p-58391-F-01, University of Ljubljana, Yugoslavia.

86) Volkenstein, M. V. (1969) Muscular contraction. Biochem. Biophys. Acta, 180, 562-572.

87) Wilkie, D. R. (1950) The relation between force and velocity in human muscle. J. Physiol., 110, 249-280.

88) Wilkie, D. R. (1956) Measurement of the series elastic component at various times during a single muscle twitch. J. Physiol., 134, 527-530.

89) Woledge, R. C. (1961) The thermoelastic effect of change of tension in active muscle. J. Physiol., 155, 187-208.

APPENDIX A EQUIVALENT MASS

Geometric diagram of the lever system employed in the physiological experiments is shown in Fig. A-1. Denoting by I the moment of inertia of the isotonic lever and by T the torque exerted round the pivot, we get the kinetic equation for the isotonic lever system:

$$I\ddot{\theta} = T = P\ r\ \cos\theta$$

where θ = angle of the isotonic lever from the vertical axis,

r = lengh of the isotonic lever from the pivot to the tip,

P = tension on muscle.

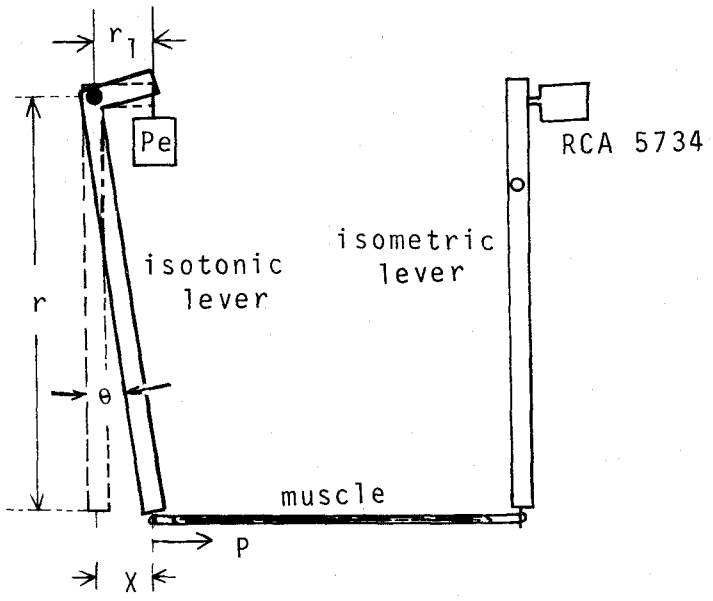

Fig. A-1 Schematic drawing of the employed lever system.

Because θ is sufficiently small, then $\cos\theta \simeq 1.0$:

$$I\ddot{\theta} \doteqdot P\ r$$

$$r\theta \doteqdot X$$

where X = displacement of the isotonic lever on the horizontal axis;
X is nearly equal to the shortening of muscle.

Hence,

$$P = (I/r^2)\ \ddot{X}$$

On the other hand, the kinetic equation of muscle is

$$P = \hat{M}\ \ddot{X}$$

where $\hat{M}$ = equivalent mass consisting of the isotonic lever and an applie load.

Namely. we can obtain

$$\hat{M} = I/r^2$$

Dimensions of the isotonic lever are r= 7cm, r_1= 0.7 cm (length from the pivot to the point of hunging a load), and the mass of the lever = 400 mg

Thus, we get

$$I = 13.7 + 0.49\ P_e \qquad (g.cm^2)$$

$$\hat{M} = 0.28 + 0.01\ P_e \qquad (g)$$

where P_e = applied load (g).

PART II

STUDY ON THE NEUROMUSCULAR CONTROL SYSTEM

CHAPTER I

INTRODUCTION

Recently, developments of prostheses, artificial limbs, manipulators and robots have extensively proceeded with advances of electronics, control theory and Biomechanisms. But these studies have left various significant problems to be solved. In particular, it has been urgently required to develop adequate control systems which are capable of controlling satisfactorily several actuating mechanisms in the artificial limbs. In view of the fact that existing control systems designed by engineers are entirely far the biological control system in respect to performance and stability, it is obviously significant to clarify magnificient functions of the motor control system from the view-point of enginnering.

The motor control system is provided with several neuromuscular reflexes at the spinal cord level that play dominant roles in the regulation of both posture and movement. One of the most important of them is undoubtedly the stretch reflex consisting of muscle spindles → alpha motoneurons → muscles. The reflex is thought to fulfill the role of the feedback system which controls length of the muscle, and thus to function in maintaining the posture. Another reflex consisting of Golgi tendon organs → alpha motoneurons → muscles must apparently function in tension control as well as in safety mechanism which protects a muscle from overloads and consequent damage. It is of interest that the position and velocity sensitivities of muscle spindles are regulated by gamma efferent signals descending from higher nervous centers. Any automatic control instruments made by engineers have never furnished such an active function. To sum up, capability of highly functional and complex control of movement would be originated from the multiple and hierachical innervations between local control loops and

higher nervous centers.

In general, the motor system has been studied in the disciplines of physiology, neurophysiology, biology and biophysics. Consequently functions of the individual physiological components have been made clear in detail, and the essential anatomy has been established. But it has been felt that only a beginning has been made in understanding how the motor control system works in the fully dynamic sense. As commonly believed, simulation study based on the concept of "analysis by synthesis" would be useful for dynamic analyses of the system.

In fact, there are many different kinds of simulation studies that attempt to elucidate the mechanism of the motor system. For example, Houk (1966)[28], and Mains and Soechting (1971)[41] have studied the stretch reflex in normal human subjects, applying a force disturbance input to the system. Young and his co-workers (Young, 1969[63]; Young et al. 1964[64]) and McRuer et al. (1968)[51] have identified dynamic characteristics of the human operator and proposed the models. Further, Houk et al. (1970)[32] have investigated the length and force feedback of cat's soleus muscles form the point of view of control theory. In addition to them, various kinds of quantitative approaches involving frquency analysis, stability analysis and others have been executed (Vickers, 1968[58]; Ishida and Umetani, 1972[33]; Hatakeyama et al. 1972)[26]. All these models, however, are not satisfactory because of fragmentary explanations of specified phenomena, although they have furnished us with useful informations in understanding the motor system. Furthermore, most of them have been involved in constructing simple quasi-linear models without regarding the nonlinear features provided in muscle spindles and muscles.

Serious problems to be settled definitely are summarized as follows: how do we employ our muscle spindles in the control of movement and posture, and why do we need this potent and highly differential gamma-spindle apparatus? What are the tasks of the tendon organs? The principal objects

of the present study are indeed to explicate these problems from an entirely new angle. A strong endeavor is made to explain the functional roles of muscle spindles and a gamma efferent system, and to clarify the mechanism of how higher nervous centers govern the several spinal reflexes.

Organization of Part II is cited below. Note that the investigations in chapters III, IV and V deal with soleus muscles of cat, and those in chapter VI with a human forearm motor system.

Chapter II gives an abridged description of the neuromuscular control system.

In chapter III, a mathematical model of muscle spindle is developed, based on physiological and anatomical data obtained from cat soleus. The model represents the responses of primary and secondary endings as a non-linear function of muscle length and frequency of fusimotor stimulation.

In chapter IV, a mathematical model of the stretch reflex of cat soleus muscle is developed. Responses of the model obtained from analog simulations are compared with the physiological data, and in the process the effects of fusimotor fibers on the stretch reflex are accounted for.

In chapter V, a mathematical model of the antagonistic neuromuscular control system at the spinal cord level is developed, based on the results obtained in chapters III and IV. The model consists of a pair of agonist and antagonist muscles, limb-load mechanical system, muscle spindles (GIa, GII afferent fibers), Golgi tendon organs (GIb afferent fibers) , alpha and gamma efferent pathways. The mechanisms of postural control, tension control and velocity control are examined.

In chapter VI, a mathematical model of a human forearm motor system is developed. The voluntary movements of intact human subjects and the responses of electrically stimulated muscles are simulated on an analog computer.

Chapter VII summarizes major findings and conclusions and also includes some discussions for further researches.

CHAPTER II

MOTOR CONTROL SYSTEM: REVIEW

2.1 GENERAL

The principal anatomical pathways of a neuromuscular control system are outlined schematically in Fig. 2.1.[34] The figure shows some of the pathways over which the spinal reflex signals are transmitted. The physiological components of the motor system may fall into four major categories;[20]

(1) muscle, which is a unidirectional force generating device,

(2) sensory organs, which are transducers that monitor system performance,

(3) neurons, which are processors that transform sensory signals into positive commands to muscles,

(4) nerve fibers, which are the transmission lines of the nervous system.

Efferent signals proceed from the spinal cord to the muscle and its receptors (muscle spindles) via the ventral spinal root. There are at least two types of efferent paths; the alpha efferent fibers which innervate the ordinary extrafusal muscle fibers, and the gamma efferent fibers which innervate the intrafusal muscle fibers of the muscle spindles. The afferent paths carrying signals from the muscle receptors enter the spinal cord via

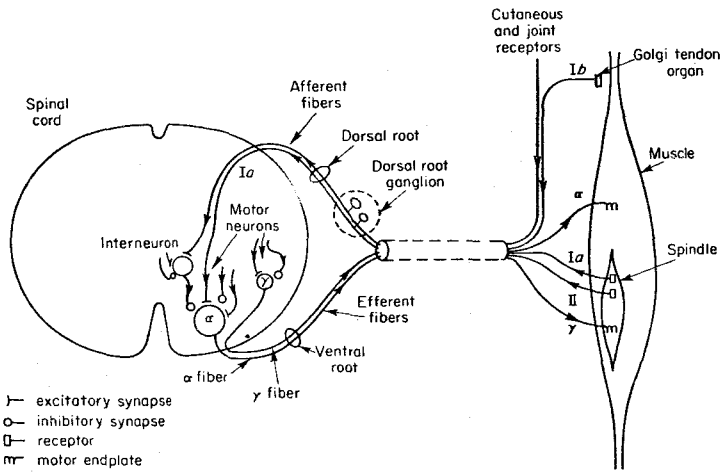

Fig. 2.1 Musculospinal reflex pathways (redrawn from Jones, 1969).[34]

the dorsal roots. These afferent fibers arise in the spindles and Golgi tendon organs of the muscle.*) Thus, alpha motoneuron (spinal ventral horn cell) receives a consequence of signals coming from both higher nervous centers and from sensory receptors**), and muscle fibers, innervated by alpha motoneuron, work together to provide fine control of limb movements.

2.2 SKELETAL MUSCLE

A skeletal muscle consists of many extrafusal muscle fibers which are innervated by alpha motoneurons, and the fibers are attached onto the relevant bone through tendons. The contractile process of muscle is schematically illustrated in Fig. 2.2 (details of structures and functions of a striated muscle were described in chapter II of part 1). Neural excitation produces

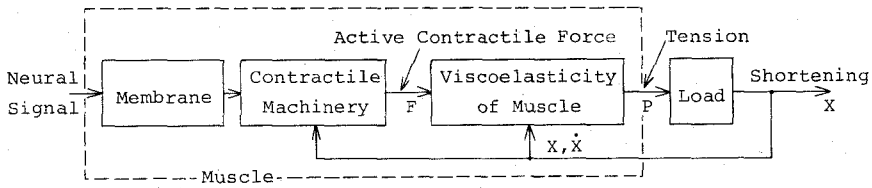

Fig. 2.2 Process of muscle contraction

a series of mechano-chemical reactions and in turn develops an active contractile force. The active force is a function of neural signals (pulse frequency) and length of muscle , and the force is transmitted to the external mechanical loading system via filtering effects of muscle viscoelasticity. That is, force and shortening of the muscle are decided by firing rates of the alpha nerve fibers and viscous elastic properties of the muscle, besides the external loading.

---

*) The dorsal roots also contains afferent fibers from receptors located in the joints, in adjacent tissue and in cutaneous layers. However, there is little quantitative knowledge of how they subserve the overall system.

**) The Renshaw cell feedback loop is not considered in the present study.

2.3 MUSCLE PROPRIOCEPTORS

a) Muscle spindle

Muscle spindle, located in parallel with the extrafusal muscle fibers, is an adjustable stretch receptor which detects length of muscle and rate of its change. According to the recent anatomical and physiological findings (Granit, 1970)[23], following features may be outlined. A simplified schematic view of a spindle is shown in Fig. 2.3 (Matthews, 1964)[49].

i) There are two types of intrafusal fibers; nuclear bag fibers and nuclear chain fibers.

ii) There are two types of afferent sensory endings; primary endings and secondary endings, which are associated with the group Ia (GIa) and group II (GII) afferent fibers, respectively.

iii) There are two functionally separated types of efferent innervation to the spindle; dynamic gamma (fusimotor) fibers (γ_1) and static gamma fibers (γ_2). Upon stimulation, dynamic gamma fibers significantly increase the dynamic responses (velocity sensitivity) of primary endings. Static gamma fibers increase the static responses (position sensitivity) of primary and secondary endings.

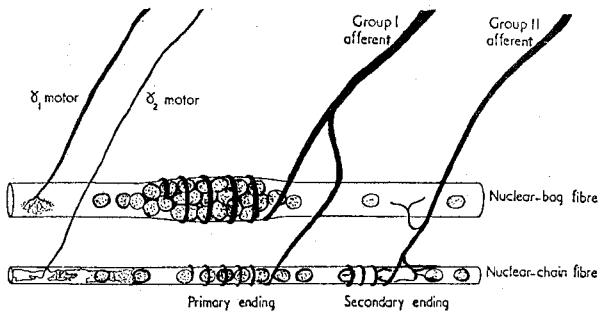

Fig. 2.3 Simplified picture of the mammalian muscle spindle (from Matthews, 1964)[49].

Namely, the pulse frequency of GIa or GII afferent fibers is a function of at least two independent quantities; efferent pulse frequency of gamma

fibers besides length and velocity of the muscle. It should be noted that position and velocity sensitivities of the spindle receptors are regulated by gamma efferent fibers.

b) Golgi tendon organs

Golgi tendon organs, located in the muscel tendons, are mechanoreceptors sensitive to a total tension on muscle because they are placed in series with it. Afferent nerve fibers from the organs are termed group Ib fibers (GIb). The tendon organs are very sensitive to the tension produced by active contraction of the muscle, while many tendon organs have a rather high threshold to passive stretch (Houk, 1967[29]; Houk and Simon, 1967[31]).

2.4 NERVE FIBERS AND ALPHA MOTONEURON

It is generally acknowledged that the particular form of a nerve pulse has no meaning to the nervous system. Rather, the position of the pulse in time contains all the information that is transmitted along nerve fibers. Thus, we consider only the flow of instantaneous pulse frequency through nerve fibers and neurons.

Time delays due to transmission along nerve fibers are directly proportional to the length of the fiber and inversely proportional to the diameter of the fiber*). Assuming the fiber length between the spinal cord and the soleus to be about 0.5 m, the corresponding time delay along each nerve fiber (alpha, gamma, GIa, GIb, GII) can be calculated. The delay is,

*) 1.0 μ in diameter is about 6 m/sec of the condicnion velocity. Alpha efferent fibers, 10-20μ in diameter, conduct at a velocity of 50-80 m/sec (cat soleus); gamma efferents, 2-8μ in diameter, 15-50 m/sec of the conduction velocity; GIa and GIb afferent fibers , 10-20μ in diameter, conduct at a velocity of 60-120 m/sec; GII afferent fibers, 4-12 μ in diameter, 30-72 m/sec of the conduction velocity.[20,24]

however, about several miliseconds at most, so that its effect is neglected in the present study.

Alpha motoneurons in the spinal cord may be recognized as an element transmitting somewhat of a replica of the algebraic sum of its excitatory and inhibitory inputs, subject to the following modifications; (i) synaptic delay of less than 1.0 msec, (ii) attenuator factor, which is somewhat dependent on the past history of inputs, e.g., post-tetanic potensiation, adaptation, fatigue, etc. , (iii) threshold.

2.5 EFFECTS OF MUSCLE RECEPTORS ON THE MOTONEURONS

The monosynaptic spinal reflex (stretch reflex) consists of a two-neuron arc; GIa afferent fibers from the spindle receptors synapse directly on the alpha motoneurons. Other pathways associated with the several spinal reflexes include one or more interneurons. The interneurons receiveng synapses from GIa and GIb fibers have been termed A and B interneurons. (Eccles, Eccles and Lundberg, 1960[15]; Jones, 1969[34]). The interneurons whose effect upon the alpha motoneurons is excitatory are termed the AE or BE interneurons, and those inhibitory are termed the AI or BI interneurons. Effects of three kinds of afferent fibers upon the alpha motoneurons are outlined below.

i) GIa fibers synapse directly on their motoneurons (homonymous), and also on those synergetic muscles (heteronymous). In addition, GIa fibers synapse on the AI interneurons of the antagonists. Reciprocal innervation thus occurs at the spinal cord level.

ii) GIb fibers from Golgi tendon organs produce inhibitory effect on homonymous and heteromymous alpha motoneurons, these pathways being via BI interneurons. In addition, GIb fibers produce excitatory effect on the alpha motoneurons of the antagonistic muscles via BE interneurons.

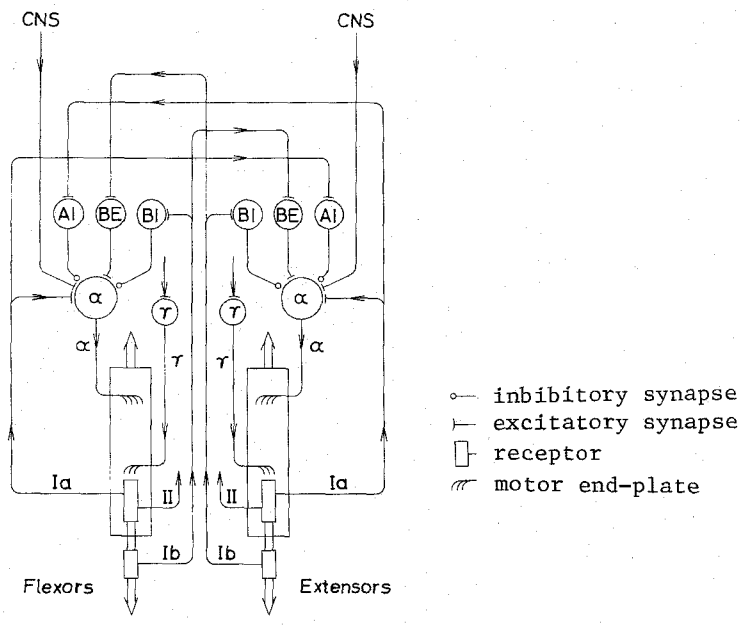

Fig. 2.4 Information-flow diagram of myotatic unit (redrawn from Jones (1969))[34].

iii) Spindle group II afferent fibers conduct more slowly and through a polysynaptic connection, but information on the effects of GII fibers upon alpha motoneurons are rather meagre. GII fibers are drawn in Fig. 2.4 without any spinal or central termination because of lack of knowledge about their terminations. A current view on the reflex action of the GII is that they produce excitation of flexor motoneurones with inhibition of extensor motoneurones. However, Matthews (1969)[50] has pointed out that the electrical stimulation of extensor GII afferent fibers may occasionally give extensor fascilitation with inhibition of flexors. Further, it was suggested by R. M. Eccles and Lundberg (1959)[17] that there might be "two alternative pathways from group II afferents onto flexor motoneurons, one excitatory and one inhibitory" and with "some sort of reciprocal linkage" between them. To sum up, there would be the possi-

bility of at least four reflex patterns associated with GII fibers; namely, flexor reflex pattern, autogenetic inhibition, autogenetic excitation and reciprocal innervation. Thus, the interneurons which mediate the reflex effects of spindle GII activity are seen to occupy a crucial position. This problem is investigated in chapter V.

2.6 ORGANIZATION OF THE NEUROMUSCULAR SYSTEM

The several flexor and extensor muscles, associated receptors, their afferent and efferent neural pathways to the motoneurons and their interconnections within the spinal cord all form a fundamental operational unit of muscles (myotatic nunit). The schematic blockdiagram of the myotatic

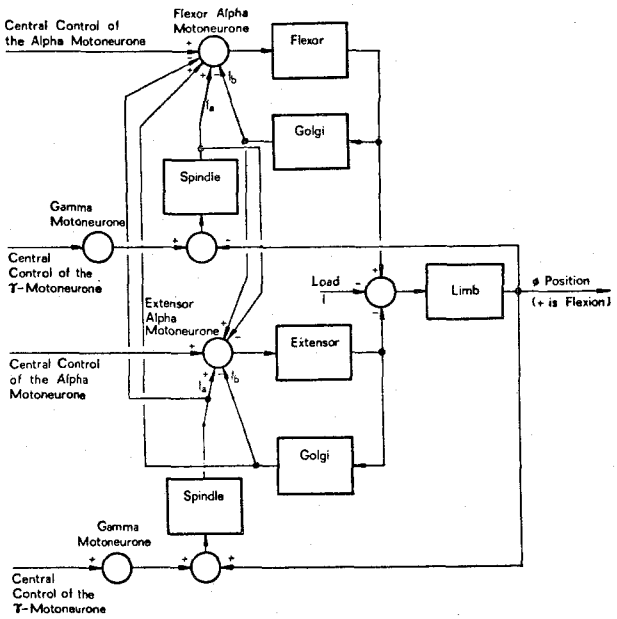

Fig. 2.5 Blockdiagram of neuromuscular control system (redrawn from Vodovnik (1971)).[61]

unit is represented in Fig. 2.5, by identifying the role of each physiological component in carrying out the spinal reflex. There are two fundamental feedback loops (spinal reflex arc) associated with the spindle and Golgi tendon organs.

The stretch reflex arc consisting of spindle group Ia afferents → alpha motoneurons → muscle has been interpreted as feedback system which controls muscle length. Note that the spindle receptor fulfills the functions of feedback transducer, comparator and controller with adjustable sensitivities. Another reflex arc, Golgi tendon organs → alpha motoneurons → muscle, is a feedback system which regulates muscle tension.

The control loop contains two reference command inputs from higher nervous centers, alpha and gamma efferent pathways. It has been commonly believed that gamma efferent input functions essentially as a position-command signal, at least for smooth, continuous movements. The second input, alpha efferent command signal produces a rapid response because of fast conduction velocity and few synapses. It is thought by most researchers that this alpha command input is normally employed for rapid voluntary motions, especially those of the skilled task and the avoidance reflex.

CHAPTER III

A MATHEMATICAL MODEL OF MUSCLE SPINDLE OF CAT SOLEUS MUSCLE

3.1 INTRODUCTION

In a recent review, Matthews (1964)[49] has pointed out that in many muscles of the cat the total number of spindle nerve fibers, including both efferent and afferent, is considerably greater than the number of the ordinary alpha motor nerve fibers which supply the extrafusal muscle fibers. This fact strongly suggests that the muscle spindle is the key organ in the regulation of muscle contraction and that it plays a dominant role in the control of both posture and movement. While a large quantity of physiological data about the mammalian muscle spindles has been accumulated by extensive studies (Matthews, 1964[49]; Lennerstrand, 1968[39]; Granit, 1970[24]), precise functions of the receptors are still far from being understood. Further, many quantitative approaches, involvong mathematical descriptions and the formulation of models of the spindle, have been attempted by many workers, but most of them have been rather meagre. Earlier approaches have been concerned with simple linear models of the lead-lag filter type(Houk, 1966[28]; Toyama, 1966[51]; McRuer et al., 1968[51]; Gottlieb et al., 1969[21]; Rudjord, 1970[55]). Recently, in order to account for the nonlinear effects of fusimotor stimulation on the dynamic characteristics of muscle spindles, more elaborated models have been developed by Crowe (1968)[12], Gottlieb et al. (1970)[22] and Angers and Delisle (1971)[6], but these models are not so satisfactory.

The purpose of the present chapter is to develop a mathematical model which can account for behavioral characteristics exhibited by mammalian muscle spindles. A special attension is paid to the nonlinear properties of the receptors, such as the effects of fusimotor stimulations on the position and velocity sensitivities. The model consisting of three distinct subcomponents, i.e., a mechanical filter, a mechano-electric transducer and an encoder, is developed, based on physiological and anatomical findings. The system

parameters concerning primary and secondary endings are determined quantitatively by simulating the transient and steady state responses of the endings. All the simulation experiments in the present work are made on an analog computer, to account for the existing physiological data obtained from the muscle spindles of cat soleus.

3.2 STRUCTURE AND FUNCTION OF MUSCLE SPINDLE

a) General

A simplified schematic view of a mammalian muscle spindle is shown in Fig. 2.3, and outline of the receptor is expressed at section 2.3. The nuclear bag fibers have a central region with few myofibrils, which is joined in series either side to the striated contractile tissue. The nuclear chain fibers are striated along their entire length with nuclei evenly distributed. The primary endings have axon branches wound around the central part of the nuclear bag fibers and also around the nuclear chain fibers. The large majority of the secondary endings are found on the nuclear chain fibers, with a minority on nuclear bag fibers. The response of these endings to muscle stretch is an increase in firing rate not only to signal the magnitude of stretch (static response), but also to signal the rate of change of stretch (dynamic response). As for the two functionally separated fusimotor fibers, although the details of spindle innervation by way of the fusimotor system is much dispute[23 24 49], it may be considered that the bag fibers receive dynamic fusimotor fibers, and the chain fibers receive static fusimotor fibers.

It is well known that there are three main transformations that occur as the spindle changes muscle length into afferent nerve pulses. Fig. 3.1 shows the illustration of transformations involved in the processes from the mechanical and neuronal stimulations to the responses in the form of afferent spikes. A mechanical filter refers to the process by which muscle

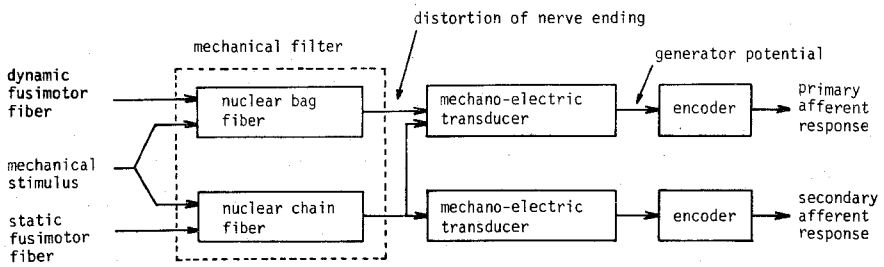

Fig. 3.1 Blockdiagram to illustrate three distinct kinds of transformation in mammalian muscle spindle.

length is converted into mechanical distortion of nerve endings. A mechano-electric transducer represents the biochemical process by which distortion of nerve endings is converted into continuous generator potential. An encoder represents the membrane breakdown process by which generator potential is encoded into discharge rate of afferent pulses. Dynamic characteristics in the responses of spindle receptors may be accounted for by a cascade combination of these three transformations.

b) Static and dynamic properties of muscle spindles

We shall present a summary of the data now available concerning the static and dynamic properties of the muscle spindles. According to the physiological literature, we use following terms of convenience; position sensitivity, dynamic index, velocity sensitivity and bias.(Lennerstrand, 1968[39]; Crowe and Matthews, 1964a[13]; Gottlieb et al., 1970[22]; Eldred et al., 1953[18]). While the terms refer to steady state behaviors after transients have died out, they seem to characterize the transfer properties of spindle receptors. In fact, as described in the following section in detail, the transfer properties of muscle spindles to mechanical input are expressed by the first order transfer function.

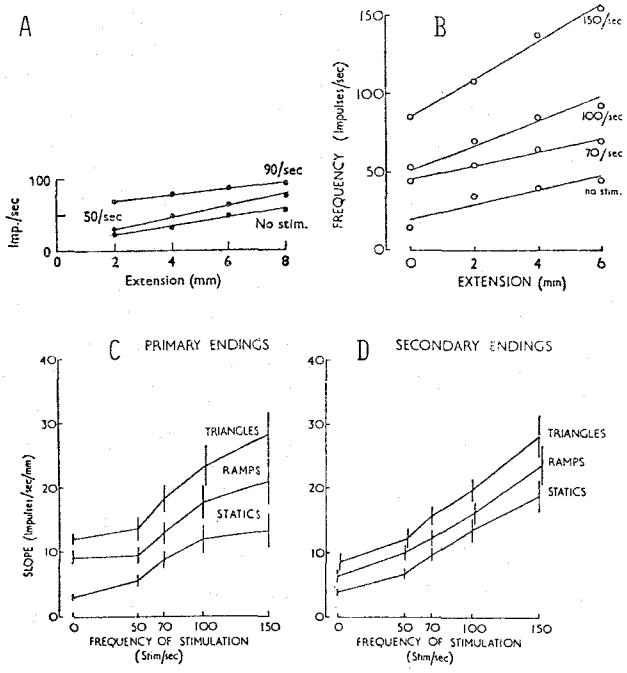

Fig. 3.2 Effects of fusimotor stimulation on the position sensitivities of primary (A, B, C) and secondary endings (D). A, the effect of dynamic fusimotor stimulation on the relation between the frequency of discharge of a primary ending and the extension applied to the cat soleus muscle. B, the effect of static fusimotor stimulation on the discharge rate-extension relation. C, D, the average effect on the position sensitivity of varying the frequency of stimulation of combined coarse ventral root filaments. Figure A, from Crowe and Matthews (1964a)[13]; B, C, D, from Brown, Lawrence and Matthews (1969).[11]

$$H(s) = \hat{K}_x + \frac{\hat{T}_x s}{1 + \hat{T} s}$$

where $\hat{K}_x$ represents the static gain of the system, i.e., position sensitivity, $\hat{T}_x$ represents a convenient description of the velocity sensitivity, and $\hat{T}$ is the lag time constant.

i) Position sensitivity

The steady state firing rates of the primary and secondary endings increase approximately linearly with the length of muscle. The slope of the

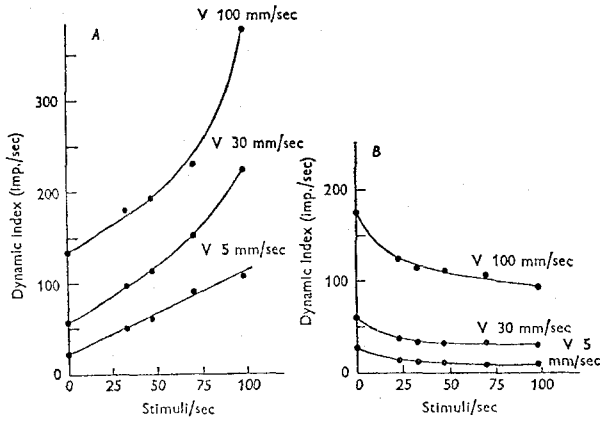

Fig. 3.3 The effect of varying the frequency of fusimotor stimulation on the size of the ' dynamic index' of a primary ending found for particular velocities of stretching. A, stimulation of dynamic fusimotor fiber; B, stimulation of static fiber. (redrawn from Crowe and Matthews (1964a)).[13]

best straight line which can be fitted to the graph of discharge frequency against length may be defined as the position sensitivity of the ending. It has been confirmed that the position sensitivity of primary endings is increased both by stimulation of dynamic fusimotor fibers and by stimulation of static fibers, while the position sensitivity of secondary endings is increased only by static fusimotor stimulation. These effects are illustrated in Fig. 3.2.

ii) Velocity sensitivity and dynamic index

The velocity sensitivity is a measure of the dynamic component of the afferent outputs which is proportional to the velocity of muscle stretch. The sensitivity has been studied experimentally by measuring the dynamic index of the ramp response (Crowe and Matthews, 1964a)[13]. The dynamic index is defined as the difference between the frequency of firing of the ending just before the end of the dynamic phase of ramp stretching and that occuring at the final length 0.5 sec after completion of the dynamic phase of stretching. Since this quantity should increase in direct propor-

TABLE III-1

EFFECTS OF FUSIMOTOR STIMULATIONS AND VELOCITY OF STRETCHING ON POSITION AND VELOCITY SENSITIVITIES AND BIAS OF SPINDLE AFFERENTS

	Dynamic fiber stimulation	Static fiber stimulation	Increase in velocity
Primary ending			
Position sensitivity	increase	increase	no effect
Velocity sensitivity	increase	slight decrease	decrease
Bias	increase	increase	no effect
Lag time constant	no effect	no effect	decrease
Secondary ending			
Position sensitivity	no effect	increase	no effect
Velocity sensitivity	no effect	no effect	decrease
Bias	no effect	increase	no effect
Lag time constant	no effect	no effect	decrease

tion to the velocity of applied stretch for the linear system, the velocity sensitivity may be defined as the slope of the relation between the dynamic index and the velocity (Appendix C).

Fig. 3.3 shows the effect of fusimotor stimulation on the dynamic index of a primary ending obtained by Crowe and Matthews (1964a)[13]. Stimulation of dynamic fusimotor fibers causes a considerable increase in dynamic index, but stimulation of static fusimotor fibers causes a slight decrease in it. This fact means that the velocity sensitivity of primary endings is increased by dynamic fusimotor stimulation, but slightly decreased by static one. On the other hand, the velocity sensitivity of secondary endings is independent of the fusimotor stimulations. Note that the sensitivities of the endings, including both primary and secondary, are decreased by increasing velocity, because the dynamic index-velocity curves of both endings appear to be convex upwards for the lower velocity of stretching.

iii) Bias

At a steady muscle length, the firing rate of spindle endings is enhanced by fusimotor stimulation, and it is approximately a linear function of the stimulation rate of either fusimotor fiber type (Bessou et al, 1968)[9]. The term ' bias' represents the tonic component of the spindle output that is independent of stretch; therefore, the bias corresponds to the y-intercept

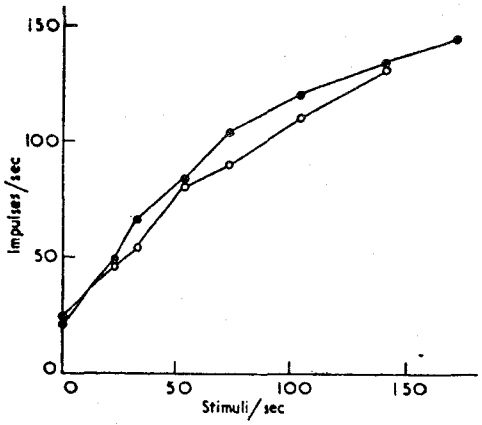

Fig. 3.4 The effect on the frequency of discharge of a primary ending, with the muscle at a constant length, of stimulating a static fusimotor fiver (●) and a dynamic fusimotor fiber (o), at various frequencies. (From Matthews, 1962)[47]

on the steady state relation between muscle length and discharge frequency. Fig. 3.4 shows the effect of varying the frequency of fusimotor stimulations upon the discharge frequency of a primary ending.

iv) Lag time constant

In addition to the nonlinear effects caused by fusimotor stimulations, we can find other nonlinear features caused by mechanical stimulus. One of them is, as described in item ii), the decrease in velocity sensitivity caused by increasing velocity of stretching. Another significant one is concerned with the lag time constant, $\hat{T}$. Estimating the responses of endings to ramp stretching, we can find that the endings begin to discharge more repidly in the rising phase of discharging, and to decay faster in the falling phase as the velocity of stretch is increased (e.g., Fig. 3.9). These facts mean that the lag time constant, $\hat{T}$, may be decreased with an increase in velocity of stretching.

The nonlinear effects described above are summarized in Table III-1. Note that the primary ending afferent is influenced by stimulation of both dynamic and static fusimotor fibers and that the secondary afferent is in-

fluenced almost solely by the static fibers. An explanation of the mechanism of different effects produced by fusimotor fibers upon the endings may be obtained by way of differences in the viscoelastic properties of the intrafusal fiber. Further, the velocity-dependences of lag time constant and velocity sensiticity may be explained together. This is discussed in section 3.5.

3.3 DEVELOPMENT OF THE MODEL

a) Mechanical filter

We have already developed a mathematical model of the skeletal muscle, as expressed in the part I of the present thesis. The model consists of a force generator and viscous and elastic components. The model is considered to be also applicable to the intrafusal fibers of spindle receptors. In fact, two kinds of intrafusal fibers, nuclear bag fibers and nuclear chain fibers, are considered to have contractile regions in series with noncontractile regions. The contractile region may be expressed by three-component model consisting of force generator, viscous and parallel elastic components. The noncontractile region may be represented only by a purely elastic component, since the viscosity of this portion may be assumed to be considerably smaller than that of contractile portion. Consequently, we propose a lumped parameter model shown in Fig. 3.5. The upper half of the figure corresponds to the nuclear bag fibers, and the lower half to the nuclear chain fibers acting in parallel with the bag fibers. Note that the noncontractile region is assumed to correspond to the sensory portion in which afferent fibers terminate. Namely, both the extension of spring E_1 of the nuclear bag fiber and that of spring E_3 of the chain fiber cause the primary ending to discharge, and that the extension of spring E_4 of the nuclear chain fiber cause the secondary ending to discharge.

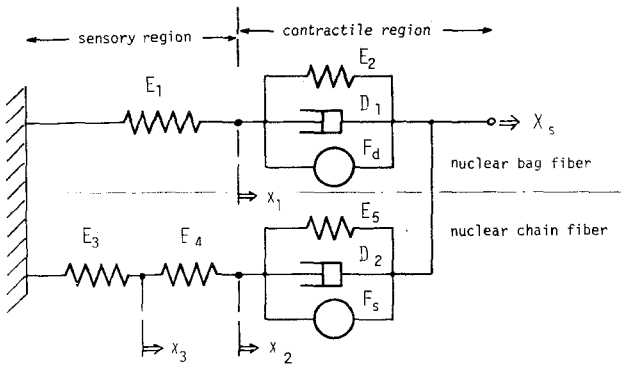

Fig. 3.5 Model of mechanical filter of mammalian muscle spindle

The mechanical filter in Fig.3.5 leads to the following equations.

$$E_1 x_1 = E_2 (X_s - x_1) + D_1 (\dot{X}_s - \dot{x}_1) + F_d \tag{3.1}$$

$$E_3 x_3 = E_4 (x_2 - x_3) \tag{3.2}$$

$$E_3 x_3 = E_5 (X_s - x_2) + D_2 (\dot{X}_s - \dot{x}_2) + F_s \tag{3.3}$$

where E_1, E_2, E_3, E_4, E_5 = spring constants,

D_1, D_2 = viscous constants,

F_d (F_s) = contractile force of nuclear bag (chain) fiber produced by stimulation of dynamic (static) gamma fiber,

X_s = extension of the muscle spindle,

x_1, x_2, x_3 = extensions.

Then it is reckoned that the extension applied to the whole muscle produces an identical pattern of extension of the spindle;

$$X_s = \nu X \tag{3.4}$$

where X = extension of the whole muscle,

ν = constant.

b) Mechano-electric transducer

We shall simply assume that the conversion of distortion of nerve endings into generator potentials is linear process, i.e., the generator poten-

tial is proportional to the extension of sensory part. It is assumed, similarly to Angers and Delisle (1971)[6], that the generator potential of the primary ending is proportional to a weighted sum of extension taken on both sensory parts of nuclear bag fiber, E_1, and chain fiber, E_3.

$$P_{g1} = c_1 x_1 + c_3 x_3 \tag{3.5}$$

where P_{g1} = generator potential of primary ending,

c_1, c_3 = constants.

Similarly, the generator potential of the secondary ending is assumed to be proportional to the extension of the sensory part of nuclear chain fiber, E_4;

$$P_{g2} = c_4 (x_2 - x_3) \tag{3.6}$$

where P_{g2} = generator potential of secondary ending,

c_4 = constant.

c) Encoder

An encoder corresponds to the process by which generator potential is converted into discharge rate of afferent spikes. According to Katz (1950)[37], the frequency of afferent spikes has been found, within physiological operating limits, to be directly proportional to the receptor potential. Thus, the frequency of spikes generated in the afferent nerve of primary ending may be given by

$$R = r_1 P_{g1} + R_o \tag{3.7}$$

where R = discharge rate of afferent spikes of the primary ending,

R_o = spontaneous discharge rate,

r_1 = constant.

Similarly, the frequency of spikes of secondary endings is written as

$$Q = r_2 P_{g2} + Q_o \tag{3.8}$$

where Q = discharge rate of afferent spikes of secondary endings,

Q_o = spontaneous discharge rate,

r_2 = constant.

d) Transfer function of the muscle spindle

Taking the Laplace transform of Eqs. (3.1)-(3.8), we obtain (see Appendix B):

$$R(s) = R_o + \left(K_x + \frac{T_x s}{1 + T_1 s} \right) X(s) + \frac{K_d}{1 + T_d s} \Gamma_d(s) + \frac{K_s}{1 + T_s s} \Gamma_s(s) \qquad (3.9)$$

$$Q(s) = Q_o + \left(K_x' + \frac{T_x' s}{1 + T_3 s} \right) X(s) + \frac{K_s'}{1 + T_s s} \Gamma_s(s) \qquad (3.10)$$

where Γ_d = frequency of stimulation of dynamic gamma fibers,

Γ_s = frequency of stimulation of static gamma fibers.

Equations (3.9) and (3.10) give the total change in frequency of afferent spikes of the primary and secondary endings, as a function of both changes in muscle length and in stimulation frequencies of static and dynamic gamma fibers.

As illustrated in Table III-1, both the position sensitivities K_x and K_x' and the velocity sensitivity T_x are changed by fusimotor stimulations, so that these properties have to be introduced into the parameters. On the basis of the physiological data in Fig. 3.2, the position sensitivities of primary and secondary endings may be expressed as

$$K_x = a_o + a_1 \Gamma_d^\circ + a_2 \Gamma_s^\circ \qquad (3.11)$$

$$K_x' = a_o' + a_2' \Gamma_s^\circ \qquad (3.12)$$

$$\Gamma_d^\circ = \mathcal{L}^{-1} \{ \Gamma_d(s) / (1 + T_d s) \}$$

$$\Gamma_s^\circ = \mathcal{L}^{-1} \{ \Gamma_s(s) / (1 + T_s s) \}$$

where a_o, a_1, a_2, a_o' and a_2' are constants.

As shown in Fig. 3.3, the dynamic index is an approximately linear function of the frequency of dynamic fusimotor stimulation. Consequently, the velocity sensitivity of primary endings may be written as

$$T_x = b_o + b_1 \Gamma_d^{\circ} \tag{3.13}$$

Because the sensitivity T_x is decreased by increasing velocity as shown in Table III-1, the parameters b_o and b_1 should depend on velocity. On the other hand, the velocity sensitivity of secondary endings, T_x', is independent of fusimotor stimulation.

e) Simulation of the model

The equations (3.9)-(3.13) are simulated on an analog computer. The blockdiagram of the model is shown in Fig. 3.6. Because of the large number of parameters involved in the equations, we proceed systematically in the simulation of the model. First, estimating appropriate steady-state responses,

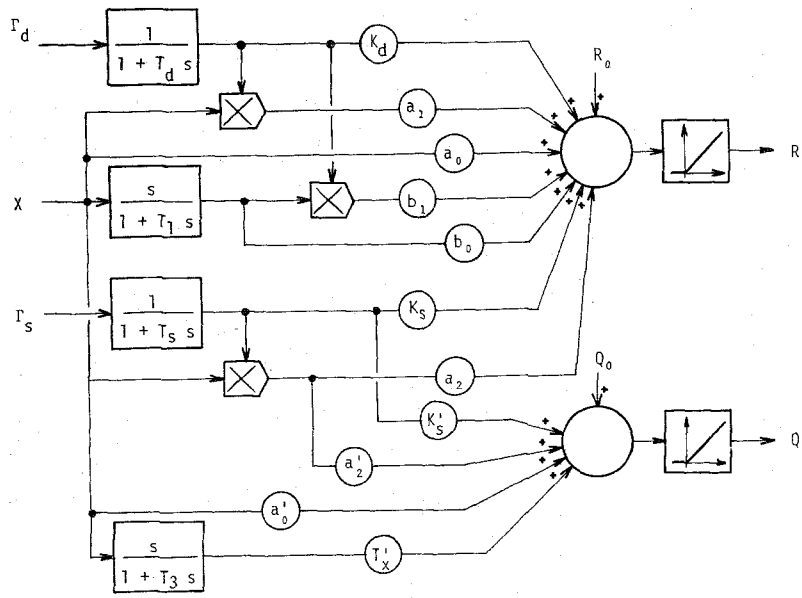

Fig. 3.6 Blockdiagram of the model simulated on an analog computer.

we identify the static gains such as a_o, a_1, a_2, a_o', a_2', K_d and K_s. Then, simulating the transient responses, we identify the dynamic parameters such as lag time constant and velocity sensitivities, b_o, b_1. Finally, we accumulate all the estimated parameters obtained from the simulations, and then calculate the mean value for each parameter after all, because considerable differences are found between the estimated parameter values of different endings, even within the same muscle.

When the velocity of stretching is varying with time, the velocity-dependent parameters, b_o, b_1, T_1 and T_3 have to be altered with time according to change in velocity. Such a simulation procedure, however, is quite difficult, so that these parameters are simply assumed to be unaltered with time in the following simulations.

3.4 RESULTS

a) Responses of primary endings

Fig. 3.7 shows the effects of changing the length of the muscle on the response of a primary ending to stimulation of a dynamic fusimotor fiber. Figures a and b are the responses of the ending to stretching the muscle by 6 mm at 5 mm/sec in the presence (b) and absence (a) of fusimotor stimulation at 90 stim/sec. Figures c and d are the responses of the same ending to fusimotor stimulation (90 stim/sec) applied after the muscle was stretched by 2 mm (c) and by 6 mm (d) at 10 mm/sec. Periods of fusimotor stimulation are shown by thick bars at the middle and length changes (ramp stretch) at the bottom. Spots represent the physiological results redrawn from the literature (Crowe and Matthews, 1964a)[13]; in the physiological recordings, a direct display of the instantaneous frequency of discharge is given by the spot of a cathode ray tube. For all the frequencygram presented in this chapter, except Fig. 3.11, physiological results are similarly represented by spots.

Values of the system parameters are estimated individually from each physiological record in Fig. 3.7, and then their mean values are calculated.

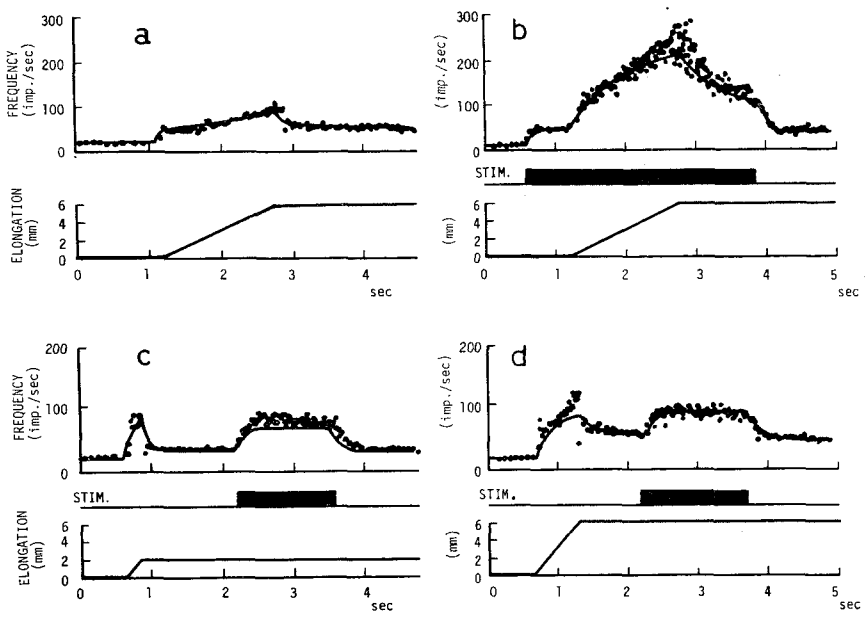

Fig. 3.7 The effect of changing the length of the muscle on the response of a primary ending to stimulation of a dynamic fusimotor fiber. Records, a, b: Response of ending to stretching the muscle by 6 mm at 5 mm/sec in the presence (b) and absence (a) of fusimotor stimulation. Records, c and d: Response of the same ending to stimulation applied after the muscle was stretched by 2 mm (c) or by 6 mm (d) at 10 mm/sec. Frequency of fusimotor stimulation in all records was 90 stim/sec. Spot, experimental result redrawn from Crowe and Matthews (1964a).[13] Solid line, response of the model obtained with the parameters in Table III-2.

TABLE III-2

PARAMETERS ESTIMATED FROM SIMULATION OF FIG. 3.7

Figure	Experimental condition			Estimated parameters							
	X mm	v mm/sec	Γ_d stim/sec	R_0 imp/sec	a_0 imp/sec / mm	a_1 imp/sec / mm / stim/sec	b_0 imp/sec / mm/sec	b_1 imp/sec / mm/sec / stim/sec	T_1 sec	K_d imp/sec / stim/sec	T_d sec
a	6	5	0	23.0	5.5		6.7		0.3		
b	6	5	90	12.0	5.6	0.031	(6.7)	0.33	0.4	0.37	0.13
c	2	10	90	18.0	5.9	0.042	5.8		0.06	0.37	0.13
d	6	10	90	12	4.9	0.025	4.4		0.12	0.37	0.13
Mean Value {Number of Measurements}				16.0{4}	5.5{4}	0.033{3}				0.37{3}	0.13{3}

The results are given in Table III-2 and the simulated responses obtained by the model with the values are shown with solid lines in Fig. 3.7. The model response shows a close agreement with the physiological result. As seen from comparison between a and b, the response of the ending under dynamic fusimotor stimulation undergoes more increase in the firing rate than under no fusimotor stimulation. This is due to the increase in position and velocity sensitivities.

Fig. 3.8 shows the effects of stimulating a static fusimotor fiber on the responses of primary endings. Values of the system parameters are estimated similarly from the physiological data.*) The result is given in Table III-3, and the model responses obtained with the values are shown in Fig. 3.8 with solid lines. As seen in the figure, the responses under static fusimotor stimulation are greater than those under no stimulation. These effects are evidently due to the increase in position sensitivity caused by the static fusimotor stimulation, but the strength of the effects produced on the various endings differs considerably. These features are shown numerically in Table III-3.

The experimental data in Fig. 3.9 are pertinent for examining the effects on the lag time constant and on the velocity sensitivity. Fig. 3.9 shows the responses of a single primary ending to stretching the muscle by 6 mm at various velocities 5, 30, 70 mm/sec. Records a, b and c are the responses of the ending in the absence of fusimotor stimulation, records d, e and f the responses during stimulating a static fusimotor fiber at 70 stim/sec, and records g, h and i the responses during stimulating a dynamic fusimotor fiber at 70 stim/sec. The period of stimulation is shown by the thick bar beneath each record, and the stretch at the bottom.

---

*) The time scale in Fig. 3.8 differs between the dynamic phase of stretching and the static phase; the recording speed during the dynamic phase was increased linearly with the velocity of stretching in order to permit better observation of the behavior of the spindle endings. The same recording is seen in Fig. 3.9 and Fig. 3.10.

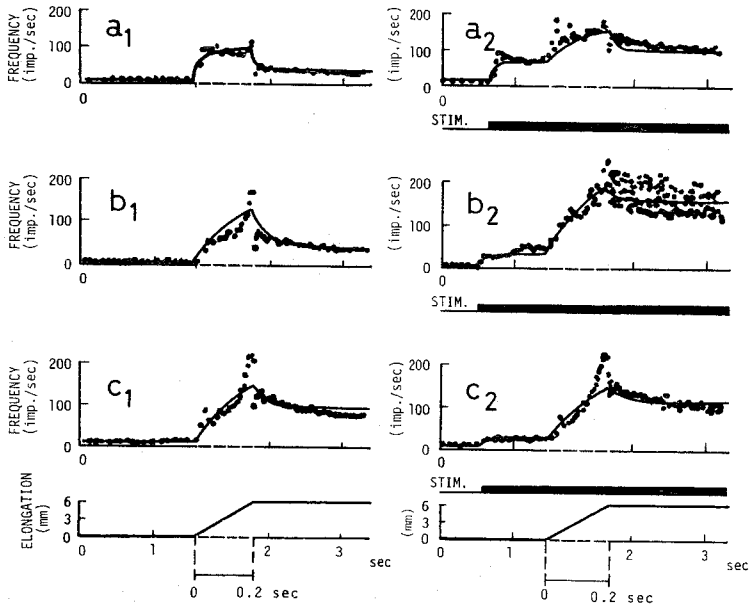

Fig. 3.8 The effect on three different primary endings (a, b, c), of stimlating the same single static fusimotor fiber. The muscle was stretched by 6 mm at 30 mm/sec in the presence (a_2, b_2, c_2) and absence (a_1, b_1, c_1) of fusimotor stimulation at 135 stim/sec. Spot, experimental result obtained by Crowe and Matthews (1964b)[14]; solid line, simulated result obtained with the parameters in Table III-3.

TABLE III-3

PARAMETERS OF THREE DIFFERENT ENDINGS ESTIMATED FROM SIMULATION OF FIG. 3.8

Figure	Γ_s stim/sec	R_0 imp/sec	a_1 imp/sec / mm	a_2 imp/sec / mm / stim/sec	b_0 imp/sec / mm/sec	T_1 sec	K_s imp/sec / stim/sec	T_s sec
a_1	0	2.0	4.2		2.0	0.013		
a_2	135	2.0	4.2	0.006	2.4	0.1	0.44	0.05
b_1	0	10.0	7.9		4.2	0.2		
b_2	135	10.0	7.9	0.13	2.0	0.1	0.32	0.05
c_1	0	13.0	12.0		3.5	0.2		
c_2	135	13.0	12.0	0.02	2.0	0.1	0.13	0.05
Mean Value {Number of Measurements}		8.0{6}	7.9{6}	0.05{3}	2.7{6}	0.12{6}	0.3{3}	0.05{3}

Amount of stretch, X = 6 mm; velocity, v = 30 mm/sec.

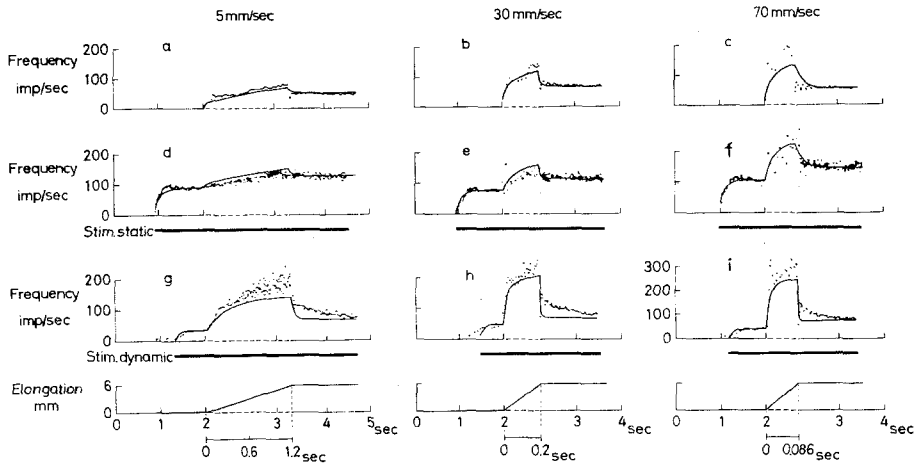

Fig. 3.9 The contrasting effects of stimulating the two kinds of fusimotor fibers on the responses of a single primary ending to stretching the muscle at various velocities. Records, a, b, c: The responses of the ending in the absence of fusimotor stimulation on stretching the muscle by 6 mm at 5, 30 and 70 mm/sec. Records, d, e, f: The responses to similar stretch applied, with stimulating a static fusimotor fiber at 70 stim/sec; period of stimulation is shown by bar beneath each record. Records, g, h, i: The responses under stimulating a dynamic fusimotor fiber at 70 stim/sec.(Note different frequency scale for i). Spot, physiological result of frequencygram redrawn from Crowe and Matthews (1964a).[13] Solid line, response of the model obtained from the parameter values given in Table III-4.

Values of the parameters are estimated from the physiological data and their mean values are calculated. The mean value for each parameter is only given in Table III-4, and the responses of the model obtained with the values (before averaged) are shown in Fig. 3.8 with solid lines. As seen in Table III-4, the parameters b_o and b_1 concerning the velocity sensitivity are decreased with an increase in velocity. This is due to the fact that the dynamic index in Fig. 3.9 has not enhanced in proportion to velocity of stretching. Similarly, the lag time constant, T_1, is smaller at the higher velocities, which corresponds to the behavior —— the discharge rate has risen and fallen more rapidly as velocity is increased.

TABLE III-4

ESTIMATED PARAMETERS OF THE PRIMARY ENDINGS

Figure's number in this paper	Reference	R_0 imp/sec	a_0 $\frac{\text{imp/sec}}{\text{mm}}$	a_1 $\frac{\text{imp/sec}}{\frac{\text{mm}}{\text{stim/sec}}}$	a_2 $\frac{\text{imp/sec}}{\frac{\text{mm}}{\text{stim/sec}}}$	K_d $\frac{\text{imp/sec}}{\text{stim/sec}}$	T_d sec	K_s $\frac{\text{imp/sec}}{\text{stim/sec}}$	T_s sec	v mm/sec	b_0 $\frac{\text{imp/sec}}{\text{mm/sec}}$	b_1 $\frac{\text{imp/sec}}{\frac{\text{mm/sec}}{\text{stim/sec}}}$	T_1 sec
Fig. 3.2	(a),Fig.9	12.0{1}	6.1{4}	0.017{8}		0.26{2}							
Fig. 3.2	(c),Fig.1	22.2{2}	3.9{8}		0.032{24}			0.517{6}					
Fig. 3.2	(c),Fig.6		3.2{18}		0.107{18}								
Fig. 3.3	(a),Fig.4									5.0	4.8{1}	0.18{4}	
										30.0	1.9{1}	0.045{4}	
										100.0	1.3{1}	0.016{4}	
Fig. 3.4	(d),Fig.5	23.2{2}				0.81{6}		0.94{7}					
Fig. 3.7	(a),Fig.8	16.0{4}	5.5{4}	0.033{3}		0.37{3}	0.13{2}			5.0	6.7{1}	0.33{1}	0.35{2}
										10.0	5.1{2}		0.09{2}
Fig. 3.8	(b),Fig.3	8.0{6}	7.9{3}		0.05{3}			0.3{3}	0.05{3}	30.0	2.7{6}		0.12{6}
Fig. 3.9	(a),Fig.2	13.3{9}	7.2{6}	-0.016{3}	0.0{3}	0.52{3}	0.1{3}	0.98{3}	0.1{3}	5.0	4.9{2}	0.15{1}	0.07{3}
										30.0	1.7{2}	0.047{1}	0.018{3}
										70.0	1.2{2}	0.021{1}	0.011{3}
Fig. 3.10	(b),Fig.10	13.0{1}	5.5{2}	0.07{2}	0.0{1}	0.29{2}		0.79{2}		10.0	5.0{2}	0.05{2}	0.05{4}
Fig. 3.11	(e),Fig.11	16.0{1}	5.0{1}	a_1+a_2=0.13{2}		K_d+K_s=1.82{2}				2.9	15.0{1}	0.31{2}	2.0{3}
Fig. 3.14	(c),Fig.7		1.3{3}		0.07{2}					5.0	3.6{3}		0.65{3}
	(a),Fig.6	7.0{4}	5.6{1}		0.0{3}			0.8{3}	0.05{3}	30.0	3.3{4}		0.05{4}
	(a),Fig.7	17.0{2}	45.6{4}	0.08{2}		0.42{2}	0.17{2}			5.0	6.3{1}	0.14{1}	0.13{2}
										50.0	2.1{1}	0.03{1}	0.03{2}
	(e),Fig.13	19.0{1}	2.1{1}	a_1+a_2 0.083{5}		K_d+K_s=1.4{5}				2.8	17.2{1}	0.19{5}	0.5{6}
	(b),Fig.2	7.0{6}	5.4{3}	0.13{3}		0.59{3}				30.0	2.87{3}	0.08{3}	0.045{6}
Mean value		12.5	4.68	0.0415	0.055	0.535	0.128	0.74	0.067	$b_0 = 1.2 + 4.3\ e^{-0.07v}$			
Standard deviation		7.8	2.1	0.062	0.042	0.154	0.027	0.25	0.023	$b_1 = 0.015 + 0.1\ e^{-0.04v} + 0.36\ e^{-0.35v}$			
Number of measurements		{39}	{58}	{21}	{54}	{21}	{7}	{24}	{9}	$T_1 = 1.8\ e^{-0.048v} + 0.93\ e^{-0.03v}$			

Reference: (a) Crowe and Matthews (1964a)[13]; (b) Crowe and Matthews (1964b)[14]; (c) Brown, Lawrence and Matthews (1969)[11]; (d) Matthews (1962)[47]; (e) Harvey and Matthews (1961)[25].

It is of significance to compare the effects of stimulating, separately and in combination, a static fusimotor fiber and a dynamic fusimotor fiber, both of which influence the same primary ending. This is achieved in four experiments. The spot in Fig. 3.10 show the frequencygram obtained from separate and simultaneous stimulations of a static and a dynamic fusimotor fiber, both at 70 stim/sec (Crowe and Matthews, 1964b)[14]. Values of the parameters are estimated from the physiological data. Estimated values (mean values) are given in Table III-4, and the simulated responses of the model obtained with the values (before averaged) are shown in Fig. 3.10, solid lines. Simultaneous stimulation of both fusimotor fibers together produce a greater increase in discharge rate of the ending than stimulation of either alone. Note that the increase in discharge rate produced by the combined

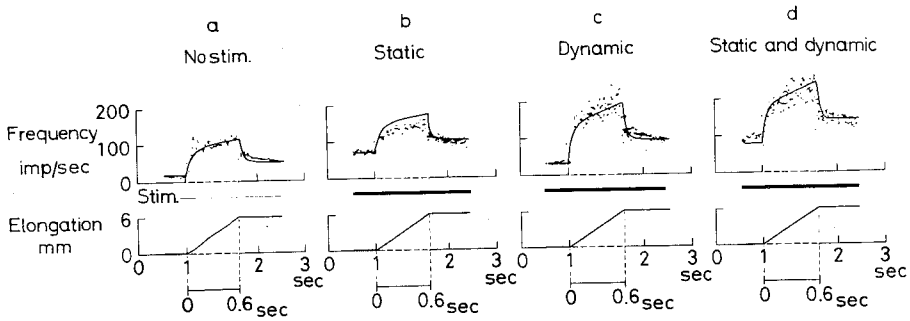

Fig. 3.10 The effects of stimulating, separately and together, a static and a dynamic fusimotor fiber, both at 70 stim/sec. The muscle was stretched by 6 mm at 10 mm/sec. Spot, experimental result of frequencygram obtainedd by Crowe and Matthews (1964b)[14]. Solid line, simulated result obtained by using the values in Table III-4.

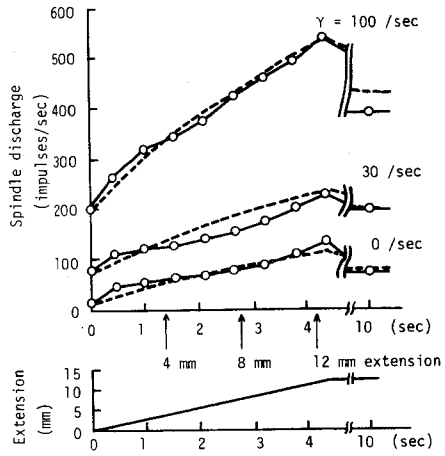

Fig. 3.11 The effect of stimulating the fusimotor fibers at various rates (0, 30, 100 stim/sec) on the response of primary ending to stretching the muscle by 12.45 mm at 2.9 mm/sec. Open circle, experimental result redrawn from Harvey and Matthews (1961)[25]. Broken line, simulated result.

stimulation is approximately equal to the sum of the increase produced by stimulating the two fusimotor fibers separately. Therefore, the principle of superposition holds for the case of fusimotor stimulations.

Open circle in Fig. 3.11 is the experimental result which shows the effects of ventral stimulation at various frequencies on the response of a primary ending to slow stretch (Harvey and Matthews, 1961)[25]. Stimulation of ventral root filaments is considered to stimulate simultaneously corresponding static and dynamic fusimotor fibers. The parameters estimated from the physiological data are given in Table III-4, and the broken line in Fig. 3.11 shows the response of the model obtained with the values. It is shown that increasing the frequency of stimulation produces an increase in the slope of the discharge rate-extension relation.

Additional physiological results are simulated in the same manner as mentioned above. Estimated values obtained from those simulations are given in Table III-4, while both physiological data and simulated responses are not shown in this paper on account of space consideration.

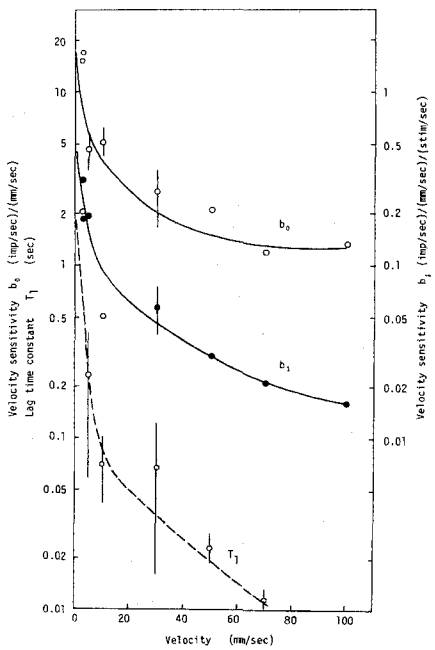

Fig. 3.12 Plot of the velocity sensitivity (b_0, b_1) and the lag time constant (T_1) of the primary endings against velocity of stretch. Vertical bar indicates the standard error of the mean for each point.

All the parameter values of the primary endings obtained by a series of simulations are collectively put in order in Table III-4. The mean values concerning the velocity-dependent parameters, b_o, b_1 and T_1, and their standard deviations (the root mean square value) are calculated as shown in the lowest row of the table. As for the velocity-dependent parameters, calculation of the mean and root mean square values is made only on the particular velocities such as 5, 10, 30 and 50 mm/sec. In Fig. 3.12, the mean value is plotted against velocity with open circle, and the root mean square is given with vertical bar. Applying the curve fitting procedure to each curve, we can express the relation with employing exponential function:

$$b_o = 1.2 + 4.7\ e^{-0.057\ v} + 5.0\ e^{-0.4\ v} \tag{3.14}$$

$$b_1 = 0.015 + 0.1\ e^{-0.04\ v} + 0.36\ e^{-0.35\ v} \tag{3.15}$$

$$T_1 = 1.8\ e^{-0.48\ v} + 0.09\ e^{-0.03\ v} \tag{3.16}$$

where v= velocity of stretching, mm/sec.

Then, the dynamic index can be calculated by introducing Eqs. (3.14) and (3.15) into the relation.

$$\text{Dynamic index} = (b_o + b_1 \Gamma_d)\ v$$

Solid line in Fig. 3.13 shows the experimental result which illustrates the effect of dynamic fusimotor stimulation on the relation between velocity and dynamic index, and broken line in the figure is the calculated curve of the dynamic index in such a manner. A quantitative coincidence is seen between physioloiical and simulated curves, while we have to notice a remarkable difference appeared only for the case at Γ_d=100 stim/sec.

b) Responses of the secondary endings

The same technique as employed for the primary endings is applied to identify the parameters concerning the secondary endings, such as a_o', a_2',

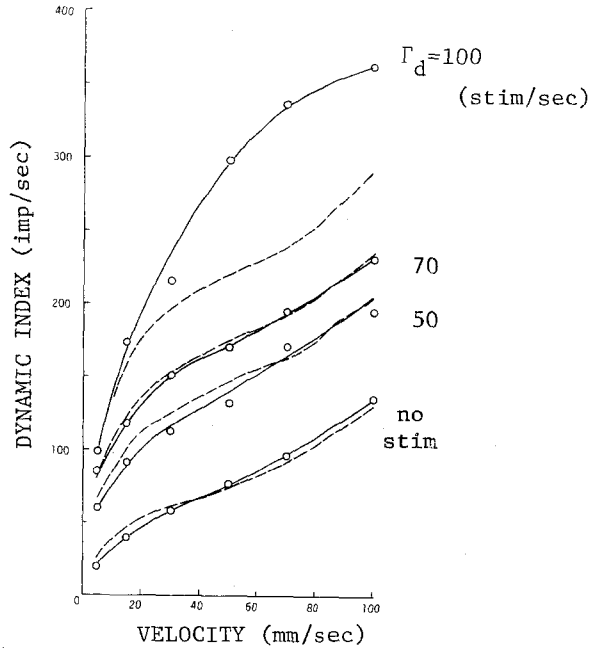

Fig. 3.13 The effect of fusimotor stimulation on the relation between dynamic index of a primary ending and velocity of stretching. Open circle, experimental result redrawn from Crowe and Matthews (1964a)[13]. Broken line, simulated curve.

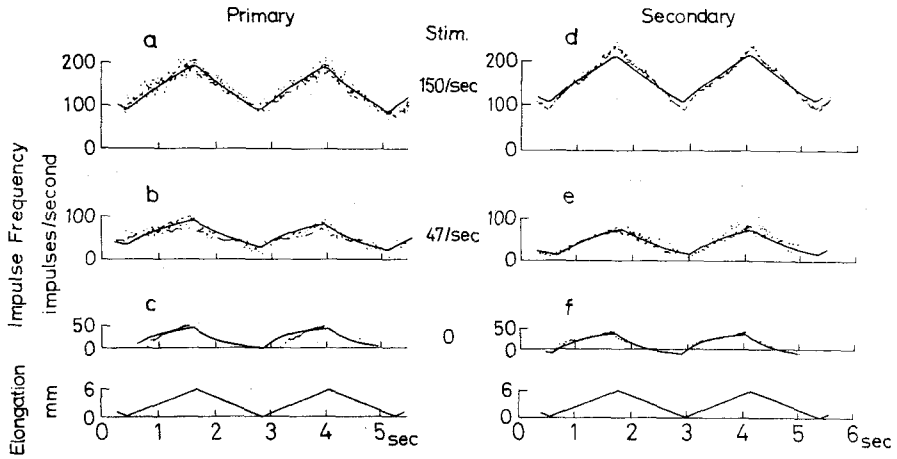

Fig. 3.14 The responses of primary and secondary endings to stretching by 6 mm at 5 mm/sec in the absence of fusimotor stimulation and during stimulating several combined coarse ventral root filaments of static type. Spot, experimental result redrawn from Brown et al. (1969)[11]. Solid line, simulated response.

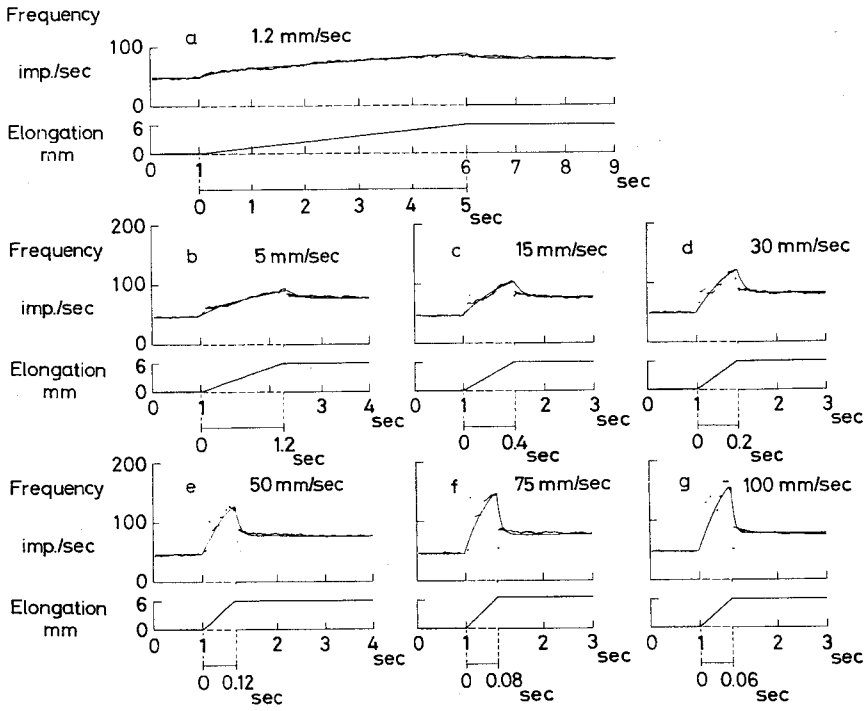

Fig. 3.15 The responses of a secondary ending to an extension of 6 mm at velocities ranging from 1.2 to 100 mm/sec. Spot, experimental result redrawn from Matthews (1963)[48]. Solid line, simulated result.

T_x', T_3, K_s and T_s. Firstly, the parameters a_o' and a_2' are determined from the static curve "statics" in Fig. 3.2 (d) that represents the relation between K_x' and Γ_s. Consequently, we obtain a_o'=4.0 (imp/sec)/mm and a_2' =0.083 (imp/sec)/mm/(stim/sec).

In turn, the transient responses of a secondary ending to triangular stretching are simulated by means of the model. The physiological data redrawn from Brown et al. (1969)[11] are shown in Fig. 3.14 with spots. The response of a primary ending to similar stretching is also represented for comparison. Both the parameters of the secondary and of the primary endings are estimated from the physiological records. Estimated values for the parameters are approximately identical between both endings; $a_o'=a_0$=1.33 (imp/sec)/mm,

$a_2'=a_2=0.07$ (imp/sec)/mm/(stim/sec), $T_x'=b_o=3.6$ (imp/sec)/(mm/sec), $K_s'=0.44$ (imp/sec)/(stim/sec), $K_s=0.65$ (imp/sec)/(stim/sec) and $T_1=T_3=0.44$ sec. Simulated responses of the model obtained with these parameters are shown with solid lines in Fig. 3.14.

Fig. 3.15 shows the responses of a secondary ending to phasic stretching at various velocities (Matthews, 1963)[48]. Parameters a_o', T_x' and T_3 are estimated from the physiological data. Estimated values are given in Table III-5, and simulated responses of the model obtained with the values are shown with solid lines in Fig. 3.15.

All the estimated parameters of the secondary endings are summarized in Table III-5, and the mean value is calculated for each parameter. Then, the

TABLE III-5

ESTIMATED PARAMETERS OF SECONDARY ENDINGS

Figure's number in this paper	Reference	Q_0 imp/sec	a_0' $\frac{\text{imp/sec}}{\text{mm}}$	a_2' $\frac{\text{imp/sec}}{\frac{\text{mm}}{\text{stim/sec}}}$	K_S' $\frac{\text{imp/sec}}{\text{stim/sec}}$	v mm/sec	T_x' $\frac{\text{imp/sec}}{\text{mm/sec}}$	T_3 sec
Fig. 3.2	(c) Fig. 6		4.0{1}	0.083{4}				
Fig. 3.14	(c) Fig. 7		1.33{3}	0.07{2}	0.44{2}	5	3.6{3}	0.44{3}
Fig. 3.15	(f) Fig. 2	43.0{7}	5.33{7}			1.2	8.0{1}	0.25{1}
						5	2.8{1}	0.21{1}
						15	2.0{1}	0.17{1}
						30	1.8{1}	0.13{1}
						50	1.4{1}	0.08{1}
						75	1.4{1}	0.06{1}
						100	1.4{1}	0.05{1}
Mean value		43.0	4.12	0.079	0.44	$T_x'=0.76+7.7\,e^{-0.4v}+1.2\,e^{-0.04v}$		
Number of measurements		{7}	{11}	{6}	{2}	$T_3=0.2\,e^{-0.036v}+0.06\,e^{-0.003v}$		

velocity-dependent parameters are plotted against velocity in Fig. 3.16. Curve c represents the velocity sensitivity — velocity relation, and curve d the lag time constant — velocity relation. Furthermore, we identify the velocity sensitivities of two additional secondary endings as a function of velocity by calculating the dynamic index — velocity curves presented in the literature (Matthews, 1963)[48]. The results obtained are plotted in Fig. 3.16, curves a and b. Remarkable differences are found among three curves a, b and c. Curve a seems to show an average feature of velocity sensitivity vs

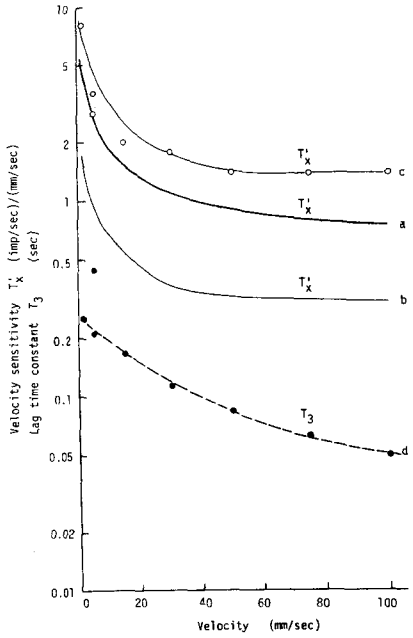

Fig. 3.16 The relations between velocity sensitivities and velocity, obtained from three different secondary endings, a,b and c. Curve, d, the relation between lag time constant of the secondary endings and velocity of stretching.

velocity relation. Applying curve fitting procedures to curves a and d, we can formulate the T_x' - v relation and the T_3 - v relation as

$$T_3 = 0.19\ e^{-0.036\ v} + 0.06\ e^{-0.003\ v} \tag{3.17}$$

$$T_x' = 0.76 + 7.7\ e^{-0.4\ v} + 1.2\ e^{-0.04\ v} \tag{3.18}$$

Both the velocity sensitivity and the lag time constant of the secondary endings are decreased by increasing velocity in the same manner as the primary endings represent, while quantitative differences are generally found between both kinds of endings.

3.5 DISCUSSION

A mathematical model of mammalian muscle spindle which consists of a mechanical filter, a mechano-electric transducer and an encoder is developed, based on the physiological and anatomical findings. Much knowledge about structure of spindle gives a basis of construction of viscoelastic model of a mechanical filter. In addition, a large quantity of experimental data on spindle behavior that has been obtained from cat's soleus muscle by P. B. C. Matthews and his coworkers, is quite available to our computer simulations; these data motivate us to make the quantitative investigations involving construction of mathematical model and estimation of system parameters. As a result we can indicate that we have a quantitative agreement, with respect to transient and steady-state features of the muscle spindles, between physiological and simulation results. Further, it should be noted that our model can account for the marked nonlinear properties of primary and secondary endings, e.g., variation of position and velocity sensitivities caused by stimulation of static and dynamic fusimotor fibers.

As suggested by Matthews (1964)[49] and Crowe (1968)[12], variation of the position and velocity sensitivities of spindle may be accounted for by way of change in the viscous and elastic properties of the intrafusal fibers. The following assumptions are introduced into the viscous and elastic properties of intrafusal fibers, based on the knowledge about the mechanical properties of the skeletal muscles.

1) Stimulation of the dynamic fusimotor fiber increases values of E_2 and D_1. The increase in D_1 is much greater than the increase in E_2.
2) Stimulation of the static fusimotor fiber produces an increase in E_5 but a relatively small increase in D_2. These assumptions 1) and 2) are the same as described by Crowe (1968).[12]
3) In addition, increasing velocity does cause an decrease in D_1 and D_2.
4) Other elastic constants , E_1, E_3 and E_4, and parameters η_1, η_2, η_3 and ν all remain always constant.

TABLE III-6

EFFECTS OF VISCOELASTICITY OF THE INTRAFUSAL FIBERS ON THE POSITION AND VELOCITY SENSITIVITIES OF THE PRIMARY AND SECONDARY ENDINGS

	Nuclear bag fiber		Nuclear chain fiber		Primary ending			Secondary ending		
	elasticity E_2	viscosity D_1	elasticity E_5	viscosity D_2	position sensitivity K_x	velocity sensitivity T_x	lag time constant T_1	position sensitivity K_x'	velocity sensitivity T_x'	lag time constant T_3
Stimulation of dynamic fiber	increase	large increase			increase	increase	slight increase			
Stimulation of static fiber			increase	slight increase	increase	slight decrease		increase	slight decrease	slight decrease
Increase in velocity		decrease		decrease		decrease	decrease		decrease	decrease

It is later discussed that these assumptions are similar to the mechanical properties exhibited by the skeletal muscle. Introducing the assumptions 1) -4) into Eq. (A-9), we can obtain Table III-6. The result is in a good agreement with what is actually observed in the responses of muscle spindle. First, significant effects of fusimotor stimulation on the position and velocity sensitivities, besides effects of velocity on the lag time constant are inclusively accounted for. Additional nonlinear effects which are not emphasized in the simulation because of less significance and of slight nonlinearity are also explained. In Table III-6, velocity sensitivity of a primary ending, T_x, is decreased by stimulation of static fusimotor fibers, which is in agreement with the feature in Fig. 3.3 (Crowe and Matthews, 1964a)[13]. Further, Table III-6 shows a slight increase in the lag time constant, T_1, caused by stimulation of dynamic fusimotor fibers. This effect is actually observed on the spindle responses as shown in Fig. 3.7 and in Fig. 3.9; stimulation of a dynamic fiber produces a response over the static part of stretch which reaches a steady state rather more slowly than in the absence of fusimotor stimulation. Now, more satisfactory model may be obtained by introducing these nonlinear properties into the model, although it becomes consequently more complicated. These effects, however, are trifling and less important in the muscle control system than the marked nonlinear effects. The model proposed in the present study is considered being sufficient as a first approximation.

We have clarified the mechanical properties of the skeletal muscle fibers of the frog by physiological recordings and by simulation studies on a computer (see chapters III and V of Part I in this paper, or Akazawa et al., 1969[3], 1971[5]). The above-mentioned assumptions 1)-4) about the viscous and elastic properties of the intrafusal fibers are introduced, based on the knowledge of skeletal muscle fibers. Firstly, we can indicate that the parallel elasticities of the nuclear chain and nuclear bag fibers, E_2 and E_5, are enhanced by stimulating dynamic and static fusimotor fibers. The following properties have to be emphasized: We have shown the existence of two kinds of the parallel elastic components; one of them is a common passive one and the other is, although physiological meaning of it can not be known, an active parallel elastic one whose elasticity is increased in proportion to an increase in the force generated in the contractile component. This fact means that the parallel elasticity is increased by stimulation of alpha motor fibers. Another feature is worthy to note. According to Rack and Westbury (1969)[54], the slope of active tension-extension curve of the cat soleus muscle is increased by stimulation frequency of alpha motor fibers. This property may also correspond to an increase in parallel elacticity phenomenologically. At any way, assuming that the intrafusal fibers have the identical mechanical properties with the extrafusal fibers, parallel elasticities, E_2 and E_5, are considered to be enhanced by fusimotor stimulations. Other series elasticities, E_1, E_3 and E_4, may be independent of fusimotor stimulation , and may be approximately constant.

On the other hand, we have also identified two kinds of viscous components in the skeletal muscle fibers. One of them is a passive viscous element which may correspond to the viscosity of the resting state. The other is a viscous-like element which represents the force-load-velocity relation of the contractile component (see chapter III of Part I of this thesis, or Mashima et al., 1972)[42]. Viscous coefficient of the passive viscous component is nearly constant or slightly decreased by an increase in velocity. Viscous-like coefficient of the viscous-

like component is decreased by increasing velocity , but increased by an increase in the force (active state) developed in the contractile component, i.e. it is increased by stimulation of alpha motor fibers. Assuming that these properties of viscosity of the extrafusal fibers are also provided in the intrafusal fibers, we can say that viscosities of the nuclear bag and chain fibers, D_1 and D_2, are increased by stimulating the dynamic and static fusimotor fibers, respectively, besides that both viscosities are decreased by increasing velocity.

3.6 CONCLUSION

1. A mathematical model of the mammalian muscle spindle which consists of three distinct transformations, a mechanical filter, a mechano-electric transducer and an encoder, is developed, based on anatomical and physiological data.

2. All the parameters were determined quantitatively, by simulating the experimental results obtained from the spindle receptors of cat soleus muscle by Matthews and his co-workers. (See Table III-4 and Table III-5).

3. The simulated responses of the model showed close agreements with the physiological results and accounted for the nonlinear effects of fusimotor fibers on the responses of spindle receptors. The model explained following nonlinear features.

i) Position sensitivity of the primary endings is increased approximately in direct proportion to the frequency of stimulation of the static and dynamic fusimotor fibers.

ii) Position sensitivity of the secondary endings is increased proportionally with an increase in stimulation frequency of the static fibers.

iii) Velocity sensitivity of the primary endings increases in direct proportion to the stimulation frequency of dynamic fusimotor fibers, while the sensitivity of the secondary endings is independent of fusimotor stimulations.

iv) The sensitivities of primary and secondary endings are together decreased by increasing velocity of stretch.

v) The lag time constants in transfer functions of lead-lag filter type for the primary and secondary endings are decreased as velocity of stretch is increased.

4. It was discussed that the nonlinear properties above mentioned, i)-v), could be accounted for by way of variations of the viscous and elastic properties of the intrafusal fibers, involving the nuclear bag and nuclear chain fibers.

CHAPTER IV

ANALYSIS OF STRETCH REFLEX IN SOLEUS MUSCLE

4.1 INTRODUCTION

Among the fundamental motor reflexes that play a major role in the muscular control of posture and movement, one of the most important is undoubtedly the stretch reflex. The purpose of the present chapter is to clarify the dynamic characteristics of the stretch reflex and the functional roles of each physiological component in its reflex, by means of analog simulations. Firstly, mathematical models of the physiological components such as muscle, muscle spindle and alpha motoneuron, are developed, based on the existing data obtained from cat soleus muscles. Then, a mathematical model of the stretch reflex is synthesized by connecting the ensemble of these sub-component models according to the neurological priciples. Finally, behaviors of the model are compared with existing physiological records, and mechanism of the stretch reflex and the roles of the gamma system in the reflex are made clear.

4.2 BRIEF REVIEW OF THE STRETCH REFLEX

Basic arc of the stretch reflex is a closed loop consisting of muscle spindle → group Ia afferent fibers → alpha motoneurons → muscle. Since the study of Liddell and Sherrington (1924)[40], most of the physiologists have recorded the muscular force that is produced as a result of stretching the muscle. That is, the change of muscle length is treated as input, and the muscular force as output. The information-flow diagram for this situation is illustrated schematically in Fig. 4.1.

A passive tension is produced by stretching the muscle, due to the viscoelasticity of passive elements such as the surface membrane, connective tissue and tendons. When the muscle is elongated, the spindle units within the muscle

respond to stretch by increasing the pulse frequencies in group Ia afferent fibers, which in turn increase the efferent signals from the alpha motoneurons to the muscle, and finally enhance the active contractile tension of muscle (active tension). The sum of the passive tension and the active tension is termed the total tension.

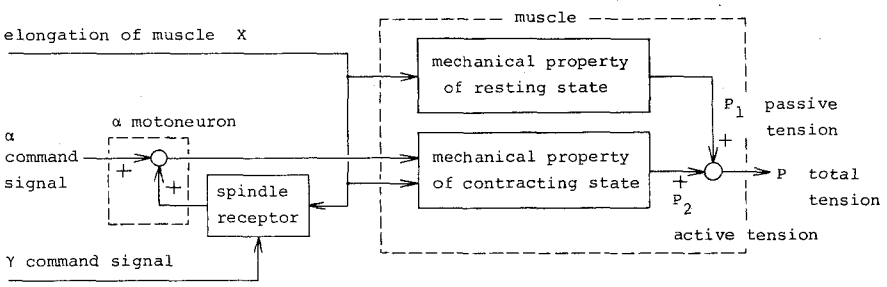

Fig. 4.1 Schematic information-flow diagram of the stretch reflex

4.3 DEVELOPMENT OF THE MODEL

a) Muscle model

A mathematical model of the skeletal muscle has been already developed in chapter V of Part I of this thesis. The model is applied here, and each parameter of the mechanical elements is identified from the physiological data obtained from cat soleus muscles. Nonlinear mechaincal properties of substantial importance are introduced into the model and otherwise are linearlized as much as possible. The mechanical model of muscle is shown in Fig. 4.2.

i) Equation of the model

The total tension is expressed as the sum of the passive tension P_1 and the active tension P_2.

$$P = P_1 + P_2 \qquad (4.1)$$

where P = total tension.

The passive tension is produced by the passive viscoelastic resistance of series elastic component (SEC_1), parallel elastic one (PEC_1) and viscous one (VC_1). The equation at the resting state is

$$\left.\begin{aligned} P_1 &= K_1 x_1 \\ P_1 &= K_p (X - x_1) + B_1 v_1 \\ v_1 &= \dot{X} - \dot{x}_1 \\ X &= X_M - X_o \end{aligned}\right\} \qquad (4.2)$$

where X_M = muscle length,

X = extension of muscle,

X_o = standard length,

x_1 = extension of SEC_1,

v_1 = velocity,

K_1 = elastic constant of SEC_1,

K_p = elastic constant of PEC_1,

B_1 = viscous constant of VC_1.

Taking the Laplace transform of Eq. (4.2), we get

$$P_1(s) = K_o(X) \frac{1 + \tau_2 s}{1 + \tau_1 s} X(s) \qquad (4.3)$$

$$K_o(X) = K_1 K_p / (K_1 + K_p), \quad \tau_1 = B_1 / (K_1 + K_p), \quad \tau_2 = B_1 / K_p .$$

Passive tension of cat soleus muscles increases exponentially with an increase in extension as demonstrated by Matthews (1959a)[45]. This result means that the elastic constants K_1 and K_p are dependent on the muscle extension. Thus, we express $K_o(X)$ as a function of extension of muscle length, X, while the time constants τ_1 and τ_2 are assumed to be constant.

The equations for the contracting muscle which consists of force generator (FG), series elastic component (SEC_2) and viscous-like component (VC_2) are expressed as follows:

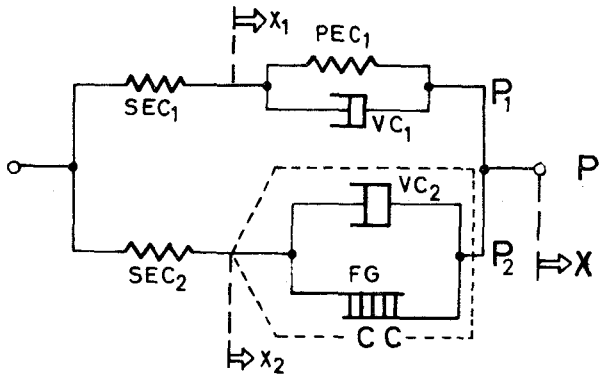

Fig. 4.2 Model of muscle. SEC, PEC, elastic component; VC, viscous component; FG, force generator; CC, contractile component; X, x_1,x_2, extension; P, total tension; P_1, passive tension; P_2, active tension

$$\left.\begin{aligned} P_2 &= K_2\, x_2 \\ P_2 &= F + B_2\, v_2 \\ v_2 &= \dot{X} - \dot{x}_2 \\ B_2 &\begin{cases} = \dfrac{F\,(P_o + a)}{P_o\,(b - v_2)} & (v_2 \leq 0) \\ = \dfrac{F\,(P_o + a')}{P_o\,(b' + v_2)} & (v_2 > 0) \end{cases} \end{aligned}\right\} \qquad (4.4)$$

where P_o = maximum isometric tension,

F = contractile force generated in FG,

x_2 = extension of SEC_2, $x_2 = 0$ at $F = 0$,

v_2 = velocity of CC,

B_2 = viscous coefficient of VC_2, function of F and v_2,

K_2 = elastic coefficient of SEC_2,

a, a', b, b' = constants of the force-velocity relation.

Slow velocity of stretching is treated in the present chapter, so that the viscous coefficient, B_2, is assumed to depend only on the contractile force.

$$B_2 = \frac{F}{P_o} B_o \tag{4.5}$$

where B_o = viscous constant of VC_2 at $F = P_o$. Then, the contractile force developed in the force generator, F , is definitely dependent on discharge rate of alpha motoneurons and the length of muscle. So we employ the following transfer function:

$$\left.\begin{aligned} F(s) &= \frac{1}{1 + \tau_o s} F_A(s) \\ F_A &= f\ (\ A,\ X_M\ ) \end{aligned}\right\} \tag{4.6}$$

where F_A = function of A and X_M,

A = firing frequency of alpha motoneuron,

τ_o = time constant.

ii) Quantitative determination of the parameters

According to the static relation between the passive tension and the length of muscle (Matthews, 1959a)[45], we can get

$$K_o(X) = 0.007\ (\ e^{0.3\ X} - 1.0\ )\ /\ X \tag{4.7}$$

where X, mm; $K_o(X)$, K_g/mm.

Analyzing tension responses to stretching cat soleus muscles at the resting state (Matthews, 1959a)[45], we estimate τ_1 = 0.5 sec and τ_2 = 1.0 sec.

The parameters of the contracting muscle are determined, based on the physiological data obtained by Rack and his co-workers (Rack and Westbury, 1969[54]; Joyce and Rack, 1969[35]). While elasticity of the series elastic component of the active muscle, K_2, increases with an increase in load or in extension, we assume the elasticity to be independent of tension and to be 1.0 Kg/mm. As seen from the data (Joyce and Rack, 1969)[35], this value

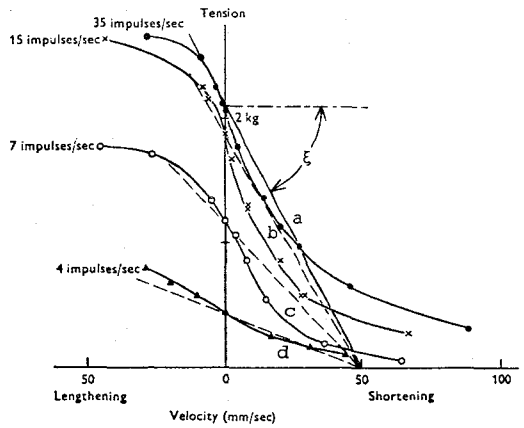

Fig. 4.3 Force-velocity relation of cat soleus muscles. Circle , experimental result redrawn from Joyce and Rack(1969)[35]; stimulation was through five channels at rates indicated on the figure. Straight lines a, b, c and d ; employed for the simulation.

corresponds with the series elasticity at half a maximum isometric tension.

The viscous constant B_o in Eq. (4.5) is estimated from the force-load-velocity curves. Fig. 4.3 shows the relation obtained by Joyce and Rack (1969)[35], which illustrates the effects of various frequencies of alpha efferent fibers under the distributed stimulation of five channels.*) The stimulation frequency more than 35 imp/sec may be regarded approximately as a tetanic stimulation frequency, and consequently the maximum tetanic tension P_o as about 2.1 Kg. For simplicity, we make an approximation, i.e. the hyperbolic force-velocity curves in Fig. 4.3 are expressed by the straight lines. In this situation, the viscous constant B_o may be taken to be a gradient of the line a.

$$B_o = \tan \xi = 2.1 / 50.0$$
$$= 0.042 \text{ Kg/(mm/sec)} \qquad (4.8)$$

*) In order to gain a better understanding of the behavior of soleus muscles under physiological conditions, Rack and his co-workers have employed a new method of subdividing ventral roots and supplying stimulating pulses to different groups of motor units in rotation; five different channels were used in Figs. 4.3, 4.4 and 4.6 in the present paper.

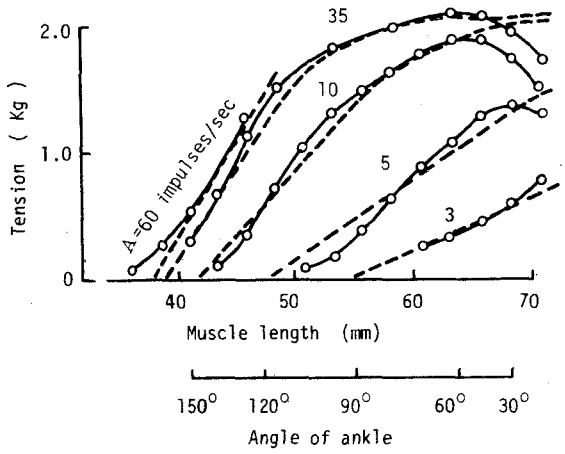

Fig. 4.4 Effects of muscle length and stimulation frequency on the active tension. Open circle, experimental result redrawn from Rack and Westbury (1969)[54]. Broken line, simulated result.

This value subsequently implies that the load-velocity curves at A=15.0, 7.0 and 4.0 imp/sec are approximated with the lines b, c and d , respectively, as shown in Fig. 4.3.

In turn, the function $F_A = f(A, X_M)$ and the time constant τ_o are determined. Solid curves in Fig. 4.4 shows the steady state relation between muscle length and active tension developed at various stimulation frequencies of alpha efferent fibers (Rack and Westbury, 1969)[54]. (* , See the last page). Applying curve fitting procedure to a series of curves, we can obtain the following equation for $f (A, X_M)$.

$$\left.\begin{aligned} F_A &= \begin{cases} 0 & (f_a \leq 0) \\ f_a & (0 \leq f_a \leq 1.4) \\ 2.1 - 0.72\, e^{-1.5 (f_a - 1.4)} & (f_a > 1.4) \end{cases} \\ f_a &= 14.2 (1.0 - e^{0.13 A})(X_M - 32.5) - 1.0 \end{aligned}\right\} \quad (4.9)$$

where dimensions of F_A, X_M and A are [Kg], [mm] and [imp/sec], respectively.

In addition, the time constant τ_o = 0.2 sec is estimated from the time courses of isometric tension development. These results are summarized in Table IV-1.

TABLE IV-1

Mechanical parameters of cat soleus muscle

$K_o(x)$	Kg/mm	$0.007(e^{0.3X}-1.0)/X$ $\quad X=X_M-X_o$, X_o=58.9 mm
τ_1	sec	0.5
τ_2	sec	1.0
P_o	Kg	2.1
K_2	Kg/mm	1.0
B_o	Kg/(mm/sec)	0.041
τ_o	sec	0.2
F_A	Kg	$=\begin{cases} 0 & (f_a \leq 0) \\ f_a & (0<f_a\leq 1.4) \\ 1.4+0.72(1.0-e^{1.5(f_a-1.4)}) & (f_a>1.4) \end{cases}$ where $f_a=14.2(1.0-e^{-0.13A})(X_M-32.5)-1.0$

X, X_M=mm; A=imp/sec.

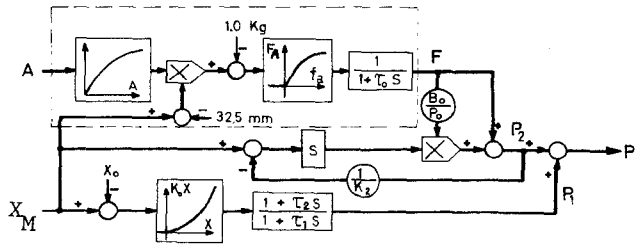

Fig. 4.5 Model of the cat soleus muscle simulated on an analog computer.

iii) Simulated results

Equations (4.1) - (4.9) are simulated on an analog computer. The block-diagram is shown in Fig. 4.5. Firstly, the steady active tension, P_2, is calculated against various values of stimulation frequency A and muscle length X_M. The result is shown with broken line in Fig. 4.4, which shows

close agreement with the physiological result. Further, the responses of isometric contraction at various muscle lengths to various frequencies of stimulation are simulated with using the program in Fig. 4.5. The results are shown with broken line in Fig. 4.6. The simulated results are in a good coincidence with the isometric tension curve obtained from the cat soleus (solid line in Fig. 4.6)

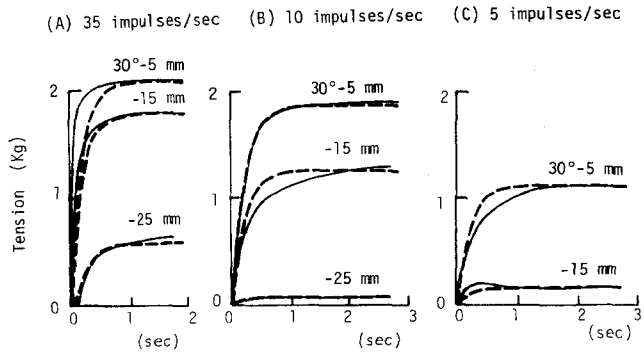

Fig. 4.6 Solid line, experimental results redrawn from Rack et al.[54] (1969); isometric tension curve obtained from different stimulus rates (distributed stimulation of five channels) at different muscle lengths. Broken line; simulated response.

b) Model of the muscle spindle

The mathematical model of muscle spindle has been developed in chapter III. The model is applied here. The discharge rate in group Ia fibers from primary endings is expressed as a function of muscle length and frequency of gamma motor stimulation. The transfer function is given as

$$R(s) = R_o + \left(K_x + \frac{T_x s}{1 + T_1 s} \right) X(s) + \frac{K_d}{1 + T_d s} \Gamma_d(s) + \frac{K_s}{1 + T_s s} \Gamma_s(s)$$

$$K_x = a_o + a_1 \Gamma_d^\circ + a_2 \Gamma_s^\circ, \qquad T_x = b_o + b_1 \Gamma_d^\circ,$$

$$\Gamma_d^\circ = \mathcal{Z}^{-1} \{ \Gamma_d(s) / (1 + T_d s) \}, \quad \Gamma_s^\circ = \mathcal{Z}^{-1} \{ \Gamma_s(s) / (1 + T_s s) \}$$

(4.10)

where R = firing frequency of group Ia fibers,

R_o = spontaneous firing frequency,

Γ_d = frequency of stimulating dynamic gamma fibers,

Γ_s = frequency of stimulating static gamma fibers.

Estimated value for each parameter is redrawn in Table IV-2 (see Table III-4). Note that the parameters b_o, b_1 and T_1 are dependent on velocity of stretching, and otherwise are constant.

TABLE IV-2

Parameters of the spindle group Ia afferent fibers

R_o	13.0	(imp/sec)
a_o	4.7	(imp/sec)/mm
a_1	0.04	(imp/sec)/mm/(stim/sec)
a_2	0.06	(imp/sec)/mm/(stim/sec)
K_d	0.54	(imp/sec)/(stim/sec)
T_d	0.13	(sec)
K_s	0.74	(imp/sec)/(stim/sec)
T_s	0.07	(sec)
b_o	$1.2+4.3\ e^{-0.07v}$	(imp/sec)/(mm/sec)
b_1	$0.015 + 0.1e^{-0.04v} + 0.36e^{-0.35v}$	(imp/sec)/(mm/sec)/(stim/sec)
T_1	$1.8e^{-0.048v} + 0.93e^{-0.03v}$	(sec)

v=mm/sec

c) *Model of the alpha motoneuron*

A significant property of firing of motoneurons within the primary firing range is the algebraical summation of reflex stimuli (Granit, 1970).[24] Thus, alpha motoneuron is expressed here as a simple analog element having the functions of algebraical summation and threshold. Namely, firing rate of the alpha motoneuron, A, is a weighted sum of impulse frequencies of GIa afferent fibrs, R, and those of the alpha efferent routes from higher centers, H_α :

$$A = \begin{cases} 0 & (A \leq 0) \\ H_\alpha + \lambda R & (A > 0) \end{cases} \quad *) \qquad (4.11)$$

where H_α = pulse frequency in alpha efferent route from higher centers,

λ = attenuation factor, constant.

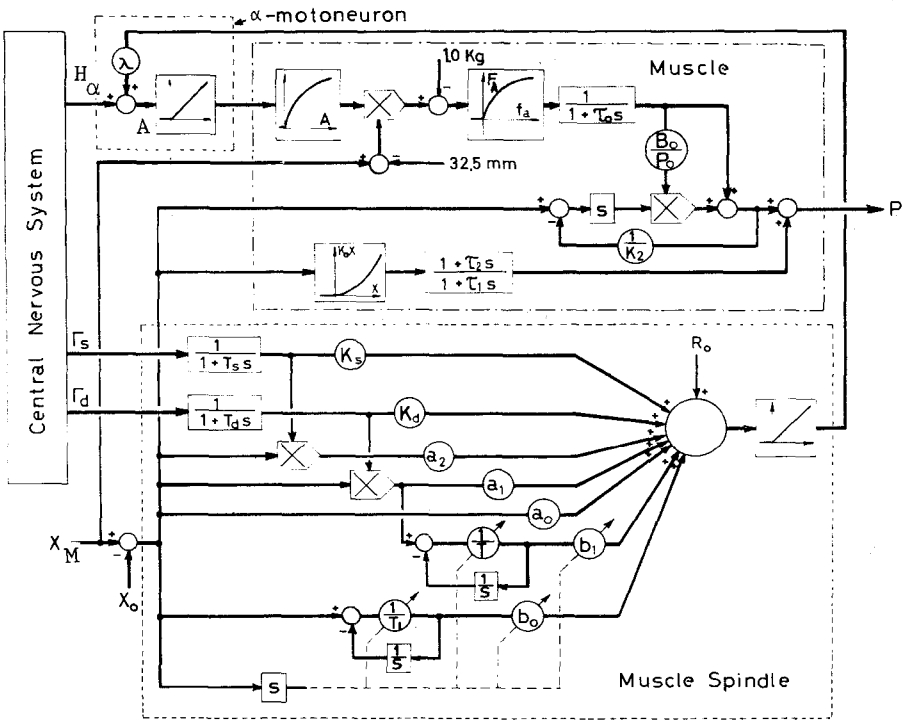

Fig. 4.7 Model of the stretch reflex.

d) Model of the stretch reflex

A mathematical model of the stretch reflex concerning cat soleus muscles can be developed by synthesizing the proposed models of muscle, muscle spindle and alpha motoneuron, according to their anatomical connections. The model is programed on an analog computer , by using Eqs. (4.1) - (4.11). The model is shown in a diagramatical form in Fig. 4.7.

*) The firing rate of alpha motoneuron, A, corresponds to the frequency of distributed stimulation of five channels of motor units (cf. Eq. (4.9)).

4.4 SIMULATION RESULTS

a) The relation between reflex tension and extension

Solid line in Fig. 4.8 is a typical rocord of the physiological data to show the stretch reflex in a soleus muscle of a decerebrate cat (Matthews, 1959a)[45]. The figure shows the increase in tension produced by extending the

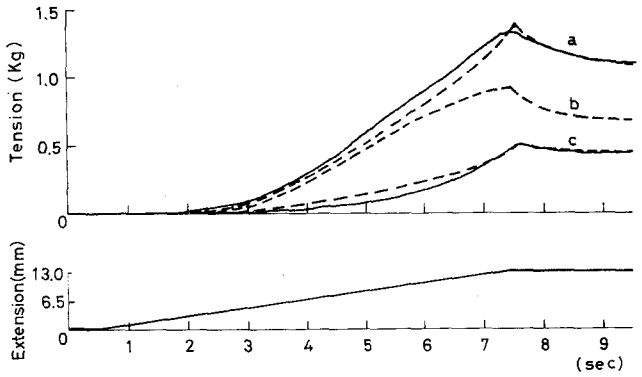

Fig. 4.8 Simulation of the stretch reflex. Solid line, physiological data redrawn from Matthews (1959a)[45]. Broken line, simulated response of the model. Curve a, total tension produced by extending the soleus muscle of a cat by 13 mm at 1.9 mm/sec; curve c, passive tension ; curve b, simulated active tension.

soleus muscle by 13 mm at 1.9 mm/sec, the extension being increased linearly with time. Curve a is the total tension recorded when the stretch reflex was present, and curve c the passive tension when the stretch reflex was completely abolished (nerve was completely anaesthetized with procaine). Broken line in Fig. 4.8 is the response obtained from the model. The simulated result shows close agreement with the experimental one. In the simulation, following values were used besides Table IV-1 and Table IV-2. Initial length of muscle before stretching was taken to be X_i=58.9 mm, spontaneous pulse frequency of alpha motoneuron to be A_i= 0.9 imp/sec, λK_x=0.15 (imp/sec)/mm, λT_x=0.28 (imp/sec)/(mm/sec) and T_1=0.69 sec.

Of course, the amount of the active tension produced by the stretch reflex could not be observed actually, so that it has been commonly determined by subtracting the passive tension from the total tension. Conveniently, time course of the active tension can be drawn directly by means of the computer simulation. Curve b (broken line) in Fig. 4.8 shows the simulated response of the active tension to the same stretching.

b) Effect of gamma activity on the stretch reflex

Influences of the activity of gamma motoneurons on the stretch reflex have been investigated in detail by Matthews (1958,[44] 1959b).[46] A typical record of the experimental results is shown in Fig. 4.9, with solid line.[46] The figure shows the total tension developed in the stretch reflex where the gamma

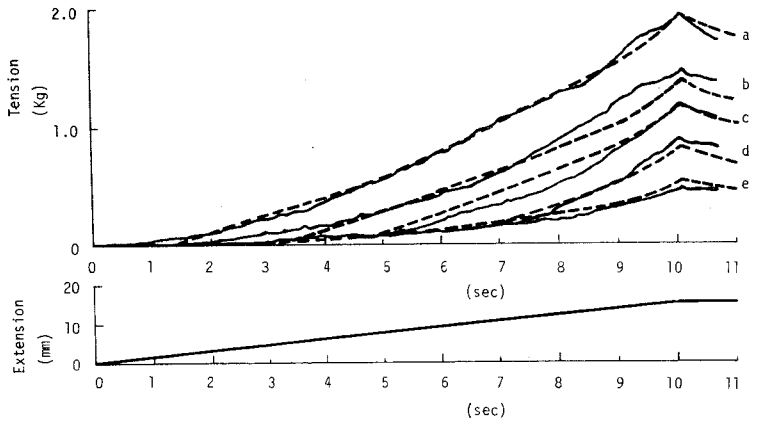

Fig. 4.9 Effects of the gamma activity on the stretch reflex.
Solid line, physiological result to show the effect on the stretch reflex of selectively paralysing the gamma efferent nerve fibers with procaine. Each record shows the total tension produced in cat soleus by extending it by 15 mm at 1.5 mm/sec. Record a was obtained before applying procaine; record e was obtained when the stretch reflex was abolished by inhibition; records b, c, d were obtained when the nerve had been exposed to procaine for 4.5, 6.5 and 10 min, respectively. Broken line, simulated response of the model.

efferent nerve fibers are paralysed selectively by the application of procaine to the muscle nerves. It was confirmed that the procaine paralysed the small gamma motor fibers before the large alpha motor fibers*). Record a was obtained before applying the procaine, record e was obtained when the stretch reflex was abolished completely by inhibition. Records b, c and d were obtained when the nerves had been exposed procaine for 4.5, 6.5 and 10 minutes, respectively. The gamma efferent fibers were believed to be paralysed to some extent gradually with time. Denoting the firing rates of gamma motonerurons in the states a , b, c and d by Γ_a, Γ_b, Γ_c and Γ_d, respectively, we may write the relations $\Gamma_a > \Gamma_b > \Gamma_c > \Gamma_d$, and A=0 in the stage e. The responses of these stretch reflexes are simulated on an analog computer with using the parameter values in Table IV-3. The simulated results are shown in Fig. 4.9, with broken lines. The responses of the model closely agree with the physiological data.

TABLE IV-3

	λR_o	λK_x	λT_x	X_i	T_1
	imp/sec	$\frac{\text{imp/sec}}{\text{mm}}$	$\frac{\text{imp/sec}}{\text{mm/sec}}$	mm	sec
a	1.45	0.15	0.28	60.2	0.69
b	1.13	0.11	0.22	60.2	0.69
c	0.91	0.09	0.75	60.2	0.69
d	0.73	0.07	0.13	60.2	0.69

*) The changes occured in the stretch reflex did not occur abruptly, but took about 5 minutes to develop. The first stage of paralysis during the first 10 minutes exposure is unaccompanied by any change in the direct motor responses of soleus to stimulating its nerve central of the anaesthetized region, and may be attributed to a selective paralysis of the gamma efferent nerve fibers.

Introducing the values in Table IV-3 into Eq. (4.10), we can estimate the pulse frequency of gamma efferent fibers in each stage ; namely, we get Γ_a=80 stim/sec, Γ_b=40 stim/sec, Γ_c =20 stim/sec and Γ_d=0 , by assuming that frequencies of both dynamic fusimotor fibers and static ones are identical ($\Gamma_d = \Gamma_s$) and λ= 0.01 (imp/sec)/(imp/sec). At the same time, we get a_o= 6.7 (imp/sec)/mm, $a_1 + a_2$ = 0.107 (imp/sec)/(stim/sec), b_0= 13.0 (imp/sec)/(mm/sec), b_1 = 0.2 (imp/sec)/(mm/sec)/(stim/sec), 0.107 $(X_i - X)_o + (K_s + K_d)$= 0.9 (imp/sec)/(stim/sec) and $A + 0.01\ R_o$ = 0.73 imp/sec. These values closely coincide with those which are estimated from the actual responses of the muscle spindles in chapter III (see Table IIV-2).

4.5 DISCUSSION

Since the pioneer work by Liddell and Sherrington (1924)[40], most of the physiologists have investigated the stretch reflex of single muscles, instead of a pair of agonist and antagonist muscles. Especially, detailed examination has been made on the soleus muscle of cat. Thus, the present simulations of the model were attempted to explain the stretch reflex in the cat soleus muscles, and then the obtained results are indicated to satisfactorily account for the dynamic characteristics of the reflex action and for the functional roles of muscle, muscle spindle and gamma efferent fibers in the reflex.

One of the difficulties encountered during the present simulations is lack of knowledge concerning the dynamic characteristic of α motoneuron, especially the attenuation ratio (λ) by which the firing rate of group Ia afferent fibers (R) is converted into that of α motoneurons (A). We thus assumed λ= 0.01 (imp/sec)/(imp/sec). This value may be recognized as being reasonable with the recent observation demonstrated by Araki (1972)[7], although the direct evidence cannot be obtained. Fig. 4.10 shows the discharge rate

of a single motoneuron produced by stimulating gruop Ia nerve fibers at various frequencies. The ratio λ must correspond exactly with the slope of the curve, A / R. It is taken to be about 0.05 (imp/sec)/(stim/sec) at the lower stimulation frequencies of R (not exceeding about 100 stim/sec). In this place,

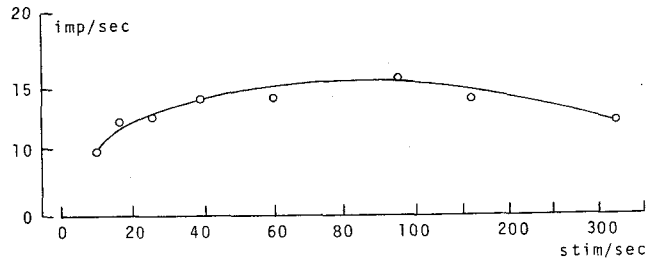

Fig. 4.10 The relation between discharge rate and stimulation frequency. Ordinate, discharge rate of a single motoneuron at the resting membrane potential; abscissa, frequency of stimulating the group Ia afferent fibers (redrawn from Araki (1972)).[7]

it has to be recalled that in the simulation, "A" is trated as the frequecy of distributed stimulation in five different groups of motor units. Namely, it is assumed in the simulation that all the motor units associated with the soleus muscle are activated. Taking them into consideration, the value of λ = 0.01 must be moderate on our simulation while it is the one-fifth of the ratio (λ= 0.05) of a single motoneuron estimated from Araki's result.

4.6 CONCLUSION

1. A mathematical model of the stretch reflex was developed, based on the physiological data obtained from cat soleus muscles. Dynamic characteristics of the reflex and the functional roles of gamma activity were explained quantitatively by analog simulations.

2. The model of muscle developed in chapter V of Part I, was applied here, while the viscous and elastic characteristics were determined from the data of cat soleus and active contractile force was expressed as a function of

muscle length and pulse frequency of alpha motoneurons.

3. The model of muscle spindle in cat soleus muscle which was developed in chapter III was applied here.

4. Alpha motoneuron was modeled as an analog element having the functions of algebraical summation and threshold.

5. Total and passive tensions produced reflexly by stretching the soleus were accounted for by the model. The response obtained from the model closely coincided with that from the soleus muscle.

6. Decrease in the active reflex tension produced by reducing the activity of gamma efferent nerve fibers (paralysing the gamma efferents by the application of procaine) was explained quantitatively in terms of the model.

CHAPTER V

ANALYSIS OF NEUROMUSCULAR CONTROL SYSTEM

5.1 INTRODUCTION

There are, at least, three fundamental spinal reflexes via spindle GIa and GII afferents and tendon GIb afferents, which play important roles in the motor control. It is now well known that contraction of a muscle is reflexly excited by responses of its spindle receptors to stretch and is reflexly inhibited by responses of its Golgi tendon organs to contraction. Nevertheless, the actual importance of each of these reflexes in the motor control remains obscure because of the lack of an experimental approach which is capable of estimating quantitatively their respective influences. Indeed, no satisfactory explanation has been given to the problems of how these fundamental reflexes work together each other and how higher nervous centers govern them to perform a certain purposeful movement.

It has been often emphasized that an activity of gamma efferent nerve fibers is of importance in regulating poture and movement (Granit, 1966,[23] 1970;[24] Matthews, 1964).[49] For instance, the measuring of length for purposes of the control becomes impossible in the absence of contributions from the gamma system. Furthermore, the gamma system has a remarkable function capable of regulating the position and velocity sensitivities of spindle receptors. However, the actual contribution of the activity of gamma efferents has never been explained in the fully dynamic sense.

In the present chapter, a mathematical model of the neuromuscular control system at the spinal level is developed. The analysis treats an unstable limb system consisting of flexor and extensor muscles, where associated muscle spindles (GIa and GII afferent fibers), Golgi tendon organs (GIb afferent fibers), alpha and gamma efferent routes are together taken into consideration. All the parameters involved are determined, based

on the physiological data obtained from cat soleus muscles. Analog simulations are made to reveal the control mechanism of the motor system, especially the roles of spindle receptors in the regulation of posture and velocity of purposeful movements, and the roles of tendon organs in the regulation of muscle tension. In addition, much effort is devoted not only to explaining the functional role of gamma activities but also to uncovering the cooperative actions of spinal reflexes and the supra-spinal control of them, i.e., selection of the spinal subprograms of control.

It is assumed in the present study that the effect of spindle GII fibers is quite opposite to the GIa afferent fibers, the feedback pathways of GIa afferent fibers operate always and the pathways of GIb and GII fibers do not operate always by a command from higher nervous centers. Therefore, three possible cases are treated here; only GIa afferent fibers operate (section 5.3), and either GIb or GII afferent fibers operate together with GIa afferent fibers (section 5.4). Under these considerations, postural control, tension control and velocity control are analysed.

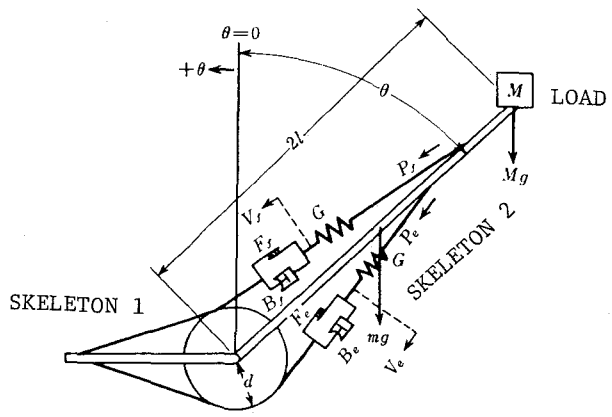

Fig. 5.1 Kinetic model of muscle-limb system.

5.2 MATHEMATICAL MODEL

a) Muscle-limb system

The system is represented diagramatically in Fig. 5.1. It is assumed

that the skeleton 2 rotates round the ankle joint in the vertical plane and the skeleton 1 is fixed. The kinetic equation concerning the rotation of this system is

$$\left.\begin{aligned} & T_f - T_e - T_d = I\frac{d^2\theta}{dt^2} + B_j\frac{d\theta}{dt} - \hat{M}\sin\theta \qquad (-\pi/2 \leq \theta \leq \pi/2) \\ & T_f = d\,P_f \\ & T_e = d\,P_e \\ & I = 4\left(M + \frac{m}{3}\right)\ell^2 \\ & \hat{M} = (2M + m)\,g\,\ell \end{aligned}\right\} \quad (5.1)$$

where T_f (T_e) = torque exerted by the flexor (extensor) muscle,

T_d = disturbance torque,

P_f (P_e) = tension of the flexor (extensor) muscle,

M = mass of the load,

I = moment of inertia consisting of the skeleton 2 (limb) and a load,

m = mass of the skeleton 2,

B_j = viscous coefficient of rotation round the ankle joint,

d = lever arm,

ℓ = half length of the skeleton 2 (see Fig. 5.1),

θ = angle of joint (its increase indicates flexion of the limb),

$\hat{M}$ = loading torque.

Note that the subscript "f" indicates flexor and "e" indicates extensor.

A mathematical model of the skeletal muscle was developed in chapter V of Part I of this thesis. The simplified model of it, consisting of a force generator, viscous-like and series elastic components, is employed here. Assuming that both flexor and extensor muscles are identical, we can get the following equations for the muscles.

$$
\left.
\begin{aligned}
P_f &= F_f - B_f\, v_f \\
P_e &= F_e - B_e\, v_e \\
v_f &= d\,(\,d\theta / dt\,) + G\,(\,dP_f / dt\,) \\
v_e &= -\,d\,(\,d\theta / dt\,) + G\,(\,dP_e / dt\,) \\
B_f &= B_o\, F_f / P_o \\
B_e &= B_o\, F_e / P_o
\end{aligned}
\right\} \qquad (5.2)
$$

where F_f (F_e) = contractile force of the flexor (extensor) muscle,

B_o = viscous constant,

B_f (B_e) = viscous coefficient of the flexor (extensor); function of the contractile force F_f (F_e),

P_o = maximum contractile force,

v_f (v_e) = shortening velocity of the viscous component of flexor (extensor),

G = compliance of the series elastic component of both muscles.

Then we assume that the contractile force, F_f or F_e, generated in the force generator, is only as a function of pulse frequency of alpha motoneuron:

$$
\left.
\begin{aligned}
F_f(s) &= \frac{f_a}{1 + \tau_o\, s}\, A_f(s) \\
F_e(s) &= \frac{f_a}{1 + \tau_o\, s}\, A_e(s)
\end{aligned}
\right\} \qquad (5.3)
$$

where A_f (A_e) = pulse frequency of alpha motoneuron which innervates the flexor (extensor) muscle,

f_a = constant,

τ_o = time constant.

b) Muscle spindle and Golgi tendon organ

A model of the muscle spindle of cat soleus muscle has been developed in chapter III. The model is applied here. Impulse frequencies of GIa and GII afferents are expressed as a function of muscle extension, X, and impulse frequency of gamma fibers. The equations about GIa are

$$\left.\begin{aligned} R_f(s) &= R_o - \left(K_{xf} + \frac{\tau_{xf}\, s}{1 + \tau\, s} \right) X(s) + \frac{K_r}{1 + \tau_r\, s}\, \Gamma_f(s) \\ R_e(s) &= R_o + \left(K_{xe} + \frac{\tau_{xe}\, s}{1 + \tau\, s} \right) X(s) + \frac{K_r}{1 + \tau_r\, s}\, \Gamma_e(s) \end{aligned}\right\} \quad (5.4)$$

and those about spindle GII afferent fibers are

$$\left.\begin{aligned} Q_f(s) &= Q_o - \left(K_{xf} + \frac{b_o\, s}{1 + \tau\, s} \right) X(s) + \frac{K_r}{1 + \tau_r\, s}\, \Gamma_f(s) \\ Q_e(s) &= Q_o + \left(K_{xe} + \frac{b_o\, s}{1 + \tau\, s} \right) X(s) + \frac{K_r}{1 + \tau_r\, s}\, \Gamma_e(s) \end{aligned}\right\} \quad (5.5)$$

$$\left.\begin{aligned} X &= d\ \theta \\ K_{xf} &= a_o + a_3\, \Gamma_f^{\circ} \\ \tau_{xf} &= b_o + b_3\, \Gamma_f^{\circ} \\ \Gamma_f^{\circ} &= \mathcal{L}^{-1}\{\Gamma_f(s) \,/\, (1 + \tau_r\, s)\} \\ K_{xe} &= a_o + a_3\, \Gamma_e^{\circ} \\ \tau_{xe} &= b_o + b_3\, \Gamma_e^{\circ} \\ \Gamma_f^{\circ} &= \mathcal{L}^{-1}\{\Gamma_e(s) \,/\, (1 + \tau_r\, s)\} \end{aligned}\right\} \quad (5.6)$$

where R_f (R_e) = impulse frequency of GIa afferent fibers of muscle spindle of the flexor (extensor) muscle,

Q_f (Q_e) = impulse frequency of spindle GII afferent fibers of the flexor (extensor) muscle,

R_o (Q_o) = spontaneous discharge frequency of GIa (GII) afferents,

Γ_f (Γ_e) = impulse frequency of gamma fibers to the flexor (extensor) muscle,

X = extension of the length of the extensor muscle, i.e. shortening of the length of the flexor muscle,

a_o, a_3, b_o, b_3 = constants,

τ, τ_r = time constants.

Special attentions should be paid to the remarkable nonlinear characteristics expressed in Eq. (5.6), i.e., the position sensitivity, K_{xf} or K_{xe}, and velocity sensitivity, τ_{xf} or τ_{xe}, are together increased with increasing gamma motor stimulations.

Recently, Houk and Simon (1967)[31] have examined in detail the properties of Golgi tendon organs in cat soleus muscles. As a result, it is shown that the sesitivity of the tendon organs is about $21 \sim 110$ (imp/sec)/Kg and that their thresholds are low, about $0.08 \sim 0.5$ Kg, with respect to P_o=2.0 Kg. Thus, the property of the Golgi tendon organ may be written as

$$\left.\begin{aligned} U_f &= K_t P_f \qquad (U_f \geq 0) \\ U_e &= K_t P_e \qquad (U_e \geq 0) \end{aligned}\right\} \quad (5.7)$$

where U_f (U_e) = impulse frequency of Golgi tendon GIb afferent fibers of the flexor (extensor) muscle,

K_t = constant of proportionality.

c) Alpha motoneuron

An alpha motoneuron may be modeled basically as an analog element that has the functions of algebraic summation and threshold. Namely, the output frequency of alpha motoneuron can be represented as

$$\left.\begin{aligned} A_f &= H_{\alpha f} + \lambda_1 R_f - \lambda_2 R_e - \varepsilon_1 Q_f + \varepsilon_2 Q_e - \delta_1 U_f + \delta_2 U_e \\ A_e &= H_{\alpha e} + \lambda_1 R_e - \lambda_2 R_f - \varepsilon_1 Q_e + \varepsilon_2 Q_f - \delta_1 U_e + \delta_2 U_f \end{aligned}\right\} \quad (5.8)$$

$H_{\alpha f}$ ($H_{\alpha e}$) = impulse frequency of alpha efferent route to the alpha motoneuron of flexor (extensor) muscle,

λ_i, ε_i, δ_i, (i=1,2) = constants.

Equations (5.1)-(5.8) are simulated on an analog computer. The blockdiagram is shown in Fig. 5.2.

As mentioned in the introduction, it is assumed that sensory signals conducting from the muscle receptor afferents, GII and GIb, to alpha motoneurons are inhibited on the interneurons by way of command signals from CNS; namely, we take $\varepsilon = \delta = 0$ in section 5.3, and $\varepsilon \neq 0$, $\delta \neq 0$ in section 5.4, while $\lambda \neq 0$ in all investigations.

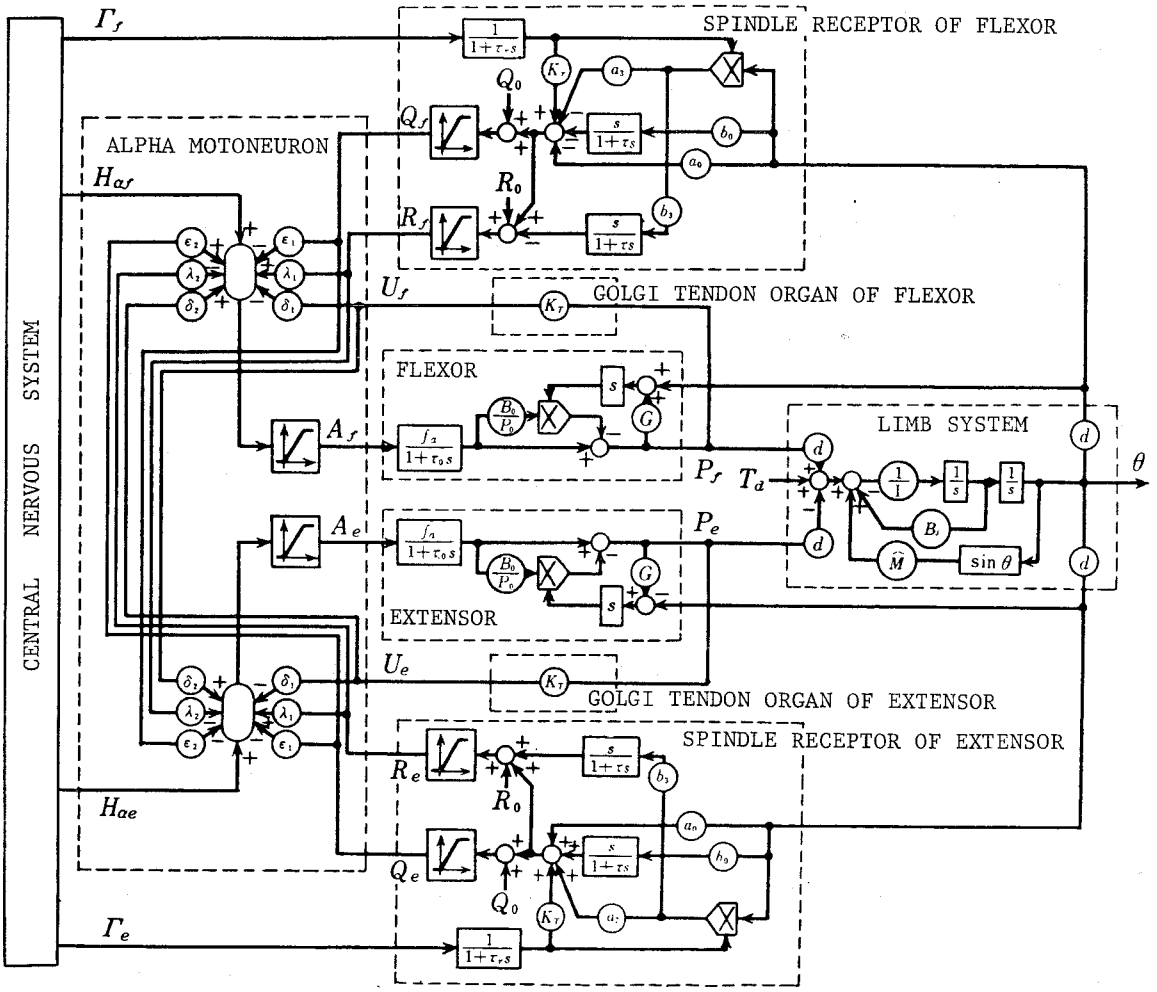

Fig. 5.2 Model of the neuromuscular control system, simulated on an analog computer.

TABLE V-1

The parameters of the model determined from the cat soleus muscles

$P_o = 0.4 \times 10^8$dyn	$a_0 = 50.0$pps/cm
$B_o = 0.8 \times 10^7$dyn(cm/sec)	$a_3 = 1.0$pps/cm/pps
$G = 0.5 \times 10^{-8}$cm/dyn	$b_0 = 20.0$pps/(cm/sec)
$f_a = 0.2 \times 10^7$dyn/pps	$b_3 = 0.5$pps/(cm/sec)/pps
$\tau_o = 0.05$sec	$K_r = 3.0$pps/pps
$B_J = 0.3 \times 10^7$dyn·cm/(rad/sec)	$\tau_r = 0.1$sec
$d = 1.25$cm	$\tau = 0.03$sec
$2l = 15.0$cm	$\lambda_1 = 0.01$pps/pps
$m = 30.0$g	$\lambda_2 = 0.01$pps/pps

d) Determination of the parameters, and normalization

Most of the system parameters are refered from the results obtained in chapters III and IV, and the other prameters are determined from the physiological data of cat soleus muscle. The results are given in Table V-1.*) Since these values would vary with each preparation and characteristics of extensor muscles are scarcely known, we take the normalization. Normalizing the equations (5.1) - (5.3) with the maximum torque $d\,P_o = T_{max}$, and making an approximation of $\sin\theta \simeq \theta(2/\pi)$, we get

$$\left.\begin{aligned} T_f^* - T_e^* - T_d^* &= I^* \frac{d^2\theta^*}{dt^{*2}} + B_j^* \frac{d\theta^*}{dt^*} - \hat{M}^* \theta^* \\ T_f^* &= F_f^* \left(1 - \frac{d\theta^*}{dt^*} - \frac{dT_f^*}{dt^*} \right) \\ T_e^* &= F_e^* \left(1 + \frac{d\theta^*}{dt^*} - \frac{dT_e^*}{dt^*} \right) \\ F_f^*(s) &= A_f^*(s) \,/\, (1 + \tau_o^* s) \end{aligned}\right\} \qquad (5.9)$$

*) We take the value of P_o of flexor and extensor muscles to be about 20 times greate than the maximum force of cat soleus muscle (see chapter IV), and the values of B_o, G are calibrated according to the ratio, 20.

$$F_e^*(s) = A_e^*(s) \;/\; (1 + \tau_o^* s)$$

$$\hat{M}^* = \frac{2}{\pi} \beta \hat{M} \;/\; T_{max}$$

$$T_{max} = d P_o$$

In Eq. (5.9), the Laplace transform variable "s" corresponds to the t*-domain ; namely, $G(s)= \int_o^\infty e^{-st^*} g(t^*)\, dt^*$, where G(s) is the Laplace transform of g(t*). This is also applied to the following equations. Eqs. (5.4)-(5.8) are normalized with the maximum values of impulse frequency of alpha motoneuron and gamma motoneuron, A_{max} and Γ_{max}, respectively.

TABLE V-2

Normalization of the parameters

$T_f^* = T_f/T_{max}$, $T_{max} = dP_o$	$A_f^* = A_f/A_{max}$	$a_o^* = a_0 G P_o/A_{max}$ $=0.5$
$F_f^* = F_f/P_o$	$\Gamma_f^* = \Gamma_f/\Gamma_{max}$	$a_3^* = a_3 G P_0 \Gamma_{max}/A_{max}$ $=3.0$
$\hat{M}^* = 2\beta\hat{M}/\pi T_{max}$	$H_{\alpha f}^* = H_{\alpha f}/A_{max}$	$b_0^* = b_0 P_o/B_o A_{max}$ $=5.0$
$I^* = I/G(dB_o)^2$	$R_f^* = R_f/A_{max}$	$b_3^* = b_3 P^o \Gamma_{max}/B_o A_{max}$ $=37.5$
$B_d^* = B_d/d^2 B_o = 0.24$	$R_0^* = R_o/A_{max} = 0$	$K_r^* = K_r \Gamma_{max}/A_{max}$ $=45.0$
$\theta^* = \theta d/P_o G = 6.25\theta$	$Q_f^* = Q_f/A_{max}$	$K_T^* = K_T T_{max}/A_{max}$
$t^* = t/B_o G = 25.0t$	$Q_0^* = Q_o/A_{max} = 0$	$\tau^* = \tau/B_o G$ $=0.75$
$\tau_o^* = \tau_o/B_o G = 1.25$	$U_f^* = U_f/A_{max}$	$\tau_r^* = \tau_r/B_o G$ $=2.5$
$\beta = P_o G/d = 0.16$		

$A_{max} = 20$pps, $\Gamma_{max} = 300$ pps.

$$\left.\begin{aligned}
R_f^*(s) &= R_o^* \mp \left(K_{xf}^* + \frac{\tau_{xf}^* s}{1 + \tau^* s} \right) \theta^*(s) + \frac{K_r^*}{1 + \tau_r^* s} \Gamma_f^*(s) \\
Q_f^*(s) &= Q_o^* \mp \left(K_{xf}^* + \frac{b_o^* s}{1 + \tau^* s} \right) \theta^*(s) + \frac{K_r^*}{1 + \tau_r^* s} \Gamma_f^*(s) \\
K_{xf}^* &= a_o^* + a_3^* \Gamma_f^{\circ *} \\
\tau_{xf}^* &= b_o^* + b_3^* \Gamma_f^{\circ *} \\
\Gamma_f^{\circ *} &= \mathcal{L}^{-1}\{\Gamma_f^*(s) \;/\; (1 + \tau_r^* s)\} \\
A_f^* &= H_{\alpha f}^* + \lambda_1 R_f^* - \lambda_2 R_e^* - \varepsilon_1 Q_f^* + \varepsilon_2 Q_e^* - \delta_1 U_f^* + \delta_2 U_e^*
\end{aligned}\right\} \quad (5.10)$$

where
$$A_f^* = \begin{cases} 0 & (A_f^* < 0) \\ A_f^* & (0 \leq A_f^* < 1.0) \\ 1.0 & (A_f^* \geq 1.0) \end{cases}$$

Eq. (5.10) represents the equation associated with the flexor muscle, where minus (-) of the compound sign ($\mp$) is taken. The equation of the extensor muscle can be obtained from Eq. (5.10) by exchanging the subscripts "f" and "e" with one another (f → e, e → f) and also by taking the plus (+) in compound signs. Normalized values are given in Table V-2, where we assume A_{max}= 20 imp/sec. Γ_{max}= 300 imp/sec, $R_o=Q_o=0$. These normalized values are used in all the following simulations.

5.3 MECHANISM OF POSITION CONTROL

In this section we consider the case in which only GIa afferent fibers are operating, and show that the impulse frequency of gamma fibers corresponds to the reference in the position control mechanism, and besides examine the contribution of gamma activity to the regulation of posture.

a) Analysis of steady state characteristics

We commence with the relation between limb position and output of each physiological element at the steady state , i.e., $d\theta/dt=0$, $d^2\theta/dt^2=0$, $dT_f/dt=0$, $dT_e/dt=0$. Figure 5.3 illustrates the relations of R_f^*, R_e^*, T_f^* and T_e^* to the angle, θ^*, in two typical cases. That is, in Fig. 5.3 (A) the efferent command signal is absent ($H_\alpha^*= H_{\alpha f}^* = H_{\alpha e}^* =0$), while $H_\alpha^*=0.25$ in Fig. (B). It is clear that in (A) both flexor and extensor muscles do not operate at the same time over a whole range, $-\pi/2 \leq \theta \leq \pi/2$, while both muscles work simultaneously around $\theta=0$ in (B).

Obviously, the limb position can be fixed at an angle where both the driving torque exerted by the muscles and the loading torque are identical. The angle θ_R is defined as the reference position. The driving torque acting on the lever (skeleton 2) is the difference between the torque exerted by the

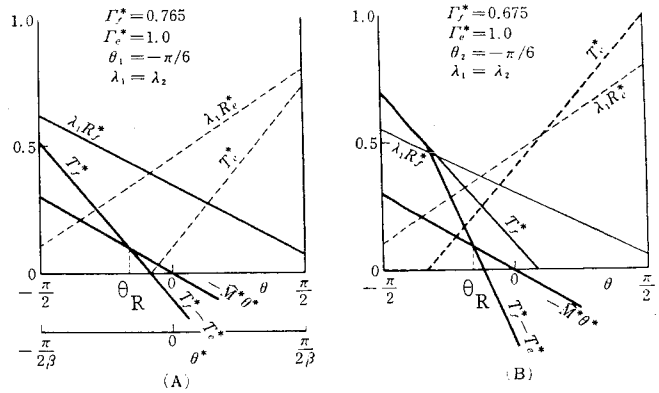

Fig. 5.3 The steady state relation between outputs of each physiological components and angle of joint, (A) $H_\alpha^*= 0$; (B) $H_\alpha^*=0.25$.

flexor and that by the extensor muscle, i.e., $T_f^* - T_e^*$. The loading torque is expressed to be $-\hat{M}^*\theta^*$. As graphically shown in Fig. 5.3, the reference angle, θ_R, is obviously where the line of $T_f^*-T_e^*$ intersects that of $-\hat{M}^*\theta^*$. Note that T_f^* and T_e^* are dependent on angle of joint and their dependences can be regulated by the gamma efferent signals, Γ_f^* and Γ_e^*. That is, the reference position θ_R^* can be varied by changing the values of Γ_f^* and Γ_e^*.

In this place, we have to consider that the driving force at the angle of θ_R is T_f^* in the case of Fig. 5.3 (A) and it is $T_f^*-T_e^*$ in (B). It is due to the property of threshold of the alpha motoneurons and spindles; namely, A_f^*, A_e^*, R_e^* and R_f^* are non-negative. Therefore, two cases should be treated.

Case I: $T_e^* = 0$ or $T_f^* = 0$ at $\theta^*=\theta_R^*$,

Case II: $T_e^* > 0$ and $T_f^* > 0$ at $\theta^*=\theta_R^*$.

Consequently, we get the following relations from Eqs. (5.9) and (5.10).

$$\left.\begin{aligned}
&\text{Case I:}\quad \theta_R^* = \frac{H_{\alpha f}^* + (\lambda_1 \Gamma_f^* - \lambda_2 \Gamma_e^*) K_r^*}{-\hat{M}^* + a_o^* (\lambda_1 + \lambda_2) + a_3^* (\lambda_1 \Gamma_f^* + \lambda_2 \Gamma_e^*)} \\
&\qquad \left(-\tfrac{\pi}{2} \leq \theta_R^* \; \beta \leq 0\right) \\
&\theta_R^* = \frac{H_{\alpha e}^* + (\lambda_1 \Gamma_e^* - \lambda_2 \Gamma_f^*) K_r^*}{-\hat{M}^* + a_o^* (\lambda_1 + \lambda_2) + a_3^* (\lambda_2 \Gamma_f^* + \lambda_1 \Gamma_e^*)} \\
&\qquad \left(0 < \theta_R^* \; \beta \leq \tfrac{\pi}{2}\right) \\
&\text{Case II:}\quad \theta_R^* = \frac{H_{\alpha f}^* - H_{\alpha e}^* + (\lambda_1 + \lambda_2)(\Gamma_f^* - \Gamma_e^*) K_r^*}{-\hat{M}^* + (\lambda_1 + \lambda_2)\{2a_o^* + a_3^* (\Gamma_f^* + \Gamma_e^*)\}} \\
&\qquad \left(-\tfrac{\pi}{2} \leq \theta_R^* \; \beta \leq \tfrac{\pi}{2}\right)
\end{aligned}\right\} \quad (5.11)$$

That is, the relation indicates that the reference position can be regulated by the gamma efferent command signals, Γ_f^* and Γ_e^*, and also by the alpha efferent signals, $H_{\alpha f}^*$ and $H_{\alpha e}^*$. Fig. 5.4 (A) shows a graphical representation of Case II of Eq. (5.11); namely, each line in the figure shows the relation between Γ_f^* and Γ_e^* for obtaining several reference positions such as $\theta_R^* = 0, \pm\pi/2, \pm\pi/3, \pm\pi/6$, against a fixed load (M=1.0 Kg).

b) Conditions necessary for maintenance of stable posture

The condition necessary for the limb to be maintained at the desired angle θ_R^* (not to fall down) is examined. For the purpose of holding the skeleton 2 stably at θ_R^*, a gradient of driving torque line, T_f^*-T_e^*, to θ^* has to be greater than that of the loading torque line, i.e. $\hat{M}^*$. For example, its necessary condition of stability is satisfied in the case of

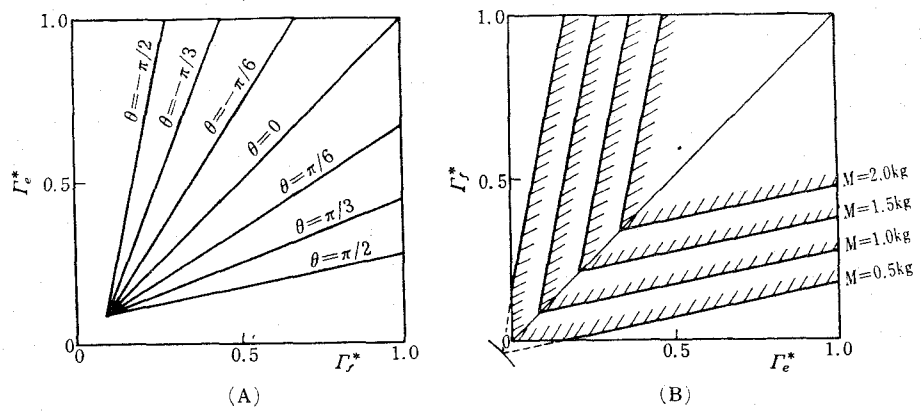

Fig. 5.4 Steady state characteristics of illustrating the effects of gamma stimulations. (A) The relation between Γ_f^* and Γ_e^*, necessary for obtaining the various reference positoons; $\theta_R = 0, \pm\pi/6, \pm\pi/3$, and $\pm\pi/2$. (B) Necessary conditions for the limb not to fall down against various loads, M= 0.5, 1.0, 1.5 and 2.0 Kg. Stable region is shown by shaped portion.

Fig. 5.3. The conditions of stability in the cases of I and II are

$$\left.\begin{aligned}
&\text{Case I:}\quad a_o^*(\lambda_1+\lambda_2)+a_3^*(\lambda_1\Gamma_f^*+\lambda_2\Gamma_e^*) > \hat{M}^* \\
&\qquad (-\pi/2 \leq \theta \leq 0) \\
&\qquad a_o^*(\lambda_1+\lambda_2)+a_3^*(\lambda_1\Gamma_e^*+\lambda_2\Gamma_f^*) > \hat{M}^* \\
&\qquad (0 \leq \theta \leq \pi/2) \\
&\text{Case II:}\quad (\lambda_1+\lambda_2)\{2a_o^*+a_3^*(\Gamma_f^*+\Gamma_e^*)\} > M^* \\
&\qquad (-\pi/2 \leq \theta \leq \pi/2)
\end{aligned}\right\} \quad (5.12)$$

The necessary conditions of stable control for the Case II are shown with the shaped upper right portions in Fig. 5.4 (B). Within the regions the limb is maintained at a certain angle subjected to Eq. (5.11). As a result it is concluded that to enhance Γ_f^* and/or Γ_e^* with an increase in load is necessary for executing a stable postural control. This result is very inter-

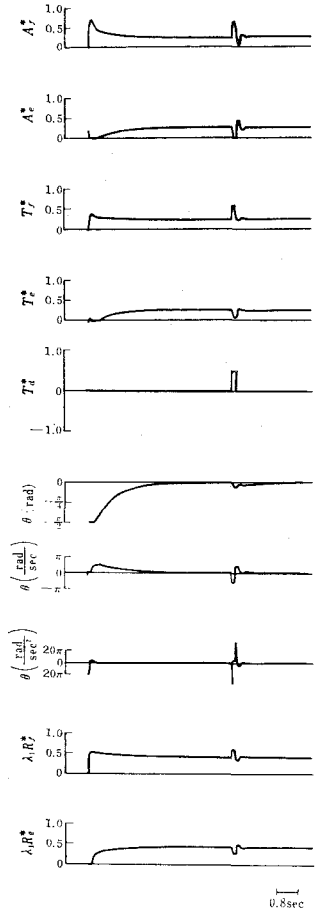

Fig. 5.5 Simulated response of postural control action to show the transient response of flexing movement and response to disturbance torque (T_d^*).

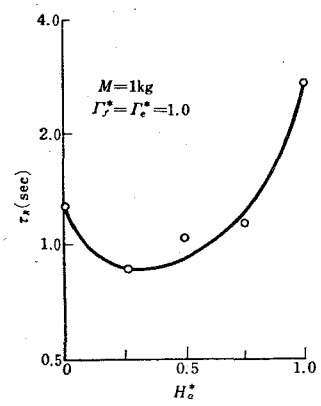

Fig. 5.6 Simulated result to show the relation between H_α^* and τ_R.

esting and worthy to be emphasized. For example, if the sensitivity of muscle spindles is constant ($a_3^* = 0$), the limb system should become unstable in terms of falling down when an applied load is increased. Thus, the role of gamma system that regulates the sensitivities of muscle spindles has an important significance in maintaining a stable position, or in the postural control of the mechanically unstable limb system.

c) Analysis of transient characteristics

Movements of flexing from $\theta = -\pi/2$ to $\theta=0$ and responses to disturbace forces are simulated on an analog computer. A typical record of the simulated results is shown in Fig. 5.5 where each waveform illustrates the time course of individual physiological element. On the simulation, applied load is taken to be 1.0 Kg, the values of alpha efferent command, $H_{\alpha f}^*$ amd $H_{\alpha e}^*$ are changed stepwisely from 0.0 to 0.25 at t=0, and similarly the values of Γ_f^* and Γ_e^* from 0.0 to 1.0 at t=0. After the system reaches to a steady state and $\theta=0$, a disturbance torque is inflicted rectangularly. As shown in the figure, the position control is carried out satisfactorily stable in the dynamic sense even against the disturbance force.

The effects of $H_{\alpha f}^*$, $H_{\alpha e}^*$, Γ_f^* and Γ_e^* on the responses are examined by repeating similar simulation experiments. Fig. 5.6 shows the effects of

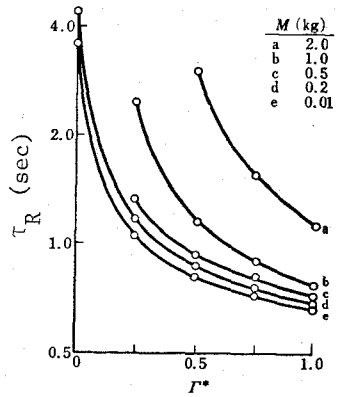

Fig. 5.7 Relation between Γ^* and τ_R, obtained from the simulation experiments for various loads at $H_\alpha^*=0.25$, $\Gamma^* = \Gamma_f^* = \Gamma_e^*$.

alpha efferent commands H_α^* ($\equiv H_{\alpha f}^* = H_{\alpha e}^*$) on the velocity of flexion movement in the rising phase from $\theta = -\pi/2$ to $\theta = 0$. In this figure is shown the relation between H_α^* and τ_R (τ_R, time constant of the rising phase), where $\Gamma_f^* = \Gamma_e^* = 0$ and $H_\alpha^* = 0$ at $t=0$, at $t>0$ $\Gamma_f^* = \Gamma_e^* = 1.0$ and H_α^* is varied but time-invariant. Around $H_\alpha^* = 0.25$, the time constant τ_R gives a minimum value. This is probably due to the following reasons. A flexion velocity is not only determined by the net driving torque, $T_f^* - T_e^* + \hat{M}^*\theta^*$ which actually drives skeleton 2 but also by the viscous forces in the muscles which tend to decrease the velocity of flexion. An increase in H_α^* leads to an increase in T_f^* and T_e^* and also to an increase in the viscous forces of the both muscles. Thus, a certain value of H_α^* would exist at which the velocity of flexion becomes maximum although an exact value can not be obtained because of two complicated effects. The value tends to become $H_\alpha^* = 0.25$ under the condition of Fig. 5.6.

The effects of gamma efferent command signals, Γ_f^* and Γ_e^*, on the velocity of flexing movements are examined. Same simulation experiments as Fig. 5.5 were done, changing the gamma activities $\Gamma^* = \Gamma_f^* = \Gamma_e^*$ and employing various values of applied load, M, and then the time constant in the rising phase of flexion, τ_R, was estimated. Fig. 5.7 shows the obtained result of the relation between Γ^* and τ_R at various loads ranging from 0.01 to 2.0 Kg. As seen from the figure, an increase in Γ^* leads to the faster movement (small value of τ_R) while increase in load, of course, leads to the lower velocity (greater value of τ_R). The values of Γ^* necessary enough to get $\tau_R = 1.2$ sec is plotted against load in Fig. 5.8, which is redrawn from Fig. 5.7. It is evident from the figure that the same value of $\tau_R = 1.2$ sec , i.e., the same velocity of flexion movement, can be achieved by increasing Γ^* in proportion to an increase in load.

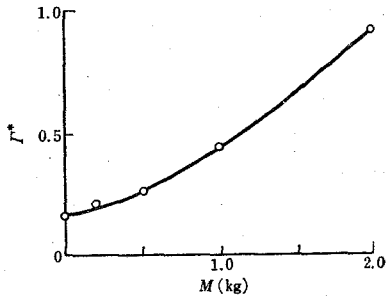

Fig. 5.8 The relation between M and Γ* at τ_R=1.2 sec: open circle, redrawn from Fig. 5.7.

d) Effect of alpha-gamma linkage

In the neural connections of motor system, there are several spinal descending pathways from higher nervous centers which regulate the funtion of myotatic unit of the spinal cord level. In particular, the cerebellar

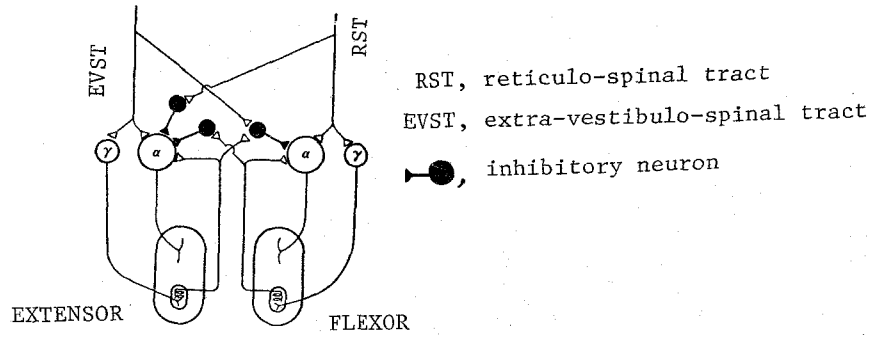

Fig. 5.9 Spinal descending pathways from cerebellum to a myotatic unit at the spinal cord level (from Ito, 1972).

efferent pathways to the spinal cord are undoubtedly the most importants of them. As shown in Fig. 5.9, impulses of the extra-vestibulo-spinal tract (EVST) make the extensor muscle superior to the flexor muscle by activating both the alpha and gamma motoneurons of the extensor (alpha-gamma linkage), and by inhibiting those of the flexor, neural impulses of the reticulo-spinal tract (RST) have opposite effects to EVST. The neuron link in Fig. 5.9 was simulated additionally to the circuit of Fig. 5.2 on an analog computer; that is, the network was introduced into the central nervous system in

Fig. 5.2. Simulation experiments were made, with using the program. Now we denote the impulse frequency of the EVST by H_e ($H_e^*=H_e/A_{max}$) and that of the RST by H_f ($H_f^* = H_f/A_{max}$). Typical records of the simulated results

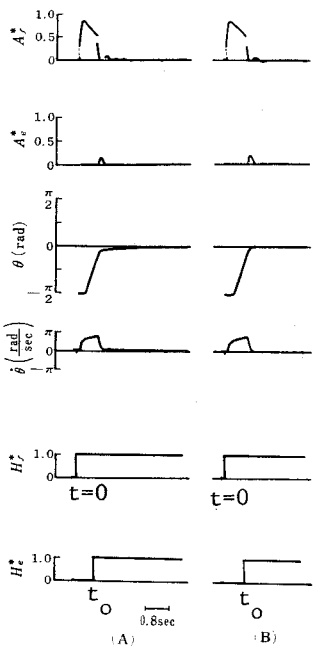

	H_{af}^*	H_{ae}^*	Γ_f^*	Γ_e^*
$t<0$, $H_f^*=0$, $H_e^*=0$	0	0	0	0
$0\leq t<t_o$, $H_f^*=1$, $H_e^*=0$	1/4	−1/4	1	0
$t_o\leq t$, $H_f^*=1$, $H_e^*=1$	0	0	1	1

Fig. 5.10 Simulated result to show the effects of alpha-gamma linkage on the postion control action. (A), instant of onset of the stimulation of the RST, t_o, was earlier; (B) t_o was moderate; inserted table, employed values; the neural connection in Fig. 5.9 was used.

are shown in Fig. 5.10. In the simulations, the EVST is activated stepwisely at t=0,i.e., H_f^* is changed from 0 to 1.0, and then the RST is activated stepwisely also at $t=t_o$, i.e., H_e^* is changed from 0 to 1.0 at $t=t_o$, when the angle of the limb θ draws near the desired angle $\theta_R=0$. The records show rapid and precise flexion movements. It seems that the switching instant, t_o, is set moderately in the case (B) of Fig. 5.10, while the instant slightly earlier in (A). At any rate, on activating the RST, the rapid flexion brought about by the stimulation of the EVST is

slowed down, and consequently the limb approaches slowly to the desired angle.

5.4 MECHANISM OF TENSION AND VELOCITY CONTROLS

In this section we consider the case in which either GIb or GII afferent pathway operates together with GIa afferents, and examine the mechanism of tension control by means of GIb afferent feedback and that of velocity control by means of GII afferent feedback.

a) Mechanism of tension control

As to a single muscle, a negative feedback system of tension control is formed via Golgi tendon organs as shown in Fig. 2.5. Apparently, reference input is given by the impulse frequency of alpha efferent routes and a controlled output is the tension generated by the muscle. Fig. 5.11 is the simulated result to show the isometric tension response to stepwise input of H_α*, where the joint is fixed at a certain angle. Curve b is the response in the presence of GIb feedback and curve a is in the absence of it. When the GIb feedback pathway is acting, isometric tension is developed faster

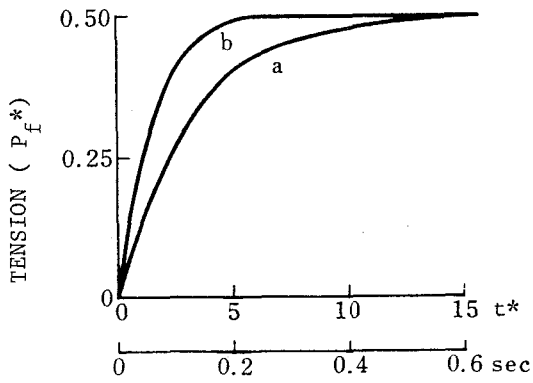

Fig. 5.11 Simulation result to show the effect of Golgi tendon GIb feedback on the tension development to step change in H_α*. Curve a, in the absence of GIb feddback, δ_1=0, H_α*=0.5; curve b, in the presence of GIb feedback, δ_1 K_T* = 1.0, H_α* = 1.0.

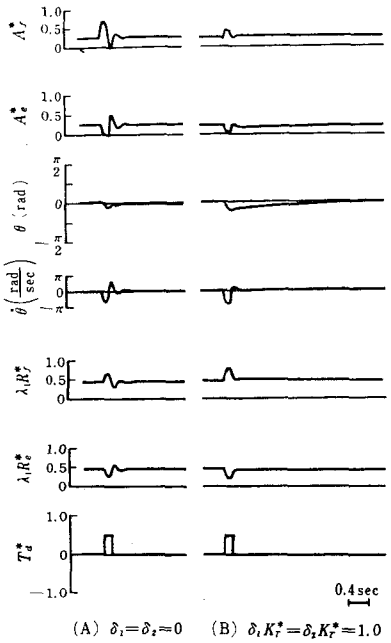

Fig. 5.12 Simulation result to show the effects of GIb feedback on the responses to disturbance torque (T_d^*). (A) In the absence of GIb feedback, $\delta_1 = \delta_2 = 0$, $H_\alpha^* = 0.25$; (B) in the presence of GIb feedback, $\delta_1 K_T^* = \delta_2 K_T^* = 1.0$, $H_\alpha^* = 0.5$; both cases, GIa feedback afferents were operating, $\Gamma_e^* = \Gamma_f^* = 1.0$, M=1.0 Kg.

Further, the effects of simultaneous operation of GIb afferent feedback pathways of both the flexor and extensor muscles are examined, i.e. $\delta_1 \neq 0, \delta_2 \neq 0$. Here we denote by P_{fo}^* and P_{eo}^*, the tension of flexor and of extensor in the absence of GIb feedback respectively, and by P_{fl}^* and P_{el}^*, the tension of flexor and extensor in the presence of GIb feedback, respectively. assuming $\delta_1 K_T^* = \delta_2 K_T^* = 1.0$, we obtain

$$\left.\begin{aligned} P_{fl}^* &= (2 P_{fo}^* + P_{eo}^*) / 3 \\ P_{el}^* &= (2 P_{eo}^* + P_{fo}^*) / 3 \end{aligned}\right\} \qquad (5.13)$$

For example, if $P_{fo}^* = 0.9$ and $P_{eo}^* = 0$, we get $P_{fl}^* = 0.6$ and $P_{el}^* = 0.3$. This fact means that difference between the tension of flexor and that of extensor is decreased by way of the effects of GIb feedback pathways and that the

tensions of both muscles tend to become identical, i.e. to be averaged. This effect of GIb on maintaining steady tension level is also demonstrated by simulating transient responses to disturbance torque. One of the results is shown in Fig. 5.12; namely, in (B), GIb pathways of both muecles are under operation, and in (A) they are not acting at all, and in either case GIa afferents do work always. It is evidently shown that the steady tension desired can be maintained by means of GIb feedback though it may be varied slightly by the disturbance. The function of tendon organs is said to be safety mechanism which prevents from damage of muscle by decreasing its excessive stretch-reflex tension developed when a large external torque is applied or when someone jumps down from high place. Simulated results in Fig 5.12 would imply this effect, namely, stretch reflex tension resulted from the disturbance torque is much smaller in the presence of GIb feedback pathway than in the absence of it.

b) Mechanism of velocity control

Functions of spindle group II afferent fibers are investigated for two typical cases , as shown in Fig. 5.13 (A) and (B). In the case (A), GII feedback loops of the extensor and flexor muscles are operating. In the case (B) only GII afferent pathway of the extensor muscle is operating; that is, this neural connection corresponds to the flexor reflex pattern of innervation. The neural connection of Fig. 5.13 (C) is quite the same as (B). Note that in (A), (B) and (C), GIa afferent fibers of the flexor and extensor muscles operate always. The steady state relations between torques (T_f^* and T_e^*) and angle are shown in the left half of the figure. Note that $T_f^*(0)$ and $T_e^*(0)$ express the torques of the flexor and the extensor muscle in the absense of GII afferent feedback, respectively, and that T_f^* and T_e^* are the respective torques in the presence of GII feedback. Corresponding neural connection of GII is shown in the right half of the figure.

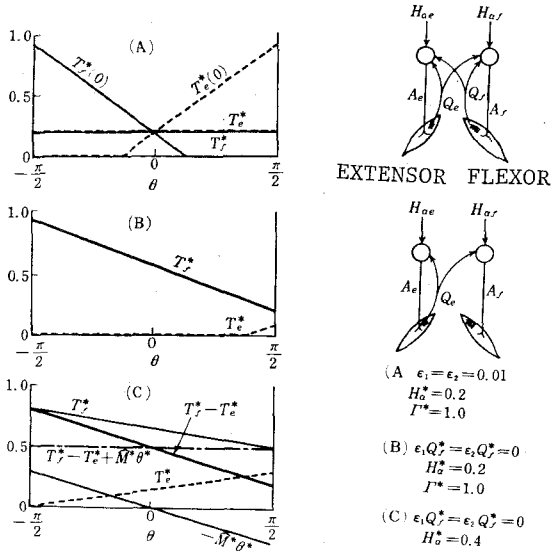

Fig. 5.13 Effect of spindle group II afferent feedback on the steady state relation between torques (T_f*, flexor; T_e*, extensor) and angle of the joint. Only neural connections of GII afferent fibers are shown in the right half , and those of GIa are not drawn while GIa feedback pathways operate always. (A) GII afferents of both the flexor and extensor muscles operate; (B),(C),only GII afferents of the extensor muscle operate. Note that the line of (T_f*-T_e*) is parallel with that of ($-\hat{M}$*θ*) in (C).

It is shown in Fig. (A) that the reflex tension developed by the GIa afferent feedback is completely inhibited by GII afferent feedback pathways. Consequently, the impulse frequencies of alpha efferent routes are conveyed directly to the muscles via alpha motoneurons, on which spindle receptors have no actual influences. Now consider the movements of skeleton 2 in the horizontal plane, i.e. $\hat{M}$=0. At the steady state, $H_{\alpha f}$* = A_f* = T_f* and $H_{\alpha e}$* = A_e* = T_e*, so that the steady state velocity, w_h* = d θ*/dt*, can be written as follows from Eqs. (5.9) and (5.10).

$$w_h^* = \frac{H_{\alpha f}^* - H_{\alpha e}^*}{H_{\alpha f}^* + H_{\alpha e}^* + B_j^*} \tag{5.14}$$

This equation means that in the horizontal movement, the velocity of flexion or extension can be controlled only by the command signals of alpha efferent routes from higher centers.

On the other hand, it is obvious that the loading torque associated with a limb and an applied load is dependent on the angle of joint; for example, the torque is maximum when the limb is at a horizontal position ($\theta = \pi/2$) and it is zero when the limb is at a vertical position ($\theta = 0$). So we attempt to explain the velocity control of flexion movements in the vertical plane, by refering the roles of gamma activity and group II afferent feedback pathways. We may begin with considering that the net torque of driving the limb is equal to the difference between torque exerted by the muscles, $T_f^* - T_e^*$, and loading torque, $-\hat{M}^* \theta^*$; namely, $T_f^* - T_e^* + \hat{M}^* \theta^*$. Therefore, when the net torque is independent of the angle of joint and maintains constant, the angular velocity of mevement can be kept constant. In the cases (B) and (C) in Fig. 5.13, the torques exerted by the flexor and extensor muscles are expressed as

$$\left.\begin{aligned} T_f^* = A_f^* &= H_{\alpha f}^* + \lambda_1 R_f^* \\ T_e^* = A_e^* &= H_{\alpha e}^* - \lambda_1 R_e^* \end{aligned}\right\} \qquad (5.15).$$

And further, if Γ_f^* does satisfy the relation:

$$\left.\begin{aligned} \lambda\ (a_o^* + a_3^* \Gamma_f^*) &= \hat{M}^*/2 \\ \lambda = \lambda_1 &= \lambda_2 \end{aligned}\right\} \qquad (5.16)$$

we can write the net torque as

$$T_f^* - T_e^* + \hat{M}^* \theta^* = H_{\alpha f}^* - H_{\alpha e}^* + 2\lambda K_r^* \Gamma_f^* \qquad (5.17).$$

Consequently, we may show that the right hand of the equation is independent of the angle of joint, θ. (See Fig. 5.13 (C)). In this situation, the steady state velocity, w_v^*, is approximately given as

$$w_v^* = \frac{H_{\alpha f}^* - H_{\alpha e}^* + 2\lambda K_r^* \Gamma_f^*}{A_f^* + A_e^* + B_j^*} \qquad (5.18).$$

Because the relation

$$A_f^* + A_e^* = H_{\alpha f}^* + H_{\alpha e}^* \qquad (5.19)$$

does hold (see Eq. (5.15)), the denominator and the numerator are independent of the angle, θ. Finally the steady state velocity w_v^* is independent

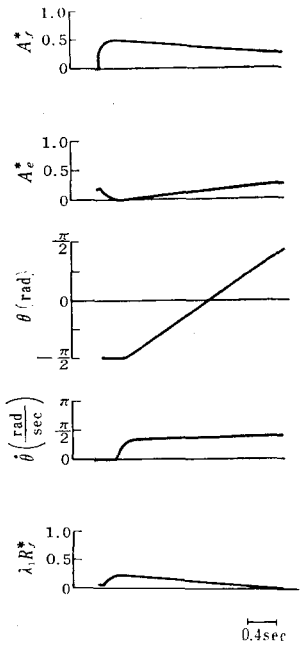

Fig. 5.14 Simulated result to show the possibility of velocity control of flexion movement. Neuronal connection, Fig. 5.13 (B); $H_\alpha^* = 0.25$, $M = 1.0$ Kg, $\Gamma_f^* = 0.34$, these values satisfy the relation of Eq. (5.16). Spindle GII afferent path, flexor reflex pattern; GIa afferent fibers operate always.

of the angle of joint. This result means that a steady velocity can be obtained by increasing Γ_f^* linearly as an applied load is increased, and that the desired steady velocity can be controlled by the impulse frequencies of alpha efferent routes, $H_{\alpha f}^*$ and $H_{\alpha e}^*$. These considerations were actually

demonstrated on an analog computer. A typical record of the simulation results of velocity control is shown in Fig. 5.14. As seen from the figure, the limb begins to flex slowly because of the inertia and other effects, and then it reaches to and maintains nearly steady velocity.

As to the effects of group II afferent feedback, following aspects may be emphasized. As shown in Fig. 5.13 (A), torque $T_e^*(0)$ developed by the effects of GIa afferents is considerably large at $0 < \theta < \pi/2$ and is increased with an increase in θ, and the extensor's torque tends to prevent the limb from flexing. On the other hand, in the presence of GII afferent feedback, the extensor muscle does scarcely operate over the whole angle, as shown in Fig. 5.13 (B) and the action of the flexor is superior to the extensor. That is, GII afferent feedback of the extensor, inhibiting the extensor's activity, can make the limb flex more smoothly.

5.5 DISCUSSION

The present work proposed and investigated two problems of interest; one problem is how and why the activity of gamma efferent fibers is employed in the regulation of posture and movement, and the other is how higher nervous centers control several spinal reflexes for the purpose of certain intended motions. The present study would be very significant in accounting for the roles of gamma activity in the motor control in the dynamic sense. Particularly, it is a very interesting result and worthy to be emphasized that gamma activities need to be enhanced with an increase in load for the purpose of maintaining the posture satisfactorily stable. Recently, Euler (1966)[19] has demonstrated the contribution of gamma activity to "load-compensation" in the respiratory control , through direct recordings of spindle afferents of the intercostal muscle; that is, the spindle activity is adjusted to compensate for changes of load. The present work seems to explain the concept of the "load-compensation" in the regulation of posture in such a quantitative form as represented by Eq. (5.11).

Granit (1970)[24] has specially emphasized that the most commonly observed effects of gamma fibers on spindles in the modest range of normal movements is undoubtedly their remarkable precise co-activation with the alpha activity, and that the cerebellum controls a neural switch directing excitation into the alpha or gamma route. As shown in Fig. 5.10, simulating the neuron links between the cerebellar efferents and the alpha and gamma motoneurons, we have examined the role of alpha-gamma linkage in the postural control in terms of the model and also demonstrated its usefulness. This investigation is quite the beginning. Indeed, we are now going to attack this dynamic problem with increasing vigor, considering the cerebellar circult elucidated by Eccles, Ito and Szentagothai (1967)[16] and applying the theory of learning control. A preliminary work along the line has been already reported (Kajiyama et al., 1973)[36]. The study has dealt with the problem of postural control of multi-link motor system, paying a special attention to the learning control function of cerebellum.

It has been suggested that the velocity control in the extremities would depend to some extent on information from joints and ligamints. The question of whether the spindles also contribute something is required to be speculated. In the present work, the possibility of velocity control has been shown in the dynamic manner , by introducing the cooperative actions of spindle group II afferents with group Ia afferents and together by considering the effects of gamma activity. On the other hand, Phillips (1969)[53] also treated an intended movement at an uniform velocity diagramatically with considering the contributions of gamma fibers, spindle GIa and GII fibers, but failed to go beyond a diagramatical illustration. The present study is more significant in accounting for the problem quantitatively. The velocity control is essentially associated with our ordinary intended movements, but the very outline has never been clarified by any physiological recordings, still less the contribution of group II afferents. At any rate, further physiological and

mathematical study which would lead to understanding of the actions of group II and group Ia afferent fibers is required in view of clarifying the mechanism of velocity control.

5.6 CONCLUSION

1. A mathematical model of the neuromuscular control system consisting of a pair of flexor and extensor muscles was developed, based on the physiological data obtained from cat soleus muscles. In terms of an analog simulation, control functions of the spinal reflexes of spindle GIa, spindle GII and tendon GIb afferent fibers, were accounted for quantitatively.

2. Activities of gamma effernet fibers were shown to correspond to reference of limb position. The relation between impulse frequency of gamma fibers, Γ, and desired angle of joint, θ_R, was represented.

3. Spindle group Ia fibers were shown to function as a PD controller in the position control system, and their gains of proportionality and differentiation are regulated by Γ. The condition necessary for stable postural control is to increase Γ in direct proportion to the increase in load.

4. Neural connections between myotaitc unit at the spinal cord and cerebellar efferent pathways were simulated, and usefulness of alpha-gamma linkage in the postural control was demonstrated.

5. Tendon group Ib fibers were shown to function effectively in the tension control of muscle.

6. The possibility of velocity control was shown by introducing synergetic action of GII afferent fibers with GIa fibers.

7. These simulations showed that one of the spinal reflexes such as position control, velocity control and tension control, could be selected by supraspinal control to the interneurons mediating GIb and GII pathways.

CHAPTER VI

MATHEMATICAL MODEL OF HUMAN FOREARM MOTOR SYSTEM

6.1 INTRODUCTION

An analysis of the kinetic muscle-limb system, consisting of antagonistic muscle pairs and limb-load element, is of significance in understanding how skillfully the muscle system works and in providing a deeper insight into the control structure of voluntary or reflex motions. The analysis will be also useful in designing more satisfactory artificial limbs or in developing new orthotic systems for the paralyzed extremities.

The present purpose is to clarify the dynamic characteristics of the human forearm system, in particular, to investigate the mutually tangled effects among th mechanical properties of muscle and the agonist-antagonist muscle action. A mathematical model of the forearm muscle-limb system is developed, based on the physiological and anatomical findings, paying a special attention to the nonlinear dynamics of muscle contraction. The most important feature of the model is variation in system parameters due to muscle tension. Dynamic properties of the system are revealed quantitatively by means of simulations on an analog computer, and the behavior of the model is compared with the physiological data obtained from the intact human subjects.

6.2 DEVELOPMENT OF A MODEL

a) Preliminary consideration

Before developing a model, it is necessary to determine which motion of the forearm need to be analyzed, to investigate throughly whatever is known about the forearm muscle-limb system and then to see what additional assumptions and approxamations should be reasonably be made. The motions studied here are flexion and extension of the forearm about the elbow joint in the horizontal

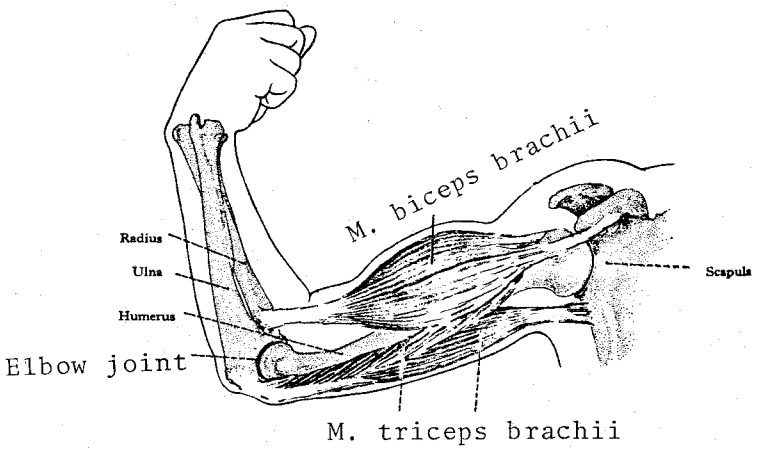

Fig. 6.1 Schematic drawing of muscle action in the forearm motor system.

plane, where the upper arm and human body are considered to be fixed. As seen in Fig. 6.1, the flexion is caused by contractions of the flexor muscles and extension by those of the extensor muscles. It is well known that biceps brachii muscle, coracobrachii muscle and brachialis muscle act together as the flexor muscle, and triceps brachii muscle and anconeus muscle act as the extensor muscle. These muscles might be simply represented as a single flexor and a single extensor muscle, respectively. Then, the forearm muscle-limb system can be shown by a mechanical model in Fig. 6.2.

Basically, mechanical property of the skeletal muscle has been represented by two-component model, consisting of the contractile component (CC) obeying the force-velocity relation and the series elastic component (SEC) (Hill, 1938[27]; Wilkie, 1950[62]; Akazawa et al., 1969[3], 1970[4], 1971[5]). Further, the CC may be separated into two elements, the force generator (FG) and the viscous-like component (VC), as shown in Fig. 6.2.(Details are mentioned in chapter V of part I of the present thesis). The correspondence of the force-velocity relation of the CC to the two components are explained as follows.

We have represented the force-load-velocity relation of the CC in a general-

lized form of Hill's hyperbolic equation (1938)[27]:

$$\left.\begin{aligned} (P + A)(v + b) &= b(F + A) \\ A &= a(F / P_o) \end{aligned}\right\} \qquad (6.1)$$

where P = load applied to the muscle (or tension on the muscle),

P_o = maximum isometric tension,

F = contractile force generated in FG,

v = velocity of shortening of CC,

a, b = dynamic constants of Hill's hyperbolic equation.

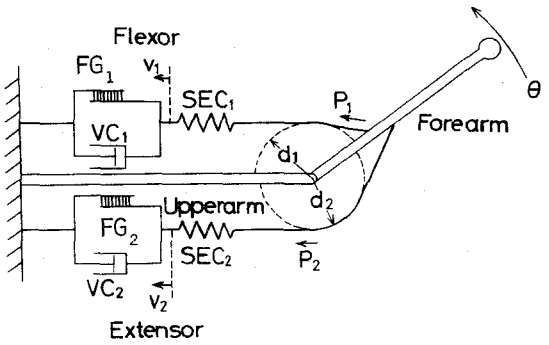

Fig. 6.2 Model of the muscle limb-system.

Then, the equation (6.1) is written as

$$\left.\begin{aligned} P &= F - B v \\ B &= \frac{F(P_o + a)}{P_o(v + b)} \end{aligned}\right\} \qquad (6.2)$$

where B = viscous coefficient of VC, function of v and F.

It is worthy to note that the viscous coefficient varies linearly with the contractile force, and consequently that the stimulation of alpha motor fibers in effect controls damping effect as well as the contractile force.

The force-velocity and tension-compliance relation obtained from the intact human subjects are shown in Fig. 6.3 and Fig. 6.4, respectively.

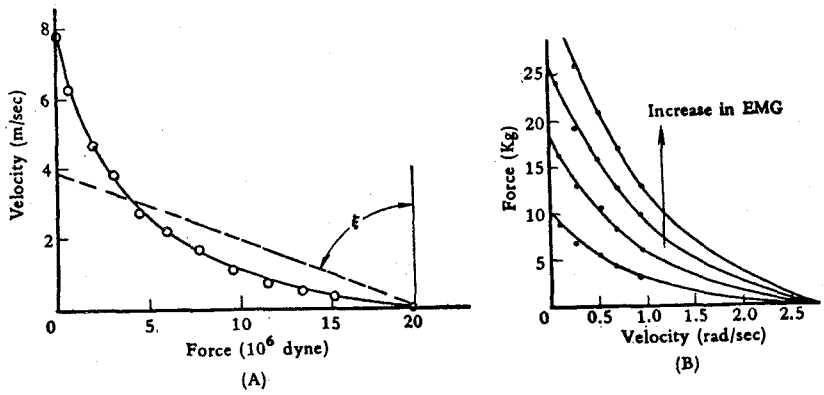

Fig. 6.3 Force-velocity relation of human skeletal muscles.
(A) The relation of forearm flexor muscle during maximum contraction, both force and velocity measured at the hand grip (from Wilkie (1950))[62].
(B) The relation of human calf muscle at four different levels of submaximal excitation (from Bigland and Lippold (1954))[10].

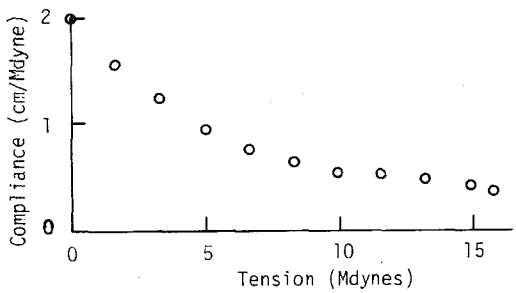

Fig. 6.4 Tension-compliance curve of the forearm flexor, both tension and compliance measured at the hand grip (from Wilkie (1950))[62].

Fig. 6.3 (A) shows the relation between forces of forearm flexor muscles and steady state velocity of shortening, in which human subject was to perform maximum contraction. Thus, the relation might represent the force-velocity relation at $F = P_o$. On the other hand, Fig. 6.3 (B) shows the effect of F on the velocity redrawn from Bigland and Lippold (1954)[10]. Four curves were obtained from the calf muscle at four different levels of submaximal excitation, i.e., at four different values of F less than P_o. Typical physiological data

of the tension-compliance relation obtained from the human flexor muscle of upper arm are shown in Fig. 6.4 (Wilkie, 1950)[62]. The compliance of SEC is not constant but decrease as the muscle tension is increased.

Although several complicated nonlinear properties of muscle have been clarified as mentioned above, dependence of viscous coefficient upon the contractile force is considered to play the most important role in the muscle motor system, so that it seems to convenient to make the following assumtions in developing the model.

(1) Viscous coefficient, B, is only as a function of the contractile force:

$$B = B_o \ (F / P_o) \tag{6.3}$$

where B_o is a viscous constant. This approximation is equivalent to linearlize the force-velocity curve as shown in Fig. 6.3 with a dashed line.

(2) Compliance of SEC, G, is assumed to be constant and independent of the tension.

(3) Both flexor and extensor muscles have identical mechanical properties, i.e., B_o and G of both muscles are identical.

In addition, following assumptions are introduced, concerning the geometry of the muscle-bone structure.

(4) Both muscles lie in the horizontal plane of the arm motion.

(5) The lever arms of both muscles are identical, $d = d_1 = d_2$, and are independent of the elbow joint angle.

(6) Dependence of maximum force, P_o, upon the elbow angle is neglected.

b) Formulation of the equation of the system

The equations associated with the mechanical system in Fig. 6.2 are now deduced. The equations with respect to the muscle itself are

$$\left.\begin{aligned} P_1 &= F_1 - B_1 v_1 \\ P_2 &= F_2 - B_2 v_2 \end{aligned}\right\} \tag{6.4}$$

$$\left.\begin{aligned} B_1 &= B_o\ (\ F_1/P_o\ ) \\ B_2 &= B_o\ (\ F_2/P_o\ ) \end{aligned}\right\} \qquad (6.5)$$

$$\left.\begin{aligned} v_1 &= d\ (d\theta/dt) + G\ (dP_1/dt) \\ v_2 &= -d\ (d\theta/dt) + G\ (\ dP_2/dt) \end{aligned}\right\} \qquad (6.6)$$

The kinetic equation for limb motion is

$$T_1 - T_2 + T_d = I\frac{d^2\theta}{dt^2} + B_j\frac{d\theta}{dt} \qquad (6.7)$$

$$\left.\begin{aligned} T_1 &= d\ P_1 \\ T_2 &= d\ P_2 \end{aligned}\right\} \qquad (6.8)$$

where θ = angle of elbow joint,

T_1 (T_2) = torque exerted by flexor muscle (extensor muscle),

d = lever arm,

I = moment of inertia of limb and hand,

B_j = viscous constant about elbow joint,

T_d = disturbance torque applied to the limb,

ω = angular velocity, $\omega = d\theta/dt$,

and subscripts 1 and 2, refer to flexor and extensor, respectively.

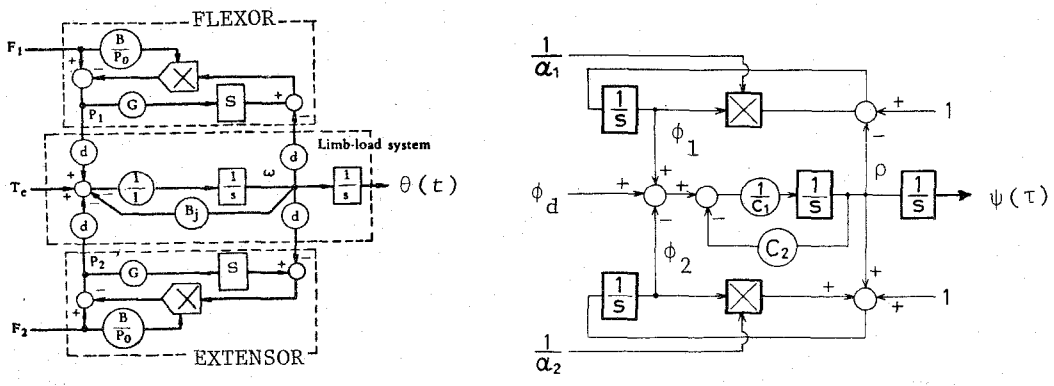

Fig. 6.5 Analog computer program of the model. (A), equations for (6.4)-(6.8). (B), nondimensional equation for Eq. (6.11).

Equations (6.4) - (6.8) can be simulated on an analog computer. The block-diagram is shown in Fig. 6.5 (A).

Since the values of the system parameters obviously may vary individually with human subjects, normalization is necessary so that the model may be applied generally. Following normalizations are made.

$$\left.\begin{aligned} \alpha_1 &= F_1 / P_o \qquad (0 \leqq \alpha_1 \leqq 1.0) \\ \alpha_2 &= F_2 / P_o \qquad (0 \leqq \alpha_2 \leqq 1.0) \\ \phi_1 &= T_1 / d\,P_o \\ \phi_2 &= T_2 / d\,P_o \\ \phi_d &= T_d / d\,P_o \end{aligned}\right\} \quad (6.9)$$

and

$$\left.\begin{aligned} \psi &= \theta\,(d / P_o) \\ \tau &= t\,(1.0 / B_o\,G) \\ C_1 &= I\,(G / d^2\,B_o{}^2) \\ C_2 &= B_j\,(1.0 / d^2\,B_o) \end{aligned}\right\} \quad (6.10)$$

As a result, we can obtain the non-dimensional equations from Eqs. (6.4) - (6.8):

$$\left.\begin{aligned} \phi_1 &= \alpha_1 \left(1 - \frac{d\psi}{d\tau} - \frac{d\phi_1}{d\tau}\right) \\ \phi_2 &= \alpha_2 \left(1 + \frac{d\psi}{d\tau} - \frac{d\phi_2}{d\tau}\right) \\ \phi_1 - \phi_2 + \phi_d &= C_1 \frac{d^2\psi}{d\tau^2} + C_2 \frac{d\psi}{d\tau} \end{aligned}\right\} \quad (6.11)$$

The analog computer program of Eq. (6.11) is shown in Fig. 6.5 (B). The inputs of the system are α_1 and α_2 which are the normalized contractile forces developed by the stimulations in the flexor and extensor muscles, respectively, and the output the normalized angle of elbow joint, ψ.

Note that α_1 and α_2 not only work as inputs but also bring about variation in system parameters, in addition that the system is time-variant

because α_1 and α_2 are as a function of time. Consider a simple case: α_1 = constant, α_2 = constant, $\phi_d = 0$. In this case, Eq. (6.11) becomes

$$\left.\begin{aligned} & A_4 \frac{d^4\psi}{d\tau^4} + A_3 \frac{d^3\psi}{d\tau^3} + A_2 \frac{d^2\psi}{d\tau^2} + A_1 \frac{d\psi}{d\tau} = \alpha_1 - \alpha_2 \\ & A_4 = C_1 \alpha_1 \alpha_2 , \qquad A_3 = C_2 \alpha_1 \alpha_2 + C_1 (\alpha_1 + \alpha_2) \\ & A_2 = C_1 + C_2 (\alpha_1 + \alpha_2) + 2 \alpha_1 \alpha_2 , \\ & A_1 = C_2 + \alpha_1 + \alpha_2 \end{aligned}\right\} \quad (6.12)$$

The difference $(\alpha_1 - \alpha_2)$ obviously acts as a net driving force to make the arm move. The terms $(\alpha_1 + \alpha_2)$ and $\alpha_1 \alpha_2$ are included in the system parameters A_4, A_3, A_2 and A_1, so that the the dynamic property can be regulated by those terms. Note that the term $(\alpha_1 + \alpha_2)$ is an indication of the overall tension level.

c) Quantitative determination of the parameters

The values of the parameters, I, d, P_o, G, B_o and B_j are calculated, based on the physiological data obtained by Wilkie (1950)[62] and Vodovnik et al. (1967).[59] The values of force, velocity and compliance in Fig. 6.3 (A) and Fig. 6.4 are measured directly at the hand grip, so that they have to be calibrated to those of the corresponding muscle. The calibration can be made in terms of lever ratio, η :

η = (lever arm)/(distance from elbow joint to hand grip)

= 4.5/32.0 = 0.14

(1) Momemt of inertia of arm and hand is taken to be 0.53×10^6 ($g.cm^2$), from Wilkie (1950).[62]

(2) Lever arm is taken to be 4.5 cm from Wilkie, which is the equivalent lever arm of biceps brachii muscle.

(3) Maximum force at the hand grip is 19.6×10^6 dyne as shown in Fig. 6.3 (A) Thus, P_o at the muscle is taken to be $19.6 \times 10^6 / \eta = 1.4 \times 10^8$ dyne.

(4) Compliance is assumed to be 0.8×10^{-6} cm/dyne at the hand grip as seen in Fig. 6.4, thus G is taken to be $0.8 \times 10^{-6} \times \eta^2 = 1.57 \times 10^{-8}$ cm/dyne.

(5) Viscous damping constant during maximum contraction at the hand is assumed to be $\tan \xi$ in Fig. 6.3 (A), thus $B_o = \tan \xi / \eta = 2.58 \times 10^6$ dyne/(cm/sec) at the muscle.

(6) According to Vodovnik et al. (1967), viscous damping constant about elbow joint is 1.2×10^7 dyne.cm/(rad/sec), thus we use $B_j = 1.0 \times 10^7$ dyne.cm/(rad/sec) in the present chapter.

(7) The dimensionless parameters, τ, ψ, C_1 and C_2 are obtained from above values.

The estimated values are summarized in Table VI-1.

TABLE VI-1

Values of the system parameters estimated

I	0.53×10^6	[g·cm²]	ψ/θ	2.0 [rad⁻¹]
d	4.5	[cm]	τ/t	25.0 [sec⁻¹]
P_0	1.4×10^8	[dyne]	C_1	0.25
G	1.57×10^{-8}	[cm/dyne]	C_2	0.2
B_0	2.58×10^6	[dyne/(cm/sec)]		
B_j	1.0×10^7	[dyne·cm/(rad/sec)]		

6.3 RESULTS

In this section, behaviors of the model are compared with the existing physiological data obtained from the human subjects. Then various types of motions are investigated to understand the dynamic properties of muscle-limb system in terms of the model. Furthermore, the behaviors of electrically stimulated muscles are explained by the model , with changing the parameters.

a) Simulation of isometric contraction

An isometric contraction of intact muscle is attained under the condition where corresponding limb is fixed. Solid line in Fig. 6.6 is an ex-

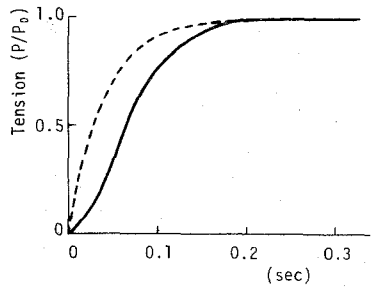

Fig. 6.6 Simulation of isometric contraction. Solid line, physiological record obtained from the forearm flexor muscle (from Wilkie, 1950).[62] Broken line, response of the model.

perimental result redrawn from Wilkie (1950).[62] In the experiment, maximal endeavor to flex the elbow was made, so that the flexor muscle was considered to generate the maximum contractile force. This contraction, therefore, may be mathematically expressed as

$$d\psi/d\tau = 0,\ d^2\psi/d\tau^2 = 0,\ \alpha_1=0\ (\tau< 0),\ \alpha_1=1.0\ (\tau> 0).$$

The isometric contraction is simulated on an analog computer using the parameters in Table VI-1. The simulated response is drawn with broken line in Fig. 6.6. The response of the model shows the faster rise in tension. It is because compliance is assumed to be constant, viscous coefficient is to be independent of velocity, and the contractile force is assumed to be stepwise,

b) Simulation of voluntary movement

There are many types of possible purposeful movements such as withdrawal, tracking and minimum-time movements. Here physiological records of the minimum-time movements obtained by Vodovnik et al. (1966)[60] are simulated, because they recorded both the elbow joint angle and the electromyograms of biceps brachii and triceps brachii muscles simultaneously. The physiological

data are shown in Fig. 6.7 (a) and (b). In the experiments, the initial and final positions of the limb were specified, and the subject was to move his limb from one position to the other in the possible shortest time.

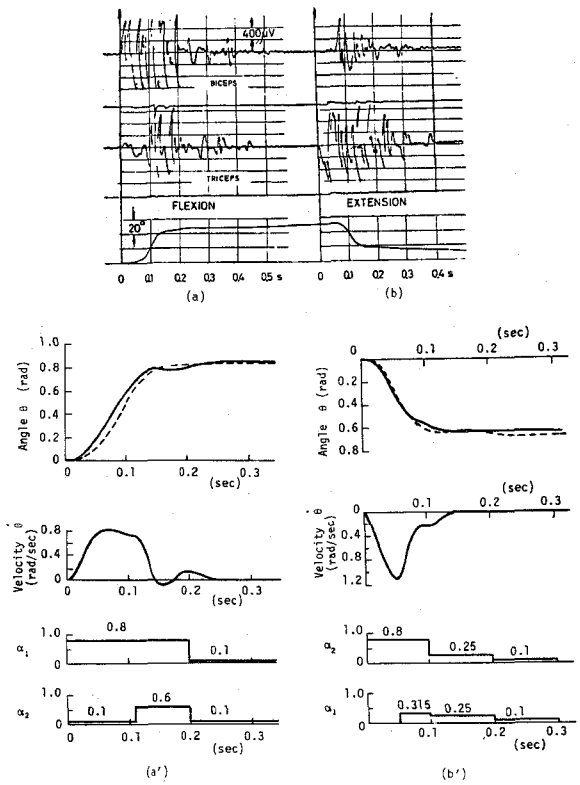

Fig. 6.7 Simulation of the minimum-time movements.
(a), (b): experimental results redrawn from Vodovnik et al. (1966)[60]; top trace, EMG of biceps; middle, EMG of triceps; bottom, elbow joint angle. (a'), (b'): solid line, simulated result of the movements; broken line, physiological result redrawn from the figures (a) and (b).

The difficulty encountered in achieving simulation of this motion arises in estimating quantitaitvely the contractile force exerted by the muscle. However, considering the fact that approximately linear relationship holds between the envelop of EMG and the isometric tension (Kuroda et al., 1970;[38]

Suzuki and Suematsu, 1969[56]; Vodovnik et al., 1966[60]), we take that the time courses of the exerting forces, $\alpha_1(t)$ and $\alpha_2(t)$, are those in Fig. 6.7 (a') and (b') which are similar to the envelops of EMG. Solid line in Fig. 6.7 (a') and (b') show the responses of the model obtained by using the values in Table VI-1. The simulated results show close agreements with the experimental records (broken lines (a') and (b') redrawn from (a) and (b), respectively).

c) Force-load-velocity relation of muscle-limb system

It is generally believed that the quick movements are achieved by alternative contractions of agonist and antagonist muscles (bang-bang mode), which seems to be in agreement with the time-optimal control theory. However, in the experimental data obtained, e.g., as seen in Fig. 6.7, there is a period when both muscles are active simultaneously. It is thus necessary to examine how the velocity of motion is regulated by the exerting forces of agonist and antagonist muscles. Such investigations may give an important clue for solving the time-optimal control problem of muscle motor system.

Fig. 6.8 (A) shows the responses of the model where the antagonist (extensor) being relaxed, the agonist (flexor) is activated with various stimulus intensities. When the exerting force is larger, the velocity rises faster and has a high steady state of velocity, although the responses become resonant. In Fig. 6.8 (B), the difference in exerting forces of both muscles, $(\alpha_1 - \alpha_2)$, is constant while the sum of both $(\alpha_1 + \alpha_2)$ varies from 1.5 to 0.5. The velocity rises more slowly and has a lower steady state when the sum is large (tension level is high). This is because the viscous force acting in the opposite direction of movement becomes larger as the sum ($\alpha_1 + \alpha_2$) is increased.

In addition, the model behaviors of slowing down, stopping and reversing are computed. One of the results is shown in Fig. 6.9. Until the switching time (broken line), the antagonist muscle being relaxed , the limb continues

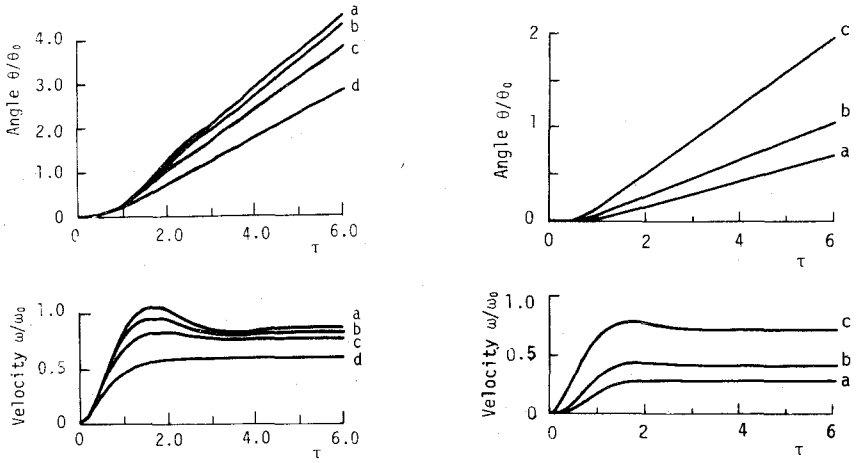

Fig. 6.8 Simulation results to show the effects of contractile force upon the velocity of movements. (A) The agonist is generating the contractile force, the antagonist being relaxed; curve a, α_1 =1.0, α_2=0; b, α_1=0.75, α_2=0; c, α_1=0.5, α_2=0; d, α_1=0.25, α_2=0. (B) Effect of tension level (α_1 + α_2) on the velocity when the difference (α_1 - α_2) is constant, (α_1-α_2)=0.5; curve a, α_1=1.0, α_2=0.5; b, 0.75, 0.25; c, 0.5, 0.0. t/τ= 40 msec, θ_o = 0.49 rad, ω_o=12.1 rad/sec.

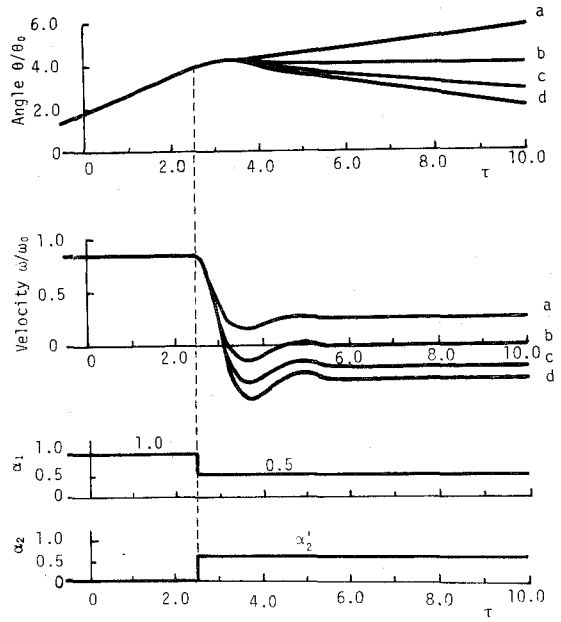

Fig. 6.9 Model responses of turning over from flexion to extension, holding and braking the flexion by changing the contractile forces of flexor and extensor muscles. curve a, α_2'=0.25; curve b, 0.5; curve c, 0.75; curve d, 1.0; t/τ =40 msec, θ_o=0.49 rad, ω_o=12.1 rad/sec, ϕ_d=0.

to flex at a constant speed by means of the agonist's contraction. Then, the agonist is inhibited and the antagonist is, in turn, excited with a specific stimulus strength according to motions. Each motion can not be performed immediately after the switching instant due to the moment of inertia of limb and to the lag time constant of muscle dynamics. We find in Fig. 6.9 c and d, that it takes about 20 msec (τ=0.5) from the switching time for the reversing motion to begin.

On the other hand, the relation between force and velocity in the steady state ($d\phi_1/d\tau=0$, $d\phi_2/d\tau=0$, $d^2\psi/d\tau^2=0$) is

$$\rho = \frac{\alpha_1 - \alpha_2}{\alpha_1 + \alpha_2 + C_2} \tag{6.13}$$

$$\rho = d\psi/d\tau$$

That is, velocity of movement is increased when the difference in forces ($\alpha_1 - \alpha_2$) is increased but decreased when the sum of them ($\alpha_1 + \alpha_2$) is increased. Furthermore, Eq. (6.13) indicates that the relation between α_1 and α_2 is linear when the velocity is constant. Solid line in Fig. 6.10 shows this relation at ρ= ±0.8, ±0.6, ±0.4, ±0.2 and 0. The maximum velocity , ρ_{max} = 0.838 is obtained at α_1=1.0 and α_2=0.

For comparison, consider a linear system in which the viscous coefficient is constant, independently of the contractile force, i.e., $B_1=\tilde{\alpha}_1 B_o$, $B_2=\tilde{\alpha}_2 B_o$, where $\tilde{\alpha}_1$ and $\tilde{\alpha}_2$ are constants. In this case, the steady state velocity is

$$\rho = \frac{\alpha_1 - \alpha_2}{\tilde{\alpha}_1 + \tilde{\alpha}_2 + C_2} \tag{6.14}$$

The velocity is dependent on the difference ($\alpha_1 - \alpha_2$) only. The relation of Eq. (6.14) is shown with broken lines in Fig. 6.10, in which ($\tilde{\alpha}_1 + \tilde{\alpha}_2$) is

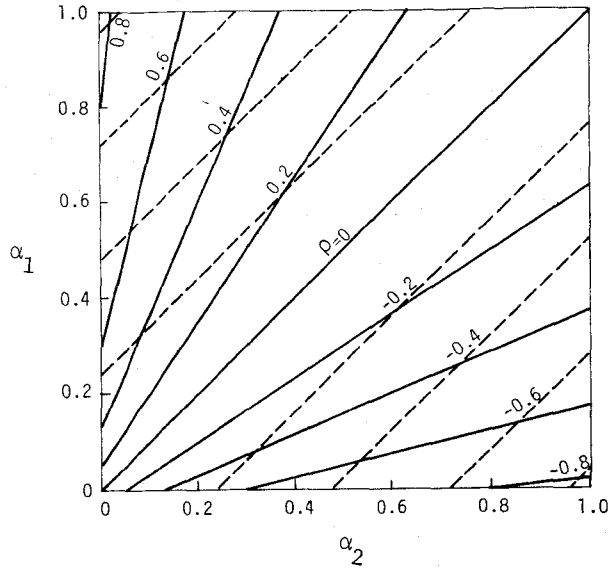

Fig. 6.10 The steady state relation between velocity (ρ) and force (α_1 and α_2). Solid line, the proposed model (viscous coefficient varies with α_1 or α_2); broken line, linear model (viscous coefficient is constant , see Eq. (6.14)).

taken to be 1.0 so as to obtain the same maximum velocity ρ_{max}=0.838 as obtained from Eq. (6.13). While broken lines of the linear system are parallel with each other, solid lines of the nonlinear model are dense near the origin. This aspect may mean that the velocity of the movements can be regulated more widely by smaller value of α_1 and α_2.

Furthermore, the responses of the model to the constant load-torque are computed. A typical response to several values of the load-torque is shown in Fig. 6.11. When the applied load is small, the velocity rises quickly and has a high steady state value. The steady state relation between load-torque is formulated as

$$\rho = \frac{\phi_d + \alpha_1 - \alpha_2}{\alpha_1 + \alpha_2 + C_2} \qquad (6.15)$$

While the load(force)-velocity relation of the intact human muscles is hyperbolic as shown in Fig. 6.3, the $\phi_d - \rho$ relation of the model becomes linear

as expressed in Eq. (3.15), which is due to the linear approximation of the force-velocity curve shown in Fig. 6.3 (A).

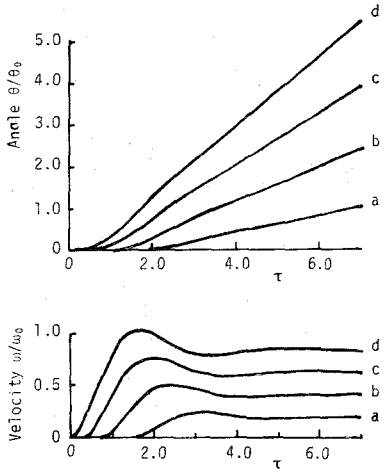

Fig. 6.11 Responses of the model to show the effects of load-torque on the velocity of movements. Curve a, applied load ϕ_d =0.75; b, 0.5; c, 0.25; d, 0. In each case, α_1=1.0, α_2=0, t/τ=40 msec, θ_o=0.49 rad, ω_o=12.1 rad/sec.

d) Response to disturbance torque

In order to examine the dynamic property of the muscle-limb system, the responses to impulsive disturbance torque are investigated, paying special attentions to the nonlinear effect of contractile force. Consider that an impulsive disturbance torque, $\phi_d = A_\phi \delta(\tau)$, is applied to the limb at τ=0 when the forearm is maintained at a certain position, with the identical contractile forces being generated by both muscles, i.e., $\alpha = \alpha_1 = \alpha_2$. Transient responses of the system to several values of α are shown in Fig. 6.12. When the exerting force is large, the responses become more resonant and the offset error from the maintained position is smaller. This property is explained analytically as follows. When α is time-invariant, Laplace transform of Eq. (3.11) yields the following relation.

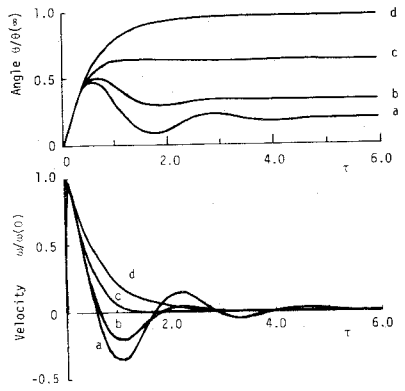

Fig. 6.12 Responses of the model to impulsive disturbance torque, $\phi_d = A_\phi \delta(\tau)$, illustrating the effects of tension level such as tense (a), moderate tense (b and c) and relaxed tension (d). Curve a, $\alpha = \alpha_1 = \alpha_2 = 1.0$; b, 0.5; c, 0.2; d, 0.1; t/τ=40 msec, $\psi(\infty)=2.656\ A_\phi$, $\rho(0)=4.0\ A_\phi$.

$$\left.\begin{aligned} \psi(s) &= \rho(s) \,/\, s \\ \rho(s) &= \frac{A_\phi\,(1+\alpha\, s)}{C_1\,\alpha\,(s^2 + 2\,\zeta\,\omega_n\, s + \omega_n^2)} \\ \text{damping ratio: } \zeta &= (C_1 + C_2\,\alpha)/\,2\sqrt{C_1\,\alpha\,(C_2 + 2\,\alpha)} \\ \text{natural frequency: } \omega_n &= \sqrt{(C_2 + 2\,\alpha)/\,C_1\,\alpha} \end{aligned}\right\} \quad (6.16)$$

where $\psi(s)$ and $\rho(s)$ are the Laplace transforms of $\psi(\tau)$ and $\rho(\tau)$, respectively. From the final value theorem, $\psi(\tau)$ at $\tau=\infty$ is

$$\psi(\infty) = \frac{A_\phi}{C_2 + 2\,\alpha}$$

Therefore, both the damping ratio and the gain to disturbance decreases as α increases. Thus if both muscles are generating large contractile forces, e.g. if muscle tone is at clamping or tensing state, the system would be highly resonant but the offset error would be small.

6.4 DISCUSSION

Although the proposed model is not, in a sense, a complete one, since neither the neural innervation in the spinal cord nor the central nervous system is taken into account at all. This simulation, however, is useful in developing an orthotic system with electrically stimulated muscle. In genaral, patients with central or peripheral lesions of their motor pathways are unable to perform useful movements with corresponding limb. In some cases, required motions can be achieved by electrical stimulation of the motor points of the muscle of interest. It is thus necessary to synthesize a control device by which the corresponding limb moves similarly as when normally innervated. An electrically stimulated muscle has, in itself, the similar mechano-chemical contractile process and properties as normally activated muscles, so that the model proposed here can be also applied to this kind of muscle by varying the parameters of muscle in Table VI-1.

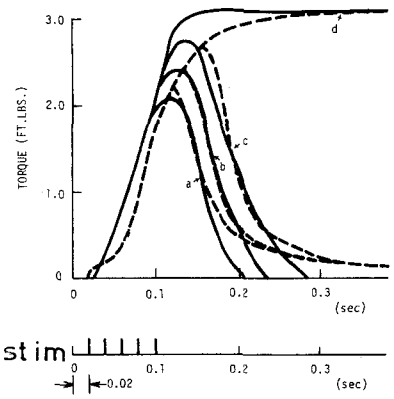

Fig. 6.13 Simulation of the isometric contraction generated by electrical stimulation at 50 Hz, Solid line, physiological record obtained from Crochetiere, Vodovnik and Reswick (1967)[65]; curve a, 3-pulse; b, 4-pulse; c, 5-pulse; d, tetanus; 1.0 [FT.LBS]= 13.5 × 10^6 dyne.cm. Dashed line, simulated responses of the model.

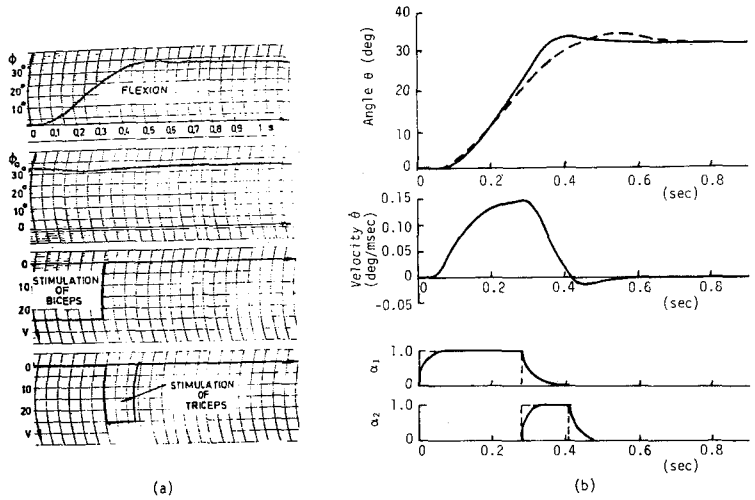

Fig. 6.14 Simulation of the flexion movement generated by electrical stimulations of biceps and triceps of upper arm. (a) Experimental record redrawn from Vodovnik et al. (1966).[60] (b) Solid line, simulated response of the model; broken line, experimental record redrawn from figure (a).

According to the physiological data concerning the electrical stimulations obtained by Vodovnik and his co-workers (Vodovnik et al., 1966,[60] 1967,[59] Crochetiere et al., 1967[65]), we take following values for the upper arm muscles electrically stimulated; $P_o = 9.4 \times 10^6$ dyne, $1/G = 4.3 \times 10^{-6}$ cm/dyne, $B_o = 0.17 \times 10^6$ dyne/(cm/sec), $B_j = 12.0 \times 10^6$ dyne.cm.sec, d=4.5 cm, $I = 0.9 \times 10^6$ g.cm^2 and time course of the contractile force F(t) is $F(t) = \mathcal{L}^{-1}\{P_o/(1 + \tau_e s)\}$, τ_e=40 msec.

Solid lines in Fig. 6.13 show the typical responses of isometric contraction of human biceps generated by electrical stimulation, where several numbers of pulses (0.2 msec-pulse at 50 Hz) were applied (Crochetiere et al. 1966).[65] Broken line is the simulated response obtained from the above values. Fig. 6.14 (a) shows the flexion movement produced by the functional electrical stimulation of biceps and triceps (Vodovnik et al., 1966),[60] and solid line in Fig. 6.14 (b) is the simulated response of the model obtained by using the

above values of the parameters. As seen from Fig. 6.13 and Fig. 6.14, simulated responses show close coincidence with the experimental responses obtained from intact human subjects. Then, the orthotic system would be thus designed by means of pertinent computer simulation studies of the proposed model, and in fact the work along the line proceeds now. This procedure is of significance in making a preliminary experiment without applying actual electrical stimulations to the patients.

6.5 CONCLUSION

A mathematical model of the muscle-limb system of the human forearm was developed, based on the physiological and anatomical findings. Simulation study on an analog computer was made to explain the dynamic properties of the system and further to validate the proposed model. The results are summarized as follows.

1. The contractile force of the muscle does not only act as driving force but also leads to variation in system parameters.

2. All the parameters were identified from the experimental data obtained from the intact human subjects.

3. Voluntary isometric and minimum-time movements were simulated by the model, showing close agreements with the experimental responses.

4. Simulation study on an analog computer showed that when the exerting force is large, the muscle-limb system becomes resonant, but the gain decreases.

5. The behaviors of electrically stimulated muscles, i.e., isometric contraction and flexion movements, were explained by the model.

CHAPTER VII

CONCLUSION

Mathematical models of muscle spindle, tendon organ, muscle, motoneuron and muscle-limb-load system were developed individually, based on the physiological data obtained from cat soleus muscles. Further, by synthesizing these elements, a model of the stretch reflex and a total model of a neuromuscular control system at the spinal level was developed. Control functions of the system, and roles of the gamma system were clarified by simulations on an analog computer. Additionally, mathematical model of a human forearm motor system was developed. Essentially conclusive remarks are enumerated as follows.

1. A mathematical model of the muscle spindle was developed, based on physiological and anatomical findings (section 3.3). Discharge rates of the primary and secondary endings were expressed as a function of muscle length, stimulation frequency of dynamic gamma fibers Γ_d and stimulation frequency of static gamma fibers Γ_s. All the parameters involved were determined quantitatively from the physiological data (section 3.4 and 3.5). Important properties revealed are cited below.

i) Position sensitivity of the primary endings is increased proportionally with an increase in Γ_d or Γ_s.

ii) Position sensitivity of the secondary endings is increased proportionally with an increase in Γ_s.

iii) Velocity sensitivity of the primary endings is increased proportionally with an increase in Γ_d, while velocity sensitivity of the secondary endings is independent of Γ_d and Γ_s.

iv) Velocity sensitivities of both endings are decreased by increasing velocity of muscle stretch.

2. A mathematical model of the stretch reflex consisting of muscle spindle (group Ia afferent fiber), alpha motoneuron and muscle, was developed.

i) All the parameters were determined quantitatively, based on the physiological data obtained from cat soleus muscles (section 4.3).

ii) The total tension, the active reflex tension and the passive tension in cat soleus produced by stretching it were simulated together on an analog computer. The responses of the model showed close agreement with the physiological data (section 4.4).

iii) Responses of the stretch reflex observed when gamma efferent nerve fibers were paralysed by procaine were simulated. The effect of gamma activity on the stretch reflex was explained quantitatively (section 4.4).

3. A mathematical model of the antagonistic neuromuscular control system was developed, based on the results obtained in chapters III and VI (section 5.3). The proposed system consists of a pair of skeletal muscles (flexor and extensor), muscle spindles (GIa and GII fibers), tendon organs (GIb fibers), alpha motoneurons, alpha and gamma efferent routes from higher centers and limb-load system. Cooperative functions of each organ and control functions of the neuromuscular control system were made clear by analog simulations of the model.

i) Impulse frequencies of the gamma efferent fibers, Γ, were shown to be equivalent to reference signal of position (angle of the joint), θ. The steady state relation between Γ and θ was represented, involving the effects of impulse frequency of alpha efferent fibers, H_{α}, (section 5.3).

ii) It was indicated that, in order to maintain a stable postural control or to perform fast movement, Γ needs to be increased with

an increase in load (section 5.3 b), c)).

iii) The neuron links of spinal descending tracts from cerebellum (extra-vestibulo-spinal tract and reticulo-spinal tract) were introduced into the model, and usefulness of alpha-gamma linkage in the postural control was revealed (section 5.3 d)).

iv) The spinal reflex arc via tendon organ group Ib fibers effectively functions in controlling muscle tension (section 5.4).

v) It was shown that velocity control was possible when spindle GII fibers act simultaneously with GIa fibers.

vi) Finally, it was suggested that the supra-spinal control to interneurons mediating the GIb and GII afferent pathways would lead to selecting one of the spinal reflexes such as postural control, tension control and velocity control.

4. A mathematical model of the muscle-limb system of a human forearm motor system was developed, based on physiological and anatomical findings.

i) All the parameters were identified from the experimental data obtained from intact human subjects (section 6.2).

ii) Both voluntary isometric and minimum-time movements and the movements generated by the contraction of electrically stimulated muscles were simulated by the model. Simulated results showed close agreement with the human data (section 6.3 and section 6.4).

iii) It was unfolded by simulations that the muscle-limb system became resonant but the gain was decreased when the force exerted by a muscle was large.

It is well known that cerebellum does play a very important role in the motor control. So it is of obvious interest to reveal the functions of cerebellum regulating the neuromuscular control system at the spinal level. A few about it has been investigated in the present work (section 5.3).

With increasing vigor, we have set about this subject, paying special attentions to the learning control functions of cerebellum.

There are eager needs to drive and control paralyzed extremities with functionally electrical stimulations. It is evident that the present work and the further study of cerebellum would be closely associated with the development of such an orthotic system. In fact, a basic approach of designing the control system is also proceeded in cooperation with the writer's colleagues, extending the findings obtained from the present work and the proposed algorithm of learning control , and further applying the pattern recognition technique to EMG.

REFERENCES

1) Agarwal, G. C., Berman, B. M. and Stark, L. (1970) Studies in postural control systems. Part I: Torque disturbance input. IEEE Trans. Syst. Sci. Cybernetics, SSC-6, 116-121.

2) Agarwal, G. C. and Gottlieb, G. L. (1969) Analysis of step tracking in normal human subjects. IEEE Trans. Man-Machine Systems, MMS-10, 132-137.

3) Akazawa, K., Fujii, K. and Kasai, T. (1969) Analysis of muscular contraction mechanism by viscoelastic model. Technol. Pepts. Osaka Univ., 19, No. 902, 577-593.

4) Akazawa, K., Fujii, K., Kasai, T. and Mashima, H. (1970) Simulation of muscular contraction based on sliding mechanism. Jap. J. Med. Electronics and Biol. Engng, 8, 203-211. (in Japanese).

5) Akazawa, K., Fujii, K. and Mashima, H. (1971) Mechanical properties of skeletal muscle. In "The Second Domestic Symp. on Biomechanism," SOBIM JAPAN, No. 13, 175-188. (in Japanese).

6) Angers, D. and Delisle, G.Y. (1971) Study of the action of static and dynamic fusimotor fibers with a mechanical model of the mammalian muscle spindle. IEEE Trans. Bio-Medical Engineering, BME-18, 175-180.

7) Araki, T. (1972) Undo Neuron no Hassha yoshiki. In "Seitai no Undokiko to sono seigyo." Mashima, H. and Ikai, M, ed., pp143-171. Tokyo: Kyorin shoin. (in Japanese).

8) Bessou, P. and Laporte, Y, (1962) Responses from primary and secondary endings of the same neuromuscular spindle of the tenuissimus muscle of the cat. In "Symposium on Muscle Receptors", (Barker, D., ed.) pp. 105-119. Hong Kong: Hong Kong University Press.

9) Bessou, P., Laporte, Y. and Pagès, B. (1968) Frequencygrams of spindle primary endings elicited by stimulation of static and dynamic fusimotor fibres. J. Physiol., 196, 47-63.

10) Bigland, B. and Lippold, O. G. J. (1954) The relation between force, velocity and integrated electrical activity in human muscle. J. Physiol., 123,214-224.

11) Brown, M. C., Lawrence, D. G. and Matthews, P. B. C. (1969) Static fusimotor fibres and the position sensitivity of muscle spindle receptors. Brain Res., 14, 157-172.

12) Crowe, A. (1968) A mechanical model of the mammalian muscle spindle. J. Theoret. Biol., 21, 1, 21-41.

13) Crowe, A. and Matthews, P. B. C. (1964a) The effects of stimulation of static and dynamic fusimotor fibres on the response to stretching of the primary endings of muscle spindles. J. Physiol., 174, 109-131.

14) Crowe, A. and Matthews, P. B. C. (1964b) Further studies of static and dynamic fusimotor fibres. J. Physiol., 174, 132-151.

15) Eccles, J. C., Eccles, R. M. and Lundberg, A. (1960) Types of neurone in and around the intermediate nucleus of the lumbosacral cord. J. Physiol., 154, 89-114.

16) Eccles, J. C., Ito, M. and Szentágothai, J. (1967) "The Cerebellum as a Neuronal Machine." Berlin: Springer Verlag.

17) Eccles, R. M. and Lundberg, A. (1959) Synaptic actions in motoneurones by afferents which may evoke the flexion reflex. Arch. ital. Biol. 94, 199-221.

18) Eldred, E., Granit, R. and Merton, P. A. (1953) Supraspinal control of the muscle spindles and its significance. J. Physiol., 122, 498-523.

19) Euler, C. v. (1966) Proprioceptive control in respiration. In "Muscular Afferents and Motor Control. Nobel Symposium I", (Granit, R., ed.), pp. 197-207. Stockholm: Almqvist and Wiksell.

20) Fujimori, B. (Editor) (1966) Japanese Handbook of Physiology, vol VII, Physiology of Motor System. Tokyo: Igaku shoin.

21) Gottlieb, G. L., Agarwal, G. C. and Stark, L. (1969) Stretch receptor models I -single-efferent single-afferent innervation. IEEE Trans. Man-Machine Systems, MMS-10, 17-27.

22) Gottlieb, G. L., Agarwal, G. C. and Stark, L. (1970) Studies in postural control systems. Part III: A muscle spindle model. IEEE Trans. Syst. Sci. Cybernetics, SSC-6, 127-132.

23) Granit, R. (Editor) (1966) "Muscular Afferents and Motor Control. Nobel Symposium I." Stockholm: Almqvist and Wiksell.

24) Granit, R. (1970) "The basis of motor control." London: Academic Press.

25) Harvey, R. J. and Matthews, P. B. C. (1961) The reponse of de-efferented muscle spindle endings in the cat's soleus to slow extension of the muscle. J. Physiol., 157, 370-392.

26) Hatakeyama, I., Saeki, Y. and Nagata, A. (1972) Analysis of the proprioceptive reflex control of muscular movement on the basis of control theory. Transactions of the Society of Instrument and Control Engineers, 8, 389-390.

27) Hill, A. V. (1938) The heat of shortening and the dynamic constants of muscle. Proc. Roy. Soc. B, 126, 136-195.

28) Houk, J. (1966) The stretch reflex in human muscle systems. In "The application of control theory to physiological systems," Milhorn,H.T. ed., pp. 283-316. London: W. B. Saunders.

29) Houk, J. (1967) A viscoelastic interaction which produces one component of adaptation in responses of Golgi tendon organs. J. Neurophysiol., 30, 1482-1493.

30) Houk, J. and Henneman, E. (1967) Feedback control of skeletal muscles. Brain Research, 5, 433-451.

31) Houk, J. and Simon, W. (1967) Responses of Golgi tendon organs to forces applied to muscle tendon. J. Neurophysiol., 30, 1466-1481.

32) Houk, J. C., Singer, J. J. and Goldman, M. R. (1970) An evaluation of length and force feedback to soleus muscles of decerebrate cats. J. Neurophysiol., 33, 784-811.

33) Ishida, A. and Umetani, Y. (1972) Analysis of the movement control system of skeletal muscles-Modeling with respect to tremor of the muscle. Transactions of the Society of Instrument and Control Engineers, 9, 160-166. (in Japanese).

34) Jones, R. W. (1969) Biological control mechanisms. In " Biological Engineering," Schwan, H. P. ed., pp. 87-203. New York: McGraw-Hill.

35) Joyce, G. C. and Rack, P. M. H. (1969) Isotonic lengthening and shortening movements of cat soleus muscle. J. Physiol., 204, 475-491.

36) Kajiyama, S., Akazawa, K., Taguchi, H. and Fujii, K. (1973) Postural control of multi-link system- Learning control model of cerebellum. 16th Jap. J. A. C. C., Tokyo, NO. 3007, 291-292. (in Japanese).

37) Katz, B. (1950) Depolarization of sensory terminals and the initiation of impulses in the muscle spindle. J. Physiol., 111, 261-282.

38) Kuroda, E., Klissouras, V., and Milsum, J. H. (1970) Electrical and metabolic acitvities and fatigue in human isometric contraction. J. Appl. Physiol., 29, 358-367.

39) Lennerstrand, G. (1968) Position and velocity sensitivity of muscle spindles in the cat. I. Primary and secondary endings deprived of fusimotor activation. Acta Physiol. Scand., 73, 281-299.

40) Liddell, E. G. T. and Sherrington, C. S. (1924). Reflexes in response to stretch (Myotatic reflexes). Proc. Roy. Soc., B, 96, 212-242.

41) Mains, R. E. and Soechting, J. F. (1971) A model for the neuromuscular response to sudden disturbances. Transaction of The ASME, J. Dynamic systems, Measurement and Control, Series G, 93, 247-251.

42) Mashima, H., Akazawa, K., Kushima, H.and Fujii, K. (1972) The force-load-velocity relation and the viscous-like force in the frog skeletal muscle. Jap. J. Physiol., 22, 103-120.

43) Mashima, H., Akazawa, K., Kushima, H. and Fujii, K. (1973) Graphical analysis and experimental determination of the active state in frog skeletal muscle. Jap. J. Physiol., 23, 217-240.

44) Matthews, P. B. C. (1958) The effect of the local application of procaine on the stretch reflex of the soleus muscle of the cat decerebrated by anaemia. J. Physiol., 140, 408-420.

45) Matthews, P. B. C. (1959a) The dependence of tension upon extension in the stretch reflex of the soleus muscle of the decerebrate cat. J. Physiol., 147, 521-546.

46) Matthews, P. B. C. (1959b) A study of certain factors influencing the stretch reflex of the decerebrate cat. J. Physiol., 147, 547-564.

47) Matthews, P. B. C. (1962) The differentiation of two types of fusimotor fibre by effects on the dynamic reponse of muscule primary endings. Quart. J. exp. Physiol., 47, 324-333.

48) Matthews, P.B. C. (1963) The response of de-efferented muscle spindle receptors to stretching at different velocities. J. Physiol., 168, 660-678.

49) Matthews, P. B. C. (1964) Muscle spindles and their motor control. Physiol. Rev., 44, 219-288.

50) Matthews, P. B. C. (1969) Evidence that the secondary as well as the primary endings of the muscle spindles may be responsible for the tonic stretch reflex of the decerebrate cat. J. Physiol., 204, 365-393.

51) McRuer, D. T., Magdaleno, R. E. and Moore, G. P. (1968) A neuro-muscular actuation system model. IEEE. MMS -9, 61-71.

52) Milsum, J. H. (1966) Biological control systems analysis. New York: Mc Graw-Hill Book Company.

53) Phillips, G. G. (1969) Motor apparatus of the baloon's hand. The Ferrier Lecture. Proc. Roy. Soc., B, 173, 141-175.

54) Rack, P. M. H. and Westbury, D. R. (1969) The effects of length and stimulus rate on tension in the isometric cat soleus muscle. J. Physiol., 204, 443-460.

55) Rudjord, T. (1970) A second order mechanical model of muscle spindles primary endings. Kybernetik, 6, 205-213.

56) Suzuki, R. and Suematsu, T. (1969) Myoelectric control system for one-function prosthetic hand. Reports of IMDE, Tokyo Medical and Dental Univ., 2, 156-162.

57) Toyama, K. (1966) An analysis of impulse discharges from the spindle receptors. Jap. J. Physiol., 16, 113-125.

58) Vickers, W. H. (1968) A physiologically based model of neuromuscular systems dynamics. IEEE Trans. Man-Machine Systems, MMS-9, 21-23.

59) Vodovnik, L., Crochetire, W. J. and Reswick, J. B. (1967) Control of a skeletal joint by electrical stimulation of antagonist. Med. and Biol. Engng., 5, 97-109.

60) Vodovnik,L., Kralj, A., Kelsin, D. and Borovsak, M. (1966) Simulation of purposeful movements by electrical stimulation of muscles. International Symposium on External Control in Human Extremities, 14-96.

61) Vodovnik, L. et al. (1971) Final report: Development of orthotic systems using functional electrical stimulation and myoelectric control. Priject No. 19-p-58391-F-01, University of Ljubljana, Yugoslavia.

62) Wilkie, D. R. (1950) The relation between force and velocity in human muscle. J. Physiol., 110, 249-280.

63) Young, L.R. (1969) On adaptive manual control. IEEE Trans. Man-Machine Systems, MMS-10, 292-331.

64) Young, L. R., Green, D. M., Elkind, J. I. and Kelly, J. A. (1964) Adaptive dynamic response characteristics of the human operator in simple manual control. IEEE Trans. Human Factors in Electronics, HFE-5, 6-13.

65) Crochetuere, W. J., Vodovnik, L. and Reswick, J. B. (1967) Electrical stimulation of skeletal muscle— A study of muscle as an actuator. Med. and Biol. Engng., 5, 111-125.

APPENDIX B

Taking the Laplace transform of Eq. (3.1), we obtain the extension of the spring E_1 as

$$x_1(s) = \frac{E_2 + s D_1}{E_1 + E_2 + s D_1} X_s(s) + \frac{1}{E_1 + E_2 + s D_1} F_d(s) \qquad \text{(A-1)}$$

Similarly taking the Laplace transform of Eqs. (3.2) and (3.3),

$$x_3(s) = e_4 \frac{E_5 + s D_2}{E_c + E_5 + s D_2} X_s(s) + \frac{e_4}{E_c + E_5 + s D_2} F_s(s) \qquad \text{(A-2)}$$

$$x_2(s) - x_3(s) = e_3 \frac{E_5 + s D_2}{E_c + E_5 + s D_2} X_s(s) + \frac{e_3}{E_c + E_5 + s D_2} F_s(s) \qquad \text{(A-3)}$$

$$e_4 = E_4/(E_3 + E_4), \quad e_3 = E_3/(E_3 + E_4), \quad E_c = E_3 E_4/(E_3 + E_4)$$

From Eqs. (3.4)-(3.6), we can ger

$$\begin{aligned} X_s(s) &= \nu X(s) \\ R(s) &= \eta_1 x_1(s) + \eta_2 x_3(s) + R_o \\ Q(s) &= \eta_3 \{x_2(s) - x_3(s)\} + Q_o \end{aligned} \qquad \text{(A-4)}$$

$$\eta_1 = C_1 r_1, \quad \eta_2 = C_3 r_1, \quad \eta_3 = C_4 r_2$$

Substituting Eqs. (A-1), (A-2) and (A-3) into Eq. (A-4),

$$R(s) = R_o + \left(k_1 + \frac{T_2 s}{1 + T_1 s} + \frac{T_4 s}{1 + T_3 s} \right) X(s) + \frac{k_2}{1 + T_1 s} F_d(s)$$

$$+ \frac{k_3}{1 + T_3 s} F_s(s)$$

$$Q(s) = Q_o + \left(K_4 + \frac{T_5 s}{1 + T_3 s} \right) X(s) + \frac{k_5}{1 + T_3 s} F_s(s) \qquad \text{(A-5)}$$

$$k_1 = \nu \left(\frac{\eta_1 E_2}{E_1 + E_2} + \frac{\eta_2 e_4 E_5}{E_c + E_5} \right)$$

$$k_2 = \eta_1 / (E_1 + E_2), \qquad k_3 = \eta_2 e_4 / (E_c + E_5) ,$$

$$k_4 = \nu \eta_3 e_3 E_5 / (E_c + E_5) , \qquad k_5 = \eta_3 C_3 / (E_c + E_5),$$

$$T_1 = D_1 / (E_1 + E_2), \qquad T_2 = \nu \eta_1 E_1 D_1 / (E_1 + E_2)^2,$$

$$T_3 = D_2 / (E_c + E_5), \qquad T_4 = \nu \eta_2 e_4 E_c D_2 / (E_c + E_5)^2$$

$$T_5 = \nu \eta_3 e_3 E_c D_2 / (E_c + E_5)^2$$

Following assumptions are introduced for simulation.

i) $T_1 \overset{\sim}{=} T_3$ for primary endings, (A-6)

ii) In the relation between the contractile forces of nuclear bag fibers and nuclear chain fibers and the static and dynamic fusimotor stimulation,

$$F_d(s) = G_d(s) \Gamma_d(s)$$
$$F_s(s) = G_s(s) \Gamma_s(s) \qquad \text{(A-7)}$$

And further,

$$\{ k_2 / (1 + T_1 s) \} G_d(s) = K_d / (1 + \tau_d s)$$
$$\{ k_3 / (1 + T_3 s) \} G_s(s) = K_s / (1 + \tau_s s) \qquad \text{(A-8)}$$
$$\{ k_5 / (1 + T_3 s) \} G_s(s) = K_s' / (1 + \tau_s s)$$

Substituting Eqs. (A-6), (A-7) and (A-8) into Eq. (A-5), we obtain

$$R(s) = R_o + \left(K_x + \frac{T_x s}{1 + T_1 s} \right) X(s) + \frac{K_d}{1 + \tau_d s} \Gamma_d(s) + \frac{K_s}{1 + \tau_s s} \Gamma_s(s) \qquad (3.9)$$

$$Q(s) = Q_o + \left(K_x' + \frac{T_x' s}{1 + T_3 s} \right) X(s) + \frac{K_s'}{1 + \tau_s s} \Gamma_s(s) \qquad (3.10)$$

where

$$\left.\begin{aligned}
K_x &= k_1 = \nu \left(\frac{\eta_1 E_2}{E_1 + E_2} + \frac{\eta_2 e_4 E_5}{E_c + E_5} \right) \\
K_x' &= k_4 = \nu \eta_3 e_3 E_5 / (E_c + E_5) \\
T_x &= T_2 + T_4 = \frac{\nu \eta_1 E_1 D_1}{(E_1 + E_2)^2} + \frac{\nu \eta_2 e_4 E_c D_2}{(E_c + E_5)^2} \\
T_x' &= T_5 = \nu \eta_3 e_3 E_c D_2 / (E_c + E_5)^2 \\
T_1 &= D_1 / (E_1 + E_2) \\
T_3 &= D_2 / (E_c + E_5)
\end{aligned}\right\} \qquad (A\text{-}9)$$

APPENDIX C

A ramp change in X_s is defined as

$$X_s(t) = 0 \qquad (t < 0)$$

$$X_s(t) = v\,t \qquad (0 < t < t_1) \tag{A-10}$$

$$X_s(t) = X_o \qquad (t \geq t_1)$$

where t_1 = the duration of dynamic stretching,

v = velocity of stretching.

The net length increase produced by the stretching, X_n, is

$$X_n = v\,t_1$$

Taking the Laplace transform of Eq. (A-10), we get

$$X_s(s) = \frac{v}{s^2}\left(1 - e^{-t_1 s} \right) \tag{A-11}$$

Denoting the bias to be R_o', then

$$R(s) = \left(K_x + \frac{T_x\, s}{1 + T_1\, s} \right) X(s) + R_o'(s) \tag{A-12}$$

$$R_o'(s) = R_o + \frac{K_d}{1 + \tau_d\, s}\,\Gamma_d(s) + \frac{K_s}{1 + \tau_s\, s}\,\Gamma_s(s)$$

Substituting Eq. (A-11) into Eq. (A-12), and then taking the inverse Laplace transforms of them, we can get

$$R(t) = R_o' \qquad (t \leq 0)$$

$$R(t) = K_x\, v\, t + T_x \left(1 - e^{-t/T_1} \right) v + R_o' \qquad (0 < t < t_1) \tag{A-13}$$

$$R(t) = K_x\, X_n + T_x\, e^{-t/T_1} \left(e^{t/T_1} - 1 \right) v + R_o' \qquad (t \geq t_1)$$

Since $R(t)$ at $t = t_1$ is R_o', and $R(t)$ at $t \to \infty$ is $R_o' + K_x X_n$, we obtain the position sensitivity to be $K_x = (R(\infty) - R(0)) / X_n$. According to

the definition of dynamic index, we may write

$$\text{Dynamic index} = R(t_1 + 0.5) - R(t_1)$$

$$= T_x \left(1 - e^{-0.5/T_1} \right) \left(1 - e^{-t_1/T_1} \right) v \qquad \text{(A-14)}$$

Taking $t_1 >> T_1$ and $0.5 >> T_1$ for equation (A-13), we can obtain

$$\text{Dynamic index} \simeq T_x v.$$